
# The impact of *Helicobacter hepaticus* infection on host immunity

**Anna Lucy Leith Heawood**

**BSc (Hons)**

Submitted in fulfilment of the requirements for the Degree of Doctor of Philosophy

School of Infection and Immunity
College of Medical, Veterinary and Life Sciences
University of Glasgow

**September 2024**

# Abstract

The mammalian immune system has evolved alongside a complex microbiota. Microbial colonization drives constant immune responses at steady state, while microbiota-derived metabolites and signals have functional impacts on host immune cells. *Helicobacter hepaticus* (*Hh*) is a member of the murine intestinal microbiota with the capacity to drive immune responses in a context-dependent manner. *Hh* stimulates strong immune regulation which counterbalances the induction of effector responses and allows persistent colonization without pathology. Whether these interactions alter how the host immune system responds in a subsequent disease setting has not previously been explored. In this thesis, we aimed to investigate how *Hh* affects the outcome of inflammatory disease and test whether *Hh* drives phenotypic and functional changes to intestinal immune cells at steady state.

Here, we demonstrate that *Hh* colonization attenuates intestinal disease severity in the DSS colitis model. This was dependent on extended colonization with *Hh* prior to colitis onset and was not present immediately following infection, suggesting a mechanism by which *Hh* primes intestinal immune responses at steady state to alter disease outcomes. We found that *Hh* colonization stimulated increased monocyte and neutrophil infiltration to the colon at steady state and drove increases to local proinflammatory cytokine transcription. However, colonic macrophages from infected mice showed suppressed cytokine responses *ex vivo*, indicating that *Hh* functionally modulates local immune cells to limit inflammatory responses. We tested whether the disease attenuating effect was dependent on recognition of *Hh* by TLR2, with the aim of elucidating the mechanism through which *Hh* affects disease outcomes. We demonstrate that disease attenuation does not require TLR2 signalling, suggesting that a different mechanism drives disease protection in *Hh* colonized animals.

This work provides insight into how host immune functions are shaped by the resident immunomodulatory microbiota. As the role of the microbiota in health and disease is becoming increasingly apparent, it is critical to develop a greater understanding of these interactions. Our work supports the conclusion that the microbiota primes the intestinal immune system at steady state, thereby altering immune responses during inflammatory settings.

# Table of Contents

# List of Tables

# List of Figures

# Acknowledgements

I firstly want to thank my PhD supervisor, Prof Kevin Maloy, for his support and supervision. Thank you for creating a lab environment that has been so much fun to work in. As much as we like to wind you up, you have always provided so much support, patience and advice, as well as all the laughs. You are always so excited about our ideas and data, no matter how small, and it has made my PhD a really great experience.

The work in this thesis would not have been possible without the support of the University of Glasgow core facilities staff. Diane, Alana, and Daniel, thank you for all your flow cytometry training and help with machine emergencies. Fiona McMonagle and Tyler Shaw, thank you for your excellent histology services. Massive thanks to all the staff at the CRF animal facility, especially Stuart and Nicola. Thank you also to Susan and Leandro from the imaging facility, while you both helped train me to use the microscopes and answered lots of questions, you also had to share an office with us for 2 years! Thanks for all the fun during that time. Finally, thank you to John Cole for performing the RNAseq analyses described in Chapter 7 and for answering all my Bioinformatics questions.

I want to thank the other members of the Maloy lab who have made this PhD experience so positive and helped so much with this project. Holly Webster, you taught me a lot about science but (more importantly) you showed me how to have fun while doing it. You contributed so much to this project, and the data from the *Hh*$^{+}$ MT system is thanks to your work in getting the models optimised and running the initial DSS experiments. Thanks for all the cups of tea/drinks, chats and support over the years. Annika Frede, you are an amazing scientist and friend and I could not have done this without you! You have also been there for me with so much support and patience, answered all my questions and helped in the lab so much. The quality of data in this thesis would be significantly worse without your input. Xiang (Jo) Li, you are the most generous and kind person and have provided so much help and support during your time in the group, I am so happy you joined us (and that you fed the fish so I didn't have to!). Anna Ahlback, you joined while I was writing this thesis and I want to thank you for being so excited about this project and reminding me to be excited too, and for putting up with my thesis moaning. Thanks also to Jo and Anna for all the

Kember cinnamon bun and coffee runs, I am glad you appreciate snacks as much as I do!

A huge thank you to Simon Milling, Allan Mowat and Georgia Perona-Wright for your advice and feedback during lab meetings, it all helped this project immeasurably. Anna Andrusaite, you have been such a good friend throughout my PhD, thank you for all the science and life discussions over lunch/wine and always being there for me. Liv, Patrick, Jack J, Annabelle - thanks for all the chat in the lab and good times at conferences & lab dinners, this PhD experience wouldn't have been the same without you! And thank you to all the other MMP members from past and present who have made the lab such a good environment to work in, and made late nights/early mornings in the lab a lot more fun.

I would lastly like to thank my friends, family, and partner Simon for all their love and support. I would not have been able to do this without you all. Thank you for everything!

# Author's Declaration

I declare that, except where reference is made to the contribution of others, this thesis is the result of my own work and has not been submitted for any other degree at the University of Glasgow or any other institution.

Signature:

Printed name: Anna Lucy Leith Heawood

# Abbreviations

AHR aryl hydrocarbon receptor
AIEC adherent-invasive E coli
AMP antimicrobial peptide
APC antigen presenting cell
BCA bicinchoninic acid
BM bone marrow
BMDM bone marrow-derived macrophage
BME basement membrane extract
CBA cytometric bead array
CD Crohn's disease
cDCs conventional dendritic cells
cLPL colonic lamina propria leukocyte
CM conditioned medium
CREB cyclic AMP response-element binding protein
DAMP damage associated molecular pattern
DEG differentially expressed gene
DSS dextran sulphate sodium
EAE experimental autoimmune encephalomyelitis
ECAR extracellular acidification rates
EEN exclusive enteral nutrition
FACS fluorescence-activated cell sorting
FBS foetal bovine serum
FcγRI Fc gamma receptor 1 (CD64)
FMT faecal microbiota transplantation
Foxp3 forkhead box P3
GALT gut-associated lymphoid tissue
GF germ-free
GI gastrointestinal
GMP granulocyte monocyte progenitor
GSEA gene set enrichment analysis
GWAS genome-wide association studies
Hh Helicobacter hepaticus
HSC haematopoietic stem cell
IBD inflammatory bowel disease
IEC intestinal epithelial cell
IESC intestinal epithelial stem cell
IL-10Rα IL-10 receptor alpha
ILC innate lymphoid cell
ILF isolated lymphoid follicle
iNOS inducible nitric oxide synthase
ip intraperitoneal
iTreg induced Treg
LP lamina propria
LPL lamina propria leukocyte
LPS lipopolysaccharide
MAdCAM-1 mucosal addressin cell adhesion molecule-1
MCP-1 monocyte chemoattractant protein-1
MDP muramyl dipeptide
MHCII major histocompatibility complex class II
MLN mesenteric lymph nodes

MNP mononuclear phagocyte
MOI multiplicity of infection
MT microbiota transfer
mTOR mammalian target of rapamycin
mTORC1/2 mTOR complex 1/2
MyD88 myeloid differentiation primary response 88
NET neutrophil extracellular trap
NF-κB nuclear factor kappa B
NLR nucleotide-binding oligomerization domain (NOD)-like receptor
NO nitric oxide
nTreg natural Treg
OCR oxygen consumption rates
pAKT phosphorylated AKT
PAMP pathogen-associated molecular pattern
PCA principal component analysis
PD-L1 programmed cell death ligand 1
PRR pattern recognition receptor
pS6 phosphorylated S6
qPCR quantitative PCR
RA rheumatoid arthritis
RAG recombination activating gene
REG regenerating islet-derived protein
RELMß resistin-like molecule ß
RIG retinoic acid inducible gene
ROS reactive oxygen species
SCFA short chain fatty acid
SCID severe combined immunodeficiency
SFB segmented filamentous bacteria
SI small intestine
SILP small intestinal lamina propria
SPF specific-pathogen free
TCR T cell receptor
Tfh T follicular helper cell
TGFß transforming growth factor ß
TLR toll like receptor
TLT tertiary lymphoid tissue
TNBS 2,4,6-trinitro benzene sulfonic acid
Treg regulatory T cell
UC ulcerative colitis
VEO-IBD very early onset IBD

# 1 Introduction

## 1.1 The intestinal environment

The environment of the intestine presents a specific challenge for the immune system. The tissue's structure, function, and high burden of microbes create a unique environment in which the immune system must be poised to defend against pathogens, while remaining tolerant to food and harmless microbial antigens. The complex physiology of the intestine, which differs across locations, means that the immune system is adapted to distinct niches throughout the gastrointestinal (GI) tract. Mouse models are used extensively to study the GI immune system due to their high genomic and anatomical similarities with humans (Hugenholtz and de Vos, 2018). In the following sections, the anatomy, functions, and distinct anatomical niches of the GI tract are discussed, with a focus on the murine gut.

### 1.1.1 Anatomy of the intestine

The murine GI tract begins at the mouth and ends at the rectum, encompassing the oesophagus, stomach, small intestine (SI), caecum, and colon (Figure 1-1) (Treuting et al., 2018b, Treuting et al., 2018a). The large intestine refers to the caecum and colon together and is partly distinct from that found in humans, as mice do not possess an appendix (Treuting et al., 2018a). The SI functions as the site of nutrient absorption, while water is absorbed in the colon, and bacterial fermentation of dietary substrates takes place throughout the large intestine (Treuting et al., 2018a). The physiology of the GI tract is adapted to these distinct functions and varies between sites. For example, the pH in the stomach is highly acidic but increases through a gradient along the length of the SI, with the highest pH found in the colon (Evans et al., 1988). Similarly, the GI tract is home to trillions of microbes, collectively termed the microbiota. The majority of microbes are found in the caecum and colon, which also support the highest levels of bacterial diversity (Gu et al., 2013). These distinct physiologies require specialised immune function, and it has been demonstrated that immune cell trafficking and receptor expression varies throughout the intestine (Stenstad et al., 2007, Price et al., 2018).

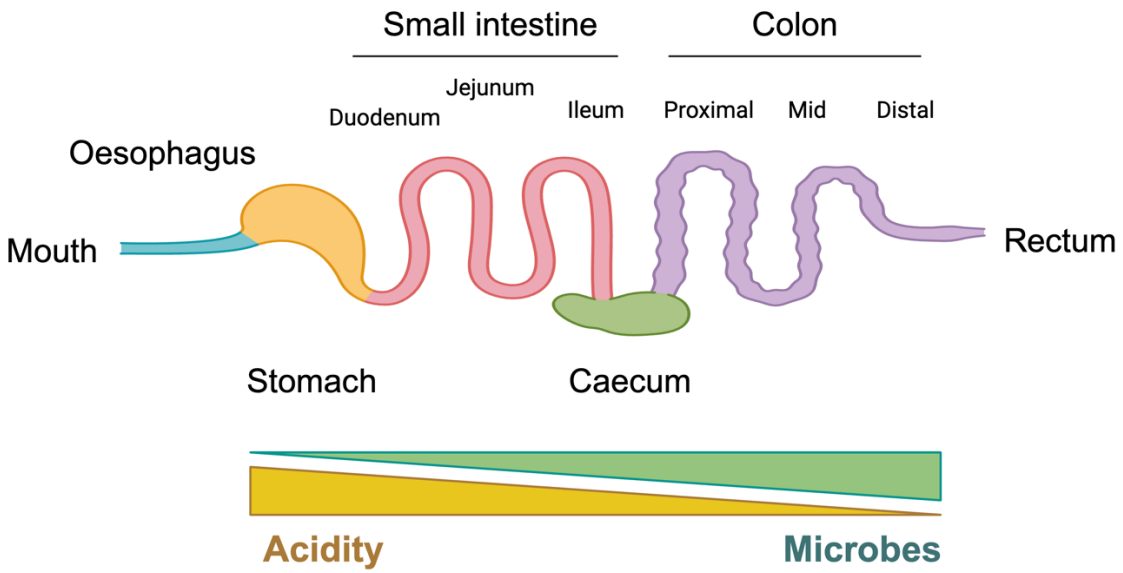


**Figure 1-1: The murine GI tract**
Starting in the mouth, the murine GI tract includes the oesophagus, stomach, SI, caecum, colon, and rectum. The SI is divided into three sections with the duodenum connecting to the stomach, followed by the jejunum, then the ileum which connects to the caecum. The colon is also divided into three with the proximal colon starting at the caecum, followed by the mid colon and ending with the distal colon which connects to the rectum. The pH is lowest in the stomach and increases in a gradient to the end of the colon, while the concentration of microbes is highest in the colon. This figure was created using BioRender.com.

The space within the small and large intestine is called the lumen, and it is here that faecal pellets are formed, and the majority of the microbiota resides (Mowat and Agace, 2014). The intestinal tissue is separated from the lumen by the epithelial barrier and mucus layer, which will be discussed in the next section. Beneath the epithelial barrier is the lamina propria (LP), which is formed of connective tissue, blood and lymphatic vessels, and contains enteric nerves, fibroblasts, and smooth muscle cells. The LP also houses one of the largest populations of immune cells in the body (Bernier-Latmani and Petrova, 2017). Underlying the LP is a thin layer of smooth muscle termed the muscularis mucosa. This is followed by the submucosa, a thicker muscle layer, and finally the serosa which contains the intestine and separates the tissue from the peritoneal cavity (Bernier-Latmani and Petrova, 2017). The majority of immune activity takes place in the epithelial barrier, LP, and muscularis mucosa, together termed the mucosa (Mowat and Agace, 2014). The appearance of the mucosa varies from the SI to the colon. The SI contains villi which project into the lumen to maximise surface area for nutrient absorption, while these are not present in the caecum and colon. Throughout the intestine are small

invaginations known as crypts which contain epithelial stem cells (Mowat and Agace, 2014). The anatomy of the intestinal mucosa is illustrated in Figure 1-2.

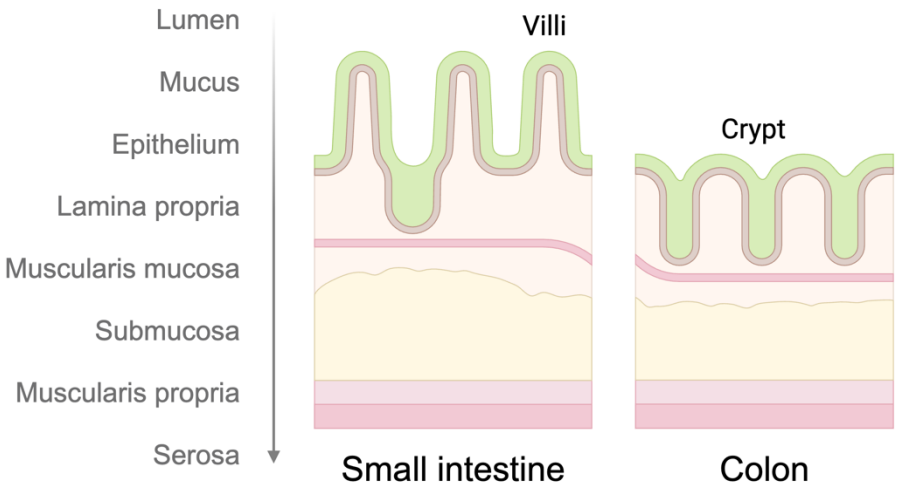


**Figure 1-2: Intestinal anatomy**
The intestinal tissue surrounds a hollow space called the lumen. A layer of mucus followed by a single layer of epithelial cells separates the lumen from the intestinal tissue. The layers of tissue start with the LP, followed by the muscularis mucosa, submucosa, muscularis propria, and finally the serosa which is the outer layer of the tissue and separates the intestine from the peritoneum. The SI contains villi and crypts, while the colon has a flatter surface and only contains crypts. This figure was created using BioRender.com.

### 1.1.2 Epithelial barrier

The intestinal epithelium exists as a single layer of intestinal epithelial cells (IECs) which form a barrier between the lumen and LP. IECs are non-haematopoietic cells derived from intestinal epithelial stem cells (IESCs). IECs have a very high turnover rate, with most mature cells being shed from the epithelium after a few days (Beumer and Clevers, 2021). IESCs constitutively proliferate and generate transit amplifying cells, which eventually differentiate into the various lineages of mature IEC (Basak et al., 2014). These lineages have distinct functions, which range from nutrient and water absorption, hormone secretion, antimicrobial functions and mucus production (Peterson and Artis, 2014). The epithelium is mostly comprised of absorptive enterocytes, but other specialised IECs include goblet cells, enteroendocrine cells, and Tuft cells. Paneth cells are also specialised IECs found in the SI but not the colon (Beumer and Clevers, 2021). Paneth cells provide growth factors to support the IESC niche in the SI (Sato et al., 2011), while this function is thought to be provided by mesenchymal cells in the colon (Degirmenci et al., 2018).

A key function of the epithelial barrier is to prevent commensal and pathogenic microbes from entering the intestinal mucosa and systemic circulation. This is achieved through the production of mucus and various immunomodulatory and bactericidal mediators (Johansson and Hansson, 2016). Mucus is secreted by goblet cells and is primarily composed of the mucin glycoprotein MUC2. Loss of MUC2 in mice leads to spontaneous colitis as well as marked changes to mucosal architecture, demonstrating its importance for intestinal homeostasis (Van der Sluis et al., 2006). Secreted mucus forms a layer which overlays the epithelium and acts as a niche for microbial colonization. This layer varies in structure and volume along the GI tract. In the SI, a single layer of mucus exists which is penetrable by bacteria. In contrast, the colon contains two mucus layers, with the outer layer colonized by microbes and the inner layer generally considered impenetrable (Johansson and Hansson, 2016). These differences are driven by the varying microbial load found in these tissues (Gu et al., 2013). As such, goblet cell numbers also increase from the SI to the colon (Johansson and Hansson, 2016). One feature of colitis is the abnormal penetration of bacteria into the inner mucus layer of the colon (Johansson et al., 2014), which could suggest that inflammation drives changes to mucus composition. Equally, altered mucus formation could be a risk factor for the development of colitis and may precede the induction of inflammation (van der Post et al., 2019).

As well as forming a physical barrier, mucus contains biochemical mediators which manage the encroachment of the microbiota. One crucial mediator is secreted IgA, which is the key antibody class associated with mucosal defence. IgA is produced by plasma cells in the tissue and is transported across the epithelium into the mucus layer and lumen. Once there, IgA binds and coats bacteria, which prevents unnecessary inflammatory responses being generated (Van der Waaij et al., 1996). It has also been proposed to inhibit bacterial motility within mucus (Johansson and Hansson, 2016). Other important components of mucus are antimicrobial peptides (AMPs), which encompass several protein families and are produced by IECs. These include defensins, cathelicidins, and C-type lectins, which generally all function by disrupting microbial cell membranes (Gallo and Hooper, 2012). C-type lectins include the regenerating islet-derived protein (REG) family, and their importance has been demonstrated through the use of genetically deficient mice. Mice lacking REGIIIγ

show changes to mucus distribution and increased contact between the epithelium and microbiota, as well as dysregulated inflammatory responses (Loonen et al., 2014). AMPs therefore play a crucial role in maintaining symbiosis with the microbiota.

While IECs are not haematopoietic immune cells, they possess many immune related functions and are important sensors of microbial and damage associated signals. IECs express a range of pattern recognition receptors (PRRs) which enable them to respond to changes in the environment (Peterson and Artis, 2014). The result of these signals include the production of cytokines and chemokines which contribute to and shape the induction of immune responses (Price et al., 2018). One example of this is the contribution of epithelial Tuft cells to type 2 immunity. Following helminth infection, the epithelium responds by expanding the number of differentiated Tuft cells. These cells produce the cytokine IL-25, which is a crucial driver for type 2 immune activation. As such, Tuft cell deficient mice show impaired type 2 immunity and increased helminth burden (Gerbe et al., 2016). In the context of *Salmonella typhimurium* infection, IEC-specific inflammasome activation results in cytokine release and reduced bacterial colonization (Rauch et al., 2017). This is accompanied by expulsion of IECs from the barrier in a form of lytic cell death, which protects against bacterial invasion of the epithelium (Rauch et al., 2017). Although PRR signalling is often associated with inflammatory responses, it has also been demonstrated that these signals are required for epithelial homeostasis (Rakoff-Nahoum et al., 2004, Cario, 2008). A mechanism is thought to exist where microbiota derived signals stimulate increased barrier function through enhancing the adhesion between epithelial cells (Peterson and Artis, 2014). Similarly, IEC PRR signalling mediated through the adaptor molecule myeloid differentiation primary response 88 (MyD88) has been shown to promote AMP production, providing protection against mortality during colitis (Asquith et al., 2010). IEC sensing of microbes therefore helps to fortify both physical and chemical components of the epithelial barrier. Together, these studies demonstrate that IECs contribute to intestinal homeostasis through diverse functions.

### 1.1.3 Intestinal lymphoid tissue

The intestine contains various forms of lymphoid tissue which serve as the main site for the priming of adaptive immune responses (Mowat and Agace, 2014). This includes several forms of gut associated lymphoid tissue (GALT) as well as the mesenteric lymph nodes (MLN), which comprise distinct nodes for draining the SI and colon (Houston et al., 2016). GALT exists beneath the epithelium in both the mucosa and submucosa, consisting of lymphoid aggregates (Mowat and Agace, 2014). In the SI, GALT includes Peyer's patches which are visible in the serosa, as well as smaller isolated lymphoid follicles (ILFs) (Jørgensen et al., 2021). The caecal patch is GALT located in the caecum and has been proposed as the key site for generation of IgA-producing plasma cells, which migrate to the colon in a microbiota-dependent manner (Masahata et al., 2014). Colonic GALT is less prominent but is present in the form of small cryptopatches and ILFs (Treuting et al., 2018a). Some forms of intestinal lymphoid tissue, such as Peyer's patches and MLN, develop prenatally in the absence of a microbiota. In contrast, cryptopatches and ILFs appear to develop in response to microbial colonisation after birth (Bouskra et al., 2008). While the MLN is the key site for naïve T cell priming, cryptopatches and ILFs mostly contain B cells and do not have segregated T cell zones (Buettner and Lochner, 2016). Peyer's patches contain both memory T cells and B cells and have also been suggested to support naïve T cell priming (Kelsall and Strober, 1996).

The MLN are the largest lymph nodes in the body due to the high level of environmental exposure which occurs in the intestine (Mowat and Agace, 2014). As distinct nodes drain the SI and colon, the unique physiologies of these tissues mean that specialised antigen uptake occurs at both sites. Antigen presenting cells (APCs) in the LP take up antigens derived from food, commensal microbes, and pathogens, before migrating to the MLN to initiate an adaptive immune response (Mowat and Agace, 2014). Various mechanisms have been proposed to explain how LP APCs access these luminal antigens. Peyer's patches and the caecal patch are overlaid with specialised epithelium including microfold (M) cells, through which luminal antigens are transported to APCs (Masahata et al., 2014). Various studies have described LP macrophages and/or dendritic cells which extend transepithelial dendrites between epithelial cells and into the lumen, allowing the sampling of luminal antigens (Mowat and Agace, 2014). It

has also been proposed that epithelial goblet cells can act as a passage through the epithelium for small soluble antigens, allowing their delivery to LP APCs (McDole et al., 2012). Importantly, enteric pathogens such as *S. typhimurium* or *H. polygyrus* utilise mechanisms which allow them to cross or breach the intestinal barrier (Tafazoli et al., 2003, Schälter et al., 2022), thus bringing antigens into the LP which can be sampled by APCs. It is likely that additional mechanisms contribute to LP antigen delivery, although this remains a topic which is not fully understood. Following antigen uptake, migratory dendritic cells in the LP enter lymphatic vessels and are transported to the MLN, where they prime naïve T cells (Schulz et al., 2009). The intestinal immune system is discussed in more detail in the following section.

## 1.2 The intestinal immune system

The immune system in different tissues is functionally specialised to the local tissue environment. In the intestine, the constant exposure to foreign materials means that the immune system must be able to tolerate harmless antigens while maintaining the ability to respond to pathogens. Many mechanisms contribute to maintaining this balance. Failure to maintain homeostasis can result in immune-mediated pathology, which is seen in inflammatory bowel disease (IBD). The immune system is composed of innate and adaptive components, where innate immune cells are the first line of defence and utilise conserved receptors to respond to microbial and danger signals. The adaptive immune system comprises T and B lymphocytes, which possess antigen specific receptors and are highly effective at responding to diverse challenges. In this section, cellular and molecular components of the intestinal immune system relevant to this thesis are discussed, many of which play important roles in maintaining intestinal homeostasis.

### 1.2.1 Intestinal myeloid cells

Myeloid cells are a subset of innate immune cells with diverse functions. They are derived originally from haematopoietic stem cells which differentiate through a common myeloid progenitor stage (Akashi et al., 2000). Differentiated myeloid cells include granulocytes (such as eosinophils and neutrophils), monocytes, macrophages, and dendritic cells. The intestinal LP is home to a

large and heterogeneous population of macrophages and dendritic cells, referred to as the mononuclear phagocyte (MNP) system (Joeris et al., 2017). Due to various shared cell surface markers and functions, for many years these cells were incorrectly classified and mistaken for each other (Tamoutounour et al., 2012). There are now established methods to distinguish specific subsets of MNP, which has allowed for analysis of individual and shared characteristics (Tamoutounour et al., 2012). The LP also contains large numbers of resident eosinophils which have recently been highlighted for their contributions to intestinal homeostasis (Arnold et al., 2018, Fallegger et al., 2022). In contrast, very few neutrophils are found in the healthy intestine, but are rapidly recruited from the blood following an inflammatory challenge (Fournier and Parkos, 2012). As inflammation resolves, neutrophils apoptose and are cleared from the tissue by phagocytosis (Fournier and Parkos, 2012). Intestinal myeloid cells and their entry from the circulation are summarised in Figure 1-3, including common cell surface markers used to identify them.

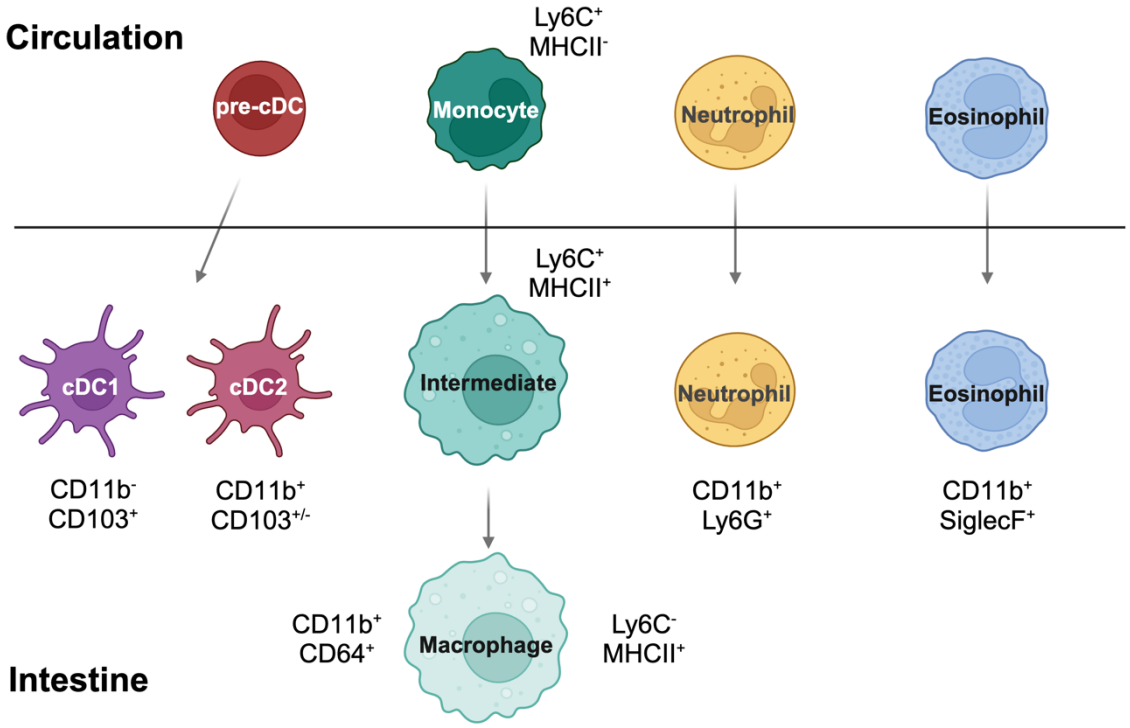


**Figure 1-3: Intestinal myeloid cells**
cDC precursors, monocytes, neutrophils and eosinophils arise in the BM before being distributed throughout the body via the circulation. These cells enter the intestine where pre-cDCs differentiate into two subsets of mature cDC, marked by differential expression of CD11b and CD103. Monocytes enter the intestine and differentiate into mature macrophages via an intermediate differentiation stage. As they differentiate monocytes lose expression of Ly6C and gain expression of MHCII, while all monocyte-macrophages express CD11b and CD64, allowing their distinction from cDCs. Neutrophils and eosinophils mature in the BM and enter the intestine as fully differentiated cells. Both cell types express CD11b, while neutrophils express Ly6G and eosinophils express SiglecF. Eosinophils can also be identified by their high granularity. This figure was created using BioRender.com.

The LP contains a large population of resident macrophages which are continuously replenished by bone marrow (BM) monocytes (Bain et al., 2014). These monocytes develop in the BM before travelling in the circulation to sites throughout the body. Upon entering a tissue, monocytes differentiate into macrophages and are imprinted with a specific phenotype reflecting the local environment. For example, stromal cells and specific signalling pathways have been shown to imprint a Kupffer cell phenotype on newly arrived monocytes in the liver (Bonnardel et al., 2019). Similarly, in the intestine, the microbiota has a clear effect on monocyte to macrophage differentiation, as mice lacking a microbiota show altered macrophage populations (Kang et al., 2020). The infiltration of monocytes to the intestine occurs constitutively at steady state, although this process is altered under inflammation. In colitis, monocyte infiltration increases but these cells fail to differentiate into mature

macrophages. Instead, proinflammatory monocytes accumulate in the tissue and are functionally distinct from resident macrophages recruited under homeostasis (Bain et al., 2013, Bain et al., 2018). One key function of intestinal macrophages is the uptake and killing of bacteria which enter the LP, which is achieved through their high capacity for phagocytosis and bactericidal functions (Bujko et al., 2017, Kang et al., 2020). They are also responsible for the clearance of apoptotic cells, including IECs (Cummings et al., 2016). In contrast to their counterparts in other tissues, intestinal macrophages do not produce an inflammatory response following microbial stimulation (Smythies et al., 2005). This lack of inflammatory cytokine production is key to maintaining intestinal homeostasis. The cytokine IL-10 is critical for this phenotype, and loss of its receptor specifically on macrophages results in spontaneous colitis (Zigmond et al., 2014).

While macrophages are capable of antigen presentation, conventional dendritic cells (cDCs) are the key APCs of the immune system. They begin life as pre-cDC progenitors in the BM, before travelling in the circulation to tissues around the body where they mature (Liu et al., 2009). Their role is to survey the tissue, acquiring antigens and sampling the environment, before travelling to the lymph node to present their antigen to a naïve T cell. This marks the end of their lifespan (Merad et al., 2013). Following this interaction, activated T cells that recognise the cognate antigens presented by cDCs are induced to express homing molecules to direct them to the correct tissue (Mora et al., 2003). Homing to the intestine occurs due to the production of retinoic acid by intestinal cDCs, which induces the expression of gut-homing molecules CCR9 and α4β7 on T cells upon activation (Iwata et al., 2004). Under homeostasis, LP cDCs are maintained in a tolerogenic state. Here, they preferentially induce the expansion of regulatory T cells (Tregs) and are essential for maintaining symbiosis with the microbiota (Loschko et al., 2016). The tolerogenic phenotype of intestinal cDCs is driven by the local environment, particularly by immune suppressive cytokines such as TGFβ (Ramalingam et al., 2012). However, upon detecting inflammatory mediators, this tolerogenic phenotype is lost and cDCs act as potent inducers of effector T cell responses. Intestinal cDCs are a heterogeneous population and can be divided into subsets based on their expression of the surface proteins CD11b and CD103 (Joeris et al., 2017). These subsets have overlapping functions

but appear to selectively induce the expansion of specific T cell subsets (Joeris et al., 2017). cDCs have been named ‘conventional’ DCs due to the presence of other DC-like cells in the body called plasmacytoid DCs (pDCs). Although pDCs bear a morphological resemblance to cDCs and are derived from similar progenitors, they possess very different functions and are specialised for the detection of viral pathogens and release of type I interferons (Merad et al., 2013).

Finally, granulocytes are polymorphonuclear myeloid cells which release their cytosolic granules upon activation. They primarily function as pathogen defence, but it is now appreciated that eosinophils, in particular, also elicit homeostatic functions which are discussed in the next section (Arnold et al., 2018, Fallegger et al., 2022). Neutrophils are rapidly recruited to sites of inflammation where they perform antimicrobial functions. In addition to phagocytosis, they generate reactive oxygen species (ROS), produce neutrophil extracellular traps (NETs), and release granules – which include AMPs, hydrolytic enzymes, proteases, and metal chelators (Fournier and Parkos, 2012). The microbiota appears to stimulate neutrophil functions, as antibiotic treatment has been shown to reduce BM neutrophil levels (Zhang et al., 2015), while mice lacking a microbiota show impaired neutrophil functions (Clarke et al., 2010, Karmarkar and Rock, 2013). Depletion of neutrophils has been shown to increase disease severity in colitis models due to greater levels of bacteria in the mucosa (Kühl et al., 2007). However, this is somewhat contradictory, as neutrophils are one of the main contributors to intestinal inflammation (Wirtz et al., 2007).

Unlike neutrophils, eosinophils are present in large numbers in the healthy intestine. They are traditionally associated with responses against extracellular pathogens, including parasites (Jung and Rothenberg, 2014). As well as releasing granules, eosinophils produce many cytokines, chemokines, and other immune mediators (Shah et al., 2020). Homeostatic functions for these cells are now being described, including the regulation of IgA production (Chu et al., 2014) and maintenance of epithelial turnover (Ignacio et al., 2022). The cytokine IFNγ has been shown to drive the recruitment of eosinophils to the intestine, where they co-localise with CD4 T cells (Gurtner et al., 2023). Furthermore, a mechanism has been described through which eosinophils contribute to Treg differentiation through their production of TGFß (Fallegger et al., 2022).

Fallegger *et al*. report that mice with a conditional knockout of *Tgfβ* specifically in eosinophils show reduced numbers of RORγt$^+$ Tregs in the intestine (Fallegger et al., 2022). Despite this, these cells have been shown to accumulate during IBD and may correlate with disease severity (Jung and Rothenberg, 2014). While much remains unknown about the functions of intestinal eosinophils, they are becoming a focus of interest in mucosal immunology due to their diverse roles in homeostasis.

### 1.2.2 Pattern recognition receptors

PRRs are evolutionarily conserved receptors which recognise pathogen or damage associated molecular patterns (PAMPs/DAMPs). They are expressed by a wide range of immune and non-haematopoietic cells and can be intracellular or expressed on the cell surface (Takeuchi and Akira, 2010). PRRs are particularly important for innate immune cells which lack specialised antigen receptors. It is through PRRs that IECs, macrophages, and cDCs survey the LP and manage the host-microbiota relationship (Fukata and Arditi, 2013). PRR ligation drives downstream signalling events which result in the production of cytokines and chemokines, thus initiating the host response to infection or damage (Fukata and Arditi, 2013). Various families of PRR exist, including toll-like receptors (TLRs) and nucleotide binding oligomerization domain (NOD)-like receptors (NLRs), which play critical roles in intestinal homeostasis and are discussed here. Other families include cytosolic DNA sensors and retinoic acid inducible gene (RIG)-I-like receptors, which are important for the host antiviral response (Thompson et al., 2011).

The TLR family includes eleven receptors, some of which are found on the plasma membrane while others are expressed in endosomes (Takeuchi and Akira, 2010). They each recognise distinct microbial ligands and mediate responses to bacterial and viral pathogens. The key TLRs for bacterial recognition are TLR2, which recognises lipoproteins, TLR4, which recognises lipopolysaccharides (LPS), and TLR5, which recognises flagellin. These are all cell surface receptors which respond to extracellular bacteria (Takeuchi and Akira, 2010). Ligation of different TLRs leads to distinct signalling cascades, resulting in specialised responses. TLR2 and TLR4 both signal through the signalling adaptor molecule MyD88, although TLR4 can also localise to endosomes where it drives an

alternative signal transduction pathway (Fukata and Arditi, 2013). Recruitment of MyD88 eventually induces translocation of the transcription factor nuclear factor kappa B (NF-κB) from the cell cytoplasm to the nucleus, resulting in transcription of NF-κB response genes (Sakai et al., 2017). NF-κB response genes include proinflammatory cytokines such as IL-1β and TNFα, as well as a range of chemokines (Sharif et al., 2007). These then drive the recruitment and activation of other immune cells.

NLRs are cytoplasmic PRRs which are activated by a range of environmental signals. These include direct recognition of microbial ligands, as well as sensing of biochemical changes to the intracellular environment (Wen et al., 2013). NLRs fall into two categories based on their ability to form inflammasome complexes (Davis et al., 2014). NLRs which do not form inflammasomes include NOD1 and NOD2, which act as intracellular receptors for bacterial peptidoglycan (Davis et al., 2014). Activation of these receptors results in a signalling cascade culminating in the activation of NF-κB and the expression of proinflammatory genes (Hasegawa et al., 2008). In contrast, activation of inflammasome-forming NLRs results in the recruitment of various adaptor proteins. Together with the NLR, these proteins form large multi-molecular complexes in the cytosol called inflammasomes, which drive the cleavage and activation of caspases (Martinon et al., 2002). Inflammasome caspases are proteolytic enzymes capable of processing the non-active pro-forms of the cytokines IL-1β and IL-18, thus leading to their secretion and enabling their proinflammatory functions (Martinon et al., 2002). Inflammasome activation can also drive pyroptosis, a proinflammatory form of cell death which activates nearby immune cells, and which can also prevent intracellular pathogen replication (Davis et al., 2014).

PRR signalling appears to have contrasting outcomes for intestinal homeostasis. As discussed previously, there is evidence that TLR signalling contributes to maintenance of epithelial barrier integrity at steady state (Rakoff-Nahoum et al., 2004, Cario, 2008). Furthermore, MyD88 signalling in IECs drives the production of AMPs, which helps to maintain symbiosis with the microbiota (Vaishnava et al., 2008). However, in the context of IBD, sustained PRR signalling results in continuous inflammatory responses and chronic pathology. As such, MyD88 signalling is required for the induction of colitis in certain murine models (Asquith et al., 2010). TLR2 and TLR4 have also been shown to be upregulated in

the mucosa of IBD patients compared to healthy controls (Hausmann et al., 2002). The importance of PRRs in the maintenance of intestinal homeostasis has been further highlighted by their genetic association with IBD (Liu et al., 2015a), discussed further in Section 1.4.

### 1.2.3 Intestinal T cells

T cells are specialised lymphocytes which possess highly specific antigen receptors. T cell receptors (TCRs) are composed of two chains: conventional T cells express the αß chains, while the γδ chains are found on a less common subset (Geisler et al., 1988). αß TCRs recognise antigen only when it has been processed by an APC and presented on the cell surface bound to a major histocompatibility complex (MHC) (Germain, 1994), and can be divided into two major subsets. $CD4^+$ T cells recognise peptides presented by MHC class II (MHCII) molecules, while $CD8^+$ T cells recognise MHCI-peptide complexes (Germain, 2002). Both subsets are derived from common lymphoid progenitors found in the BM, which migrate to the thymus where T cell development takes place (Germain, 2002). Thymic development involves a series of maturation steps in which the TCR is tested for its ability to recognise MHC and signal through its receptor. Further steps also ensure that self-reactive TCRs, which could be potential drivers of autoimmunity, are not selected (Germain, 2002). T cells leave the thymus expressing either CD4 or CD8 and migrate to peripheral lymph nodes throughout the body as naïve T cells. For the purpose of this thesis, only $CD4^+$ T cells are discussed.

Once in the lymph node, naïve T cells encounter cDCs carrying antigen from peripheral tissues. Upon recognition of an antigen matching its TCR specificity, T cells require three signals for activation. The first signal is the antigen presented in the context of MHC, which causes a synapse to form between the T cell and cDC and functions to hold the two cells together (Smith-Garvin et al., 2009). The second signal is costimulation: these are signals from other receptors on the T cell surface, whose ligands are expressed by APCs. One such receptor is CD28, which recognises costimulatory molecules CD80 and CD86 (Smith-Garvin et al., 2009). The third signal comes from cytokines produced by the APC, which direct T cell differentiation and provide survival and proliferation cues (Curtsinger et al., 2003). Recognition of cognate antigen in the absence of co-stimulation

signals results in T cell anergy, while the three signals together drive differentiation and proliferation of the T cell clone (Curtsinger et al., 2003). After this is complete, activated T cells migrate to the tissue where their antigen originated (Mora et al., 2003), and carry out effector functions.

Naïve $CD4^+$ T cells can differentiate into various subsets based on the surrounding cytokine environment. Each subset requires distinct cytokines for differentiation and plays a unique role in the immune response. Thus, T cell polarisation allows for fine tuning of the response to combat different types of pathogens (Hilligan and Ronchese, 2020). The main $CD4^+$ T cell subsets are Th1, Th2, Th17, and Treg, which all show distinct functions. The cytokines required for subset polarisation, as well as the phenotype and roles of each subset, are depicted in Figure 1-4. The key subsets discussed in this thesis are Th1 and Th17 effectors, which are involved in the host response to bacteria, and Tregs, which regulate immune responses and maintain homeostasis (Hilligan and Ronchese, 2020). Mice lacking a microbiota reportedly have fewer Th1 and Th17 cells, indicating that the microbiota drives expansion of these subsets at steady state (Sorini et al., 2018). Specific bacterial species preferentially induce different subsets, with the *Clostridia* family generally driving Treg responses while segmented filamentous bacteria (SFB) drive Th17 expansion (Sorini et al., 2018).

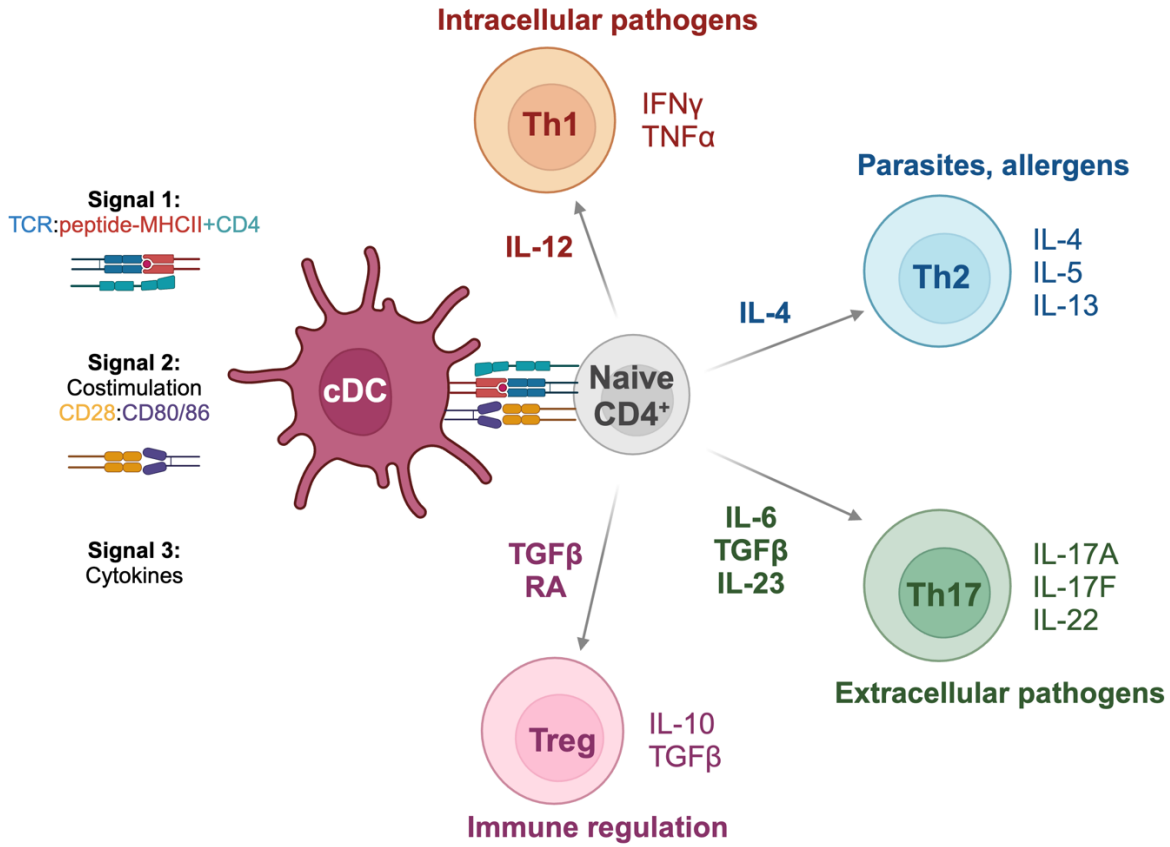


**Figure 1-4: CD4⁺ T cell activation and polarisation**
Naïve CD4⁺ T cells are polarised into different effector subsets based on the cytokine environment at the time of activation. They require three signals for activation: ligation of the TCR by a peptide-MHCII complex, costimulatory signals, and activating cytokines. Th1 cells differentiate in response to IL-12 and produce IFNγ and TNFα for targeting intracellular pathogens like bacteria and viruses. Th2 cells require IL-4 for differentiation and produce type 2 cytokines IL-4, IL-5, and IL-13. They are involved in the response to parasites and allergens. Th17 cells differentiate in response to IL-6, TGFβ, and IL-23, and produce IL-17A, IL-17F, and IL-22 for the response to extracellular pathogens including bacteria and fungi. Tregs differentiate in response to TGFβ and retinoic acid, then produce IL-10 and TGFβ for immune regulation and maintenance of homeostasis. This figure was created using BioRender.com.

Tregs are the critical cell type required to maintain the intestinal immune system in a tolerogenic state. They are identified by expression of the transcription factor forkhead box P3 (Foxp3) and high CD25 (Tanoue et al., 2016). Treg function was identified by the findings that their depletion caused multi-organ autoimmune disease (Sakaguchi et al., 1995), and that they were capable of suppressing colitis driven by naïve T cells (Powrie et al., 1993). Tregs produce the critical regulatory cytokine IL-10 which is required for maintenance of intestinal homeostasis (Rubtsov et al., 2008). They also produce TGFß, a cytokine with roles in CD4⁺ T cell regulation, immune suppression, and healing (Li et al., 2007). Two subsets of Treg exist based on their development. The first are called natural Tregs (nTreg) and develop in the thymus based on a specific selection process (de Lafaille and Lafaille, 2009). The second are induced in the periphery from naïve CD4⁺ T cells, when the TCR is activated under certain

conditions. This subset are therefore termed induced Tregs (iTreg) and are most prevalent at mucosal sites, particularly the intestine (de Lafaille and Lafaille, 2009). In the gut, iTreg differentiation requires TGFß and retinoic acid production by cDCs (Sun et al., 2007). Many iTregs are specific for commensal bacteria and dietary materials, demonstrating how tolerance to harmless antigens is achieved (Lathrop et al., 2011, Kim et al., 2016). While microbiota-reactive T cells are found in healthy individuals, the distribution and phenotype of these cells are altered in IBD (Hegazy et al., 2017). Furthermore, it has been suggested that commensal-reactive T cells can be redirected during inflammation, for example following pathogen infection, resulting in conversion to a Th1 phenotype (Hand et al., 2012). The importance of Tregs in intestinal homeostasis is further highlighted in Sections 1.4 and 1.5, where IBD and experimental murine colitis models are discussed.

## 1.3 Microbiota

The microbiota is the collective term for the trillions of microbes which reside in the mammalian body. These include bacteria, protozoa, fungi, and viruses, and are mostly found at mucosal sites which have an environmental interface. Mammalian hosts have coevolved with their microbiota, resulting in a complex symbiotic relationship. While the mammal provides a habitat and energy source for microbes, the microbiota in turn provides a range of beneficial functions for host physiology (Belkaid and Harrison, 2017). The impact of the microbiota on host immune function is only beginning to be understood, with recent studies highlighting how microbial composition can impact therapeutic and vaccine outcomes (Rosshart et al., 2017, Collins and Belkaid, 2018). Here, the beneficial effects of the microbiota are discussed, including the key mechanisms by which microbial colonization impacts immune system development and function.

### 1.3.1 Physiological functions of the microbiota

The microbiota impacts host physiology in a multitude of ways. Crucially, microbes perform various metabolic functions which produce nutrients and useful metabolites for host physiological processes (Sommer and Bäckhed, 2013). This includes the digestion of dietary fibre, which results in the production of short chain fatty acids (SCFA) from indigestible complex polysaccharides

(Morrison and Preston, 2016). Components of the microbiota can also carry out *de novo* vitamin synthesis, including vitamin K and various B vitamins (Hill, 1997). Dietary vitamin A is metabolised to produce retinoic acid, which is an important regulator of host gene expression and immunity (Bonakdar et al., 2022). While the host is capable of performing this metabolism, the gut microbiota performs a vital contribution to this process (Bonakdar et al., 2022). Another example is the metabolism of bile acids. These are produced in the liver and released into the SI after food ingestion. While the majority are reabsorbed, some travel to the large intestine where they are metabolised by the microbiota to produce secondary bile acids (Wahlström et al., 2016). Secondary bile acids are recognised by various receptors, driving gene transcription and impacting cellular metabolic processes (Wahlström et al., 2016). Thus, the microbiota increases the metabolic capacity of the host, and aids in the production of nutrients and immune mediators. Another major benefit of the microbiota is its occupation of niches which would otherwise be targeted by pathogens. This is termed colonization resistance, and the importance of this effect can be demonstrated by the increased susceptibility to infection which comes with antibiotics use (Caballero-Flores et al., 2023).

Host development and morphogenesis also appear to be regulated by the microbiota, particularly in the GI tract. Germ-free (GF) mice lack a microbiota and reportedly show reduced intestinal surface area, impaired epithelial proliferation, and decreased peristalsis (Sommer and Bäckhed, 2013). The gut microbiota has been shown to induce vascular remodelling, driven by a complex signalling loop which drives angiogenesis (Reinhardt et al., 2012). Furthermore, the formation of lymphoid tissue is regulated by the presence of microbes. The microbiota is required for certain types of GALT development, including the maturation of ILFs (Bouskra et al., 2008). Tertiary lymphoid tissue (TLT), thought to develop at sites of inflammation, functions as an additional site for adaptive immune priming (Garcia-Villatoro et al., 2024). The microbiota has been implicated in TLT formation, through a mechanism involving the aryl hydrocarbon receptor (AHR). The ligands for AHR include tryptophan metabolites, produced by microbes through the metabolism of dietary components (Garcia-Villatoro et al., 2024). Together, these studies provide

evidence of the important impact the microbiota has on host physiology and development.

### 1.3.2 Shaping of the immune system by the microbiota

The mammalian immune system has been shaped by its co-evolution with the microbiota. Only in the last two decades has the extent of this impact been appreciated, as new tools have allowed for in depth analysis of the microbiome. Still, much of what we know about microbial effects comes from GF animals, which were first generated in the 1940s (Yi and Li, 2012). Now, the process of rederivation has enabled embryos from any genetic strain to be raised in a GF environment, allowing the interplay between specific immune components and the microbiota to be studied (Hooper et al., 2012). Antibiotics have been used for years to test how microbiota depletion affects host physiology. While this is a cheaper and easier alterative to GF, it is not entirely effective as some microbes are unaffected (Hooper et al., 2012). Another important advance has been the development of next-generation sequencing technologies. Bacterial genomes include a conserved 16S ribosomal RNA subunit, which contains unique sequences specific to individual bacterial species. Sequencing of this subunit has resulted in a much greater understanding of microbiome complexity and has provided a platform to study how the microbiota changes in different contexts of health and disease (Hooper et al., 2012). Despite this, many microbial sequences belong to species which have not yet been characterised. The advent of new culture techniques to investigate previously unstudied species will allow for further advances in our understanding of host-microbiota interactions.

The key events which shape microbiota composition are birth and weaning (Bäckhed et al., 2015). The neonatal immune system is thought to have an immature phenotype, with microbial colonization playing a fundamental role in education and maturation of immune function (Gollwitzer and Marsland, 2015). Alterations to early life microbial exposure, for example through antibiotics, can drive long term changes to microbiota composition. Many chronic immune-driven pathologies have been linked to early life events (Gollwitzer and Marsland, 2015). A crucial timepoint occurs at weaning, as the increase in microbial exposure drives an immune response known as the ‘weaning reaction’ (Al Nabhani et al., 2019). This reaction is characterised by production of

proinflammatory and antimicrobial mediators, including TNFα and IFNγ, as well as the generation of Tregs (Al Nabhani et al., 2019). Prevention of this reaction using antibiotics results in pathological imprinting of the immune system, driving increased susceptibility to colitis, airway inflammation, and cancer (Al Nabhani et al., 2019). GF mice show various immune defects, including reduced intestinal T cell numbers and an increased Th2:Th1 ratio (Gensollen et al., 2016). Altered numbers and function of airway myeloid cells in the GF lung drive increased susceptibility to allergic airway inflammation (Herbst et al., 2011). GF animals also show elevated serum IgE levels, the antibody class associated with type 2 allergic responses. Microbial exposure during a specific early window is required to limit IgE production, protecting against anaphylactic responses (Cahenzli et al., 2013). Importantly, GF mice show marked impairment to BM haematopoiesis, resulting in decreased numbers of neutrophils and monocytes in the BM and a reduction in splenic macrophage numbers (Khosravi et al., 2014).

It is now understood that, rather than ignoring it, the immune system constantly generates microbiota-specific responses. These responses function to manage the symbiotic relationship between microbes and the host. The key factor which differentiates these responses from those against a pathogen is the absence of inflammation, leading to the term 'homeostatic immunity' (Belkaid and Harrison, 2017). The outcome of these homeostatic responses for immune function are only beginning to be understood. For example, microbiota-derived antigens are recognised by many B and T cell clones, leading to robust antibody and T cell responses (Ansaldo et al., 2021). Microbiota-specific IgG is induced at steady state but has been shown to protect against systemic infection with the pathogen *Salmonella typhimurium* (Zeng et al., 2016). Individual species, such as *Bacteroides fragilis*, have been shown to drive T cell expansion and lymphoid organogenesis (Mazmanian et al., 2005). These responses appear to protect against colitis (Mazmanian et al., 2008). Colonization of the skin with *Staphylococcus epidermis* was reported to induce $CD8^+$ T cells which produce IL-17A and protect against fungal infection (Naik et al., 2015). As well as adaptive immune priming, the microbiota also modulates innate responses. One example is the priming of neutrophil functions by microbiota-derived PAMPs, resulting in protection against systemic *Staphylococcus aureus* infection (Clarke et al., 2010). These studies illustrate many ways in which the microbiota impacts host

immunity, providing beneficial immune priming which protects against disease outcomes.

### 1.3.3 Dysbiosis and disease

With the increasing body of evidence surrounding the beneficial functions of the microbiota, it stands to reason that perturbations to these functions can have harmful effects on the host. The term 'dysbiosis' describes alterations or imbalance of the microbiota and is often associated with disease – both in the intestine and throughout the body (Levy et al., 2017). Many factors can drive dysbiosis, including diet, infection, inflammation, therapeutics, and antibiotics. Host genetics also have an important effect, particularly genes associated with immunity and the intestinal barrier (Levy et al., 2017). The problem with the association between dysbiosis and disease is determining whether dysbiosis is a cause or correlation. Many of the factors which drive dysbiosis are present in a disease setting, and in the event that dysbiosis precedes disease, it is unlikely that this would be picked up in an asymptomatic patient. This has been attempted in patients who are at risk of developing rheumatoid arthritis (RA), a chronic autoimmune condition affecting the joints. At risk individuals were identified based on the presence of autoantibodies and new musculoskeletal symptoms but did not yet present with clinical RA (Rooney et al., 2021). These individuals showed significant differences in microbiota composition compared to healthy controls (Rooney et al., 2021). While this suggests that dysbiosis may precede clinical RA, it is still unclear when this dysbiosis occurs relative to autoantibody production and symptom onset. Another study addressed the same question in asymptomatic individuals who were positive for genetic polymorphisms associated with RA (Wells et al., 2020). They found that genotype was associated with alterations to the gut microbiota in the absence of disease, again suggesting that dysbiosis may be an early event in RA pathogenesis (Wells et al., 2020).

While it is still unclear whether dysbiosis plays a causative role in autoimmune and inflammatory disease, the idea of targeting the microbiota as a therapeutic approach is gaining interest. Dysbiosis can encompass various features, including a loss of commensal species, loss of diversity, and an increase in opportunistic pathogens or 'pathobionts' (discussed in Section 1.5) (Levy et al., 2017).

Attempts to reverse these effects have been made using pro- and prebiotics, which involve the administration of live beneficial species or ingredients which stimulate commensal growth, respectively (Walker and Lawley, 2013). However, due to factors such as colonization resistance, these approaches have limited efficacy (Walker and Lawley, 2013). Another example is faecal microbiota transplantation (FMT). This involves the transplantation of faecal microbes from healthy donors to a patient experiencing dysbiosis, with the aim of remodelling their microbiota (Yang et al., 2023). It was initially used as a treatment for *Clostridia difficile* infection, which often occurs after antibiotics use when commensal species are depleted (Yang et al., 2023). Now, clinical trials testing the efficacy of FMT for other conditions are underway. One study reported that FMT successfully induced remission in a cohort of IBD patients (Moayyedi et al., 2015). However, other studies found no significant changes to disease (Rossen et al., 2015). It is clear that a greater understanding of host-microbiota interactions is required for successful therapeutic targeting of the microbiota. The next section covers IBD, including involvement of the microbiota.

## 1.4 Inflammatory bowel disease

IBDs are chronic inflammatory conditions affecting the GI tract. The two most common forms are Crohn's disease (CD) and ulcerative colitis (UC), which display distinct disease mechanisms and locations (Kaplan, 2015). Both diseases involve a complex interplay between genetic susceptibilities and environmental drivers which ultimately leads to a breakdown of intestinal homeostasis and immune-mediated pathology (Friedrich et al., 2019). IBD presents as a relapsing-remitting condition, with symptoms including diarrhoea, cramping, abdominal pain, weight loss, and rectal bleeding (Veauthier and Hornecker, 2018). Without treatment, IBD can cause severe complications, including intestinal perforation, bowel obstruction, abscesses, cancer, and malnutrition. Other extraintestinal complications include osteoporosis, thrombotic events, anaemia, and depression (Veauthier and Hornecker, 2018). IBD is associated with industrialised countries, with incidence in the Western world increasing since the 20$^{th}$ century, and prevalence now increasing throughout Asia, South America, and other more recently industrialised areas (Kaplan, 2015). The increasing global burden of IBD presents a huge cost to healthcare systems. While therapeutic advances have been made, many patients do not respond to treatment. There is a need for

increased understanding of disease mechanisms in order to develop personalised treatment based on disease stratification.

### 1.4.1 IBD pathogenesis

While the specific trigger for IBD is unknown, a key event in the pathogenesis is the breakdown of epithelial barrier function (Friedrich et al., 2019). This occurs due to a combination of genetic and environmental risk factors, which cause altered epithelial barrier function, microbial translocation, and a dysregulated immune response (Neurath, 2014). The result of this can be subclinical, acute, or chronic inflammation affecting distinct areas of the GI tract and leading to tissue damage and other complications (Neurath, 2014). Genome-wide association studies (GWAS) have linked over 200 genetic loci with IBD, identifying the involvement of genes associated with epithelial barrier function, innate immunity, adaptive immunity, autophagy, and microbial sensing (Jostins et al., 2012, Liu et al., 2015a, Uhlig and Powrie, 2018). Environmental risk factors include the microbiota and dysbiosis, diet, infections, smoking, and stress (Neurath, 2014).

It is clear that disruption to microbial sensing pathways and loss of intestinal barrier function leads to an altered relationship with the microbiota in IBD. For example, mutations in *NOD2* have been associated with CD risk in European cohorts (Liu et al., 2015a). NOD2 recognises muramyl dipeptide (MDP), a component of bacterial peptidoglycan (Girardin et al., 2003). Mice deficient in NOD2 show microbial dysbiosis, reduced expression of antimicrobial genes, and altered Peyer's patch composition (Al Nabhani et al., 2016). Another IBD susceptibility gene is *CARD9*, which encodes a signal adaptor protein downstream of many PRRs (Lamas et al., 2016). Studies in *Card9*$^{-/-}$ mice again showed dysbiosis as a result of the deficiency and demonstrated a link between CARD9 and tryptophan metabolism (Lamas et al., 2016). Tryptophan metabolites stimulate immune responses through the AHR, which has been shown to contribute to maintenance of epithelial barrier integrity (Metidji et al., 2018). These studies highlight the importance of microbial recognition pathways in the maintenance of intestinal homeostasis and emphasize how defects in these pathways can disturb homeostasis and lead to altered barrier function. IBD patients often present with 'leaky gut' syndrome, defined as increased intestinal

permeability (Camilleri, 2019). This results in translocation of bacteria and bacterial products from the intestinal lumen into the tissue and systemic circulation. Bacterial DNA has been reported in the serum of IBD patients (Gutiérrez et al., 2009) and has been associated with increased risk of hospitalization (Gutiérrez et al., 2016). Together, these alterations to the host-microbiota relationship can result in excessive inflammatory responses, causing the pathology in IBD (Neurath, 2014).

Cytokines produced by both the innate and adaptive immune systems drive inflammation in IBD, playing a fundamental role in pathogenesis (Neurath, 2014). Mutations to *IL23R*, the IL-23 receptor, have been associated with both CD and UC (Liu et al., 2015a), indicating a role for this cytokine which is discussed further in Section 1.5.2. Inflammation is initiated by innate-derived cytokines downstream of PRR signalling, including IL-1β and IL-18 produced following inflammasome activation (Friedrich et al., 2019), and genetic knockout of these cytokines has been shown to ameliorate disease in murine colitis models (Impellizzeri et al., 2018). Furthermore, IL-1β has been implicated in driving colitis caused by loss of IL-10 signalling, which can be treated with an IL-1 receptor antagonist (Shouval et al., 2016). Another key cytokine in IBD is TNFα, derived largely from monocytes and macrophages. It is produced at high levels in experimental colitis (Powrie et al., 1994) and has been associated with epithelial cell death (Pott et al., 2018). Importantly, targeting of TNFα as a therapeutic option was instigated after the finding that its neutralization was protective against disease in various murine colitis models (Powrie et al., 1994, Kojouharoff et al., 1997). Indeed, much of our understanding of the cytokine networks driving inflammatory disease has been gained through the use of blocking antibodies to study the effect of individual cytokines on disease outcome. Today, many of the therapeutics licensed for use against IBD target elements of different cytokine signalling pathways. These include multiple antibodies targeting TNFα (Danese et al., 2015) and targeting the shared subunit of IL-12 and IL-23 (Feagan et al., 2016). Additional therapeutics targeting IL-23, JAK signalling pathways downstream of cytokine receptor engagement, and other elements of Th17 effector responses are currently in clinical development (Moschen et al., 2019). The key events which occur during IBD pathogenesis are summarised in Figure 1-5.

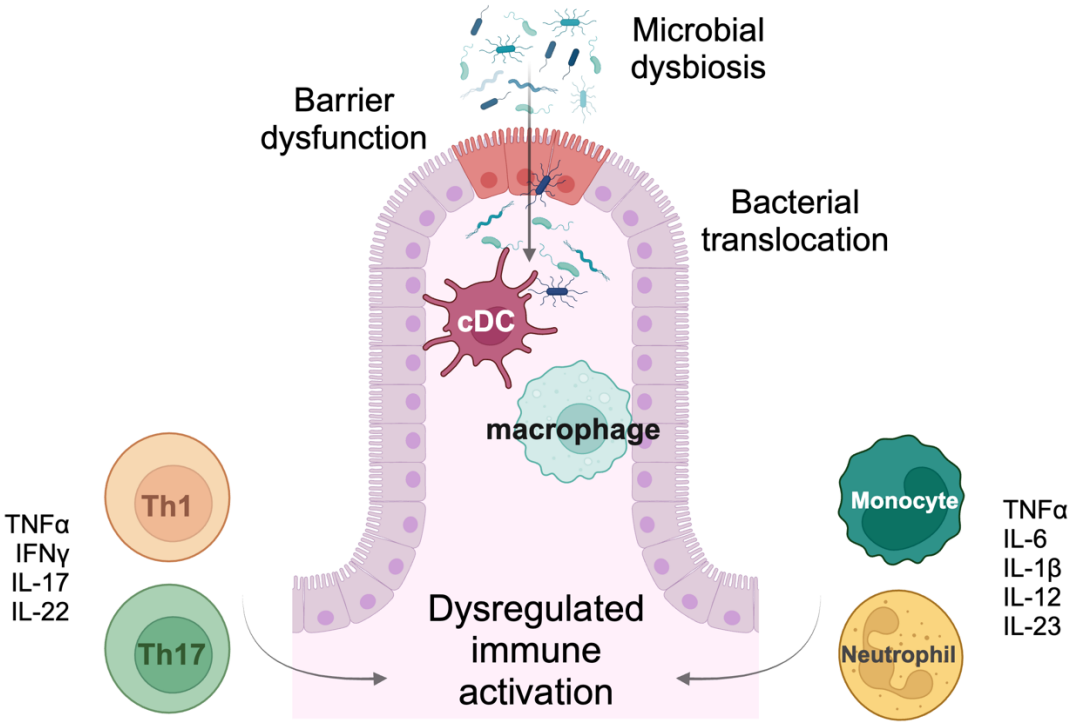


**Figure 1-5: Summary of events in IBD pathogenesis**
IBD involves an altered relationship with the microbiota, characterised by dysbiosis, host barrier dysfunction, and bacterial translocation into host tissue. Microbial antigens activate innate immune responses from cDCs and macrophages which produce cytokines to recruit and activate other immune cells. This leads to the infiltration of monocytes and neutrophils and differentiation of Th1 and Th17 cells. Defects in immune regulation result in a dysregulated immune response which leads to continued tissue damage and chronic pathology. This figure was created using BioRender.com.

## 1.4.2 T cells in IBD

Since the finding that naïve CD4 T cells could drive colitis in the absence of Tregs (Powrie et al., 1993), much work has been done to define the role of different effector T cell populations in IBD. The production of polarising cytokines by innate immune cells drives the differentiation of specific effector populations (Friedrich et al., 2019). IL-12 induces differentiation of Th1 cells, while IL-23 (along with IL-6 and TGFß) supports Th17 differentiation and function (Teng et al., 2015). Both subsets contribute to intestinal inflammation, as evidenced in murine colitis models (Morrison et al., 2013). In IBD patients, not only are Th17-associated genes implicated through GWAS (Liu et al., 2015a), but Th17 cells have been shown to infiltrate the site of inflammation (Pène et al., 2008). Elevated IL-17 levels have been demonstrated in the colon and serum during both active UC and CD (Fujino et al., 2003). Despite this, a clinical trial targeting IL-17 in CD was discontinued due to adverse effects and ineffectiveness (Hueber et al., 2012). This was suggested to be due to important homeostatic

effects of IL-17 in the intestine which had not previously been understood (Hueber et al., 2012). Conversely, IL-23 has been shown to promote a more pro-inflammatory Th17 phenotype. It is required for the acquisition of IFNγ production by Th17 cells (Hirota et al., 2011), while also limiting Treg activity in colitis models (Izcue et al., 2008). Indeed, IL-23 is required to drive disease in many murine colitis models (Hue et al., 2006, Kullberg et al., 2006, Buonocore et al., 2010), and clinical trials targeting IL-23 have shown good efficacy as a treatment for CD (d'Haens et al., 2022). These studies demonstrate the heterogeneity of intestinal Th17 responses, which is discussed further in Section 1.5.2.

The homing of T cells to the intestine is mediated by various adhesion and signalling molecules (Soler et al., 2009). To home to the intestine, T cells are required to express the integrin $\alpha_4\beta_7$ and the chemokine receptor CCR9 (Mora et al., 2003). The imprinting of this gut-homing phenotype occurs following antigen presentation by intestinal cDCs (Mora et al., 2003). As such, another therapeutic which has shown success in IBD is Vedolizumab, an antibody targeting the $\alpha_4\beta_7$ integrin (Sandborn et al., 2013). Vedolizumab inhibits the binding of $\alpha_4\beta_7$ to its ligand mucosal addressin cell adhesion molecule-1 (MAdCAM-1), thus preventing the infiltration of activated T cells to the intestine (Soler et al., 2009). The efficacy of this treatment highlights the requirement for T cells to drive the chronic pathology associated with IBD. However, IBD remains a heterogeneous disease, and not all patients respond to Vedolizumab. A current focus of IBD research is the search for potential biomarkers to identify response or non-response to different biologic treatments (Boden et al., 2018, Soendergaard et al., 2018). This could allow for the stratification of patients by disease mechanism and corresponding personalised treatment plans, thus avoiding unnecessary healthcare costs and patient side effects.

### 1.4.3 The microbiota in IBD

IBD has been associated with alterations to intestinal microbiota composition, including decreased diversity and changes to the relative abundance of specific bacterial families (Frank et al., 2007, Willing et al., 2010, Erickson et al., 2012, Pisani et al., 2022). What is less clear is whether these alterations are a cause or effect of the inflammation and other changes to barrier and immune functions

associated with IBD. Regardless, the ensuing dysbiosis is associated with changes to the metabolic output of the microbiota, with knock-on effects on host physiology and immune function (Gilbert et al., 2016). One example of this is the production of SCFA, which are produced by bacterial fermentation of dietary carbohydrates and have many documented beneficial effects on host immune and epithelial cells (Furusawa et al., 2013, Chang et al., 2014, Zheng et al., 2017). Patients with IBD have significantly reduced levels of faecal SCFAs (Huda-Faujan et al., 2010), demonstrating one mechanism by which dysbiosis can affect immune function and homeostasis in IBD.

The specific microbial changes associated with IBD tend to include proportional decreases in certain bacteria, such as the Firmicutes phylum, and relative increases in others, including Proteobacteria (Ni et al., 2017). However, studies in twins and family members have demonstrated that these changes are associated with IBD status, rather than as a result of genetics or shared environment (Willing et al., 2010, Joossens et al., 2011). The timing of the dysbiosis in relation to disease onset, however, remains unclear. Other factors which have been shown to independently drive dysbiosis in addition to inflammation include the use of antibiotics and diet (Lewis et al., 2015). Conversely, therapeutics to reduce inflammation can reverse dysbiosis (Lewis et al., 2015). The interplay between these factors in IBD presents a challenge for unpicking the contribution of specific environmental triggers to pathogenesis. Another example is the effect of infections on IBD susceptibility. Certain strains of adherent-invasive *Escherichia coli* (AIEC) have been linked with IBD, although to a differing extent in CD and UC (Darfeuille-Michaud et al., 1998, Martinez-Medina and Garcia-Gil, 2014). AIEC can invade epithelial cells and may facilitate bacterial translocation by weakening epithelial barrier strength, as well as being potent inducers of TNFα (Martinez-Medina and Garcia-Gil, 2014). However, these species are also found in the microbiota of healthy individuals. Their pathogenicity may only arise in the presence of a weakened intestinal barrier, such as those found in IBD patients, so it is difficult to discern whether these species drive IBD or simply potentiate disease in susceptible individuals. Nonetheless, *Clostridium difficile* infection in IBD patients has been associated with increased mortality compared to uninfected IBD (Ananthakrishnan et al., 2008), indicating that enteric infections can worsen disease severity.

The importance of the microbiota in IBD pathogenesis has also been emphasised through the success of therapeutics which act by modulating microbial composition. For example, antibiotics have been suggested to improve clinical outcomes and even induce remission in IBD patients when trialled as a therapeutic (Khan et al., 2011, Wang et al., 2012). This is in contrast to the use of antibiotics acting as a risk factor for IBD development (Lewis et al., 2015). This apparent contradiction suggests that while antibiotics can act as a trigger for dysbiosis, once this dysbiosis and disease has developed it may be beneficial to remove the bacteria which act as a target for dysregulated inflammatory responses. Similarly, a very successful treatment for paediatric CD is exclusive enteral nutrition (EEN), which has been shown to induce remission in a high percentage of patients and promote intestinal healing (Svolos et al., 2019). EEN is a diet-based treatment option, which appears to work by modulating microbiota composition and altering metabolite production (Gerasimidis et al., 2014). EEN excludes gluten, lactose, and alcohol from the diet, and is importantly very low in fibre (Svolos et al., 2019). This presents another contradiction, as low fibre intake is associated with the Western diet, which acts as another risk factor for IBD (Simpson and Campbell, 2015). Lack of fibre has been associated with a decrease in Firmicutes and increase in Proteobacteria species in non-IBD individuals (Simpson and Campbell, 2015). However, it appears that once IBD has developed, modulating the microbiota through lack of fibre can have beneficial outcomes (Svolos et al., 2019). These studies again highlight the complexity of IBD and demonstrate the need for increased understanding of host-microbiota interactions in this context.

### 1.4.4 Mouse models of IBD

While there are many aspects of IBD pathogenesis which remain poorly understood, murine disease models have provided major insights into pathogenetic mechanisms and therapeutic options. These models have helped to increase understanding of mucosal immunology, and the mechanisms required to maintain intestinal homeostasis. Different models vary in their mechanism of induction, pathogenesis, and involvement of the microbiota (Kiesler et al., 2015). While no model perfectly recapitulates IBD, different models can be used to study specific aspects of the mucosal inflammatory response. Several of the

most commonly used IBD models are discussed below, although others exist which have also provided important insights.

Among the most prevalently used is dextran sulphate sodium (DSS) induced colitis. This model involves the administration of DSS, a sulphated polysaccharide, into the drinking water of rodents, causing colonic epithelial injury (Kiesler et al., 2015). The subsequent barrier dysfunction causes pathological inflammatory responses targeted against the microbiota, resulting in an acute colitis (Kiesler et al., 2015). Alternatively, multiple rounds of treatment can be used to induce chronic inflammation, and disease severity develops in a reproducible, dose-dependent manner (Eichele and Kharbanda, 2017). Crucially, DSS drives colitis in severe combined immunodeficiency (SCID) mice, which lack T and B cells, demonstrating the ability of the innate immune system to drive pathology in this model (Dieleman et al., 1994). Thus, DSS colitis has been used to study the contribution of innate cells, including macrophages and neutrophils, to intestinal pathology (Kiesler et al., 2015). The epithelial barrier damage induced by DSS resembles the pathology found in UC but does not capture the full heterogeneity or complexity of IBD (Eichele and Kharbanda, 2017). Furthermore, the mechanism of disease induction is likely to be quite different in human IBD, and there are key differences in the T cell responses induced in chronic DSS models compared to IBD (Kiesler et al., 2015). However, as in human disease, DSS causes microbiota alterations which are likely driven by, or exacerbated by, the ongoing inflammatory response (Håkansson et al., 2015). The microbiota has also been shown to play a key role in regulating the severity of DSS colitis, with specific bacterial species associated with either disease protection or aggravation (Forster et al., 2022). Despite this, it has been reported that DSS can induce colitis in GF mice, suggesting that there are microbiota-independent mechanisms which contribute to disease (Bylund-Fellenius et al., 1994). Together, the DSS model has provided a reproducible and inexpensive means to study intestinal immune pathology, although it does not mimic every aspect of human disease.

Other common chemically induced colitis models involve a different mechanism of disease induction. The 2,4,6-trinitro benzene sulfonic acid (TNBS) and oxazolone models work by intrarectal administration of haptenating agents. The result of this is the induction of chronic T cell responses targeted against

hapten-modified host proteins (Wirtz et al., 2007). The T cell responses differ in each model, with Th1 being the dominant effector response in TNBS colitis, while oxazolone induces Th2 responses (Kiesler et al., 2015). As in DSS colitis, these T cell responses bear differences to those seen in IBD. A different model which more accurately recapitulates IBD T cell responses is T cell transfer colitis (Powrie et al., 1993). This system involves the adoptive transfer of naïve CD4 T cells into lymphopenic recipients, such as SCID or recombination activating gene (RAG) $^{-/-}$ mice. This causes T cell-mediated inflammatory responses targeted against the microbiota, due to the lack of Tregs in these recipients. In contrast, when Tregs are transferred along with naïve T cells, colitis is prevented (Powrie et al., 1993). The T cell responses induced in this setting are more representative of those seen in IBD, with a mixed Th1 and Th17 response induced. Furthermore, inflammation is prevented in IL-23$^{-/-}$ mice, demonstrating the requirement for this cytokine (Hue et al., 2006). As with human IBD, pathology in this model is dependent on the microbiota (Aranda et al., 1997). T cell transfer colitis is therefore a useful system to study bacteria induced T cell responses and immunopathology, although it bears limitations due to the use of immunodeficient mouse strains.

Finally, mice lacking IL-10 have been shown to develop spontaneous colitis (Kühn et al., 1993). This is important as polymorphisms to the *IL10* gene have been shown to contribute to both CD and UC susceptibility (Franke et al., 2008, Franke et al., 2010). Indeed, deficiencies in IL-10 and its receptor are associated with very early onset IBD (VEO-IBD), which is a severe form of IBD with distinct clinical manifestations and therapeutic responsiveness (Zhu et al., 2017). In *Il10*$^{-/-}$ mice, the inflammation is characterised by IL-12/23 and IFNγ production, although Th2 effector cytokines such as IL-13 can become apparent at later stages of disease (Spencer et al., 2002). Critically, IL-10 deficiency does not cause colitis in GF mice, demonstrating that pathology in this model is driven by dysregulated responses to the microbiota (Sellon et al., 1998). Furthermore, colitis develops to some extent in mice with a Treg-specific IL-10 deletion, which highlights the indispensable function of these cells in regulating intestinal homeostasis (Rubtsov et al., 2008). Colitis driven by loss of IL-10 signalling is examined further in the following section, as the role of specific bacterial species in the induction of intestinal pathology is discussed.

# 1.5 *Helicobacter hepaticus* as an experimental model

## 1.5.1 Characterisation of *Helicobacter hepaticus*

*Helicobacter hepaticus* (*Hh*) was first characterised in immunodeficient mouse strains which spontaneously developed chronic hepatitis (Ward et al., 1994, Fox et al., 1994). It was initially isolated from the liver but was found to primarily colonize the caecal and colonic mucosae. Further characterisation determined that *Hh* required low oxygen concentrations for survival, had a flagellated, spiral morphology, and was gram-negative (Ward et al., 1994, Fox et al., 1994). Analysis of the 16S subunit led to its identification as a novel enterohepatic *Helicobacter* species, with high sequence similarity to *Helicobacter muridarum* (Ward et al., 1994, Fox et al., 1994). *Helicobacter* species fall in the Proteobacteria phylum and are found naturally in the microbiota of various mammals, occupying distinct niches along the GI tract (Ménard and Smet, 2019). The most well characterised species found in humans is *Helicobacter pylori*, which colonizes the gastric epithelium and infects around half of the human population, causing gastric cancer in a subset of people (Malfertheiner et al., 2023). In contrast, *Hh* infects the murine large intestine and is not generally found in humans, although case studies have been published reporting its presence in patients with liver diseases (Hamada et al., 2009). Unlike the majority of microbes residing in the GI tract, *Hh* colonizes the surface of the epithelium and is able to penetrate the mucus layer (Chan et al., 2005). This allows *Hh* to colonize the space within epithelial crypts, an area which was previously thought to be sterile.

Despite this initial link between *Hh* and hepatitis and hepatocellular tumours, these pathologies only occur as a result of colonization in certain inbred mouse strains (Ward et al., 1994, Fox et al., 1994). Around the same time, reports were published demonstrating that mice deficient in IL-10 develop spontaneous intestinal inflammation (Kühn et al., 1993, Berg et al., 1996). This was also found to occur in various other immunodeficient mouse strains, including those lacking T and B cells such as SCID mice, and athymic mice (Ward et al., 1996, Foltz et al., 1998). These strains and others developed spontaneous intestinal pathology, characterised by typhlitis (inflammation of the caecum), colitis, and in some cases, rectal prolapse (Ward et al., 1996, Foltz et al., 1998). Many of

these mice were found to be naturally infected with *Hh*, yet, interestingly, immunocompetent animals showed no disease (Ward et al., 1996). Furthermore, disease did not develop in GF animals, indicating that a microbial component was required (Cahill et al., 1997). Cahill *et al*. then confirmed that *Hh* was sufficient to drive this pathology by infecting immunodeficient mice and performing adoptive transfer of naive CD4 T cells, which led to a severe disease resembling human IBD (Cahill et al., 1997). It was then demonstrated that infection of IL-$10^{-/-}$ mice with *Hh* resulted in the same chronic colitis (Kullberg et al., 1998). These early studies established a link between *Hh* and intestinal inflammation and crucially demonstrated that this inflammation only occurs in the absence of immune regulation.

The finding that *Hh* did not cause disease in immunocompetent animals led to its later classification as a 'pathobiont' (Chow et al., 2011). This term was designated to describe microbes which generally behave as commensal, symbiotic members of the microbiota, but which have the capacity to induce pathology under specific conditions (Chow et al., 2011). This context-dependent response sets these species apart from traditional pathogens and provides an interesting model to study how harmful immune responses are normally controlled. These pathobiont species are found in the microbiota of all mammals and include various *Helicobacter* species as well as bacteria from other families (Jeffery et al., 2022). These species tend to drive pathology in the absence of key immune regulatory elements, such as IL-10 signalling, Tregs, or TGFβ, or in hosts with mutations in genes associated with antimicrobial functions (Jeffery et al., 2022). It is clear that pathobionts exert a range of effects on host immunity, although these effects are only beginning to be understood. Recent work comparing the microbiome of wild mice to that of laboratory mice demonstrated that, compared to wild mice, pathobionts are underrepresented in laboratory animals (Rosshart et al., 2019). Wild animals had far higher relative abundance of Proteobacteria and Helicobacteraceae compared to conventional laboratory mice (Rosshart et al., 2019). This again highlights the caveats of using laboratory animals for research, as the vast differences in their microbial content can lead to differences in immune function and response to therapeutics (Rosshart et al., 2017, Rosshart et al., 2019). However, pathobiont species are still found in many laboratory animals, which presents challenges for producing reproducible data

across animal facilities. For example, *Hh* has been recorded in both laboratory mice and those from commercial vendors, including mice that are technically classified as specific-pathogen free (SPF) (Shames et al., 1995, Taylor et al., 2007). This remains an issue despite the existence of sensitive screening assays (Ge et al., 2001, Feng et al., 2005).

### 1.5.2 Pathogenesis of *Hh* induced colitis

The characterisation of *Hh* and the finding that its infection alone could trigger disease in genetically susceptible hosts led to its use as a model of bacteria induced IBD. Research went into understanding the pathogenesis of the disease and determining the immune mechanisms which drive it. Previous work using the naïve ($CD45RB^{high}$) $CD4^+$ T cell transfer model of colitis had determined that differentiated effector T cells drove colitis in immunodeficient mice, while co-transfer of $CD45RB^{low}$ T cells (now understood to be Tregs) prevented colitis (Powrie et al., 1993). Interestingly, *Hh* colonization was reported to drive colitis in the absence of T and B cells, although transfer of $CD45RB^{high}$ T cells exacerbated disease (Cahill et al., 1997). The induction of T cell-independent colitis by *Hh* was confirmed using $RAG^{-/-}$ mice, which lack T and B cells and develop innate immune driven intestinal pathology (Maloy et al., 2003). As in the T cell transfer model, Tregs contained within the $CD45RB^{low}$ fraction were able to suppress *Hh* induced colitis driven by both T cell-dependent and independent mechanisms (Kullberg et al., 2002, Maloy et al., 2003). Suppression of pathology by Tregs was dependent on IL-10 and TGFß (Maloy et al., 2003).

Colitis driven by *Hh*, as well as other models of IBD, were initially thought to be mediated by the Th1-inducing cytokine IL-12 (Kullberg et al., 1998, Kullberg et al., 2001). Treatment with anti-IFNγ or anti-TNFα did not attenuate established disease, although anti-IFNγ had been shown to prevent colitis induction when administered at the time of *Hh* infection (Kullberg et al., 1998, Kullberg et al., 2001). In these studies, only anti-IL-12 abrogated established pathology (Kullberg et al., 2001). This conclusion was later contested by the finding that the IL-12 cytokine consists of two subunits, p40 and p35, of which the p40 subunit is shared with a related cytokine, IL-23 (Kullberg et al., 2006, Hue et al., 2006). Early antibodies targeting IL-12 had in fact targeted the p40 subunit, thus also neutralising IL-23 responses. Further investigations that selectively targeted the

unique IL-12p35 or IL-23p19 subunits determined that IL-23, and not IL-12, is essential for development of colitis in response to *Hh*, both by T cell-dependent and innate mechanisms (Kullberg et al., 2006, Hue et al., 2006). Soon afterwards, *IL23R* polymorphisms were associated with IBD in humans (Duerr 2006), highlighting its importance in driving chronic intestinal pathology. Together, these discoveries changed our understanding of the mechanisms driving IBD. At a similar time, IL-23 was implicated in the pathogenesis of other models of inflammatory diseases, including experimental autoimmune encephalomyelitis (EAE), a model for multiple sclerosis (Cua et al., 2003). These results subsequently led to clinical testing of antibodies targeting IL-23 and related pathways in the context of various autoimmune and inflammatory diseases, including IBD (Moschen et al., 2019). Today, Ustekinumab is a licensed treatment for IBD and other conditions, which targets both IL-12 and IL-23 (Feagan et al., 2016, Sands et al., 2019), while Risankizumab selectively targets IL-23p19 and has shown efficacy in phase 3 clinical trials for CD (d'Haens et al., 2022). The use of mouse models, including *Hh* colitis, in determining the cytokine networks and mechanisms driving IBD have therefore been instrumental in the search for new therapeutic strategies.

IL-23 was originally considered a driver of Th17 responses, however, elevated Th1 responses were also implicated in *Hh* induced colitis (Kullberg et al., 2006, Hue et al., 2006). This suggested IL-23 could induce different effector T cell responses depending on the context (Kullberg et al., 2006). Using IL-17A-reporter mice, it was later shown that *Hh* infection of T cell-sufficient hosts induced differentiation of Th17 cells that could be programmed to stop IL-17A production and begin secreting IFNγ, mimicking a Th1 response (Morrison et al., 2013). These cells have become known as ‘exTh17 cells’ and have been reported in various autoimmune and inflammatory conditions (Hirota et al., 2011). Along with their ability to switch to a Th1-like phenotype and contribute to inflammatory pathologies, Th17 cells have also been reported to be able to develop into regulatory cells expressing IL-10 (Xu et al., 2020). These studies demonstrate the plasticity of CD4 T cell responses in various contexts, including bacteria-induced inflammation. Additionally, during *Hh* colitis, the Th17 response itself appears heterogeneous and has been shown to differ between locations within the GI tract (Morrison et al., 2015). Morrison *et al*. reported that loss of IL-17A had a worsening effect on

caecal pathology, suggesting that IL-17A may have protective functions in the cecum. In contrast, loss of IL-22 was protective in the colon, but not the cecum, indicating that IL-22 may selectively drive pathology in the colon (Morrison et al., 2015). They attributed these differences to varying expression of Th17 cytokine receptors in different locations within the intestine. Given that *Hh* colonisation varies throughout the intestine, and the newer evidence that innate PRRs are differentially expressed by location (Price et al., 2018), it seems likely that the reasons for different responses in distinct areas of the GI tract are complex and involve an interplay of microbial, innate, and adaptive factors.

The discovery of innate lymphoid cells (ILCs) furthered our understanding of the innate response during *Hh* induced colitis. It was known that IL-23 also drove innate mediated colitis but the specific pathways underpinning innate pathology were less well understood. Buonocore *et al*. classified the ILC response to *Hh* in $RAG^{-/-}$ mice, demonstrating that these cells were increased in the intestine following *Hh* infection and responded to IL-23 by producing IL-17 and IFNγ (Buonocore et al., 2010). It has since been shown that IL-22 and IL-1β contribute to innate colitis via signalling to ILCs (Coccia et al., 2012, Eken et al., 2014). Macrophages are also involved in driving innate pathology in T cell independent *Hh* colitis models. Following infection, monocytes infiltrate the intestine and mature into macrophages, where they begin secreting IL-23 and IL-1β – thus contributing to intestinal pathology (Arnold et al., 2016). More recently it was confirmed that the macrophages contributing to inflammation in *Hh* induced colitis are immature, derived from infiltrating monocytes and express intermediate levels of the maturation marker CX3CR1 (Bain et al., 2018). This indicates that tissue resident mature macrophages do not change phenotype during colitis, but rather the increased monocytic infiltration augments pathology.

Finally, the role of the greater microbiota in the pathogenesis of *Hh* colitis has become a focus of interest. GF $IL\text{-}10^{-/-}$ mice do not develop colitis when monocolonized with *Hh*, despite similar colonization levels (Nagalingam et al., 2013). This indicates that induction of colitis is dependent on other microbial species present in the host's microbiota. It has also been shown that the ability of *Hh* to drive disease in $IL\text{-}10^{-/-}$ mice varies by animal facility (Yang et al., 2013). IL-10 deficient animals from two facilities demonstrated clear differences

in their response to *Hh* infection, with mice from one facility showing robust disease while those from the second had no significant pathology (Yang et al., 2013). Animals from the two facilities had marked differences in their microbiota composition, again implicating other microbial components in the pathogenesis of *Hh* colitis. Similarly, infection with the related pathobiont *Helicobacter bilis* drives IBD-like disease following a sub-pathological dose of DSS (Gomes-Neto et al., 2017). Disease severity in this model also varies greatly with microbiota composition, with *H. bilis* monocolonization driving only mild inflammation, while the presence of a microbiota resulted in severe pathology (Gomes-Neto et al., 2017). These differences are likely due to the competition for resources which exists between species in the microbiota, resulting in altered expression of virulence factors and changes to metabolic output of individual species (Jeffery et al., 2022). These changes driven by the presence of other microbes appear to be required for the pathogenicity of *Hh*, although work remains to be done to characterise the specific mechanisms by which *Hh* drives disease.

### 1.5.3 Recognition of *Hh* by the immune system

While the pathogenesis of *Hh* induced colitis has been well studied, less understood are the mechanisms by which *Hh* is recognised and tolerated in immunocompetent hosts. To gain insight into the crosstalk between the host and its microbiota, it is important to understand which cell types recognise and respond to microbe derived signals – and the outcomes of these interactions for the host. Much work has been done to characterise the T cell response to *Hh* in different contexts. During *Hh* colitis, the T cell pool is dominated by Th1 and Th17 effectors (Kullberg et al., 2006, Xu et al., 2018). At steady state, *Hh* preferentially induces expansion of Tregs and T follicular helper cells (Tfh) (Xu et al., 2018). These Tregs and their production of IL-10 are indispensable for preventing an inflammatory response to *Hh* (Kullberg et al., 2002). Using T cell receptor (TCR) transgenic mice, Xu *et al*. showed that the same *Hh*-specific T cell clone can produce either a Treg or Th17 response to *Hh* depending on the presence or absence of IL-10 signalling (Xu et al., 2018). In another study, it was shown that a T cell clone specific for *Hh*, and capable of driving colitis in infected $RAG^{-/-}$ mice, recognises part of the *Hh* flagellar hook protein (Kullberg et al., 2003). In addition to T cell mediated responses, *Hh* induces robust

antibody production. Within 4 weeks of infection *Hh*-specific IgG2a/b and IgG1 antibodies can be detected in the serum, while IgA is present in stool (Whary et al., 1998, Kullberg et al., 1998). It is interesting to consider the requirement for these IgG antibody responses, as they do not result in clearance of *Hh* but may play a role in fine-tuning the immune response through Fc receptor interactions (Ben Mkaddem et al., 2019).

Although Tregs are crucial to prevent the development of colitis, it is also likely that a range of innate signals respond to *Hh* and contribute to promoting a tolerised response. TLR ligands are expressed by commensal microbes as well as pathogens (Rakoff-Nahoum et al., 2004), and promote protective responses in addition to inflammation. It has been reported that commensal bacteria are recognised by TLRs in the intestine and that this response is critical for maintaining homeostasis (Rakoff-Nahoum et al., 2004). It is becoming increasingly evident that TLR responses are heterogeneous and often context dependent. It is therefore important to determine which receptors respond to *Hh* and what the outcome is in different contexts. Asquith *et al*. used mice deficient in MyD88 to assess the importance of TLR signals in the induction of *Hh* colitis. Using selective depletion of MyD88 in haematopoietic cells, they demonstrated that TLR signalling on leukocytes was necessary for induction of *Hh* driven inflammation, while signalling from epithelial cells was insufficient for colitis induction (Asquith et al., 2010). Instead, they suggested that epithelial TLR signalling promotes survival from microbial invasion via antimicrobial peptide production.

It was initially reported that TLR2 was the key TLR involved in recognition of *Hh* (Mandell et al., 2004). However, these results were produced using cells transfected with human TLRs, with the limitation that *Hh* is a murine pathogen and may exhibit different specificities for murine TLRs. Later studies using $TLR2^{-/-}$ mice demonstrated that TLR2 was not required for *Hh* induced innate immune or T cell-mediated colitis (Boulard et al., 2010). A role for TLR2 has been described for maintaining intestinal homeostasis (Cario, 2008) and it is therefore possible that TLR2-mediated recognition of *Hh* does occur but does not drive an inflammatory response, but rather a protective one. It has since been shown than *Hh* produces a polysaccharide which is recognised by TLR2, and which promotes IL-10 production in macrophages at steady state (Danne et al.,

2017). Interestingly, TLR2 expression has also been reported on Tregs, and is reportedly required for the establishment of Treg-mediated tolerance towards the commensal microbe *Bacteroides fragilis* (Round et al., 2011). Whether Treg expression of TLR2 plays a role in the host response to *Hh* has not yet been reported. It has also been proposed that *Hh* soluble factors may antagonise TLR signalling in IECs (Sterzenbach et al., 2007). Although it was demonstrated that co-incubation of IECs with *Hh* reduced subsequent responses to *E. coli* LPS, these data were obtained using an immortalised cell line (Sterzenbach et al., 2007). It remains to be determined whether similar responses are elicited in primary IECs. Finally, mutations to NLR signalling genes have been associated with susceptibility to IBD (Rubino et al., 2012). Recognition of the microbiota by NLRs has been shown to promote systemic effects on the immune system, including priming of neutrophil responses (Clarke et al., 2010). Mice deficient in NOD2 reportedly show increased bacterial burden when colonized with *Hh* (Petnicki-Ocwieja et al., 2009). This suggests a potential role for this receptor in controlling the extent of *Hh* colonization, although this finding has not been subsequently validated. Together, these data demonstrate that multiple cell types and signalling pathways respond to *Hh* in different contexts.

## 1.6 Hypothesis and aims

It is clear from the literature that the host interacts with *Hh* through a range of innate and adaptive signals. However, the outcome of these interactions for host immune function remains poorly understood, especially at steady state. The majority of research surrounding *Hh* has focussed on the induction of colitis in immunodeficient mice, while the consequences of infection in immunocompetent hosts is only beginning to be explored. Furthermore, while the T cell response to *Hh* has been characterised in detail, far less is known about how this infection influences innate immune phenotype and function. In this thesis, we aimed to explore the relationship and interactions between *Hh* and its murine host, focussing on cells of the innate immune system. We aimed to determine whether the range of interactions between *Hh* and the host contribute to shaping immune function at steady state. We postulated that the dominant regulatory responses induced as a result of *Hh* colonization may alter how the host responds in an inflammatory disease setting.

We therefore hypothesised that *Hh* colonization alters host intestinal immune functions at steady state, resulting in increased regulatory responses and reduced inflammation following inflammatory challenge. To test this hypothesis, we explored the following objectives:

1. Test whether *Hh* colonization alters the outcome of disease challenge.

2. Determine how *Hh* affects the immune environment in the intestine at steady state, including phenotyping of local myeloid populations and cytokine expression.

3. Determine whether *Hh* has functional effects on macrophages at steady state.

4. Explore the signalling pathways responding to *Hh* and address their contribution in a disease setting.

5. Explore how *Hh* affects epithelial barrier composition and function.

This work aims to contribute to our understanding of host-microbiota interactions and the mechanisms by which the microbiota affects host immune function. Using *Hh* infection as an experimental model, we hope to provide further insight into how pathobiont species modulate host immunity and affect disease outcomes.

# 2 Methods

## 2.1 Mice

Wild-type C57BL/6 mice were obtained from Envigo (Huntingdon, UK) and maintained in individually ventilated cages under specific pathogen free (SPF) conditions at the Central Research Facility, University of Glasgow, UK. Procedures were performed in accordance with UK Home Office regulations under a Project Licence and Personal Licences issued by the UK Home Office. Mice were routinely screened to confirm the absence of *Helicobacter spp*. Female mice were used for all experiments at age 6-12 weeks.

## 2.2 *Helicobacter hepaticus* infections

### 2.2.1 Bacterial culture

*Helicobacter hepaticus* type strain 51449 (ATCC) (Fox et al., 1994) was cultured in tryptone soya broth (Oxoid) containing 10% foetal bovine serum (FBS) and Skirrow Campylobacter selective supplement (Oxoid). Cultures were grown microaerophillically for up to 4 days at 37°C in a shaking incubator at 110 RPM, as described (Maloy et al., 2003).

### 2.2.2 Direct *Helicobacter hepaticus* infection

The concentration of *Hh* cultures were estimated using the equation 1 $OD_{600}$ = $1x10^8$ CFU/mL (Waisman and Becher, 2014). Bacteria were assessed for viability using the LIVE/DEAD BacLight Bacterial Viability kit (ThermoFisher) then centrifuged at 5000 G for 10 mins to pellet bacteria and resuspended at $5x10^8$ CFU/mL in sterile PBS. Mice were infected with 0.2mL *Hh* in PBS by oral gavage.

### 2.2.3 *Hh*$^+$ microbiota transfer

Colonies of mice bred at the University of Glasgow (various genotypes) were tested for naturally occurring *Hh* colonization by screening stool for the *Hh*-specific gene *p25* (Feng et al., 2005) (described in Section 2.18). A cohort of confirmed *Hh*$^+$ University of Glasgow mice were then used as microbiota donors for the purpose of transferring *Hh* colonization to uninfected SPF C57BL/6 mice.

Transfer of the *Hh*$^+$ microbiota was achieved by co-housing up to 4 SPF C57BL/6 mice (Envigo) with one *Hh*$^+$ mouse (University of Glasgow) for 1-week. This microbiota transfer resulted in *Hh*$^+$ C57BL/6 mice which were originally SPF but now contained the transferred *Hh*$^+$ microbiota from the University of Glasgow donors. For experimental use, these primary recipient *Hh*$^+$ C57BL/6 mice were used as microbiota donors, whereby 4 uninfected experimental mice (C57BL/6, Envigo) were co-housed with one infected donor for 1-week to allow microbiota transfer. The original *Hh*$^+$ University of Glasgow mice used for primary microbiota transfer were donated by Marieke Pingen, University of Glasgow.

## 2.3 DSS colitis

Mice were given 2% dextran sulphate sodium (DSS) (molecular weight ~40,000, Alfa Aesar) in drinking water for 4 days, with fresh 2% DSS in water supplied on day 2. On day 4, animals were switched back to normal drinking water until the experiment end point on day 8. Control animals received normal drinking water. Mice were weighed daily during the 8-day DSS protocol and assessed for clinical signs of DSS-induced disease, receiving a disease score out of 16. Disease scores were based on 4 parameters (weight loss, bleeding, stool consistency, general appearance) with a maximum score of 4 for each.

## 2.4 TLR2 antibody blockade

Mice were treated with purified anti-mouse CD282 (TLR2) clone QA16A01 (mouse IgG1, κ) recombinant antibody (BioLegend) to block TLR2 signalling. Animals received 100μg antibody once weekly for the duration of the experiment (4 doses total). Antibody was administered by intraperitoneal injection in 0.2mL sterile PBS. Control animals received purified mouse IgG1, κ isotype control antibody (BioLegend) at the same dose.

## 2.5 *In vivo* Pam3csk4 challenge

Mice were treated with Pam3csk4 (synthetic triacylated lipopeptide, TLR2/1 agonist) (InvivoGen). Mice received either 10μg or 100μg Pam3csk4 by intraperitoneal injection in 0.2mL sterile PBS and were culled after 4h.

## 2.6 Serum collection

Animals were euthanised and cardiac puncture performed immediately afterwards using a 25-gauge needle to collect blood. Blood samples were stored in 1.5mL Eppendorfs for 4h at RT before centrifuging at 5000 G for 8 mins at RT. The serum layer was then transferred to a new 1.5mL Eppendorf and stored at -80℃ for downstream analyses.

## 2.7 Cell isolation

### 2.7.1 Isolation of lamina propria leukocytes

Colons and SI were harvested and opened longitudinally before being washed in PBS and cut into pieces. Tissues were stored at 4℃ in HBSS (no calcium, no magnesium) (ThermoFisher) supplemented with 10% FBS. For lamina propria leukocyte (LPL) isolation, tissues were transferred to HBSS supplemented with 2mM EDTA (ThermoFisher) and incubated at 37℃ in a shaking incubator at 220 RPM for 15 mins before repeating this step a 2$^{nd}$ time in new EDTA-HBSS. Colon tissue was then digested at 37℃ for 15 mins in a shaking incubator at 220 RPM with 0.65mg/mL collagenase D, 0.5mg/mL collagenase V, 30µg/mL DNAse I, and 1mg/mL dispase (all Sigma-Aldrich). SI were digested in 0.5mg/mL collagenase VIII (Sigma-Aldrich) under the same conditions. Digestion was performed in complete R10 medium (RPMI-1640 supplemented with 10% FBS, 100U/mL penicillin, 100µg/mL streptomycin, 2mM L-glutamine, and 50 µM ß-mercaptoethanol – all Gibco). Digested samples were passed through 100µm and 40µm filters to obtain single cell suspensions. Cells were then centrifuged twice in R10 at 400G for 10 mins at 4℃.

### 2.7.2 Isolation and culture of bone marrow-derived macrophages

Bone marrow was isolated from the femurs and tibias of 2-3 mice by centrifuging at 400 G for 1 min RT. Red blood cells were lysed using ACK Lysing Buffer (Gibco) according to the manufacturer's instructions. Bone marrow cells were centrifuged at 400 G for 10 mins at 4℃ before being counted and seeded in petri dishes at 5x10$^5$ cells/mL for a total of 5x10$^6$ cells per dish. Cells were seeded in R10 supplemented with 30ng/mL murine M-CSF (BioLegend). Cells were left to differentiate for 6 days and given fresh R10 containing M-CSF on day 3.

Differentiated bone marrow-derived macrophages (BMDMs) were harvested in ice-cold PBS supplemented with 3mM EDTA to allow detachment from petri dishes.

## 2.8 Flow cytometry

### 2.8.1 Surface staining

Up to $5x10^6$ cells per sample were stained with surface antibodies for flow cytometry analysis. All staining steps were carried out in PBS supplemented with 2% FBS and 2mM EDTA (FACS buffer). Cells were first incubated with Fixable Viability Dye (Invitrogen) and TruStain FcX (anti-mouse CD16/32) antibody (BioLegend) for 20 mins at 4℃ to exclude dead cells and minimise non-specific antibody binding, respectively. Cells were washed at 400 G for 5 mins at 4℃ then stained with a combination of surface antibodies (listed in Table 2-1) for 30 mins at 4℃. Cells were washed again and fixed in Fixation Buffer (BioLegend) for 30 mins at 4℃, then washed and stored in FACS buffer at 4℃ until acquisition. All surface antibodies were used at 1/200 dilution except anti-CD45 (1/400) and were obtained from BioLegend.

| Target | Clone |
|---|---|
| CD45 | 30-F11 |
| CD3 | 17A2 |
| CD45R (B220) | RA3-6B2 |
| CD11b | M1/70 |
| Ly6G | 1A8 |
| IA/IE | M5/114.15.2 |
| CD64 | X54-5/7.1 |
| Ly6C | HK1.4 |
| CD11c | N418 |
| CD80 | 16-10A1 |
| CD86 | GL-1 |
| CD274 (PD-L1) | 10F.9G2 |
| CD206 | C068C2 |
| Tim-4 | RMT4-54 |
| CD4 | RM4-5 |

**Table 2-1: Surface antibodies used for flow cytometric analyses**

### 2.8.2 Phosphorylated protein staining

For intracellular staining of phosphorylated proteins, up to $2x10^6$ cells per sample were first incubated with Viability Dye, TruStain FcX, and surface

antibodies as described above (2.8.1). Cells were then washed and fixed for 30 mins at 37℃ in pre-warmed Fixation Buffer (BioLegend). Cells were washed and permeabilized using True-Phos Perm Buffer (BioLegend) overnight at -20℃. Permeabilized cells were washed at 1000 G for 5 mins at RT then stained with antibodies against phosphorylated S6 (clone cupk43k) and phosphorylated Akt1 (clone SDRNR) (both Invitrogen) for 30 mins at RT in FACS buffer. Cells were washed and stored in FACS buffer at 4℃ until acquisition.

### 2.8.3 Mitochondrial labelling dyes

For assessment of mitochondrial activity, up to $2x10^6$ cells per sample were incubated with 250nM MitoSpy Red CMXRos and MitoSpy Green FM (both BioLegend) in complete R10 at 37℃ for 30 mins. Cells were washed at 400 G for 5 mins at 4℃ then incubated with Viability Dye, TruStain FcX, and surface antibodies as described above (2.8.1). Cells were fixed using Fixation Buffer (BioLegend). MitoSpy Green was detected in the FITC channel (filter 530/30) and MitoSpy Red was detected in the PE channel (filter 585/15). Data were acquired using a BD LSR Fortessa (BD).

### 2.8.4 Fluorescence activated cell sorting (FACS)

Colonic LPL were isolated and stained with Viability Dye, TruStain FcX, and surface antibodies as described above (2.8.1). Cell suspensions were passed through a 35µm strainer (StemCell) prior to sorting by FACS. $CD11b^+CD64^+Ly6C^-MHCII^+$ macrophages were sorted using a BD FACS Aria IIU or FACS Aria III (BD) with a 100µm nozzle. Macrophages were sorted into R10 and stored at 4℃ prior to counting and stimulation.

## 2.9 pHrodo phagocytosis assay

After isolation, LPL were seeded at $5x10^5$ cells per well in a 96 well plate in 0.2mL R10 and incubated for 2h at 37℃ to allow adherent cells to attach to plate. Non-adherent cells were washed off and adherent LPL were incubated with either 1mg/mL or 0.1mg/mL pHrodo Red *Escherichia coli* BioParticles (Invitrogen) in PBS for 30mins at 37℃. Cells were then washed and stained with surface antibodies to detect macrophages as described in Section 2.8.1. pHrodo

fluorescence was detected in the PE channel (filter 585/15) and data were acquired using a BD LSR Fortessa (BD).

## 2.10 Macrophage stimulations

FACS-sorted LPL macrophages were seeded at $3x10^4$ cells per well in 0.2mL R10 and BMDMs were seeded at $2x10^5$ cells per well in 0.2mL R10. Macrophages were either left unstimulated or treated with 100ng/mL LPS from *Escherichia coli* (Sigma-Aldrich), 100ng/mL Pam3csk4 (InvivoGen), or 1µg/mL Zymosan A from *Saccharomyces cerevisiae* (Sigma-Aldrich). For infection of macrophage cultures with *Hh*, bacterial cultures were grown and measured as described (Section 2.2) and centrifuged at 5000 G for 10 mins at RT. Bacteria were resuspended in complete R10 (without penicillin-streptomycin) and administered to macrophage cultures at multiplicity of infection (MOI) = 10. Macrophages were incubated for 16h at 37℃ and 5% $CO_2$ following stimulation. Culture supernatants were harvested and stored at -20℃ for downstream analyses.

## 2.11 alamarBlue metabolic health assay

Metabolic activity of FACS-sorted macrophages was assessed using alamarBlue (Invitrogen) as a correlate of cell viability. alamarBlue contains resazurin which is cell permeable and is reduced to resorufin inside living cells. This reaction can be quantified using absorbance due to the red colour of resorufin. Macrophages were seeded at $3x10^4$ cells per well in 180µL R10 and 20µL alamarBlue before being left to incubate for 16h at 37℃. Absorbance was measured at 570nm/600nm using a plate reader.

## 2.12 Cytometric bead array

The concentrations of IL-6, TNFα, MCP-1, and IL-10 in serum or stimulated macrophage culture supernatants were measured using the BD Cytometric Bead Array Flex Set kits (BD Biosciences). Serum samples were assayed at 1/2 dilution and FACS-sorted macrophage supernatants were assayed undiluted. Data were acquired using a BD FACS Canto II (BD).

## 2.13 Primary colonic organoid culture

### 2.13.1 Generation of L-WRN conditioned medium

L-WRN cells were obtained from ATCC (CRL-3276) and cultured as described (Miyoshi and Stappenbeck, 2013), using 0.5mg/mL Geneticin G418 (Invitrogen) and 0.5mg/mL Hygromycin B (Sigma-Aldrich) for selection of stable clones. Conditioned medium (CM) was generated containing L-WRN-secreted Wnt3a, R-spondin 3 and noggin as described(Miyoshi and Stappenbeck, 2013). CM was produced in CM base medium: Advanced DMEM F12 (Gibco) supplemented with 20% FBS, 100U/mL penicillin, 100µg/mL streptomycin, and 2mM L-glutamine (all Gibco). Final CM was filtered through a 0.2µm filter (Sigma-Aldrich) and diluted to 50% in CM base medium before aliquoting and storing at -20℃.

### 2.13.2 Isolation of colonic crypts

Colons were harvested and fat and stool gently removed. Colonic crypts were isolated as described (Fan et al., 2016). Briefly, colons were inverted and washed in 30mL PBS before incubation in 30mL PBS supplemented with 20mM EDTA for 30 mins at 37℃. Colons were transferred to 30mL new ice-cold PBS (one colon per tube) and vortexed to release crypts from the tissue. Crypts were centrifuged twice at 100 G for 2 mins at 4℃ to remove debris and single cells before counting. The desired number of crypts were then centrifuged at 500 G for 3 mins to pellet crypts prior to seeding (described in next section).

### 2.13.3 Organoid culture and passage

Organoids were cultured and passaged as described(Fan et al., 2016). Crypts were seeded in Cultrex Ultimatrix RGF Basement Membrane Extract or Cultrex RGF Basement Membrane Extract Type 2 Select (BME – both BioTechne). Crypts were seeded at 400 crypts/well in 25µL BME and plates were incubated upside-down for 10 mins at 37℃ for BME to solidify. 400µL 50% CM was added to wells and organoids were left to grow for 5-6 days and given fresh 50% CM on day 3. Organoids were passaged on day 5-6 by removing medium and incubating in ice-cold CM base medium. Organoids were disrupted by pipetting up and down to dissolve BME and break apart the organoid structures into smaller pieces and single cells. Disrupted organoids were washed at 300 G for 5 mins at 4℃ and

counted before being seeded in fresh BME as previously. Organoids were passaged 3-4 times before use.

### 2.13.4 Organoid immunofluorescent staining

Organoids were passaged as described previously and seeded onto the Nunc Lab-Tek II Chamber Slide System (Thermo Scientific). At day 5, medium was removed from wells and organoids were fixed in 200µL per well 4% paraformaldehyde Image-iT Fixative Solution (Thermo Scientific) for 20 mins at RT. Organoid immunofluorescent staining was carried out as described (Drurey et al., 2021). Organoids were stained with Rabbit anti-Mouse Ki67/MK167 (clone 1297A – BioTechne) at 1/2000 dilution overnight at 4℃ before staining with Goat anti-Rabbit IgG conjugated to AF647 (Abcam) at 1/500 dilution for 1h at RT. Slides were mounted with Vectashield Mounting Medium with DAPI (Vector Laboratories). Slides were imaged using a Nikon A1-R Confocal Microscope and image files viewed using ImageJ/Fiji (Schindelin et al., 2012).

### 2.13.5 Organoid stimulations

At day 5 post-passage, medium was removed from organoid wells and either replaced with 50% CM (unstimulated wells) or 50% CM supplemented with 20ng/mL recombinant mouse IFNγ (BioLegend), 1µg/mL Pam3csk4 (InvivoGen), or 20ng/mL recombinant mouse IL-22 (BioLegend). Organoids were stimulated in triplicate for 6h at 37℃ for harvest of RNA, or 16h for harvest of culture supernatants for ELISA assays. Culture supernatants were stored at -20℃.

## 2.14 CXCL1 and CXCL2 ELISA

The concentrations of CXCL1 and CXCL2 in stimulated organoid supernatants were measured using the mouse CXCL1/KC and CXCL2/MIP-2 DuoSet ELISA kits according to the manufacturer's instructions (BioTechne). Supernatants were assayed at 1/5 dilution for CXCL1 and 1/2 dilution for CXCL2. Absorbance was measured at 450nm/540nm using a plate reader.

# 2.15 RNA extraction

## 2.15.1 RNA extraction from tissue

1cm sections of distal colon were harvested and stored in RNA*later* Stabilization Solution (Invitrogen) at -80℃. Tissue samples were transferred to QIAzol Lysis Reagent and homogenised in a TissueLyser twice for 1 min at 25Hz using a 5mm Stainless Steel Bead (all Qiagen). Samples were centrifuged at 12,000 G for 5 mins at RT and supernatants transferred to a new 1.5mL Eppendorf. Supernatants were mixed with chloroform and incubated for 3 mins at RT before centrifuging at 12,000 G for 15 mins at RT. The aqueous layer containing RNA was harvested and mixed with 100% ethanol at 1.5X volume. Purification of RNA was carried out using the RNeasy Mini Kit with DNA digestion using the RNase-free DNase Set (both Qiagen). RNA concentration and quality were measured using a NanoDrop Spectrophotometer. RNA was stored at -80℃.

## 2.15.2 RNA extraction from epithelial crypts and organoids

Epithelial crypts were isolated as described in Section 2.13.2 and counted. $5x10^4$ crypts were removed for RNA extraction and centrifuged at 500 G for 5 mins at 4℃. Crypts were resuspended in 700µL RLT buffer (Qiagen) supplemented with 1% ß-mercaptoethanol (Sigma-Aldrich) for lysis. Organoids were harvested for RNA by removing medium from wells and adding 350µL RLT + ß-mercaptoethanol (2X organoid wells pooled per RNA sample). All lysates were homogenised using QIAshredder homogenisers (Qiagen). RNA was then purified using the RNeasy Mini Kit and RNase-free DNase Set (both Qiagen). RNA concentration and quality were measured using a NanoDrop Spectrophotometer. RNA was stored at -80℃.

# 2.16 cDNA synthesis

Complementary DNA was synthesised from RNA using the High-Capacity cDNA Reverse Transcription Kit (Applied Biosystems). For colon tissue samples 2000ng RNA was converted to cDNA, while for organoids 200-400ng RNA was used (concentration was kept consistent for all samples in each experiment). Reverse transcription cycling parameters are listed in Table 2-2. Resultant cDNA was diluted 1/10 in nuclease-free $H_20$ and stored at -20℃.

| | |
|---|---|
| 25℃ | 10 mins |
| 37℃ | 120 mins |
| 85℃ | 5 mins |
| 4℃ | ∞ |

**Table 2-2: Reverse transcription cycling parameters**

# 2.17 DNA extraction

## 2.17.1 DNA extraction from stool and caecal contents

2 fresh faecal pellets per mouse were collected in 1ml PBS and faecal DNA was either immediately extracted or samples were stored at -20℃ until extraction. Caecal contents were collected in 1mL PBS and stored at -20℃ until extraction. Faecal/caecal DNA was extracted and purified using the QIAamp PowerFecal Pro DNA Kit (Qiagen). DNA concentrations were measured using a NanoDrop Spectrophotometer. DNA was stored at -20℃.

## 2.17.2 Genomic DNA extraction from bacterial culture

*Hh* bacterial cultures were grown as described in Section 2.2.1 and centrifuged at 5000 G for 10 mins at RT to pellet bacteria. Bacterial genomic DNA was extracted using the PureLink Genomic DNA Mini Kit (Invitrogen) following the manufacturer's protocol for gram negative bacteria. DNA concentrations were measured using a NanoDrop Spectrophotometer. DNA was stored at -20℃ before being used to prepare a standard curve for *Hh* DNA quantification (described in Section 2.19.2).

# 2.18 PCR and gel electrophoresis

*Helicobacter hepaticus* DNA was detected by PCR of the *p25* gene using forward primer ATGGGTAAGAAAATAGCAAAAAGATTGCAA and reverse primer CTATTTCATATCCATAAGCTCTTGAGAATC (Feng et al., 2005) (IDT). Per sample the PCR reaction mixture contained 12.5µL GoTaq Green Master Mix 2X (Promega), 6.5µL nuclease-free $H_20$, 2µL forward and 2µL reverse primer at 10µM working concentration. Faecal DNA was diluted to 100ng/µL in nuclease-free $H_20$ and 2µL added to the reaction. The PCR cycling parameters are listed in Table 2-3. Amplicons were analysed by 1% agarose gel electrophoresis containing 0.01% SYBR safe DNA Gel Stain (Invitrogen).

| | | | |
|---|---|---|---|
| | 94℃ | 2 mins | |
| Denature | 94℃ | 1 min | 30 cycles |
| Anneal | 55℃ | 1 min | |
| Extend | 72℃ | 1 min | |
| | 72℃ | 10 mins | |
| | 4℃ | ∞ | |

**Table 2-3: Cycling parameters for *p25* PCR**

# 2.19 Quantitative RT-PCR

## 2.19.1 Murine cDNA analysis

Quantitative real-time PCR (qPCR) was performed using PowerUp SYBR Green Master Mix and the QuantStudio 7 Flex Real-Time PCR System (both Applied Biosystems). Per sample the qPCR reaction mixture for each gene of interest contained: 5µL SYBR Green Master Mix 2X, 0.5µL forward and 0.5µL reverse primer at 10µM working concentration. cDNA samples were added at 4µL per reaction and analysed in triplicate, with gene expression levels for each sample normalised to the housekeeping gene *Rps29* (encoding ribosomal protein S29). Differences in gene expression were determined using the $2^{-\Delta\Delta C(t)}$ method (Schmittgen and Livak, 2008) and a nuclease-free $H_20$ sample was analysed to confirm the absence of contamination. The cycling parameters and dissociation curve conditions are listed in Table 2-4, with primer sequences and sources listed in Table 2-5. All primers were obtained from IDT.

| **Cycling parameters** | | | |
|---|---|---|---|
| UDG activation | 50℃ | 2 mins | Hold |
| Dual-lock DNA polymerase | 95℃ | 2mins | Hold |
| Denature | 95℃ | 15 secs | 40 cycles |
| Extend | 60℃ | 1 min | |
| **Dissociation curve conditions (melt curve)** | | | |
| 1 | 1.6℃/sec | 95℃ | 15 secs |
| 2 | 1.6℃/sec | 60℃ | 1 min |
| 3 | 0.15℃/sec | 95℃ | 15 secs |

**Table 2-4: qPCR cycling parameters and dissociation conditions**

| Gene | Forward sequence | Reverse sequence | Source |
|---|---|---|---|
| *Rps29* | ACGGTCTGATCCGCAAATAC | CATGATCGGTTCCACTTGGT | Graham Heieis, University of Glasgow |
| *Tnfa* | CCTGTAGCCCACGTCGTAG | GGGAGTAGACAAGGTACAACCC | (Price et al., 2018) |
| *Ifny* | TGAGTATTGCCAAGTTTGAG | CTTATTGGGACAATCTCTTCC | Holly Webster, University of Glasgow |
| *Il1B* | TTTTCCTCCTTGCCTCTGAT | GAGTGCTGCCTAATGTCCCC | (Du et al., 2021) |
| *Il6* | CTCTGGGAAATCGTGGAAATG | AAGTGCATCATCGTTGTTCATACA | (Wongchana and Palaga, 2012) |
| *Il17a* | ATCCCTCAAAGCTCAGCGTGTC | GGGTCTTCATTGCGGTGGAGAG | Holly Webster, University of Glasgow |
| *Il22* | TTTCCTGACCAAACTCAGCA | CTGGATGTTCTCGTCGTCAC | Holly Webster, University of Glasgow |
| *Il10* | CTGAAGACCCTCAGGATGCG | TGGCCTTGTAGACACCTTGGTC | Holly Webster, University of Glasgow |
| *Retnlb* | TCTCCCTTTTCCCACTGATAG | TCTTAGGCTCTTGACGACTG | (Pei et al., 2016) |
| *Nos2* | GTTCTCAGCCCAACAATACAAGA | GTGGACGGGTCGATGTCAC | (Price et al., 2018) |
| *Lgr5* | CTCCAACCTCAGCGTCTTC | GTCAAAGCATTTCCAGCAAGA | (Nusse et al., 2018) |
| *Muc2* | ACCACAATCTCTACTCCCATCT | TCCAGTCAGACCAAAAGCAG | (Nusse et al., 2018) |
| *Chga* | CGCTCCTTGGCACCTTG | TGTCAGCCCTGAGTGTCT | (Nusse et al., 2018) |
| *Atoh1* | AGCTTCCTCTGGGGGTTACT | TTCTGTGCCATCATCGCTGT | (Guo et al., 2018) |
| *Dclk1* | CAGCCTGGACGAGCTGGTGG | TGACCAGTTGGGGTTCACAT | (Gerbe et al., 2016) |
| *Villin1* | ATGACTCCAGCTGCCTTCTCT | GCTCTGGGTTAGAGCTGTAAG | (Moon et al., 2014) |
| *RegIIIy* | CAGACAAGATGCTTCCCCGT | GCAACTTCACCTTGCACCTG | (Guo et al., 2018) |
| *Camp* | CTTCAACCAGCAGTCCCTAGACA | TCCAGGTCCAGGAGACGGTA | (Natsuga et al., 2016) |
| *Il25* | ACAGGGACTTGAATCGGGTC | TGGTAAAGTGGGACGGAGTTG | (Von Moltke et al., 2016) |
| *Il33* | GTATTCCAACTCCAAGATTTCCC | CATGCAGTAGACATGGCAGA | (Nusse et al., 2018) |
| *Ccl20* | GCCTCTCGTACATACAGACGC | CCAGTTCTGCTTTGGATCAGC | (Price et al., 2018) |
| *H2Ab1* | TGCTACTTCACCAACGGGAC | ACGTACTCCTCCCGGTTGTA | Julie Worrell, University of Glasgow |
| *Myd88* | CTAGGACAAACGCCGGAACT | ATTAGCTCGCTGGCAATGGA | (Koliaraki et al., 2019) |
| *RegIIIB* | ATGGCTCCTACTGCTATGCC | GTGTCCTCCAGGCCTCTTT | (Todoric et al., 2020) |

**Table 2-5: qPCR primer sequences and sources**

### 2.19.2 *Hh* quantification qPCR

*Hh* DNA was quantified in faecal/caecal DNA samples by qPCR of the gene *CdtB* using forward primer TCGTCCAAAATGCACAGGTG and reverse primer CCGCAAATTGCAGCAATACTT (Ge et al., 2001) (IDT). To generate a standard curve, a serial dilution of *Hh* DNA was produced using DNA extracted from *Hh* bacterial cultures as described in Section 2.17.2, with a top concentration of 25ng/µL *Hh* DNA. All DNA samples were analysed in triplicate and added at 4µL per reaction for a total of 20ng DNA per reaction. Reaction mixtures, cycling parameters and reagents/equipment were as described in Section 2.19.1.

### 2.19.3 Bacterial DNA analysis of faecal samples

The relative abundance of bacterial genes specific to different phyla, genera and species were quantified in total faecal DNA samples. DNA was added at 4µL per reaction for a total of 20ng DNA per reaction and analysed in triplicate, with gene expression levels for each sample normalised to the pan-bacteria 16S gene. Differences in gene expression were determined using the $2^{-\Delta\Delta C(t)}$ method (Schmittgen and Livak, 2008). Reaction mixtures, cycling parameters and reagents/equipment were as described in Section 2.19.1. Primer sequences and source are listed in Table 2-6.

| Specificity | Forward sequence | Reverse sequence | Source |
|---|---|---|---|
| Pan-bacteria | CGGTGAATACGTTCCCGG | TACGGCTACCTTGTTACGACTT | (Doonan et al., 2019) |
| Bacteroidetes | GTTTAATTCGATGATACGCGAG | TTAAGCCGACACCTCACGG | |
| Firmicutes | GGAGCATGTGGTTTAATTCGAAGCA | AGCTGACGACAACCATGCAC | |
| Proteobacteria | TCGTCAGCTCGTGTCGTGA | CGTAAGGGCCATGATG | |
| Lactobacillaceae | TGGAAACAGGTGCTAATACCG | GTCCATTGTGGAAGATTCCC | |
| Bifidobacterium | CTCCTGGAAACGGGTGG | GGTGTTCTTCCCGATATCTACA | |
| *Escherichia coli* | GTTAATACCTTTGCTCATTG | ACCAGGGTATCTAATCCTGTT | |
| SFB | GACGCTGAGGCATGAGAGCAT | GACGGCACGGATTGTTATTCA | |

**Table 2-6: Bacterial DNA primer sequences and source**

# 2.20 Protein quantification from faecal samples

## 2.20.1 Stool processing

Faeces were collected from inside the colon and stored in 1mL sterile PBS at -80℃ until processing. Stool samples were homogenised in PBS using a TissueLyser twice for 1 min at 25Hz using a 5mm Stainless Steel Bead (both Qiagen). Stool samples were centrifuged at 12,000 G for 15 mins at 4℃ and supernatants were transferred to a new 1.5mL Eppendorf and stored at -80℃ for subsequent protein quantification.

## 2.20.2 BCA assay

The total protein content in faecal samples was measured by Pierce bicinchoninic acid (BCA) assay (Thermo Scientific) following the manufacturer's protocol for assaying in microplates. Faecal samples were assayed at 1/2 dilution while also performing the S100A8 ELISA described next, for the purpose of normalising S100A8 concentration to the total protein content per sample. Absorbance was measured at 562nm using a plate reader.

### 2.20.3 S100A8 ELISA

The concentration of S100A8 (Calprotectin subunit) in faecal samples was measured using the mouse S100A8 DuoSet ELISA kit (BioTechne) according to the manufacturer's instructions. Samples from non-DSS controls were assayed undiluted, while samples from DSS-treated mice were assayed between 1/10 and 1/1000 dilution. Absorbance was measured at 450nm/540nm using a plate reader. S100A8 protein concentrations were normalised to the total protein content per sample.

## 2.21 Histology

### 2.21.1 Processing, embedding, and sectioning

Approximately 1cm sections of proximal, mid, and distal colon were cut using a scalpel blade as depicted in Figure 2-1. Fat and stool were gently removed and samples were transferred to 10% neutral buffered formalin (Sigma-Aldrich) and fixed for 24h at RT, before being transferred to 70% ethanol for storage at RT until processing. Tissue was embedded into paraffin blocks and sectioned at 5µm thickness using a microtome. Sections were loaded onto positively charged slides and dried overnight at RT before being stored at 4℃ until staining. For the experiments in Chapter 3, samples were processed, embedded and sectioned by a Histology Technician from the University of Glasgow Cellular Analysis Facility.

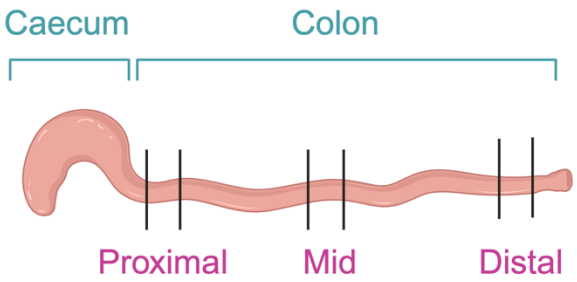


**Figure 2-1: Colon samples for histological examination**
Histology samples were taken from the proximal, mid, and distal colon to produce transverse sections. This illustration was created using BioRender.com.

### 2.21.2 H&E staining

Slides were incubated in an oven at 60℃ for 30-60 mins to melt the paraffin, before being deparaffinised and rehydrated through a series of incubations in xylene and a graded alcohol series (xylene 3 mins x2, 100% ethanol 3 mins x2, 90% ethanol 3 mins x2, 70% ethanol 3 mins x2, distilled water 2 mins). Slides were stained with Harris Haematoxylin for 2 mins before being rinsed in running water. Differentiation was carried out by incubating slides in 1% acid/alcohol, running water, and Scott's Tap Water Substitute for 30 secs each. Slides were then counter stained by first incubating in 70% ethanol and then in Eosin Y Stain 1% (alcoholic) for 30 secs and 3 mins, respectively. Slides were then dehydrated using the reverse graded alcohol series described above until incubation in xylene. Coverslips were mounted over tissue sections using DPX Mounting Medium. All reagents were obtained from CellPath. For the experiments in Chapter 3, H&E staining was performed by a Histology Technician from the University of Glasgow Cellular Analysis Facility.

### 2.21.3 Histological colitis scoring

Following H&E staining, slides were digitized using a NanoZoomer slide scanner (Hamamatsu) and sections were viewed using Aperio ImageScope software (Leica Biosystems). Colon histopathology was assessed in a blinded, semiquantitative fashion as described (Forster et al., 2022). Scores from the mid and distal colon were averaged to provide a mean histology score between 0 and 12 for each mouse, with 12 being the most severe and 0 showing no pathology. A summary of the histological scoring scheme is provided in Table 2-7.

| A | **Epithelium** | Hyperplasia | and/or | Goblet Cell Depletion | and/or | Loss of epithelial cells | | |
|---|---|---|---|---|---|---|---|---|
| | 0 | None | | None | | None | | |
| | 1 | Mild (1.5X) | | Mild (25%) | | Mild | | |
| | 2 | Moderate (2-3X) | | Marked (25-50%) | | Marked | | |
| | 3 | Severe (>3X) | | Substantial (>50%) | | Substantial | | |
| **B** | **Inflammation in lamina propria** | | | | | | | |
| | 0 | None - few leukocytes | | | | | | |
| | 1 | Mild - some increase in leukocytes at tips of crypts OR many lymphoid follicles | | | | | | |
| | 2 | Moderate - marked infiltrate (notable broadening of crypt) | | | | | | |
| | 3 | Severe - dense infiltrate throughout | | | | | | |
| **C** | **Area affected (% of section)** | | | | | | | |
| | 0 | None | | | | | | |
| | 1 | Up to 25% | | | | | | |
| | 2 | 25-50% | | | | | | |
| | 3 | >50% | | | | | | |
| **D** | **Markers of severe inflammation** | Loss of crypt structure | and/or | Submucosal inflammation | and/or | Edema | and/or | Crypt abscesses |
| | 0 | None | | None | | None | | None |
| | 1 | Mild | | Mild | | Mild | | Few (<5) |
| | 2 | Marked | | Marked | | Marked | | Many |
| | 3 | Substantial | | - | | - | | - |

**Table 2-7: Histological scoring scheme**
Each category is scored between 0-3. High scores are achieved either due to additive scores of multiple factors (e.g. moderate hyperplasia AND marked goblet cell depletion in category A) or due to the severe manifestation of one factor in the category (e.g. substantial crypt structure loss in category D).

## 2.22 Bulk RNA sequencing and analysis

RNA was extracted from epithelial crypts as described (Section 2.15.2) and mRNA libraries prepared with poly A enrichment by Novogene, UK. Bulk RNA sequencing was performed using the Illumina Sequencing platform with PE150 (Novogene). The DESeq2 package was used for differential gene expression analysis in R studio. Unless indicated otherwise, all analyses were performed by John Cole, University of Glasgow, using Searchlight software in R studio (Cole et al., 2021).

## 2.23 Statistical analyses

Flow cytometry analysis was performed using FlowJo software (Treestar). With the exception of RNA sequencing analysis, all statistical analyses were performed using GraphPad Prism software. Data are shown as mean and standard deviation. For comparisons with two variables, statistical differences were calculated using a two-way ANOVA with multiple comparisons. For comparisons with one variable, data were tested for normality using the Shapiro-Wilk normality test. Where data were normally distributed, a Student's t-test was used for comparisons between two groups and a one-way ANOVA with Tukey's multiple comparisons correction was used for comparisons between multiple groups. Where data were not normally distributed, a Mann Whitney U test (two groups) or a Kruskall-Wallis test with Dunn's multiple comparisons correction (multiple groups) were used. Significance was determined based on *p*-value where *$p < 0.05$, **$p < 0.01$, ***$p < 0.001$, ****$p < .0001$.

## 2.24 Illustrations

All illustrations were created using BioRender.com with an academic subscription.

# 3 *Helicobacter hepaticus* attenuates disease in the DSS colitis model

## 3.1 Introduction

Much of the research surrounding *Hh* focusses on its ability to trigger IBD-like inflammation in genetically susceptible hosts. However, immune competent animals tolerate the infection long-term, without induction of pathogenic inflammation (Cahill et al., 1997).There is evidence that *Hh* drives strong regulatory responses, both by induction of *Hh*-specific Tregs (Xu et al., 2018) and effects on the innate compartment, including macrophages (Danne et al., 2017). These regulatory effects are thought to counterbalance the induction of pro-inflammatory responses, including Th1 and Th17 induction, thereby allowing a dominant tolerance to be established.

The intestinal microbiota is known to play a key role in the development of various human diseases, most notably IBD, but not limited to those affecting the gut (Gilbert et al., 2016, Erickson et al., 2012, Willing et al., 2010, Miyauchi et al., 2023). It is also becoming increasingly evident that the microbiota can be protective against disease. Much research has attempted to identify specific bacterial species and families which play either a disease-driving or protective role in different settings (Roy et al., 2017, Forster et al., 2022, Surana and Kasper, 2017) but the nature of these interactions and the mechanisms behind them are not fully understood. Species such as *Hh* are termed ‘pathobionts’, referring to microbes which normally behave as commensals but have the capacity to drive inflammation in certain contexts (Jeffery et al., 2022). These species are known to actively engage the immune system and alter intestinal homeostasis in a context-dependent manner. In the case of *Hh*, immune competent hosts produce *Hh*-specific antibodies (Nilsson et al., 2000) and T cell responses (Xu et al., 2018, Kedmi et al., 2022, Kullberg et al., 2002), as well as recognising the bacteria through a range of innate pathogen recognition receptors (PRRs) (Asquith et al., 2010, Boulard et al., 2010, Sterzenbach et al., 2007). This constant level of immune activity in response to *Hh* suggests there is a crosstalk of interactions which occurs between the bacteria and host.

We hypothesised that this relationship may have evolved to have beneficial outcomes for the host. We chose to test this using the DSS model of IBD, in which the epithelial barrier in the colon is chemically damaged resulting in a massive inflammatory response targeted against the microbiota (Kiesler et al., 2015). It is well known that the disease severity in this model is dependent on the microbiota (Forster et al., 2022, Hernández-Chirlaque et al., 2016) but the effect of *Hh* in this setting has not yet been described.

## 3.2 Aims

In this chapter I aimed to set up two methods of *Hh* infection, the first a natural infection by microbiota transfer, and the second a direct infection with a well characterised *Hh* type strain (Ward et al., 1994, Kullberg et al., 2002). I then aimed to test how colonization with *Hh* affected the outcome of a disease challenge in the gut. For this purpose, I used the DSS model of colitis. I quantified disease activity using clinical parameters and histopathological analysis and then determined the effect of *Hh* infection and disease challenge on immune cell populations in the gut, focussing on innate myeloid cells which are known to be the drivers of DSS colitis (Stevceva et al., 2001). Finally, I aimed to determine whether the timepoint following *Hh* infection had an impact on the effect against disease outcome.

## 3.3 Results

### 3.3.1 The effect of microbiota transfer on DSS-induced disease

As many laboratory mouse colonies are naturally infected with Hh (Shames et al., 1995), we first aimed to establish whether animals housed at the University of Glasgow were *Hh* colonized. We used PCR to screen stool from various colonies and identified several harbouring the *Hh*-specific gene *p25* (Feng et al., 2005) (data not shown). We also confirmed that C57BL/6 mice supplied by Envigo were PCR negative for both general *Helicobacter* spp., based on the presence of *Helicobacter*-specific 16S rRNA, and *Hh* (data not shown). In addition to being colonized with *Hh*, we reasoned that the mice bred at the University would contain a more diverse microbiota than the mice bred by Envigo under Specific Pathogen Free (SPF) conditions. We chose to study the effects of this

microbiota containing natural *Hh* colonization by utilising a model of microbiota transfer through co-housing. We co-housed C57BL/6 SPF mice obtained from Envigo with a *Hh*-colonized microbiota donor from the University facility and found that by day 7, the recipient mice were all PCR positive for *Hh p25* (Figure 3-1A-B). We then used these C57BL/6 *Hh*$^+$ microbiota primary recipients as donors for subsequent microbiota transfer experiments (Figure 3-1C).

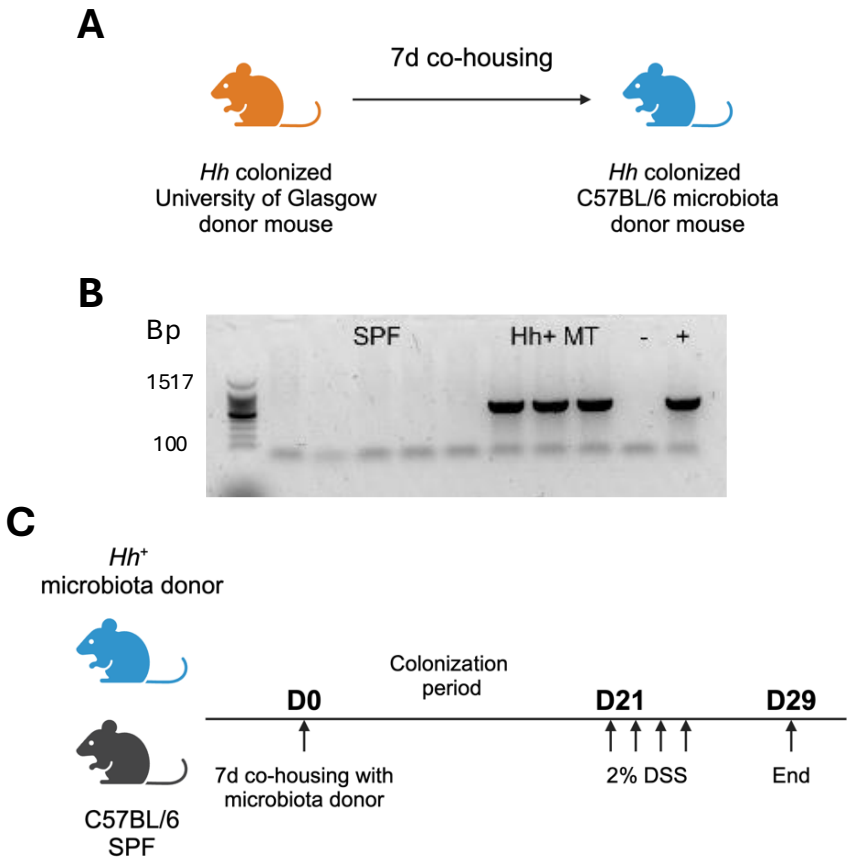


**Figure 3-1: Schematic of *Hh*$^+$ microbiota transfer and DSS treatment**
C57BL/6 mice were co-housed with *Hh*-colonized University of Glasgow donor mice for 7-days and used as microbiota donors for subsequent experiments (A). Experimental mice were co-housed with *Hh*$^+$ microbiota donors for 7-days and stool samples screened for the presence of *Hh* DNA using PCR of the *Hh*-specific gene *p25*. PCR amplicons were assessed for *p25* presence using gel electrophoresis (B). Following co-housing, mice were left for a further 14-days to allow bacterial colonization. On day 21 mice were administered 2% DSS in drinking water or given normal water as controls. After 4 days all mice were switched back to normal water for a final 4 days (C).

Following 7 days in which experimental mice were either left as naïve controls or co-housed with *Hh*$^+$ microbiota donors, mice were left for a further 2 weeks to allow the transferred *Hh*$^+$ microbiota to stabilise. We then determined whether mice which received this *Hh*$^+$ microbiota transfer (MT) had an altered response when challenged with DSS to induce colitis. Mice were treated with 2% DSS for 4 days before being returned to normal drinking water for a final 4 days (Figure 3-1C). At this timepoint, the inflammation caused by DSS is driven primarily by

myeloid cells, including gut infiltrating monocytes and neutrophils (Stevceva et al., 2001).

Mice treated with DSS were assessed daily for clinical symptoms, including stool consistency, bleeding, general appearance, and weight loss. We found that mice which had received *Hh*$^+$ MT had significantly reduced disease activity based on these parameters (Figure 3-2A). DSS treatment caused substantial weight loss in naïve animals, with many mice losing ~20% of their starting weight. In comparison, *Hh*$^+$ MT recipients were protected against severe weight loss, and many had returned almost to their starting weight by the end of the experiment (Figure 3-2B).

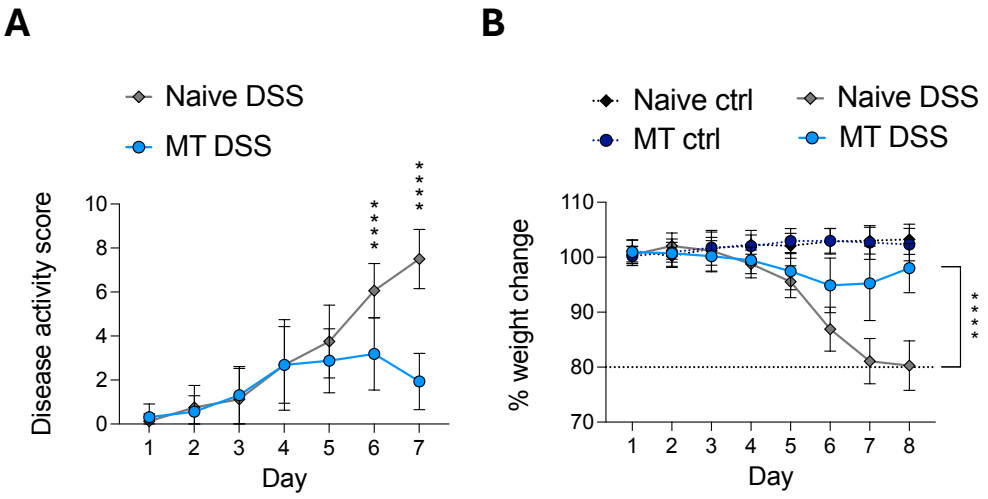


**Figure 3-2: *Hh*$^+$ microbiota transfer attenuates DSS-induced clinical disease**
C57BL/6 littermate cohorts were left untreated (Naïve) or colonized with *Hh*$^+$ microbiota (MT) and then administered 2% DSS in drinking water, as described in Fig.1B. Following DSS administration mice were assessed daily for clinical disease activity (A) and weight change (B). Data are shown as mean ± SD and pooled from 3 independent experiments with n=4-6 per experiment. Statistical significance was determined by 2-way ANOVA (significance *p< 0.05, **p<0.01, ***p< 0.001, ****p< .0001). In (B) the statistical significance is shown for day 8.

We next assessed the colon for immune cell populations, as this is the key site of DSS-induced disease (Wirtz et al., 2007). Colons were enzymatically digested and immune cells identified by flow cytometry (Figure 3-3). We focussed on the myeloid compartment because of the role of these cells in DSS-induced pathology (Bento et al., 2012). Neutrophils were identified as CD11b$^+$Ly6G$^+$ and monocytes and macrophages as CD11b$^+$CD64$^+$. The CD64$^+$ population was then divided into monocytes, intermediate monocyte-macrophages, and mature macrophages based on expression of Ly6C and MHCII (Bain and Mowat, 2014).

Conventional dendritic cells (cDCs) were $CD64^{-}CD11c^{+}MHCII^{+}$ (Langlet et al., 2012) and eosinophils were $CD11b^{+}Ly6G^{-}MHCII^{-}$ cells with high side-scatter, indicating high granularity (Bain et al., 2018). Initially our colon digests yielded low cell numbers (<$5x10^{6}$ cells isolated per colon), even from DSS-treated samples (Figure 3-4A), but the digests were optimised by switching from frozen aliquots of diluted enzymes to using fresh enzymes and this greatly improved the cell yields. In later experiments cell yields were mostly >$5x10^{6}$, per colon, with most DSS samples yielding ~$1x10^{7}$ cells (Figure 3-4A). Isolated cells were generally more than 60% viable, with comparable viability between groups, apart from a small increase in viability of naïve DSS samples compared to naïve controls (Figure 3-4B). Immune cells were identified as $CD45^{+}$, and their proportion and numbers were greatly increased in the DSS-treated groups, with no difference between naïve and MT (Figure 3-4C). CD11b is expressed by granulocytes, monocytes, macrophages, and certain subsets of cDC in the colon. The proportion of $CD11b^{+}$ cells was also greatly increased following DSS treatment, but this was significantly less in the *Hh*$^{+}$ MT group compared to naïve (Figure 3-4D). This difference was not reflected in the absolute number of CD11b expressing cells, although upon pooling the data the low cell yields from earlier experiments may have affected this (Figure 3-4D).

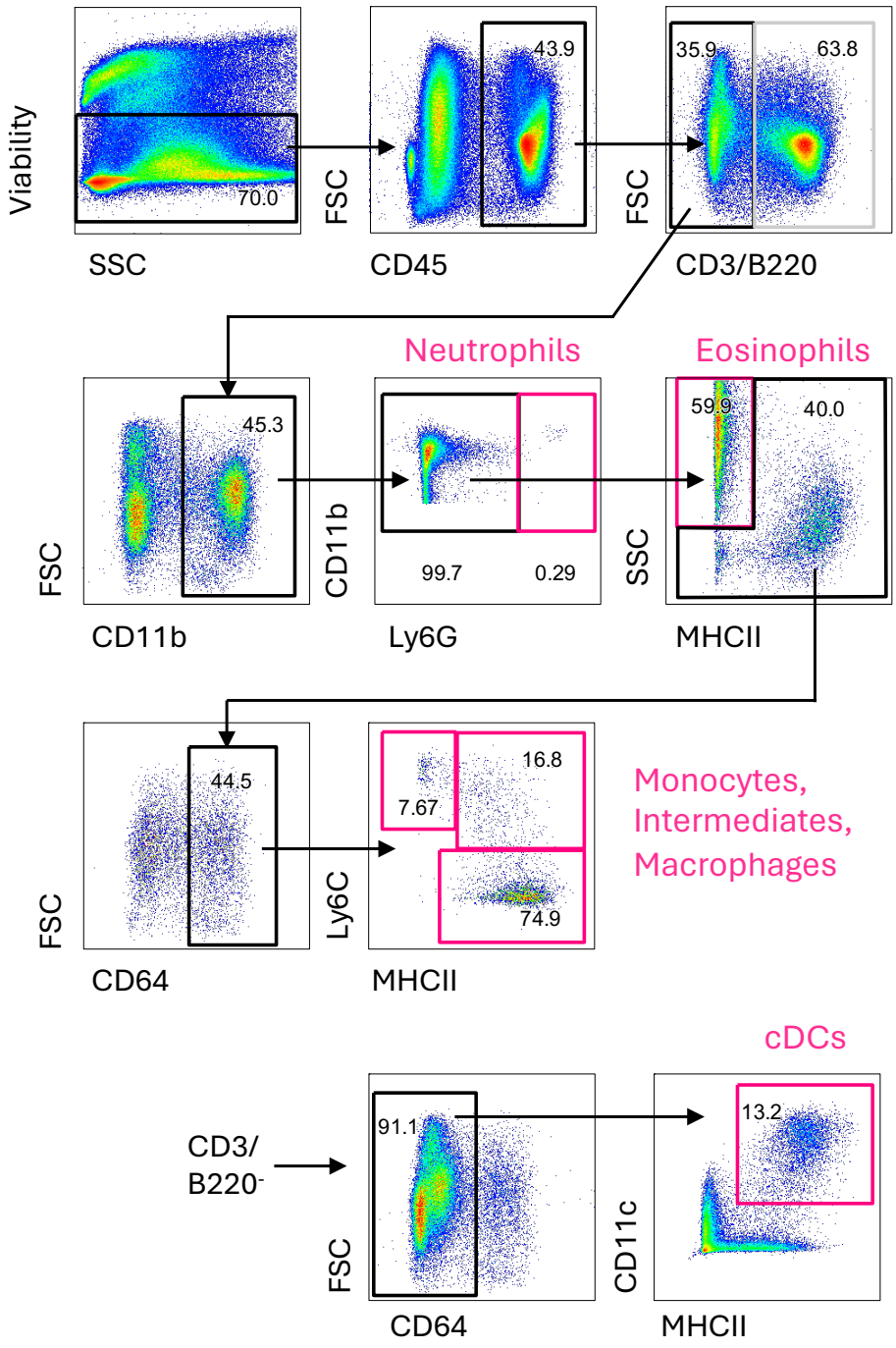


**Figure 3-3: Gating strategy for identification of intestinal myeloid cell subsets**
Single cells were pre-selected and myeloid subsets first identified as live, CD45$^{+}$, CD3$^{-}$, B220$^{-}$. Neutrophils, eosinophils, and monocyte-macrophages were CD11b$^{+}$. Neutrophils were Ly6G$^{+}$ and eosinophils were MHCII$^{-}$ with high side scatter (SSC). Monocyte-macrophages were CD64$^{+}$ and further divided based on expression of Ly6C and MHCII. cDCs were CD64$^{-}$, CD11c$^{+}$, MHCII$^{+}$. Dot plots are shown from 1 representative naïve sample.

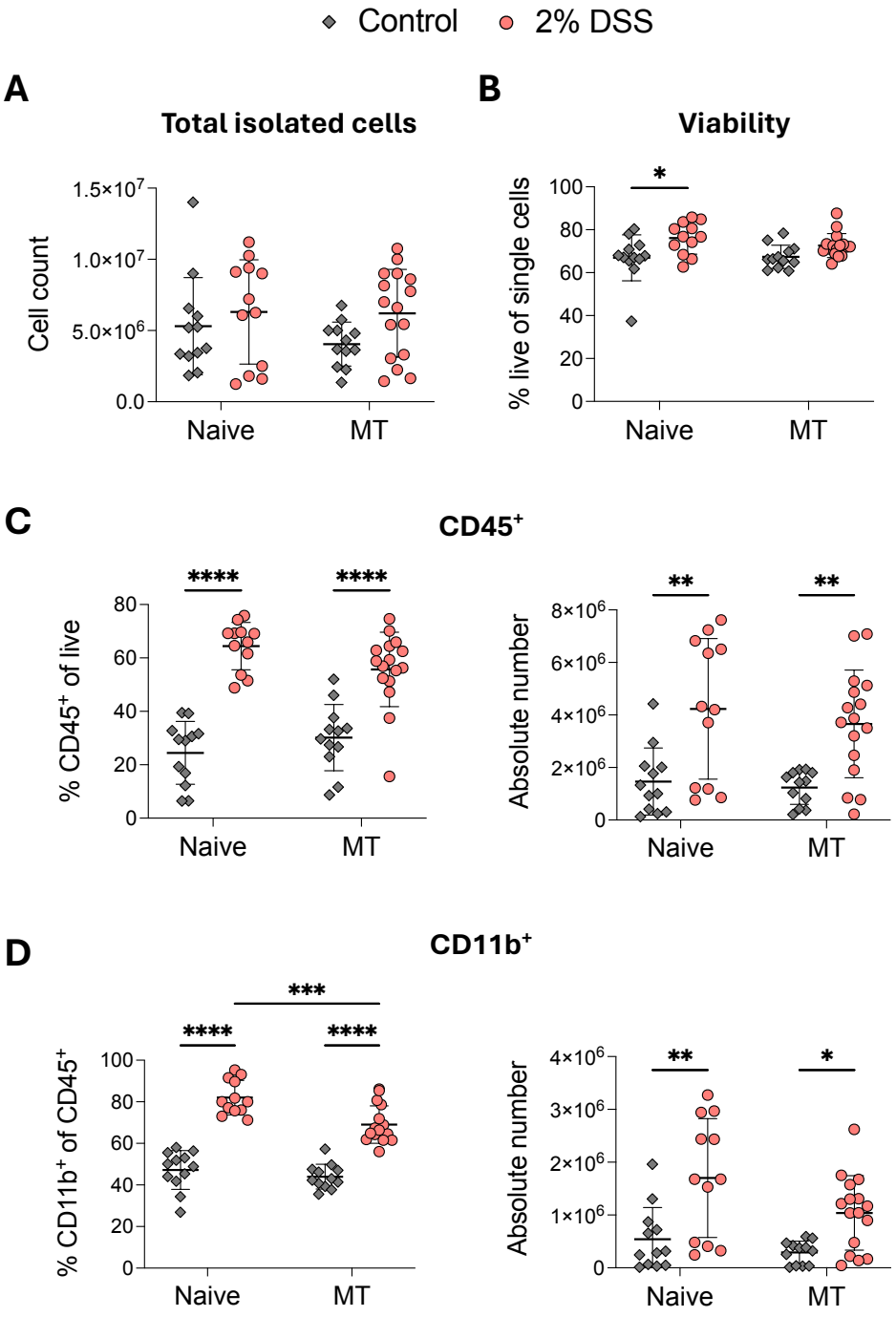


**Figure 3-4: DSS treatment drives colonic immune infiltration**
C57BL/6 littermate cohorts were left untreated (Naïve) or colonized with *Hh*$^+$ microbiota (MT) and then administered 2% DSS in drinking water, as described in Fig.1B. Colonic LP leukocytes were isolated using enzymatic digestion and the total isolated cells counted manually using trypan blue (A). Cells were assessed by flow cytometry for viability (B) and the frequency and absolute number of CD45$^+$ (C) and CD11b$^+$ (D) cells were calculated. Data are shown with mean ± SD and pooled from 3 independent experiments with n=4-6 per experiment. Statistical significance was determined by 2-way ANOVA (significance *p< 0.05, **p<0.01, ***p< 0.001, ****p< .0001).

We next confirmed that there was significant neutrophil accumulation in the colon following DSS treatment (Figure 3-5), as previously reported (Stevceva et al., 2001). However, DSS-induced neutrophil infiltration was significantly attenuated in the *Hh*$^+$ MT group, both in terms of cell proportion and number

(Figure 3-5). Similarly, there was a significant increase in colonic monocytes following DSS treatment, which was again significantly attenuated in the group which had received *Hh*$^+$ MT (Figure 3-6). In the gut, the macrophage population is largely replenished by bone-marrow derived monocytes. These cells are recruited at a higher rate during inflammation and once in the gut begin to differentiate into mature macrophages via an intermediate stage (Bain et al., 2013). The proportion and number of intermediate cells was increased following DSS treatment, but the number of these cells was significantly reduced in the *Hh*$^+$ MT group (Figure 3-7A). We observed a proportional decrease in mature macrophages following DSS treatment, due to the reciprocal increase in monocytes and intermediate cells within the CD64$^+$ population (Figure 3-7B). However, no differences in the number of mature macrophages were observed between any of the groups (Figure 3-7B). There were also no differences in the proportion or number of colonic cDCs between treatment groups (Figure 3-8). Finally, we saw significant increases in the number of eosinophils in the colon following DSS treatment, which was comparable between both the naïve and *Hh*$^+$ MT groups (Figure 3-9).

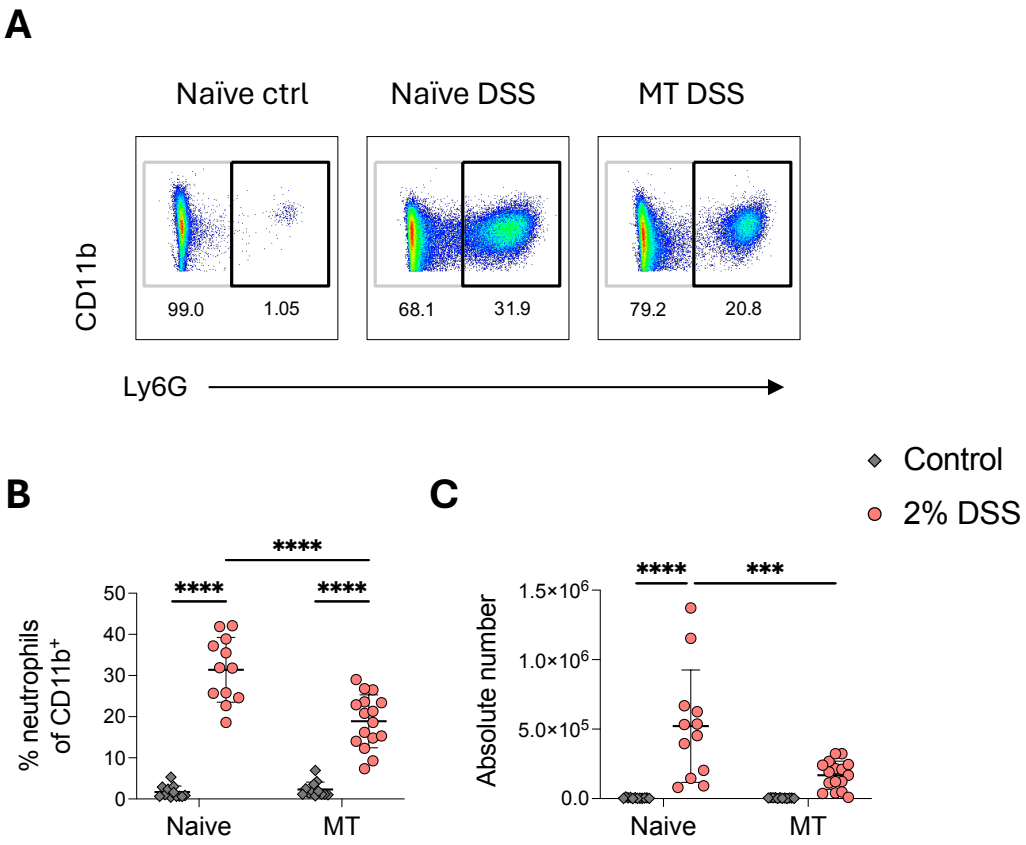


**Figure 3-5: *Hh*$^+$ microbiota transfer attenuates DSS-induced neutrophil infiltration**
C57BL/6 littermate cohorts were left untreated (Naïve) or colonized with *Hh*$^+$ microbiota (MT) and then administered 2% DSS in drinking water, as described in Fig.1B. Representative dot plots of colonic CD11b$^+$Ly6G$^+$ neutrophils (A), quantification of neutrophil frequencies (B) and absolute numbers (C) are shown. Data are shown with mean ± SD and pooled from 3 independent experiments with n=4-6 per experiment. Statistical significance was determined by 2-way ANOVA (significance *p< 0.05, **p<0.01, ***p< 0.001, ****p< .0001).

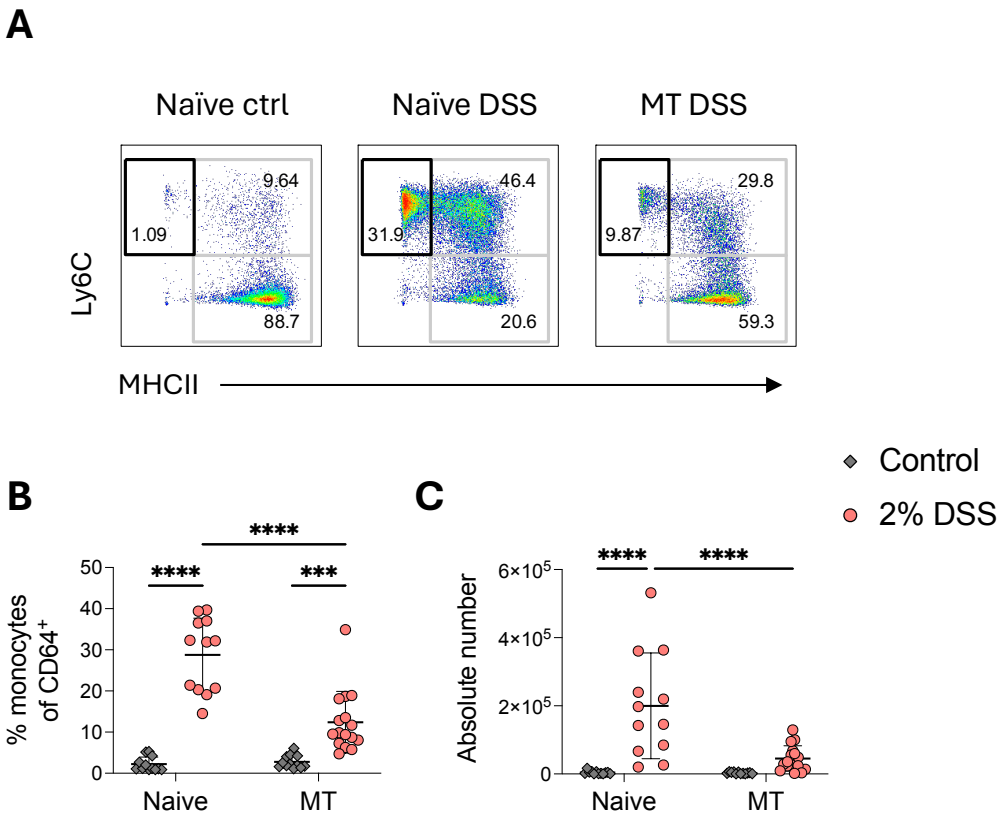


**Figure 3-6: *Hh*$^{+}$ microbiota transfer attenuates DSS-induced monocyte infiltration**
C57BL/6 littermate cohorts were left untreated (Naïve) or colonized with *Hh*$^{+}$ microbiota (MT) and then administered 2% DSS in drinking water, as described in Fig.1B. Representative dot plots of colonic CD11b$^{+}$CD64$^{+}$ monocyte-macrophages divided by expression of Ly6C and MHCII (A), quantification of Ly6C$^{+}$MHCII$^{-}$ monocyte frequencies (B) and absolute numbers (C) are shown. Data are shown with mean ± SD and pooled from 3 independent experiments with n=4-6 per experiment. Statistical significance was determined by 2-way ANOVA (significance *p< 0.05, **p<0.01, ***p< 0.001, ****p< .0001).

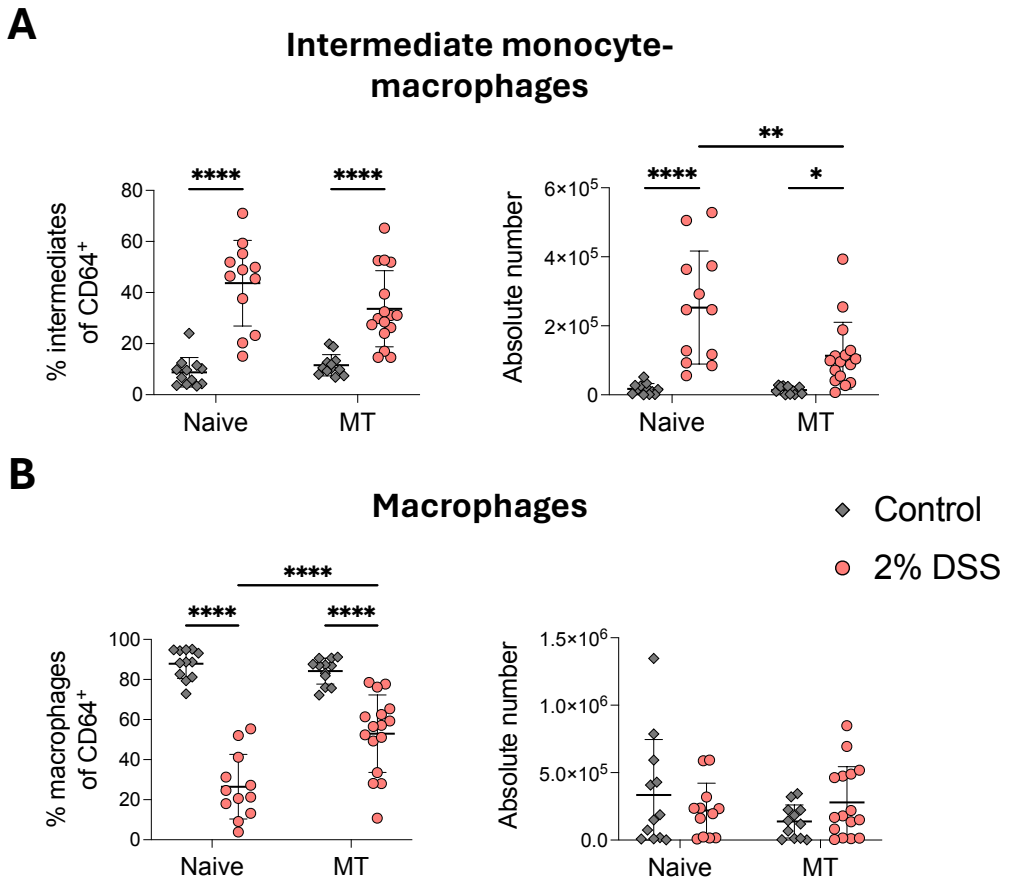


**Figure 3-7: Changes to intermediate and mature macrophages following *Hh*$^{+}$ microbiota transfer and DSS treatment**
C57BL/6 littermate cohorts were left untreated (Naïve) or colonized with *Hh*$^{+}$ microbiota (MT) and then administered 2% DSS in drinking water, as described in Fig.1B. The frequency and absolute number of colonic Ly6C$^{+}$MHCII$^{+}$ intermediate monocyte-macrophages (A) and Ly6C$^{-}$MHCII$^{+}$ mature macrophages (B) are shown. Data are shown with mean ± SD and pooled from 3 independent experiments with n=4-6 per experiment. Statistical significance was determined by 2-way ANOVA (significance *p< 0.05, **p<0.01, ***p< 0.001, ****p< .0001).

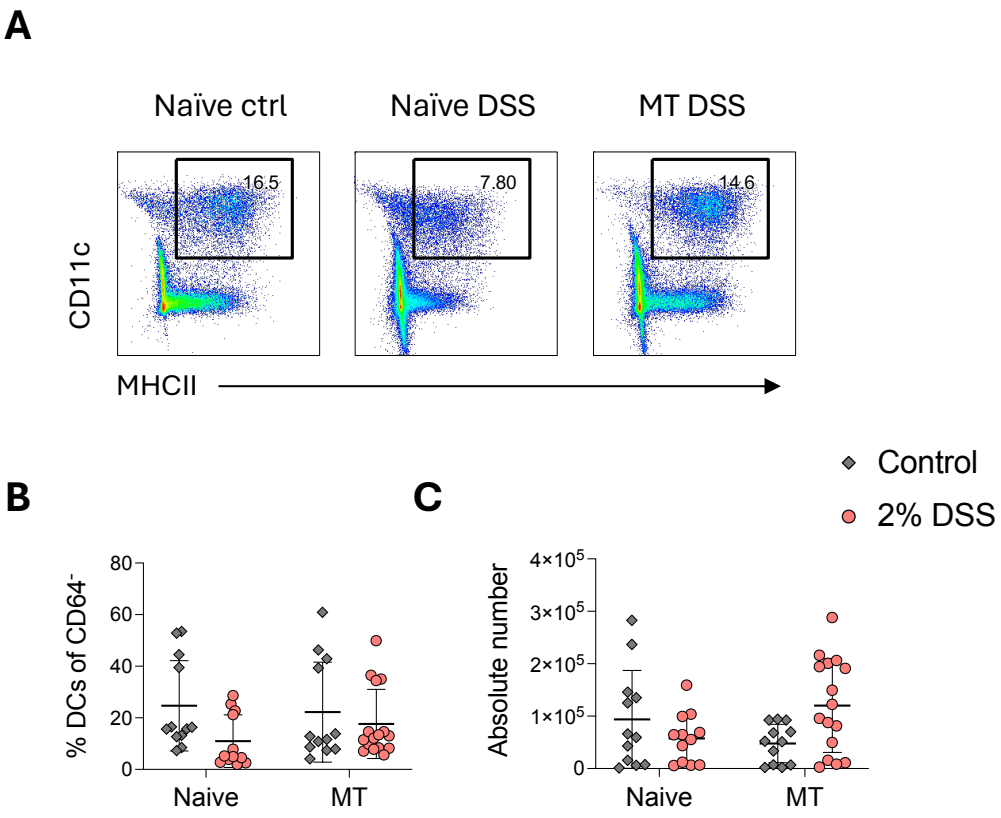


**Figure 3-8: *Hh*$^+$ microbiota transfer and DSS treatment do not alter colonic cDC**
C57BL/6 littermate cohorts were left untreated (Naïve) or colonized with *Hh*$^+$ microbiota (MT) and then administered 2% DSS in drinking water, as described in Fig.1B. Representative dot plots of colonic CD64$^-$CD11c$^+$MHCII$^+$ cDCs (A), quantification of cDC frequencies (B) and absolute numbers (C) are shown. Data are shown with mean ± SD and pooled from 3 independent experiments with n=4-6 per experiment. Statistical significance was determined by 2-way ANOVA (significance *p< 0.05, **p<0.01, ***p< 0.001, ****p< .0001).

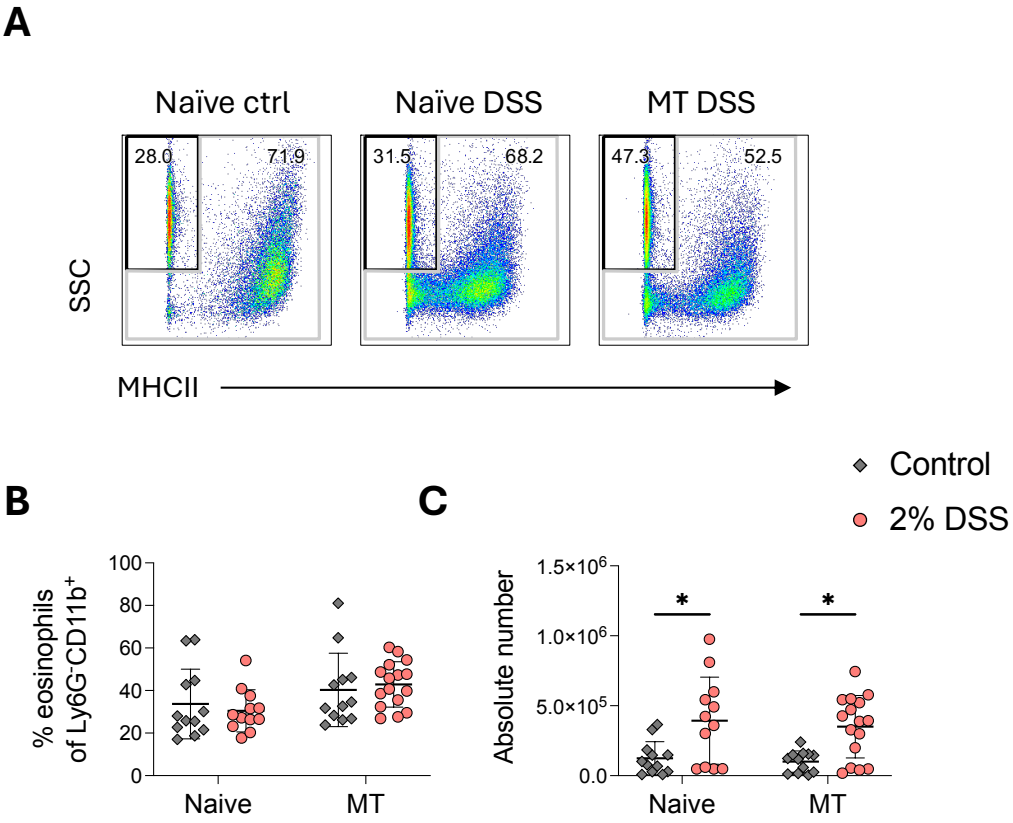


**Figure 3-9: *Hh*⁺ microbiota transfer does not alter DSS-induced eosinophil accumulation**
C57BL/6 littermate cohorts were left untreated (Naïve) or colonized with *Hh*⁺ microbiota (MT) and then administered 2% DSS in drinking water, as described in Fig.1B. Representative dot plots of colonic $CD11b^{+}SSC^{hi}MHCII^{-}$ eosinophils (A), quantification of eosinophil frequencies (B) and absolute numbers (C) are shown. Data are shown with mean ± SD and pooled from 3 independent experiments with n=4-6 per experiment. Statistical significance was determined by 2-way ANOVA (significance *p< 0.05, **p<0.01, ***p< 0.001, ****p< .0001).

These data demonstrate that transfer of a microbiota containing *Hh* was able to lessen the clinical severity of DSS-induced disease. Furthermore, the inflammatory infiltrate was significantly reduced in DSS-treated *Hh*⁺ MT recipients. These mice showed reduced numbers of colonic neutrophils and monocytes following DSS treatment, suggesting that the extent of inflammation was attenuated. At this stage, we reasoned that the differences in the *Hh*⁺ MT group may be caused by *Hh* acting alone, by *Hh* acting in conjunction with other species in the transferred microbiota, or in a *Hh*-independent manner as a result of a different element of the donor microbiota. We therefore next sought to determine whether *Hh* colonization was sufficient to drive the protection against DSS-induced disease.

### 3.3.2 *Hh* colonization is sufficient to protect against DSS-induced disease

To test the specific effects of *Hh* on disease outcome, we set up a model of direct *Hh* infection. For this purpose, we used a type strain of *Hh* which has been well characterised (Ward et al., 1994, Kullberg et al., 2002). We cultured the bacteria microaerophillically as described (Maloy et al., 2003) and C57BL/6 SPF mice were either inoculated by oral gavage with one dose of $1x10^8$ CFU *Hh* or given sterile PBS (Figure 3-10A). As in the *Hh*$^+$ MT system, we left the mice for 21 days to allow *Hh* to fully establish colonization before beginning DSS treatment. Firstly, we assessed if levels of *Hh* colonization were comparable between the *Hh*$^+$ MT and direct *Hh* infection recipients, by quantifying *Hh* levels in caecal contents using qPCR of the *Hh*-specific gene *CdtB* (Ge et al., 2001). We observed no difference in levels of *Hh* DNA between mice which had received *Hh*$^+$ MT and mice which had been directly infected by oral gavage with *Hh* (Figure 3-10B). *Hh* levels were also not affected by DSS treatment (Figure 3-10B).

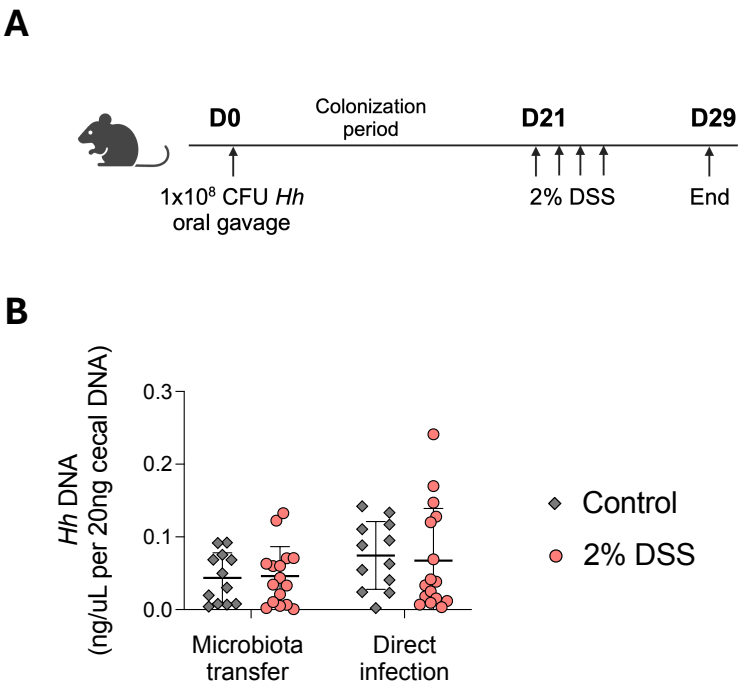


**Figure 3-10: *Hh* colonization by direct infection**
C57BL/6 littermates were administered 1x10$^8$ CFU *Hh* or given PBS by oral gavage and left for 21 days to allow bacterial colonization. On day 21 mice were administered 2% DSS in drinking water or given normal water as controls. After 4 days all mice were switched back to normal water for a final 4 days (A). *Hh* colonization was quantified in caecal content by qPCR of *CdtB* (B). *Hh* colonization was also quantified in C57BL/6 littermate cohorts colonized with *Hh*$^+$ microbiota (MT) and then administered 2% DSS in drinking water, as described in Fig.1B. Data are shown with mean ± SD and pooled from 3 independent experiments with n=4-6 per experiment. Statistical significance was determined by 2-way ANOVA (significance *p< 0.05, **p<0.01, ***p< 0.001, ****p< .0001).

As previously, the mice were monitored for symptoms of DSS-induced disease. The PBS-treated group showed significant disease activity following DSS treatment, combined with substantial weight loss (Figure 3-11A-B). In comparison, the group colonized with *Hh* displayed reduced clinical symptoms and significantly less weight loss (Figure 3-11A-B). We measured colon length as an additional indicator of disease severity, as inflammation causes a thickening of the colon tissue which results in shortening of total colon length (Yan et al., 2009). We observed significantly reduced colon lengths in both DSS-treated groups, although to a significantly lesser extent in the *Hh* infected animals (Figure 3-11C). We carried out histological assessment of the mid and distal colon for intestinal pathology and identified samples in both DSS-treated groups which showed cardinal signs of inflammation, characterised by epithelial hyperplasia, leukocyte infiltration, loss of crypt structure, and oedema (Figure 3-12) (Wirtz et al., 2007, Bonfiglio et al., 2021). However, the *Hh* colonized group overall had a significantly decreased histology score compared to the PBS-

treated group, indicating that *Hh* colonization reduced DSS-induced intestinal pathology (Figure 3-12).

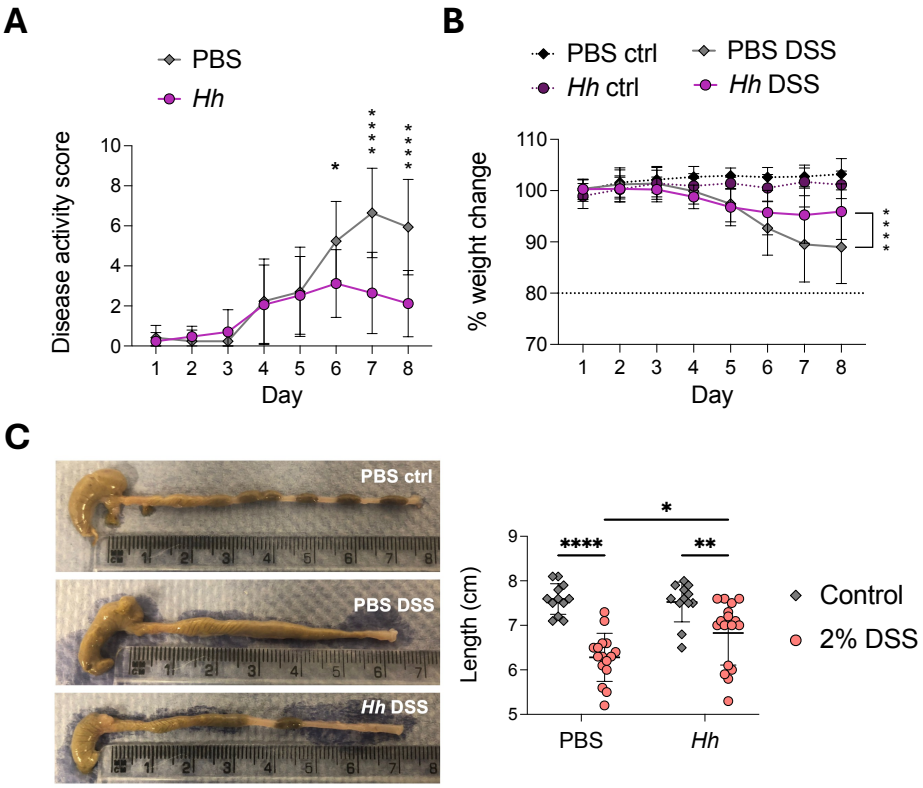


**Figure 3-11: *Hh* colonization attenuates DSS-induced disease**
C57BL/6 littermates were infected with 1x10$^8$ CFU *Hh* or given PBS by oral gavage and administered 2% DSS in drinking water. Following DSS administration mice were assessed daily for clinical disease activity (A) and weight change (B). Representative pictures of colon length are shown (C – left) with lengths quantified (C – right). Data are shown as mean ± SD and pooled from 3 independent experiments with n=4-6 per experiment. Statistical significance was determined by 2-way ANOVA (significance *p< 0.05, **p<0.01, ***p< 0.001, ****p< .0001). In (B) the statistical significance is shown for day 8.

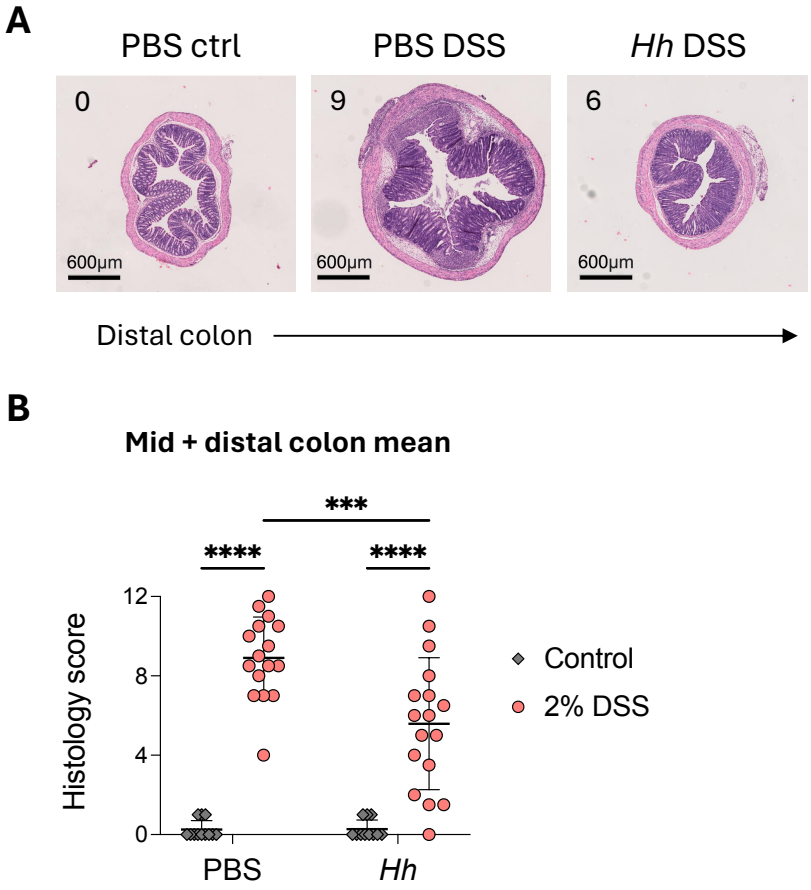


**Figure 3-12: *Hh* colonization attenuates DSS-induced intestinal inflammation**
C57BL/6 littermates were infected with 1x10$^8$ CFU *Hh* or given PBS by oral gavage and administered 2% DSS in drinking water. Representative H&E staining of the distal colon from untreated control (left), uninfected DSS (middle), and *Hh*-colonized DSS (right) mice are shown (A). Sections were scored blind for signs of histological inflammation and the mean scores from the mid and distal colon were quantified (B). The scores for the representative samples in (A) are shown in the top left of each image. Data are shown with mean ± SD and pooled from 3 independent experiments with n=4-6 per experiment. Statistical significance was determined by 2-way ANOVA (significance *p< 0.05, **p<0.01, ***p< 0.001, ****p< .0001).

Upon isolation of cells from the colon, we observed a significant increase in the total cell yield from both DSS-treated groups compared to untreated controls, although this was significantly less in the *Hh*-colonized group (Figure 3-13A). Viability of isolated cells was comparable between all treatment groups (Figure 3-13B). The numbers of CD45$^+$ immune cells and CD11b$^+$ myeloid cells were greatly increased in the colons of DSS-treated mice, but this accumulation was significantly lower in *Hh*-colonized DSS-treated mice (Figure 3-13C-D). Similarly, we found a clear reduction in the level of colonic neutrophil infiltration in *Hh*-infected DSS-treated mice compared to the DSS-treated controls (Figure 3-14). This was mirrored in the level of colonic monocytes, which were again significantly reduced in the *Hh*-infected DSS-treated group compared to the DSS-treated controls (Figure 3-15). The remaining CD64$^+$ cells were analysed, and

while there was an increase in the proportion of intermediate cells following DSS treatment, this was reciprocated with a proportional decrease of mature macrophages (Figure 3-16), as previously observed in Figure 3-7. While there were no proportional differences in the intermediate cells between both DSS-treated groups, they were significantly fewer in number in the *Hh*-colonized DSS-treated group (Figure 3-16A). However, the numbers of mature macrophages did not differ with *Hh* colonization (Figure 3-16B). Proportionally, there were no differences in cDC or eosinophil frequencies between any of the treatment groups, although both cell types increased in number following DSS treatment, and eosinophil numbers were reduced in *Hh*-infected DSS-treated group compared to the DSS-treated controls (Figure 3-17, Figure 3-18).

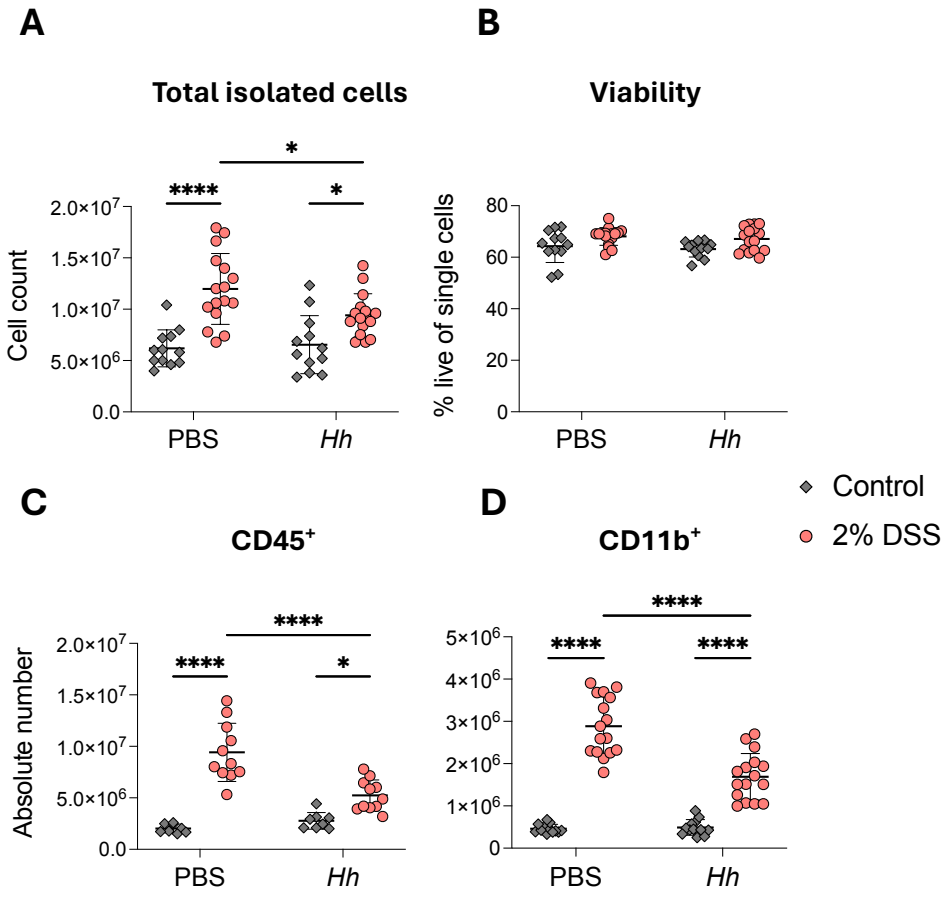


**Figure 3-13: *Hh* infection attenuates DSS-induced colonic leukocyte infiltration**
C57BL/6 mice were infected with 1x10$^8$ CFU *Hh* or given PBS by oral gavage and administered 2% DSS in drinking water. Colonic LP leukocytes were isolated using enzymatic digestion and the total isolated cells counted manually using trypan blue (A). Cells were assessed by flow cytometry for viability (B) and the absolute number of CD45$^+$ (C) and CD11b$^+$ (D) cells were calculated. Data are shown with mean ± SD and pooled from 3 independent experiments with n=4-6 per experiment. Statistical significance was determined by 2-way ANOVA (significance *p< 0.05, **p<0.01, ***p< 0.001, ****p< .0001).

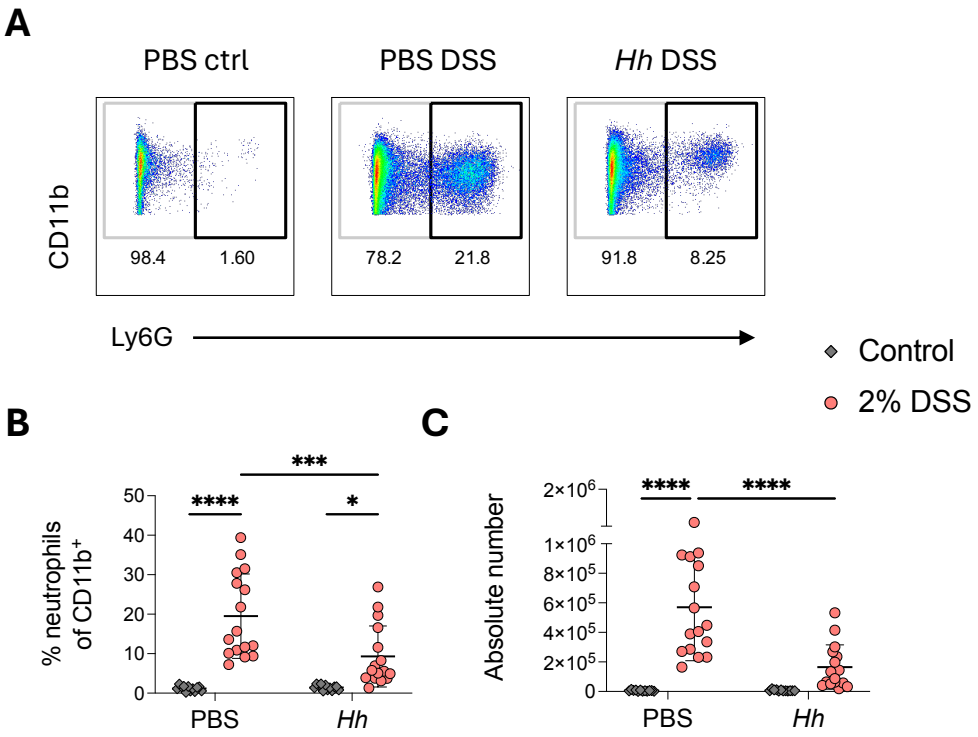


**Figure 3-14: *Hh* attenuates DSS-induced neutrophil infiltration in the colon**
C57BL/6 mice were infected with 1x10$^8$ CFU *Hh* or given PBS by oral gavage and administered 2% DSS in drinking water. Representative dot plots of colonic CD11b$^+$Ly6G$^+$ neutrophils (A), quantification of neutrophil frequencies (B) and absolute numbers (C) are shown. Data are shown with mean ± SD and pooled from 3 independent experiments with n=4-6 per experiment. Statistical significance was determined by 2-way ANOVA (significance *p< 0.05, **p<0.01, ***p< 0.001, ****p< .0001).

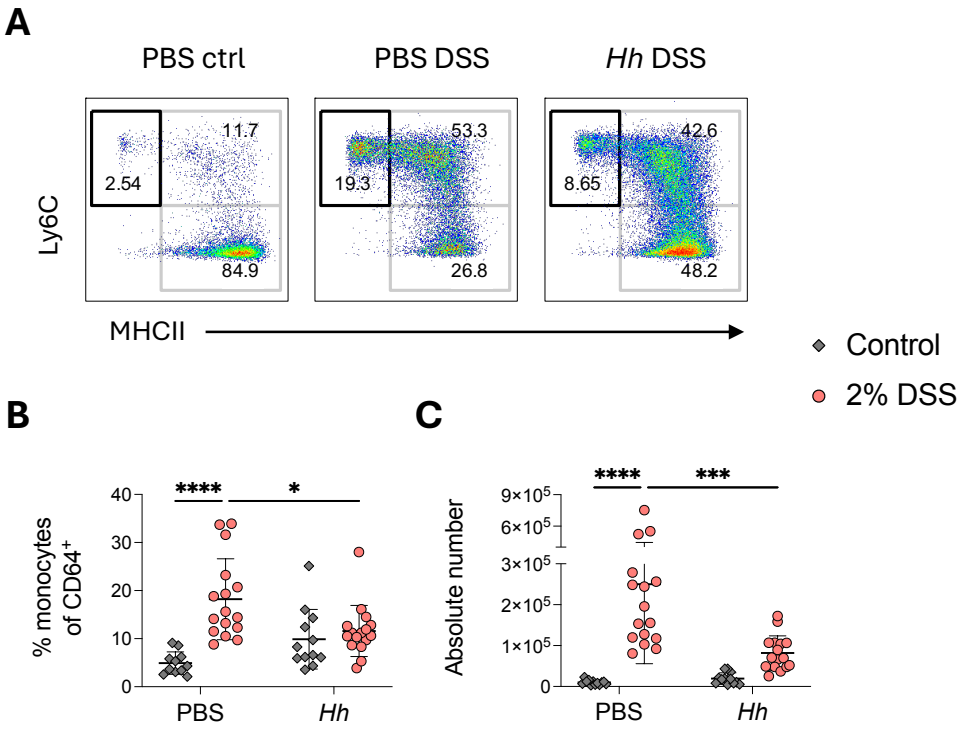


**Figure 3-15: *Hh* attenuates DSS-induced monocyte infiltration in the colon**
C57BL/6 mice were infected with 1x$10^8$ CFU *Hh* or given PBS by oral gavage and administered 2% DSS in drinking water. Representative dot plots of colonic $CD11b^+CD64^+$ monocyte-macrophages divided by expression of Ly6C and MHCII (A), quantification of $Ly6C^+MHCII^-$ monocyte frequencies (B) and absolute numbers (C) are shown. Data are shown with mean ± SD and pooled from 3 independent experiments with n=4-6 per experiment. Statistical significance was determined by 2-way ANOVA (significance *p< 0.05, **p<0.01, ***p< 0.001, ****p< .0001).

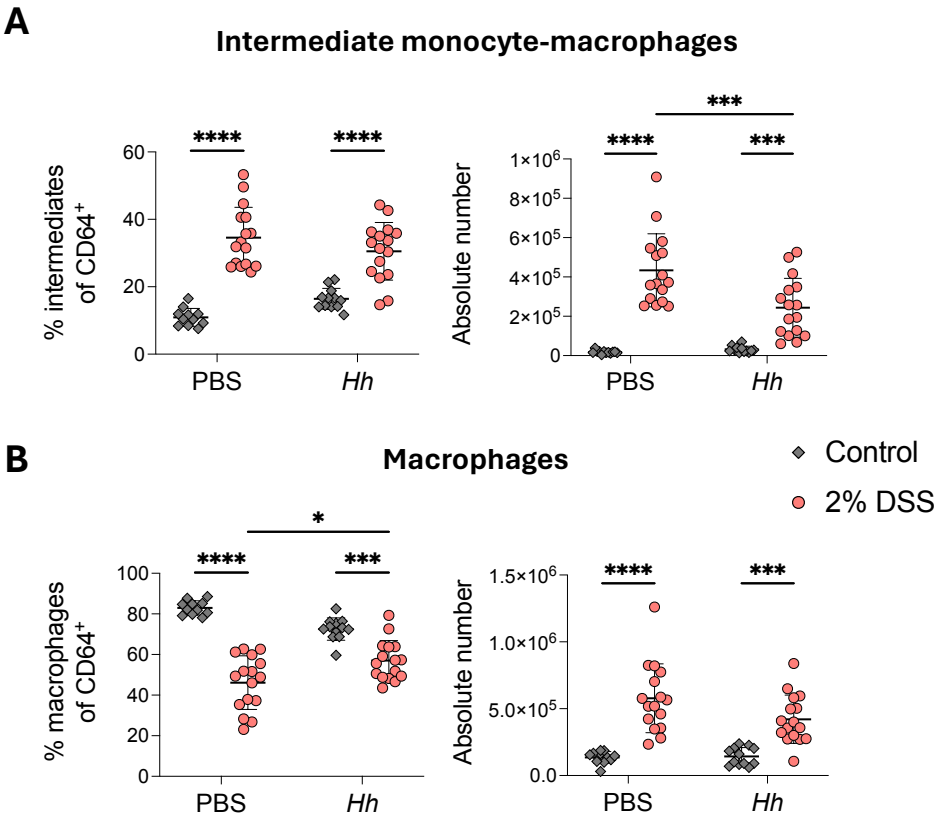


**Figure 3-16: Changes to intermediate monocyte-macrophages and mature macrophages in the colon following *Hh* colonization and DSS**
C57BL/6 mice were infected with 1x$10^8$ CFU *Hh* or given PBS by oral gavage and administered 2% DSS in drinking water. The frequency and absolute number of colonic Ly6C$^+$MHCII$^+$ intermediate monocyte-macrophages (A) and Ly6C$^-$MHCII$^+$ mature macrophages (B) are shown. Data are shown with mean ± SD and pooled from 3 independent experiments with n=4-6 per experiment. Statistical significance was determined by 2-way ANOVA (significance *p< 0.05, **p<0.01, ***p< 0.001, ****p< .0001).

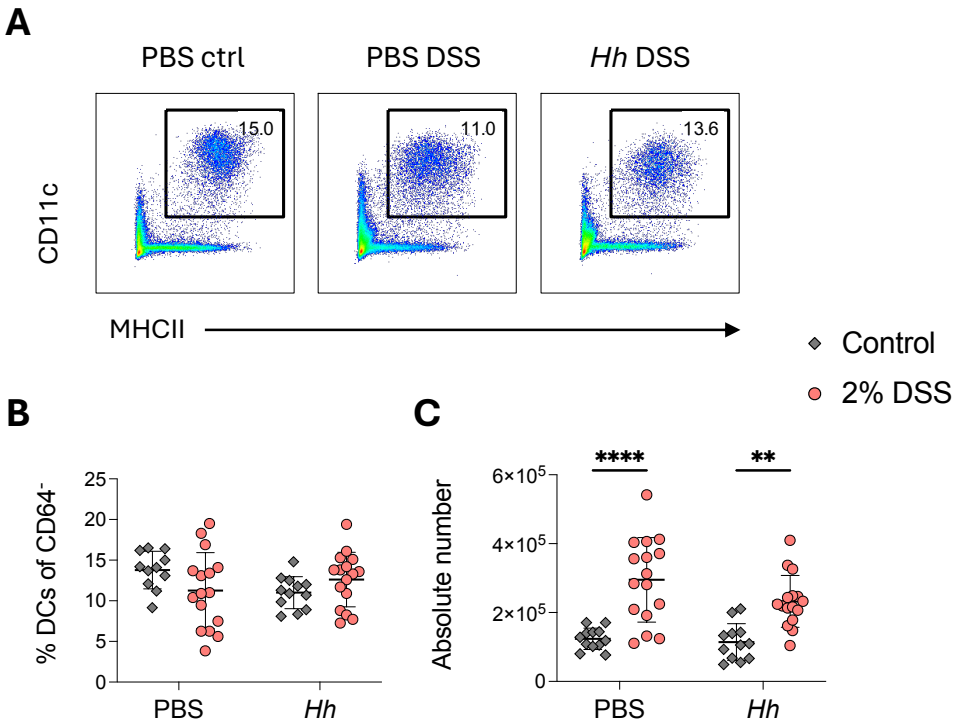


**Figure 3-17: *Hh* colonization has no impact on DSS-induced cDC accumulation in the colon**
C57BL/6 mice were infected with 1x$10^8$ CFU *Hh* or given PBS by oral gavage and administered 2% DSS in drinking water. Representative dot plots of $CD64^-CD11c^+MHCII^+$ colonic cDCs (A), quantification of cDC frequencies (B) and absolute numbers (C) are shown. Data are shown with mean ± SD and pooled from 3 independent experiments with n=4-6 per experiment. Statistical significance was determined by 2-way ANOVA (significance *p< 0.05, **p<0.01, ***p< 0.001, ****p< .0001).

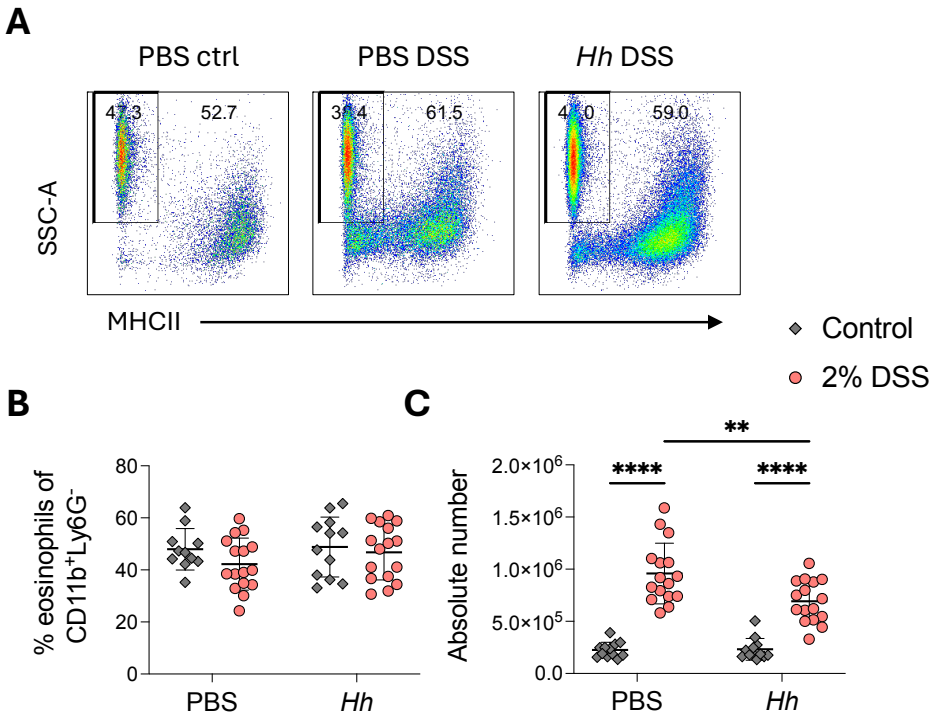


**Figure 3-18: *Hh* attenuates DSS-induced eosinophil accumulation in the colon**
C57BL/6 mice were infected with 1x10$^8$ CFU *Hh* or PBS by oral gavage and administered 2% DSS in drinking water. Representative dot plots of CD11b$^+$SSC$^{hi}$MHCII$^-$ colonic eosinophils (A), quantification of eosinophil frequencies (B) and absolute numbers (C) are shown. Data are shown with mean ± SD and pooled from 3 independent experiments with n=4-6 per experiment. Statistical significance was determined by 2-way ANOVA (significance *p< 0.05, **p<0.01, ***p< 0.001, ****p< .0001).

To summarise, using a direct infection to colonize mice with *Hh* had a comparable impact on DSS colitis as we observed following transfer of the naturally *Hh*-containing microbiota. We therefore concluded that *Hh* was sufficient to limit the severity of DSS-induced disease. Further analyses of the effect of *Hh* in this model were therefore carried out using the direct infection system.

### 3.3.3 Phenotyping of colonic macrophages and cDCs following *Hh* colonization and DSS treatment

We next determined whether there were phenotypic differences in colonic myeloid cells following *Hh* infection and DSS treatment. The majority of macrophages in the steady state intestine are mature Ly6C$^-$MHCII$^+$ cells which are highly phagocytic and unresponsive to TLR stimulation (Bain et al., 2013). In the context of inflammation, increased monocyte infiltration results in an expansion of inflammatory macrophages that are functionally distinct from the mature macrophages (Bain et al., 2018). These macrophages recruited during

inflammation produce inflammatory mediators, including TNFα, IL-6 and IL-1β, and CD11c has been used as a marker for this inflammatory macrophage phenotype in the gut (Corbin et al., 2020). We therefore analysed its expression on the Ly6C$^-$MHCII$^+$ macrophage population. We observed a substantial increase in the frequency of CD11c$^+$ macrophages following DSS treatment, in line with the reported expansion of these cells in inflammatory settings (Figure 3-19A). However, we saw no difference in the frequency of CD11c$^+$ colonic macrophages between uninfected and *Hh*-colonized DSS-treated mice (Figure 3-19A), despite the significant difference in the size of the monocyte infiltrate between these groups (Figure 3-15). We also assessed the colonic macrophage pool for expression of programmed cell death ligand 1 (PD-L1), which was shown to be upregulated on macrophages in inflammatory settings (Yamazaki et al., 2002). Indeed, we saw a marked upregulation of PD-L1 by colonic macrophages following DSS treatment, which was attenuated in the *Hh*-infected DSS group (Figure 3-19B).

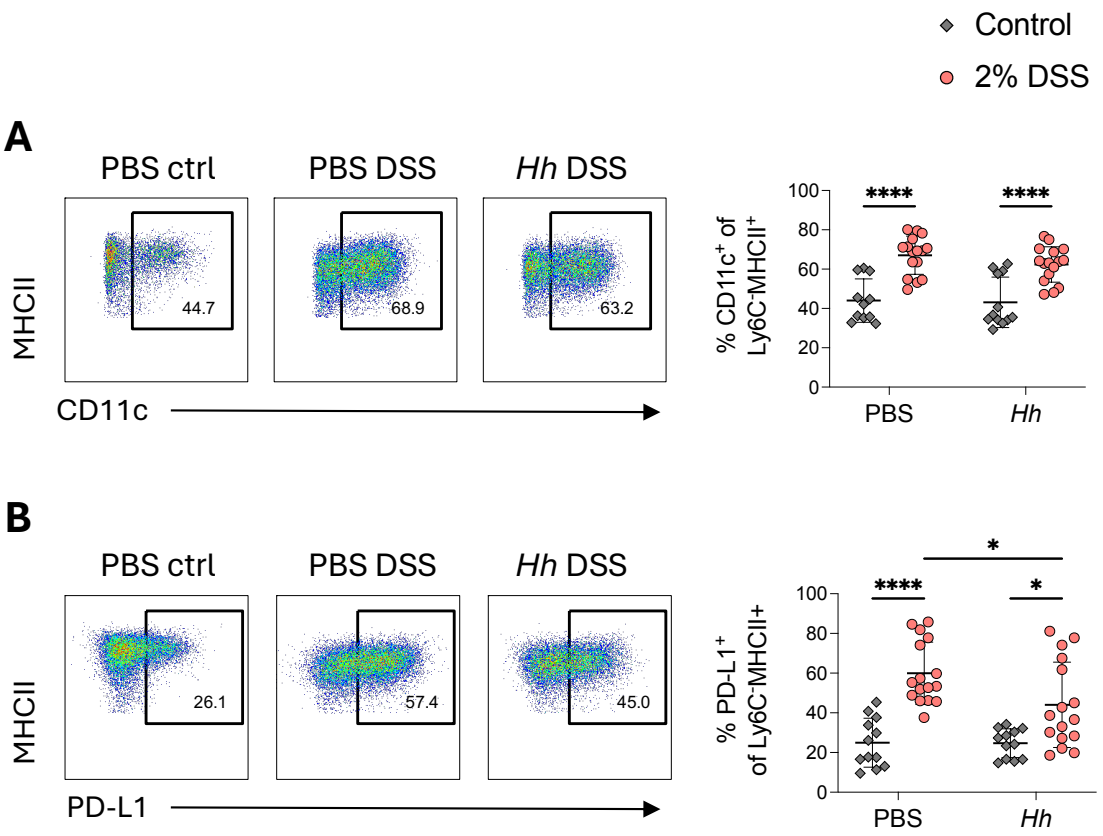


**Figure 3-19: DSS drives expansion of inflammatory macrophages in the colon**
C57BL/6 mice were infected with 1x$10^8$ CFU *Hh* or given PBS by oral gavage and administered 2% DSS in drinking water. Colonic macrophages were identified as $CD11b^+CD64^+Ly6C^-MHCII^+$ and analysed for expression of CD11c (A) and PD-L1 (B). Representative dot plots (left) and quantification of frequencies (right) are shown. Data are shown with mean ± SD and pooled from 3 independent experiments with n=4-6 per experiment. Statistical significance was determined by 2-way ANOVA (significance *p< 0.05, **p<0.01, ***p< 0.001, ****p< .0001).

We next measured the expression of co-stimulatory molecules CD80 and CD86, which are expressed on APCs and involved in T cell activation. Intestinal macrophages have been shown to exhibit low expression of these molecules, but this can be altered in patients with IBD (Rogler et al., 1998, RUGTVEIT et al., 2003). We saw that like CD11c and PD-L1, CD80 was significantly upregulated on colonic macrophages from DSS-treated mice, although the extent of CD80 upregulation was reduced with *Hh* colonization (Figure 3-20A). Conversely, we saw decreased CD86 expression following DSS treatment, with no significant effect of *Hh* colonization (Figure 3-20B). The expression of these molecules was also measured on colonic cDCs. CD80 expression was not altered on colonic cDCs following DSS treatment, although we saw a slight reduction in its expression in the *Hh*-colonized groups (Figure 3-21A). No differences in the expression of CD86 were observed on cDCs (Figure 3-21B).

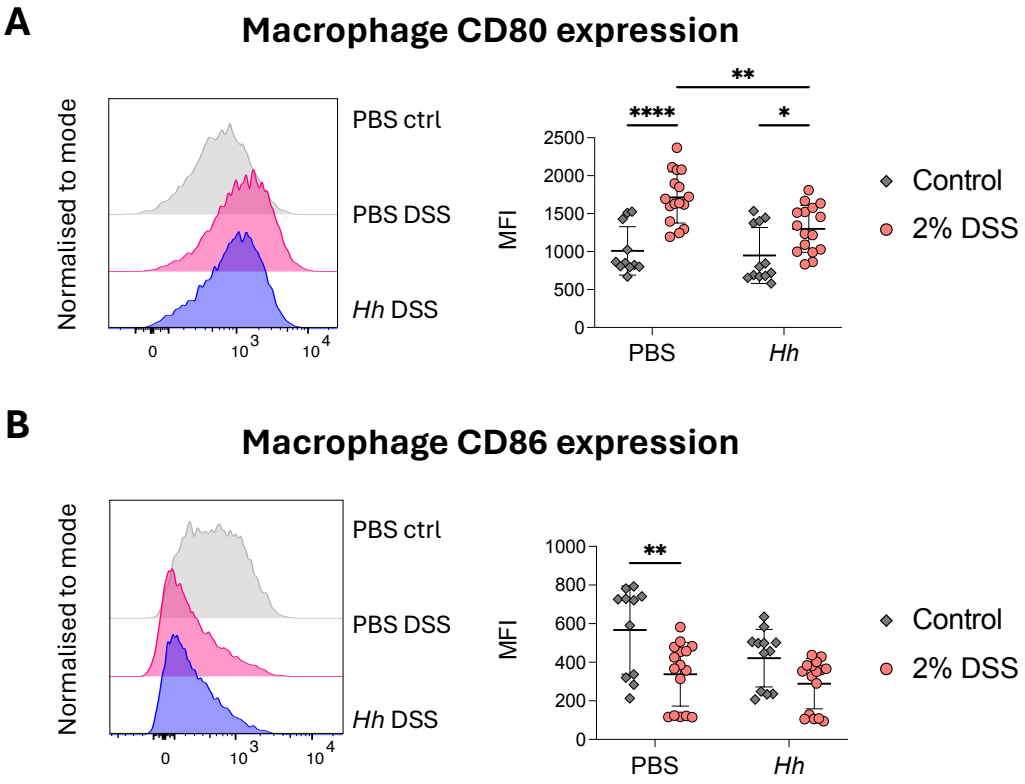


**Figure 3-20: Changes to colonic macrophage co-stimulatory molecule expression following *Hh* infection and DSS**

C57BL/6 mice were infected with 1x$10^8$ CFU *Hh* or given PBS by oral gavage and administered 2% DSS in drinking water. Colonic macrophages were identified as $CD11b^+CD64^+Ly6C^-MHCII^+$ and the MFI of CD80 (A) and CD86 (B) expression within the macrophage pool were calculated. Representative histograms showing the proportion of CD80/86-expressing macrophages (left) and quantification of MFI (right) are shown. Data are shown with mean ± SD and pooled from 3 independent experiments with n=4-6 per experiment. Statistical significance was determined by 2-way ANOVA (significance *p< 0.05, **p<0.01, ***p< 0.001, ****p< .0001).

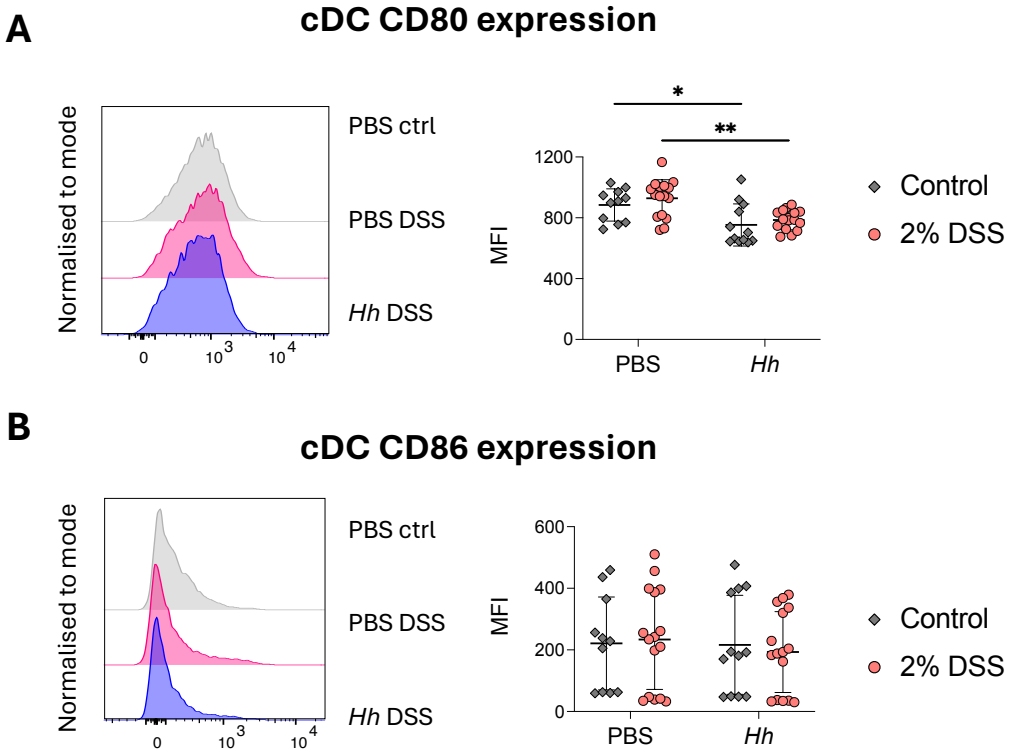


**Figure 3-21: Changes to cDC co-stimulatory molecule expression following *Hh* infection and DSS**
C57BL/6 mice were infected with 1x10$^8$ CFU *Hh* or given PBS by oral gavage and administered 2% DSS in drinking water. Colonic cDCs were identified as CD64$^-$CD11c$^+$MHCII$^+$ and the MFI of CD80 (A) and CD86 (B) expression within the cDC pool were calculated. Representative histograms showing the proportion of CD80/86-expressing cDCs (left) and quantification of MFI (right) are shown. Data are shown with mean ± SD and pooled from 3 independent experiments with n=4-6 per experiment. Statistical significance was determined by 2-way ANOVA (significance *p< 0.05, **p<0.01, ***p< 0.001, ****p< .0001).

These data demonstrate that the colonic macrophage pool develops an inflammatory phenotype following DSS treatment, as characterised by increased expression of CD11c, PD-L1 and CD80. However, colonic macrophages from *Hh*-colonized DSS-treated mice exhibited reduced upregulation of PD-L1 and CD80, although not CD11c. This further confirms that *Hh* colonization attenuates the extent of DSS-induced inflammation.

### 3.3.4 Quantification of intestinal and systemic cytokines following *Hh* infection and DSS treatment

We next examined the inflammatory response to DSS on a functional level. DSS induces expression of inflammatory cytokines IL-6 and TNFα in the colon from around day 2-3 of treatment, while by day 8 high levels of IL-1ß, IFNγ, IL-17 and IL-22 can also be detected (Nunes et al., 2018). *Hh* infection in immunocompetent mice drives expression of regulatory IL-10 (Xu et al., 2018,

Danne et al., 2017) by T cells and macrophages, while in the context of *Hh*-induced colitis the response is dominated by IL-23, IL-1ß, IL-17, IFNγ and IL-22 (Kullberg et al., 2006, Coccia et al., 2012, Morrison et al., 2015). We aimed to determine how infection with *Hh* might alter the cytokine response to DSS. Using qPCR to analyse transcription in whole distal colon tissue, we observed significant increases in expression of *Tnf*, *Ifnγ*, *Il17a*, and *Il22* at day 8 following DSS (Figure 3-22). Expression of *Il1ß* and *Il6* also increased in the DSS groups, although not to a significant level (Figure 3-22). No significant differences between the PBS and *Hh*-colonized groups were apparent, although there was a notable spread in expression of *Ifnγ*, *Il1ß*, *Il6*, and *Il22* within the *Hh*-infected DSS group, with many mice exhibiting comparable gene expression to the non-DSS control groups (Figure 3-22). Additionally, we saw a slight increase in *Il17a* expression in the *Hh*-infected control mice compared to the PBS controls, although this did not reach statistical significance (Figure 3-22). Taken together, this shows that treatment with DSS induced clear upregulation of inflammatory cytokines in the colon, which was largely comparable between the uninfected and *Hh*-colonized mice.

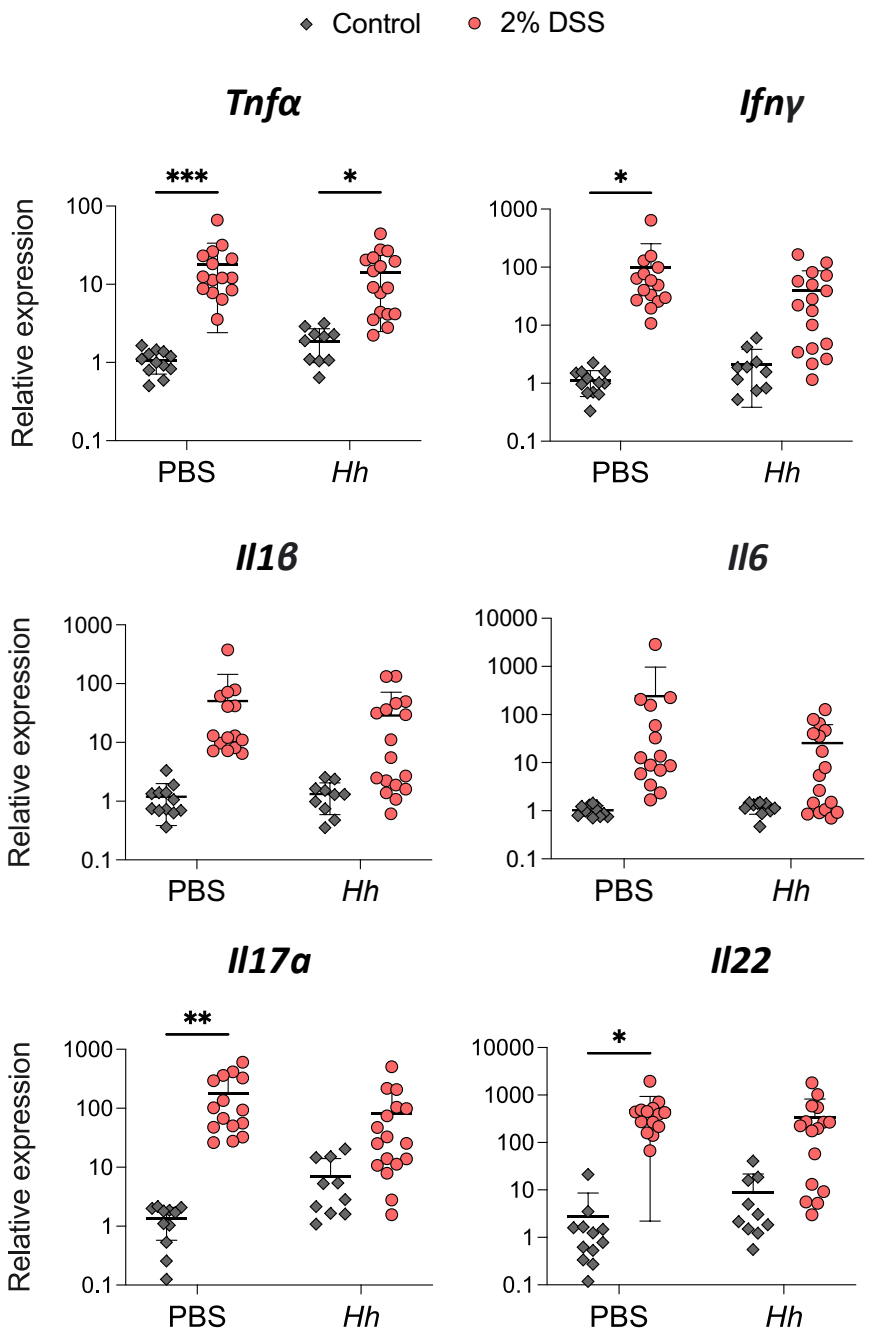


**Figure 3-22: DSS drives increased inflammatory cytokine gene expression in the colon**
C57BL/6 mice were infected with 1x10$^8$ CFU *Hh* or given PBS by oral gavage and administered 2% DSS in drinking water. A section of distal colon was isolated and expression of indicated genes measured using qPCR. Differences in gene expression were determined using the $2^{-\Delta\Delta C(t)}$ method, with gene expression normalised to the housekeeping gene *Rps29* and data shown as fold change relative to the PBS control group. Data are shown with mean ± SD and pooled from 3 independent experiments with n=4-6 per experiment. Statistical significance was determined by 2-way ANOVA (significance *p< 0.05, **p<0.01, ***p< 0.001, ****p< .0001).

In addition to assessment of inflammatory cytokines, we also analysed expression of the regulatory cytokine IL-10. *Il10* transcription was similar between the control and DSS-treated PBS samples, and there was no difference between the uninfected and *Hh*-colonized control groups (Figure 3-23A). However, when treated with DSS, we saw a significant upregulation of *Il10* only

in the *Hh*-infected mice. As IL-10 plays an important role in suppressing intestinal inflammation (Kühn et al., 1993), we hypothesised that increased *Il10* expression in *Hh*-infected mice may be responsible for the reduced inflammatory responses observed with DSS treatment. To address this hypothesis, we tested whether there was an inverse correlation between *Il10* transcription and histological inflammation, as described in Figure 3-12. We observed no correlation between these factors in the DSS-treated PBS group (Figure 3-23B). However, in the *Hh*-colonized DSS group, we observed a significant positive correlation between *Il10* transcription and histology score (Figure 3-23B). This indicates that rather than increased IL-10 driving a reduced inflammatory response in infected mice, *Hh* may prime the immune system to respond to inflammation with an increased regulatory IL-10 response. This could potentially contribute to the reduced disease severity seen in the *Hh*-colonized mice, although this hypothesis requires further testing.

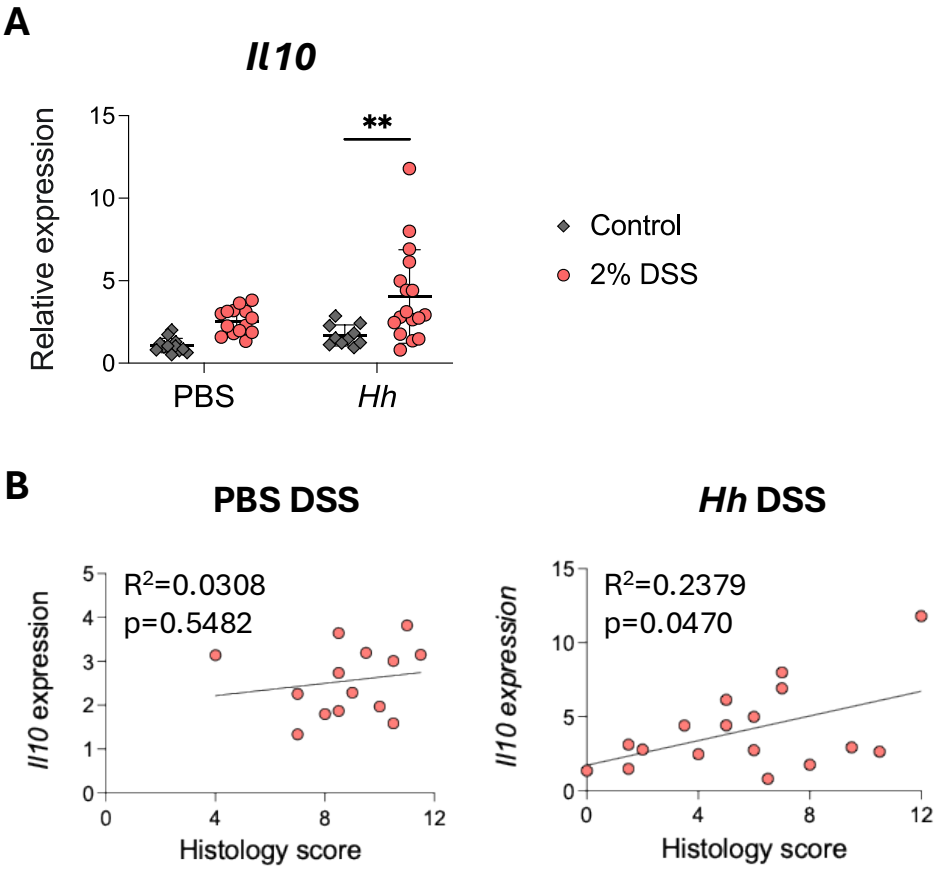


**Figure 3-23: *Hh* drives increased *Il10* transcription following DSS challenge**
C57BL/6 mice were infected with 1x10$^8$ CFU *Hh* or given PBS by oral gavage and administered 2% DSS in drinking water. A section of distal colon was isolated and expression of *Il10* measured using qPCR (A). Differences in gene expression were determined using the $2^{-\Delta\Delta C(t)}$ method, with gene expression normalised to the housekeeping gene *Rps29* and data shown as fold change relative to the PBS control group. Data are shown with mean ± SD and statistical significance was determined by 2-way ANOVA (significance *p< 0.05, **p<0.01, ***p< 0.001, ****p< .0001). Histology scores were obtained as described (Figure 3-12) and a simple linear regression performed between *Il10* expression and histology score (B). Data are pooled from 3 independent experiments with n=4-6 per experiment.

We next aimed to determine whether the inflammation induced by DSS shown here was present only in the colon, or if a systemic cytokine response could be detected. We measured the concentration of TNFα and IL-6 in the serum and initially detected negligible levels of these cytokines (data not shown). We then used samples from *Salmonella typhimuirum*-infected mice with known systemic inflammation as a positive control for this assay, and we were able to detect clear presence of both TNFα and IL-6 in the serum (Figure 3-24A). For both cytokines, the level in naïve samples was below the reliable detection limit of the assay (Figure 3-24A). In the DSS-treated samples, we observed similarly low levels of TNFα, and although we were able to detect IL-6 in the serum, there was a notable spread in the concentration between the 2 samples tested and one fell at the lower end of the detection range (Figure 3-24A). We concluded

that the DSS challenge had not induced a systemic inflammatory response at the timepoint tested here. To further confirm this, we measured the spleen mass in our different treatment groups, as an enlarged spleen is a hallmark of systemic inflammation. We observed no differences in spleen weight, either as a result of DSS treatment or *Hh* infection (Figure 3-24B). We therefore opted not to carry out further assessment of systemic inflammation in this model.

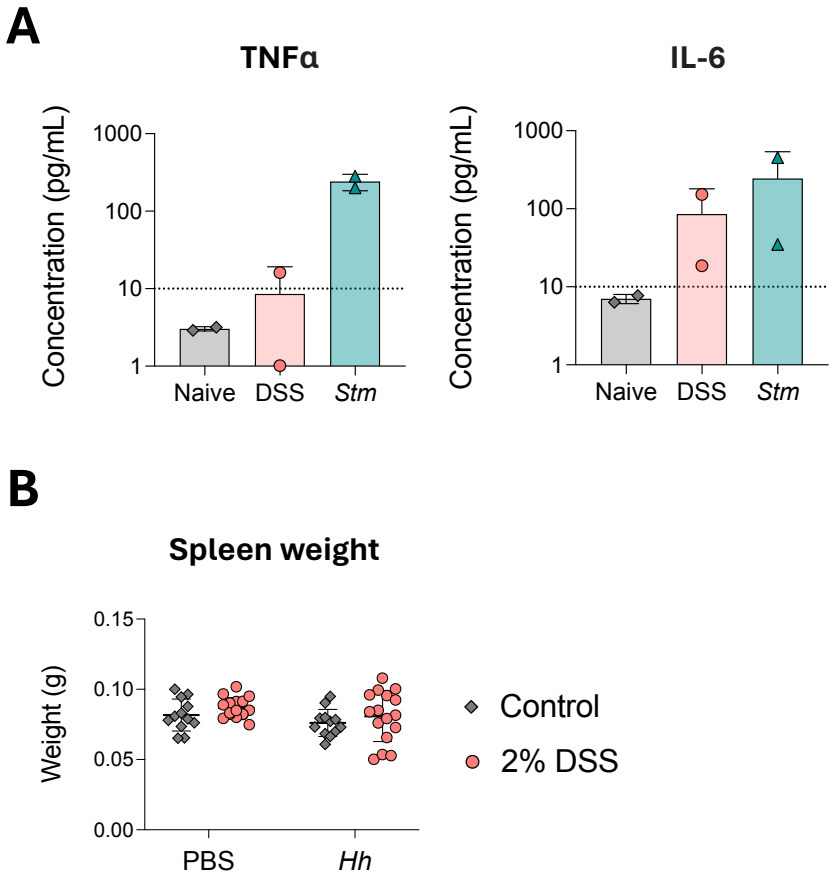


**Figure 3-24: DSS challenge did not induce significant systemic inflammation**
C57BL/6 mice were infected with 1x10$^8$ CFU *Hh* or given PBS by oral gavage and administered 2% DSS in drinking water. Mice from a separate experiment were infected with 5x10$^7$ CFU *Salmonella typhimurium* by oral gavage. The concentrations of TNFα and IL-6 in the serum of 2 uninfected non-DSS, 2 uninfected DSS-treated, and 2 *S. typhimurium* infected mice were measured by CBA. The lower detection limit of the assay is indicated (A). Spleens were collected at DSS experimental endpoint and weights quantified (B). Data are shown with mean ± SD and in (B) are pooled from 3 independent experiments with n=4-6 per experiment. Statistical significance was determined by 2-way ANOVA (significance *p< 0.05, **p<0.01, ***p< 0.001, ****p< .0001).

### 3.3.5 Assessment of antimicrobial responses following *Hh* infection and DSS treatment

Administration of DSS causes changes to the composition of the colonic microbiota (Håkansson et al., 2015, Munyaka et al., 2016), as well as damage to the epithelial barrier which can result in penetration of bacteria into the mucus

layer (Johansson et al., 2014). Disruption of the epithelial barrier is associated with translocation of bacterial antigens and luminal bacteria into the tissue (Fukata et al., 2005). These changes are accompanied by an inflammatory response targeted against the microbiota, including the induction of antimicrobial responses. We postulated that *Hh*-infected animals might exhibit increased antimicrobial responses, as a result of the close interactions between this microbe and host cells. We reasoned that increased antimicrobial activity could be beneficial during DSS-induced disease, as it could help to control the extent of bacterial spread.

We analysed colonic expression of *Retnlb*, which encodes resistin-like molecule ß (RELMß), an antimicrobial protein with bactericidal activity which has been shown to contribute to maintaining segregation between the epithelial barrier and the microbiota (Propheter et al., 2017). DSS treatment caused a marked upregulation in *Retnlb* transcription, but this was significantly reduced in the *Hh*-colonized DSS-treated mice (Figure 3-25A). In the control, non-DSS groups, we saw no difference in *Retnlb* expression between uninfected and *Hh*-infected mice (Figure 3-25A). We next measured expression of *Nos2*, encoding inducible nitric oxide synthase (iNOS). This enzyme is activated following exposure to inflammatory cytokines to produce the free radical nitric oxide (NO) (Soufli et al., 2016)Among other functions, it has been described to have antimicrobial effects, particularly against intracellular pathogens (Fang, 1997), and to play a role in maintaining bacterial homeostasis in the gut (Matziouridou et al., 2018). We observed a strong upregulation of *Nos2* in the colon following DSS treatment, which was again significantly attenuated in *Hh* infected DSS-treated mice (Figure 3-25B).

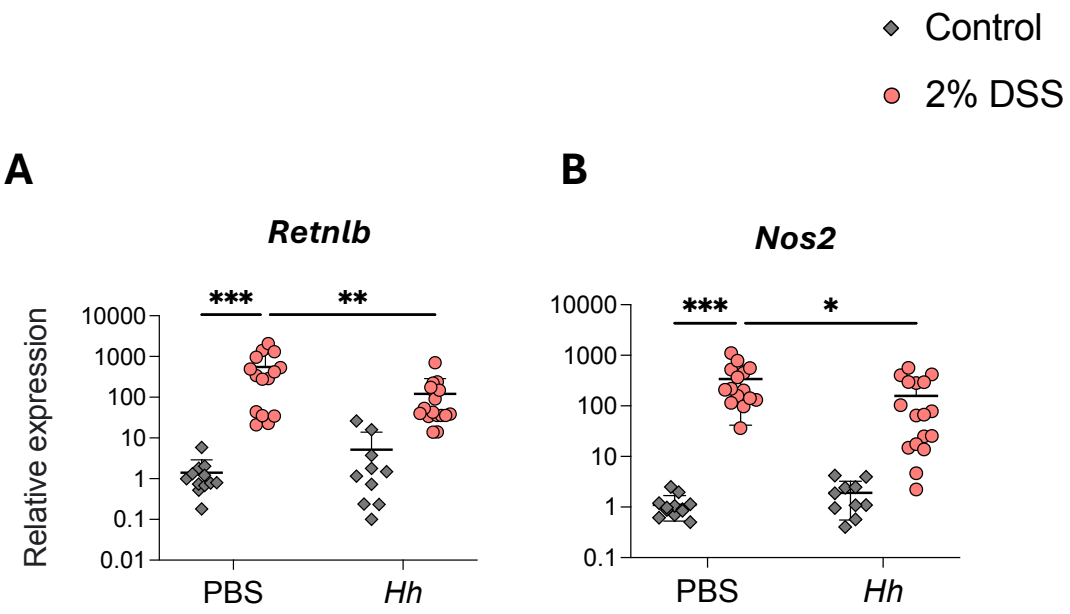


**Figure 3-25: *Hh* reduces DSS-induced antimicrobial gene expression in the colon**
C57BL/6 mice were infected with 1x108 CFU Hh or given PBS by oral gavage and administered 2% DSS in drinking water. A section of distal colon was isolated and expression of Retnlb (A) and Nos2 (B) measured using qPCR. Differences in gene expression were determined using the 2-ΔΔC(t) method, with gene expression normalised to the housekeeping gene Rps29 and data shown as fold change relative to the PBS control group. Data are shown with mean ± SD and pooled from 3 independent experiments with n=4-6 per experiment. Statistical significance was determined by 2-way ANOVA (significance *p< 0.05, **p<0.01, ***p< 0.001, ****p< .0001).

Finally, we measured levels of Calprotectin, a complex consisting of the S100A8 and S100A9 proteins. Faecal Calprotectin is associated with inflammation and is widely used as a biomarker for IBD, as it correlates with endoscopic assessment of disease activity and is non-invasive (Røseth et al., 1997, Konikoff and Denson, 2006). Calprotectin is produced largely by neutrophils, but also by other innate immune cells such as macrophages, and epithelial cells. It has a range of functions including antimicrobial effects due to its ability to chelate metal ions and sequester iron from bacteria, thus inhibiting bacterial growth (Nakashige et al., 2015, Jukic et al., 2021). Faecal Calprotectin concentrations have been shown to correlate with measures of intestinal permeability, as increased permeability is associated with barrier damage and translocation of the complex from the tissue into the luminal space and stool (Berstad et al., 2000). Calprotectin levels are therefore not only an indicator of inflammatory and antimicrobial responses, but also of barrier damage. As such, we observed a marked significant increase in the concentration of S100A8 in the stool following administration of DSS (Figure 3-26). As with expression of *Retnlb* and *Nos2*,

levels of S100A8 were significantly reduced in *Hh*-colonized DSS-treated mice when compared to the DSS control mice (Figure 3-26).

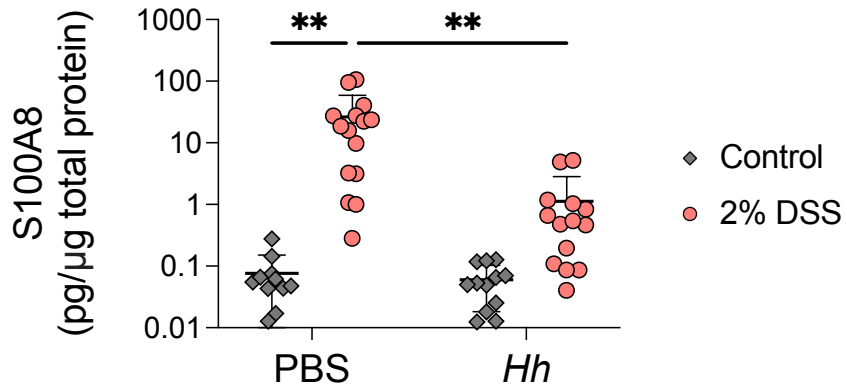


**Figure 3-26: *Hh* reduces DSS-induced faecal Calprotectin levels**
C57BL/6 mice were infected with 1x10$^8$ CFU *Hh* or given PBS by oral gavage and administered 2% DSS in drinking water. Stool was collected at experiment endpoint and the concentration of S100A8 measured by ELISA. Concentrations were normalised to total protein content measured by BCA. Data are shown with mean ± SD and pooled from 3 independent experiments with n=4-6 per experiment. Statistical significance was determined by 2-way ANOVA (significance *p< 0.05, **p<0.01, ***p< 0.001, ****p< .0001).

Taken together, these data show that antimicrobial responses appear elevated following treatment with DSS. Mice colonized with *Hh* showed reduced DSS-induced antimicrobial gene expression and lower levels of faecal Calprotectin compared to uninfected animals. Rather than *Hh* increasing antimicrobial responses to limit DSS-induced disease, it may be the case that colonized mice exhibit reduced barrier damage following treatment, therefore leading to less bacterial exposure and subsequent antimicrobial action.

### 3.3.6 *Hh*-mediated disease protection is dependent on length of time after infection

At this stage, we had established that *Hh* infection is sufficient to limit the disease severity following administration of DSS. To conclude this chapter, we finally aimed to determine whether this protection is apparent immediately after infection, or if it is dependent on the extended colonization period which we had implemented in previous experiments. We hoped this would begin to elucidate the mechanisms underlying the disease protection and tell us more about the cell types which may be involved. For example, induction of a primary T cell response takes ~7-14 days, so beginning DSS treatment before this timepoint would likely remove any effect of *Hh*-specific T cells. Similarly, any

effects of *Hh* on the innate immune compartment may take repeated interactions over time to drive alterations in phenotype and function. We also reasoned that the levels of *Hh* colonization may increase over time, so perhaps bacterial burden would be lower at earlier timepoints and therefore have a reduced effect on the immune system. This is addressed in the next chapter.

In these experiments, we infected mice with *Hh* by MT and then immediately begin DSS administration after the 7-day co-housing period (Figure 3-27). We observed no difference in either the disease activity scores or weight loss between the control and *Hh*$^+$ MT DSS-treated groups (Figure 3-28). Additionally, the proportion and number of colonic neutrophils (Figure 3-29) and monocytes (Figure 3-30) were comparable regardless of *Hh* colonization. We confirmed that the infection had indeed been successful as all *Hh*$^+$ MT recipients were PCR positive for *p25* and the levels of *Hh* DNA in caecal content, as quantified by qPCR for *CdtB*, were also comparable to previous experiments (data not shown). We therefore concluded that the *Hh*-mediated protection against DSS disease was not present at early timepoints following infection.

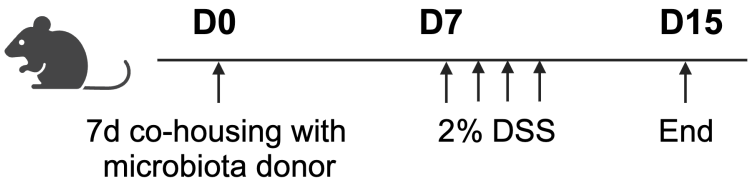


**Figure 3-27: Schematic for DSS challenge at early timepoint following *Hh* infection**
C57BL/6 mice were co-housed with microbiota donors for 7 days. On day 7 microbiota donors were removed and recipient mice were administered 2% DSS in drinking water or given normal water as controls. After 4 days all mice were switched back to normal water for a final 4 days.

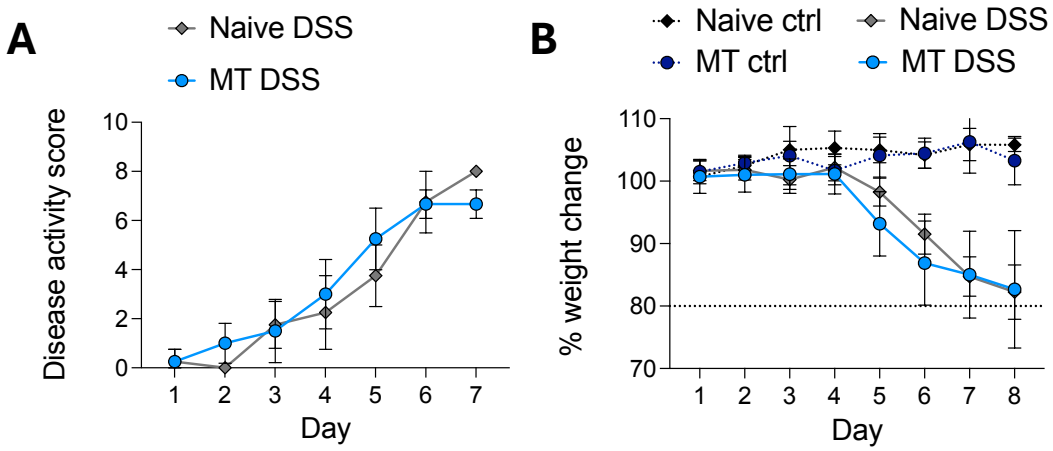


**Figure 3-28: *Hh*-mediated attenuation of DSS-induced disease is not present immediately after infection**
C57BL/6 littermate cohorts were left untreated (Naïve) or colonized with *Hh*$^{+}$ microbiota (MT) for 7 days and then administered 2% DSS in drinking water, as described in Fig.1-27. Following DSS administration mice were assessed daily for clinical disease activity (A) and weight change (B). Data are shown as mean ± SD and pooled from 3 independent experiments with n=4-6 per experiment. Statistical significance was determined by 2-way ANOVA (significance *p< 0.05, **p<0.01, ***p< 0.001, ****p< .0001).

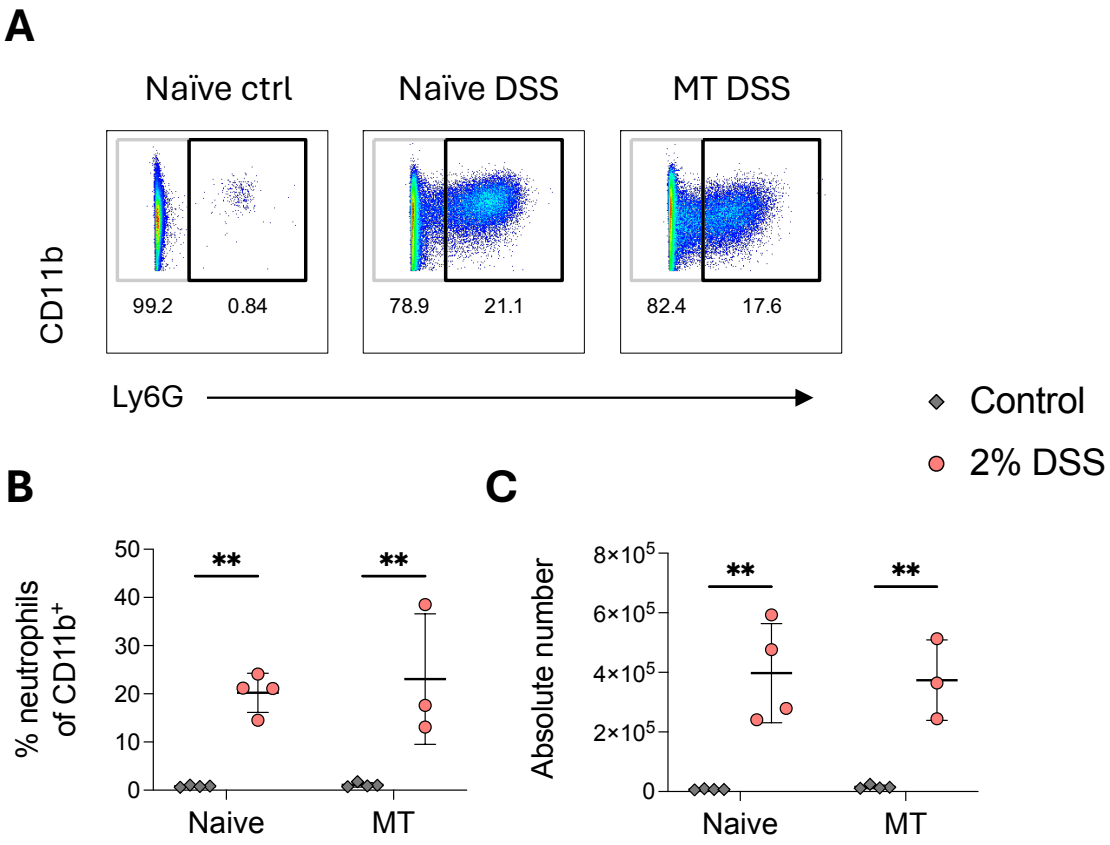


**Figure 3-29: *Hh*-mediated attenuation of DSS-induced neutrophil infiltration is not present immediately after infection**
C57BL/6 littermate cohorts were left untreated (Naïve) or colonized with *Hh*$^+$ microbiota (MT) for 7 days and then administered 2% DSS in drinking water, as described in Fig.1-27. Representative dot plots of colonic neutrophils (A), quantification of neutrophil frequencies (B) and absolute numbers (C) are shown. Data are shown with mean ± SD and are representative of one experiment with n=3-4. Statistical significance was determined by 2-way ANOVA (significance *p< 0.05, **p<0.01, ***p< 0.001, ****p< .0001).

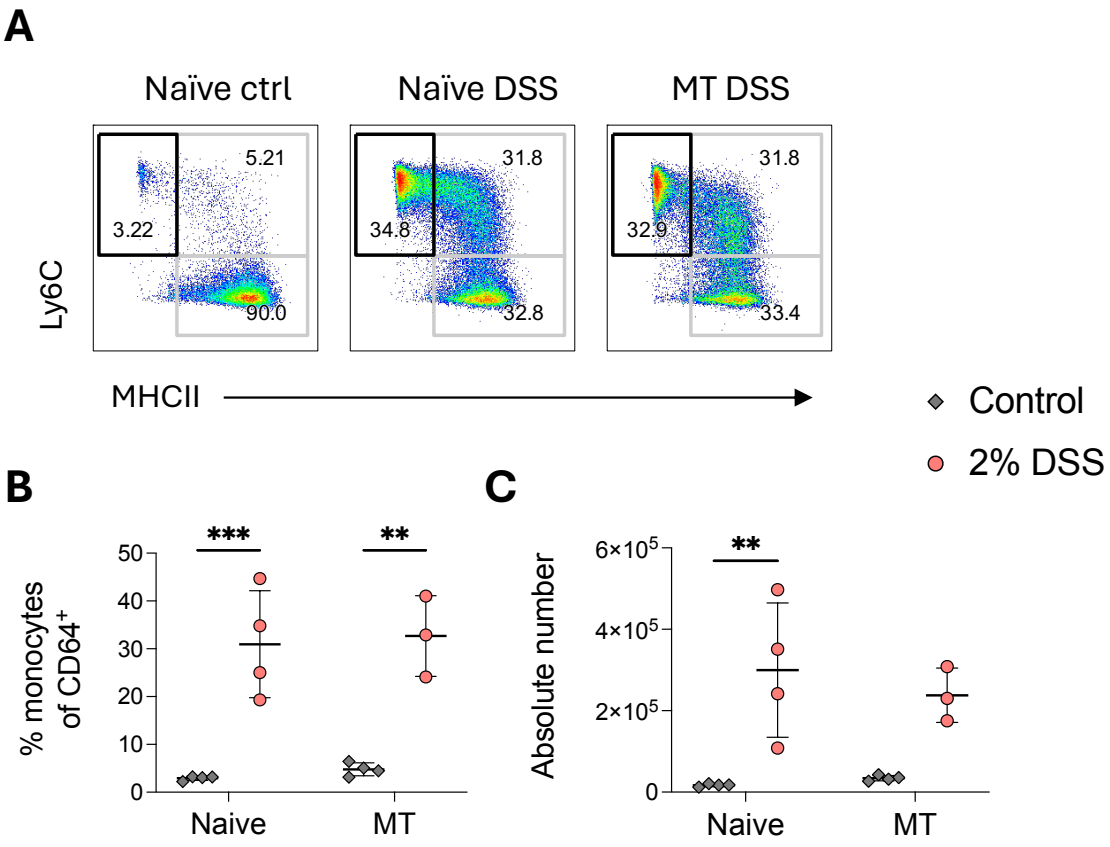


**Figure 3-30: *Hh*-mediated attenuation of DSS-induced monocyte infiltration is not present immediately after infection**
C57BL/6 littermate cohorts were left untreated (Naïve) or colonized with *Hh*$^{+}$ microbiota (MT) for 7 days and then administered 2% DSS in drinking water, as described in Fig.1-27. Representative dot plots of colonic monocyte-macrophages (A), quantification of monocyte frequencies (B) and absolute numbers (C) are shown. Data are shown with mean ± SD and are representative of one experiment with n=3-4. Statistical significance was determined by 2-way ANOVA (significance *p< 0.05, **p<0.01, ***p< 0.001, ****p< .0001).

## 3.4 Discussion

While *Hh* has been studied extensively as a model for bacteria-induced colitis, less well understood are its effects on immunocompetent hosts. Recent literature has highlighted the dominant regulatory effects of *Hh* on the immune system at steady state (Danne et al., 2017, Xu et al., 2018, Kedmi et al., 2022), but whether these effects shape the host's response during a disease or infectious challenge remains unclear. Here, using two approaches for colonizing mice with *Hh*, we explored the impact of *Hh* on DSS-induced disease, including the composition and phenotype of the colonic innate immune compartment, cytokine responses, and antimicrobial functions. We also tested whether the timepoint following *Hh* infection impacted the disease-attenuating effect we had observed.

### 3.4.1 Natural versus direct *Hh* infection methods

In recent years, the importance of microbiota standardization between experimental mice has become widely understood (McCoy et al., 2017). Due to the vast range of effects the microbiota exerts on its host, differences between animal facilities, and even between colonies in the same facility, can influence experimental outcomes. We identified animals bred at the University of Glasgow which harboured natural colonization with *Hh*. We chose to study the effect of the *Hh*-containing microbiota identified from our facility, with the aim to not only explore the effects of *Hh* on its host, but also to demonstrate how the natural microbiota of different animal colonies can impact immune function.

The use of co-housing for the purpose of microbiota transfer is often used as a method of standardizing microbial composition between animals. Despite this, it has been reported to have mixed efficacy, with some describing only partial normalization of the microbiota (Robertson et al., 2019), and others achieving more comparable composition after co-housing (Caruso et al., 2019). Importantly, not all species transfer at the same rate, and the transfer can be asymmetric, meaning that the resultant microbial composition will more closely resemble one of the original hosts (Caruso et al., 2019). We tested whether co-housing was sufficient to transfer *Hh* colonization and found that within 7 days of co-housing the *Hh* infection transfers to recipient animals. However, we have

not yet carried out extensive characterisation of this microbial transmission, and the exact composition of the donor microbiota and the extent of its transfer to recipient animals remains to be determined. This caveat should be considered when interpreting the results of the MT system in this thesis. Although we have validated the specific effects of *Hh* using a direct infection method, the contribution of additional microbes in the MT recipients cannot formally be excluded. Indeed, a recent large-scale study of DSS colitis reported a surprising degree of disease variation within a colony of C57BL/6 mice that were maintained in a single SPF breeding facility in the absence of intestinal *Helicobacter spp* (Forster et al., 2022). Microbiota sequencing revealed that cohorts that exhibited either very severe or very mild DSS colitis had different abundances of distinct bacterial species and that mono-colonization of GF mice with these individual species could reproduce different DSS disease outcomes (Forster et al., 2022). However, in our study, we observed very similar results using microbiota transfer or direct infection with *Hh*, suggesting that from the transferred microbiota, *Hh* may be the dominant species driving effects on the host. Nevertheless, it has been reported that direct *Hh* infection can alter the relative composition of the microbiota (Kuehl et al., 2005), which could potentially contribute to the observed effects. To explore whether the protective effects of *Hh* might be linked to altered abundance of other microbiota species that can affect DSS severity, it will be important to fully sequence the microbiota before and after DSS challenge, in the presence or absence of *Hh*.

### 3.4.2 *Hh*-mediated protection against DSS-induced disease severity

The effects of microbial composition on disease outcome and severity are not fully understood. This extends not only to human disease, but also to animal models, which do not completely recapitulate disease mechanisms and therapeutic effects. Differences in microbial composition and diversity are thought to be a contributing factor to this, with much work now being done using laboratory mice with “dirty” microbiomes that resemble those of wild mice, and more closely model human responses (Rosshart et al., 2019, Hamilton et al., 2020). Pathobiont species such as *Hh* are present in wild mouse microbiotas but often lacking in laboratory and SPF animals. Understanding how

species like this impact host immunity and affect disease and therapeutic outcomes will provide important insight into how the microbiota modulates host responses, which in turn can be used to inform clinical decisions.

DSS-induced colitis is a widely used model of IBD, in which the microbiota plays a documented role in disease severity (Hernández-Chirlaque et al., 2016, Forster et al., 2022, Rath et al., 2001). However, the mechanisms behind these effects have not yet been elucidated, and it is still unclear why certain bacterial species affect disease outcome while others do not. DSS-induced colitis develops normally in GF animals, indicating that there are microbiota-independent pathways driving disease which are not completely understood (Bylund-Fellenius et al., 1994). Following DSS treatment, GF mice reportedly suffer worsened epithelial injury than microbiota-sufficient animals (Hernández-Chirlaque et al., 2016), suggesting that the microbiota plays an important disease-limiting role, despite its implication in driving pathological inflammatory responses in this model. Here, we have demonstrated that colonization with *Hh* substantially reduces the severity of DSS-induced disease. *Hh* infection attenuated almost every indicator of disease severity and colonic inflammation, including weight loss and clinical symptoms, histopathological changes, and inflammatory infiltrate.

The underlying mechanisms by which *Hh* limits DSS-induced disease severity remain to be defined. It could potentially be the result of multiple mechanisms acting in conjunction, across various arms of the immune system. From studies using *Hh*-induced colitis models, we know that the bacteria has the capacity to affect multiple cell types in the gut, including T cells (Kullberg et al., 2002), ILCs(Buonocore et al., 2010), and monocytes and macrophages(Bain et al., 2018). Work done *in vitro* has also demonstrated functional effects of *Hh* on IECs (Sterzenbach et al., 2007, Liyanage et al., 2013). The potent effect of *Hh* on the T cell compartment has been heavily studied both in the context of colitis and at steady state. At steady state, *Hh* preferentially drives the induction of Tregs in the colon (Xu et al., 2018), and increased numbers of Tregs could contribute to the protective effect we have documented here. Multiple studies in which mice are treated with a probiotic or bacterial species which alters the balance of Treg and Th1/Th17 induction in the gut have demonstrated a disease-attenuating effect in the DSS colitis model (Park et al., 2018, Hartog et al., 2015), including

infection of mice with *Helicobacter pylori*, a human pathogen related to murine *Hh* (Zhang et al., 2018). However, these studies do not demonstrate that it is specifically alterations to the T cell compartment which drive protection, or whether these changes may be redundant when combined with effects on other cell types.

The rationale for an innate-mediated mechanism of disease protection comes from the timing and acute nature of the DSS regimen used here. The experimental endpoint falls on day 8 following DSS treatment, which is too early for induction of a primary T cell response as a result of DSS-induced barrier breach and exposure to bacterial antigens. While tissue resident memory T cells may become activated, including *Hh*-reactive Tregs, the brunt of the response is driven by myeloid cells and the epithelial barrier. Any *Hh*-mediated effects on their functions could act to limit their inflammatory response in this setting. There have been reports of *Hh* having a limiting effect on innate responses to PAMPs (Sterzenbach et al., 2007, Chow and Mazmanian, 2010), however these studies were carried out in cell lines and lack the environmental context of an *in vivo* infection. In later chapters, the effect of *Hh* on the myeloid and epithelial compartments are explored, with the aim of determining the extent of *Hh*-mediated functional effects on these cell types and to explore potential mechanisms of *Hh*-driven disease protection.

### 3.4.3 Phenotypic and functional effects of *Hh* on the gut landscape

We assessed various indicators of colonic inflammation, including phenotypic analysis of myeloid cells, cytokine transcription, and markers associated with antimicrobial responses. We identified expansion of CD11c-expressing macrophages in the colon following DSS treatment. This population has been reported to transcribe antimicrobial molecules and produce high levels of inflammatory cytokines (Corbin et al., 2020, Uematsu et al., 2006), and in the context of *Hh*-induced colitis, their production of IL-23 is required to trigger pathology (Arnold et al., 2016). This population is therefore likely to be key in contributing to DSS-induced disease. Although we saw a marked reduction in colonic monocyte infiltration in *Hh*-infected mice, we observed no difference in the proportion of $CD11c^+$ macrophages. This suggests that while myeloid

infiltration might be altered in infected animals, the inflammatory environment in the DSS-treated gut is still sufficient to drive the expansion of inflammatory macrophages. Despite this, other markers of an inflammatory macrophage phenotype, PD-L1 and CD80, were also upregulated following DSS treatment, but significantly reduced in *Hh*-infected mice. This is conflicting but indicates that expression of these molecules on macrophages may be controlled by different pathways, and that *Hh* may modulate these pathways to different extents. The PD-1/PD-L1 axis is involved in limiting T cell responses, and is best known as a blockade target in cancer immunotherapy (Errico, 2015), while its expression on macrophages is thought to contribute to immunosuppressive tumour microenvironments (Hartley et al., 2018). Blockade of PD-L1 has been reported to polarise tumour macrophages towards a more pro-inflammatory phenotype (Xiong et al., 2019). Its upregulation in inflammatory environments is likely a mechanism by which the immune system controls the extent of the inflammatory response. CD80 and CD86 are in the same family of molecules as PD-L1, termed the B7 superfamily, consisting of costimulatory and coinhibitory molecules (Park et al., 2023). Upregulation of these molecules is differentially induced by various stimuli, including PRR signalling (Park et al., 2023). Recognition of microbes and their products, including *Hh*, could therefore be involved in controlling their expression, and may explain why we see differences in these molecules in *Hh*-infected mice. The effects of *Hh* on the macrophage compartment are further explored in later chapters.

Cytokine networks are key to guiding intestinal homeostasis and mediating the response to infection. Upon breakdown of barrier function, cytokines derived from innate cells initiate intestinal inflammation, and in the development of chronic disease help to shape the adaptive immune response (Friedrich et al., 2019). We observed marked upregulation of *Tnfa*, *Ifnγ*, *Il17a* and *Il22* transcription in the colon of DSS-treated mice. Upregulation of *Il1β* and *Il6* were also apparent, although not to a statistically significant level. Unlike the clinical disease indicators and cellular infiltrate, there were no significant differences in inflammatory cytokine transcription between uninfected and *Hh*-colonized mice. These data are conflicting as it could be expected that numbers of inflammatory monocyte-macrophages and neutrophils would correlate with cytokine production, given that these cells produce many of the cytokines tested

(Friedrich et al., 2019). It may be due in part to the gap between cytokine transcription and protein translation, and alternative measurements of cytokine production should be undertaken to provide a more complete assessment. We observed the highest transcription of *Il10* in DSS-treated, *Hh*-infected mice, which showed clear upregulation compared to all other treatment groups. Despite the known increase in Tregs following *Hh* infection, these data suggest that at steady state, IL-10 is produced at a comparable level between infected and uninfected mice. However, upon inflammatory challenge, *Hh* appears to drive an increased propensity for IL-10 production. This idea is supported by the significant positive correlation which we observed between *Il10* transcription and histological inflammation in the *Hh*-infected group. These data suggest that *Hh* may prime the immune system to produce increased IL-10 following an inflammatory challenge. Despite this, measuring cytokine transcription in whole tissue does not allow for identification of the specific cell types producing each cytokine, and it is unclear whether this increased IL-10 is a result of production by Tregs, macrophages, or another cell type, and which cells are responding. Expression of the IL-10 receptor alpha (IL-10Rα) on macrophages has been shown to be protective in the context of DSS-induced colitis and T cell mediated colitis (Li et al., 2014, Li et al., 2015), indicating that macrophages are likely to be a key cell type responding to IL-10 in this context. It would be useful to examine the expression of IL-10Rα on different colonic immune cells, including macrophages, to determine whether *Hh* alters its expression and could potentially affect IL-10 responsiveness. Further work therefore remains to be done to assess the potential role of IL-10 signalling in *Hh*-mediated protection against DSS-induced disease.

As DSS-induced colitis is a model of barrier breach, the dysregulated inflammatory response which ensues is accompanied by antimicrobial responses designed to eliminate invading microbes. We observed increased expression of *Retnlb* and *Nos2* following DSS treatment, confirming that the loss of barrier integrity was accompanied by a significant antimicrobial response. RELMß, encoded by *Retnlb*, is produced by goblet cells in response to bacterial stimuli and its production is greatly reduced in GF animals (He et al., 2003). Mice lacking RELMß show penetration of pathogens such as *Citrobacter rodentium* into the colonic crypts (Bergstrom et al., 2015), indicating a role for RELMß in

maintaining bacterial segregation. Mice with a knockout of *Retnlb* also show elevated levels of epithelial-associated Proteobacteria, including *Helicobacter* species (Propheter et al., 2017). Despite this, we saw no difference in *Retnlb* expression between *Hh*-infected and uninfected control mice, and a reduction in expression in the *Hh*-colonized DSS group compared to uninfected DSS. These data suggest that *Hh* does not drive upregulation of RELMβ. The reduction in DSS-induced *Retnlb* in *Hh*-colonized mice is possibly a result of reduced barrier damage and subsequent exposure to microbial PAMPs. *Nos2* showed the same expression pattern, with reduced expression in the *Hh*-colonized group following DSS treatment. While iNOS, encoded by *Nos2*, is not a traditional antimicrobial peptide, it has been shown to have antimicrobial functions and involvement in regulating bacterial load in the gut (Matziouridou et al., 2018). *Nos2* is upregulated in colonic epithelial cells in mice colonized with epithelial-adherent SFB or *Cr* (Atarashi et al., 2015), but again was not upregulated here by *Hh* infection alone. Its expression is induced by inflammatory cytokines (Soufli et al., 2016), so the reduction we observed may be due to decreased cytokine signalling in infected animals – although there were no significant differences in DSS-induced inflammatory cytokine transcription in *Hh*-infected mice. We lastly measured levels of faecal Calprotectin, which were again notably increased following DSS treatment and reduced with *Hh* infection. This complex was used as an indicator of antimicrobial functions, but also as a surrogate marker for barrier damage and neutrophil accumulation (Jukic et al., 2021). Taken together, it is difficult to interpret whether the reduction in antimicrobial markers we have measured is indicative of a reduction in barrier damage and breach, or the result of decreased pro-inflammatory infiltrate and mediator production. To clarify this issue, further work should be done to directly assess the DSS-induced barrier damage in this system, for example by employing a method such as the FITC-dextran permeability assay (Volynets et al., 2016).

### 3.4.4 The impact of infection and disease challenge timing

Our final aim for this chapter was to test whether *Hh*-mediated disease protection was impacted by the length of time the animals had been infected. We hoped this would begin to elucidate the mechanism behind the protective effect, as the length of time post-infection could indicate which elements of the immune system may be altered by the bacteria. In other studies investigating

the effect of infection on experimental colitis, various timepoints of colitis induction have been tested. One study which reported a protective effect of *H. pylori* colonization waited until 4 weeks post-infection to begin DSS treatment (Zhang et al., 2018), while another group infected with *Lactobacillus acidophilus* 3 days after DSS administration (Park et al., 2018). It is likely that the protective effects described in these studies are therefore mediated by different mechanisms. As well as bacteria-mediated protection, much work has been done demonstrating the alleviating effects of helminth infections in experimental colitis models (Heylen et al., 2014). Helminths produce a range of immunomodulatory molecules to evade and suppress host responses (McSorley et al., 2013), and the mechanisms by which these alter host immunity and protect against inflammatory disease are well characterised. One mechanism described is the helminth-induced activation of Tregs (White et al., 2020), and this mechanism could potentially play a role in the *Hh*-mediated disease protection described here. Given the length of time required for induction of a naïve T cell response, we postulated that immediately following MT there would not yet be *Hh*-induced Treg expansion. Indeed, at this early timepoint, infected mice did not show attenuated disease or reduced colonic myeloid infiltration following DSS. As the inflammation in this system is driven largely by myeloid cells, a potential mechanism of protection could involve Treg-mediated effects on the myeloid compartment. Tregs have been shown to directly inhibit innate driven intestinal pathology, dependent on their production of IL-10 and TGFβ (Maloy et al., 2003), and their role in *Hh*-mediated protection from DSS requires further investigation. Studies using *Hh*-induced colitis models have employed a T cell transfer system to demonstrate the protective function of Tregs in this context (Kullberg et al., 2002, Maloy et al., 2003). A similar system could be used here, whereby Tregs from infected animals are transferred into uninfected hosts before DSS treatment, to determine whether these cells are sufficient to attenuate colitis symptoms. Alternatively, the role of Tregs could be tested by depleting these cells prior to DSS administration and assessing whether the protective effect of *Hh* remains in their absence.

Another potential mechanism is direct modulation of the myeloid compartment by *Hh*. There is substantial evidence of microbiota-driven effects on the development and function of myeloid cells. Myelopoiesis in the BM appears to be

directly affected by the level of complexity in the microbiota, with GF animals exhibiting reduced numbers of BM monocytes and granulocyte monocyte progenitors (GMPs) (Balmer et al., 2014a), and treatment with antibiotics reducing granulocytosis (Deshmukh et al., 2014). This microbiota-driven myelopoiesis is dependent on TLR signalling (Balmer et al., 2014a). As the gut is a tissue where the macrophage pool is constantly replenished by BM monocytes (Bain et al., 2014), it is possible that *Hh* could mediate effects on the BM which then impact the intestinal myeloid compartment. Alterations to BM haematopoiesis may take an extended amount of time to affect the macrophage pool in the gut, which could again explain why we do not see limiting effects on disease severity in mice only colonized with *Hh* for a short time. Once in the gut, the local environment plays a key role in shaping the functions of resident myeloid cells. Microbiota-derived signals have been shown to directly regulate macrophage functions, with the SCFA butyrate having an attenuating effect on the production of inflammatory mediators by colonic macrophages (Chang et al., 2014). In line with this, treatment with antibiotics has the opposite effect, increasing the frequency of inflammatory colonic macrophages and causing marked changes to their metabolic profile (Scott et al., 2022). *Hh* has been shown to directly drive an anti-inflammatory phenotype in gut macrophages (Danne et al., 2017), and it is likely that this mechanism may contribute to the effect we have demonstrated. Whether any direct effects of *Hh* on the myeloid compartment are present immediately after infection or require repeated interactions remains unclear. In the next chapter, the difference in the gut landscape at different timepoints following *Hh* infection is explored, with the aim of determining why the protective effect is not present early after infection and further elucidating how *Hh* alters the immune environment of its host.

### 3.4.5 Concluding remarks

In conclusion, we report that colonization with *Hh* has an attenuating effect on disease severity in the DSS colitis model. We show that *Hh* infection alleviates clinical colitis symptoms, including weight loss, and attenuates histopathological signs of intestinal disease. Inflammatory infiltrate to the colon was also markedly reduced in infected mice, and there were accompanying changes to macrophage phenotypes which are consistent with a reduction in inflammation. This protective effect was dependent on an extended colonization period prior

to colitis onset and was not apparent when animals were immediately challenged with DSS following infection. These data provide new insight into the effects of *Hh* on the immune system and demonstrate that infection with pathobiont species can have beneficial outcomes for the host.

# 4 *Helicobacter hepaticus* modulates intestinal immune homeostasis at steady state

## 4.1 Introduction

In Chapter 3, we identified a protective effect of *Hh* colonization against disease outcome in the DSS colitis model. To explore the mechanisms driving this altered response, we first require a greater understanding of the effects of *Hh* on its host at steady state. The concept of homeostatic immunity has been described in recent years, in which the crosstalk of interactions between the host and its microbiota drives a range of microbiota-specific immune responses in the absence of inflammation (Belkaid and Harrison, 2017, Ansaldo et al., 2021). It is likely that homeostatic immunity driven by *Hh* alters the intestinal immune environment, so that when challenged with DSS or another inflammatory trigger, the response and outcome are altered.

Exposure to microbiota-derived signals has a vast array of effects on host immunity and physiology. These effects range from local signals in the gut influencing the composition and functions of resident cells (Schulthess et al., 2019, Goto et al., 2014, Furusawa et al., 2013, Atarashi et al., 2011), to far-reaching effects on systemic immunity and immune cell development (Clarke et al., 2010, Balmer et al., 2014a, Khosravi et al., 2014). As our understanding of host-microbiota crosstalk increases, the differences between laboratory animals and wild animals, or indeed humans, are becoming more evident. While the mammalian immune system co-evolved with a diverse microbiota, laboratory animals are usually maintained in highly controlled, pathogen-free environments. The result is a distinct difference in the microbial composition and immune function of these animals compared to wild counterparts (Abolins et al., 2017, Rosshart et al., 2017, Rosshart et al., 2019). The immune system of laboratory mice has been described to resemble more closely that of a newborn rather than adult human, a phenotype which can be partially rescued by co-housing with non-laboratory mice (Beura et al., 2016). Wild mice show increased proportions of splenic neutrophils, highly activated NK cells, and increased proportions of effector T cells compared to laboratory mice (Abolins et al., 2017). Despite this, they also show increased proportions of Tregs and reduced cytokine responses when stimulated with PAMPs (Abolins et al., 2017). This

suggests that increased microbial exposure has a regulatory effect on immune activity, and it has been proposed that in this way the microbiota sets the threshold for immune activation (Ansaldo et al., 2021). Importantly, this has implications for therapeutic strategies, with studies describing how the microbiota can determine responses to anticancer immunotherapies and vaccines (Kroemer and Zitvogel, 2018, Collins and Belkaid, 2018, Reese et al., 2016). Similarly, animals with microbiotas resembling those of wild mice more accurately model human responses to therapeutics (Rosshart et al., 2017, Rosshart et al., 2019). It is therefore important that we develop a greater understanding of the host-microbiota crosstalk, particularly the mechanisms by which the microbiota shapes the immune system in homeostasis and how this alters outcomes in disease and therapeutic settings.

The effects of *Hh* on the intestinal T cell pool have been well documented. As previously described, *Hh* drives induction of RORγt$^{+}$ Tregs and Tfh cells at steady state (Xu et al., 2018, Kedmi et al., 2022), while in the context of *Hh*-driven colitis, the T cell pool is dominated by Th1 and Th17 cells (Morrison et al., 2013, Hue et al., 2006). In contrast, there have been few reports of *Hh*-mediated effects on the intestinal innate immune compartment at steady state. In the absence of T cells, *Hh* drives innate-mediated colitis (Maloy et al., 2003), and MyD88 signalling on myeloid cells is required for induction of innate or T cell-mediated *Hh*-driven colitis (Asquith et al., 2010). At steady state, a *Hh*-derived metabolite has been shown to induce an anti-inflammatory gene signature in macrophages (Danne et al., 2017), indicating that the bacteria may have direct functional effects on intestinal myeloid cells. However, further characterisation of the myeloid pool in *Hh* colonized animals remains to be carried out. Finally, it is also important to consider potential effects of *Hh* on the composition of the microbiota itself. Changes to microbial diversity and abundance can have downstream effects on immune function, and introducing a new species into this complex ecosystem could result in changes to immune homeostasis. There is evidence that upon infection with *Hh*, it becomes the dominant community member colonizing the caecal mucosa, therefore impacting microbial diversity (Kuehl et al., 2005). Gaining further insight into the impact of *Hh* colonization on the microbial community could help decipher direct and indirect effects of *Hh* on immune function.

## 4.2 Aims

Here I aimed to phenotype the colonic myeloid pool following *Hh* colonization at steady state. I tested two timepoints following infection to determine how the response to *Hh* develops over time, with potential implications for the disease outcomes described in Chapter 3. I also examined intestinal cytokine expression to give further insight into *Hh*-induced immune function at these timepoints. I then assessed the myeloid pool in the SI, a tissue that is not colonized by *Hh*, with the aim of determining whether *Hh* induces only local changes to immunity or whether it has the capacity to have further reaching effects. Finally, I aimed to determine whether *Hh* drives changes to faecal microbial composition, which could cause downstream effects on the immune landscape.

## 4.3 Results

### 4.3.1 *Hh* alters colonic myeloid cell recruitment at different timepoints post-infection

To understand the effects of *Hh* on the immune system at steady state, we utilised the two *Hh* infection methods described in Chapter 3. Here, we focussed on examining the intestinal myeloid compartment, as the effect of *Hh* on these cells at steady state has not been well documented, despite their contribution to pathology in *Hh*-induced colitis models (Bain et al., 2018, Arnold et al., 2016, Asquith et al., 2010). Colons were harvested at two timepoints post-infection, day 7 and day 21, as we observed different outcomes at these timepoints when mice were challenged with DSS in Chapter 3. cLPL (colonic lamina propria leukocytes) were analysed by flow cytometry, and starting with mice receiving $Hh^+$ MT, we observed a trend towards increased numbers of $CD45^+$ immune cells at day 7, which was reduced to comparable levels with naïve controls by day 21 (Figure 4-1A). No differences in numbers of $CD11b^+$ or $CD64^+$ cells were observed at either timepoint (Figure 4-1B-1C). As expected, there were very few neutrophils present in the cLPL of naïve mice, and $Hh^+$ MT had no significant impact on colonic neutrophil proportions or numbers at either time point (Figure 4-2).

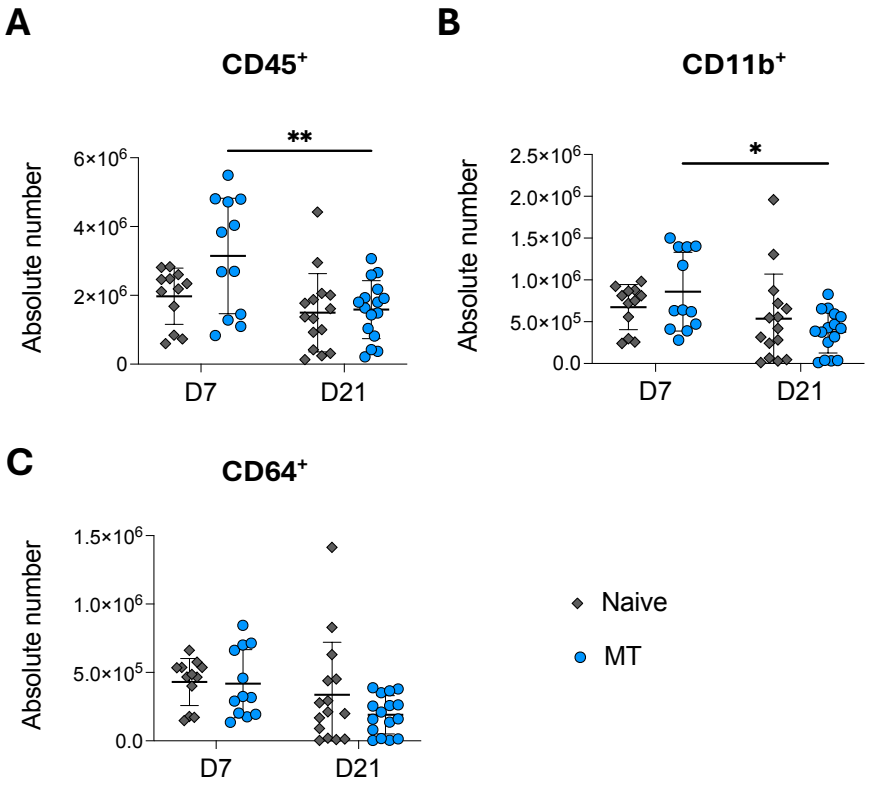


**Figure 4-1: *Hh*⁺ MT drives increased immune infiltration to the colon at day 7**
C57BL/6 littermate cohorts were left untreated (Naïve) or colonized with *Hh*⁺ microbiota (MT) for 7- or 21-days. Colonic LP leukocytes were isolated using enzymatic digestion and the absolute number of CD45⁺ (A), CD11b⁺ (B), and CD64⁺ (C) cells were calculated. Data are shown with mean ± SD and pooled from 3 (D7) or 4 (D21) independent experiments with n=4 per experiment. Statistical significance was determined by 2-way ANOVA (significance *p< 0.05, **p<0.01, ***p< 0.001, ****p< .0001).

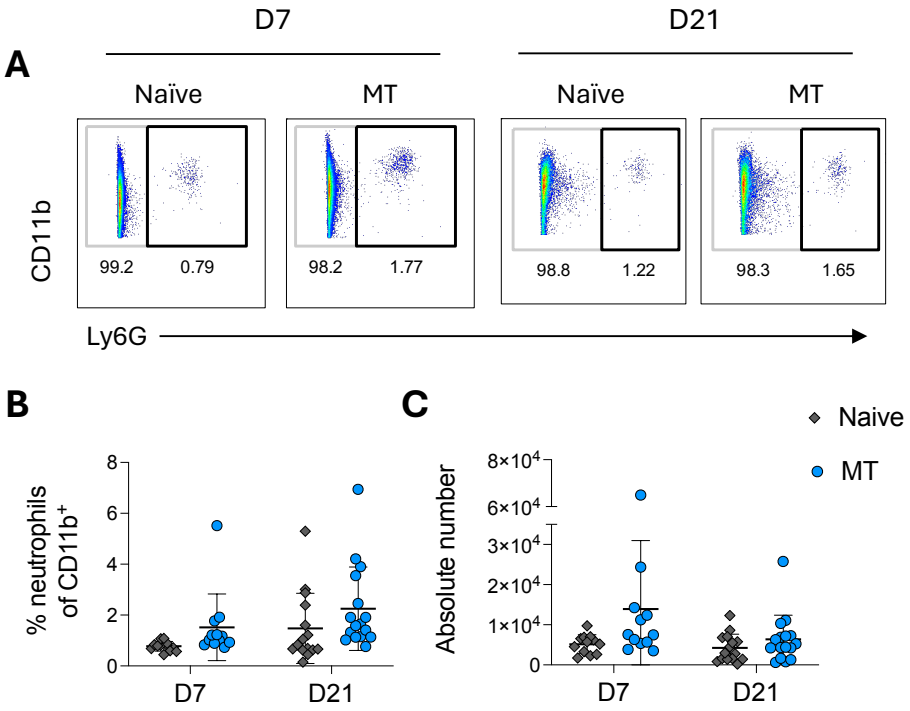


**Figure 4-2: *Hh*⁺ MT does not impact colonic neutrophil accumulation**
C57BL/6 littermate cohorts were left untreated (Naïve) or colonized with *Hh*⁺ microbiota (MT) for 7- or 21-days. Representative dot plots of colonic CD11b⁺Ly6G⁺ neutrophils (A), quantification of neutrophil frequencies (B) and absolute numbers (C) are shown. Data are shown with mean ± SD and pooled from 3 (D7) or 4 (D21) independent experiments with n=4 per experiment. Statistical significance was determined by 2-way ANOVA (significance *p< 0.05, **p<0.01, ***p< 0.001, ****p< .0001).

We next analysed the colonic monocyte-macrophage pool. At day 7 post-*Hh*⁺ MT, there was a significant increase in the proportion and number of infiltrating monocytes (Figure 4-3). However, by day 21 this was reduced, with monocyte levels comparable between the naïve and *Hh*⁺ MT groups (Figure 4-3). We observed a similar trend with levels of intermediate monocyte-macrophages (Figure 4-4A), which is likely reflective of the fact that these cells are a differential intermediate arising from infiltrating monocytes (Bain et al., 2014). Macrophage frequencies were decreased in *Hh*⁺ MT recipients at day 7 (Figure 4-4B), due to the proportionate increase in monocytes and intermediate cells. However, no differences in macrophage numbers at either timepoint were observed (Figure 4-4B). Similarly, we saw no significant differences in cDC proportions or numbers between the naïve and *Hh*⁺ MT groups (Figure 4-5). Lastly, *Hh*⁺ MT recipients showed a substantial increase in eosinophil frequency and number at day 7, although by day 21 no difference between naïve and *Hh*⁺ MT animals was apparent (Figure 4-6). These data show that following transfer of the *Hh*-containing microbiota, recipients experienced a transient increase in monocyte and eosinophil infiltration to the colon early after transfer. However,

by day 21 the proportion and number of these cells were comparable between naïve mice and *Hh*$^{+}$ MT mice, indicating that over time the myeloid cell response to the new microbiota is controlled.

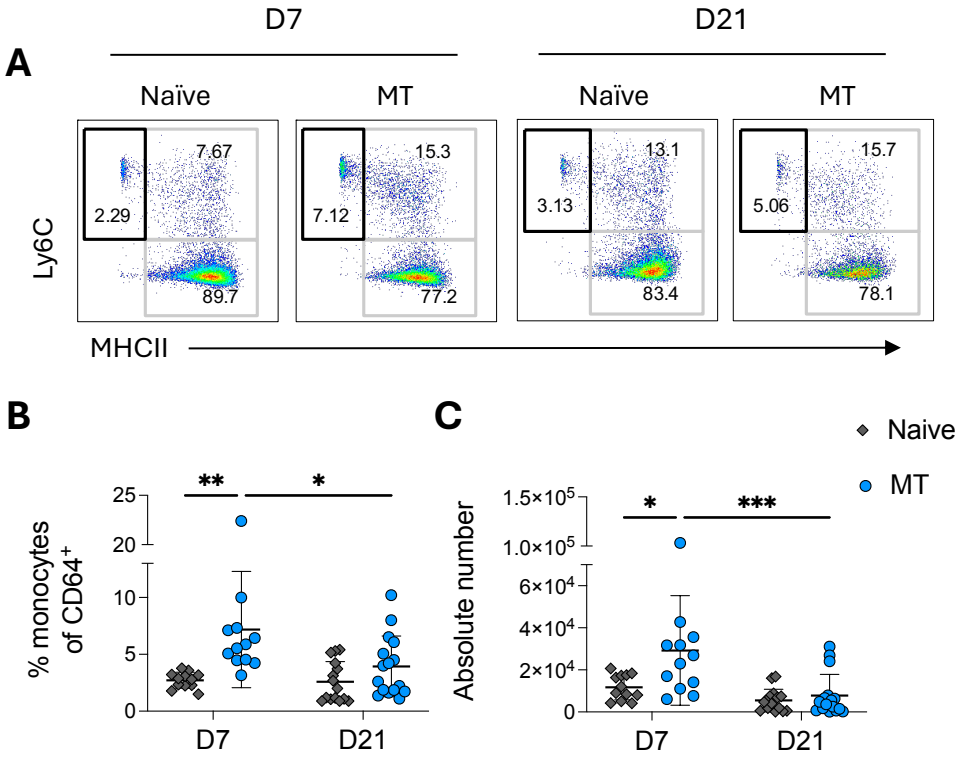


**Figure 4-3: *Hh*$^{+}$ MT induces increased monocyte infiltration to the colon at day 7**
C57BL/6 littermate cohorts were left untreated (Naïve) or colonized with *Hh*$^{+}$ microbiota (MT) for 7- or 21-days. Representative dot plots of colonic CD11b$^{+}$CD64$^{+}$ monocyte-macrophages divided by expression of Ly6C and MHCII (A), quantification of Ly6C$^{+}$MHCII$^{-}$ monocyte frequencies (B) and absolute numbers (C) are shown. Data are shown with mean ± SD and pooled from 3 (D7) or 4 (D21) independent experiments with n=4 per experiment. Statistical significance was determined by 2-way ANOVA (significance *p< 0.05, **p<0.01, ***p< 0.001, ****p< .0001).

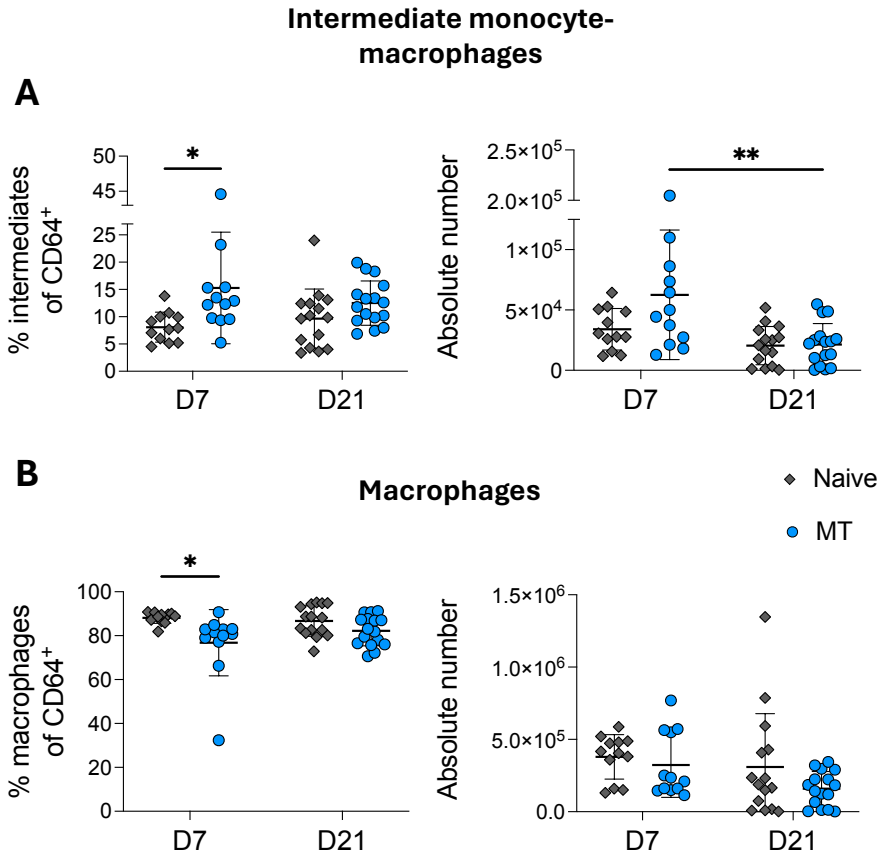


**Figure 4-4: *Hh*$^+$ MT drives increased accumulation of colonic intermediate monocyte-macrophages at day 7**
C57BL/6 littermate cohorts were left untreated (Naïve) or colonized with *Hh*$^+$ microbiota (MT) for 7- or 21-days. The frequency and absolute number of colonic Ly6C$^+$MHCII$^+$ intermediate monocyte-macrophages (A) and Ly6C$^-$MHCII$^+$ mature macrophages (B) are shown. Data are shown with mean ± SD and pooled from 3 (D7) or 4 (D21) independent experiments with n=4 per experiment. Statistical significance was determined by 2-way ANOVA (significance *p< 0.05, **p<0.01, ***p< 0.001, ****p< .0001).

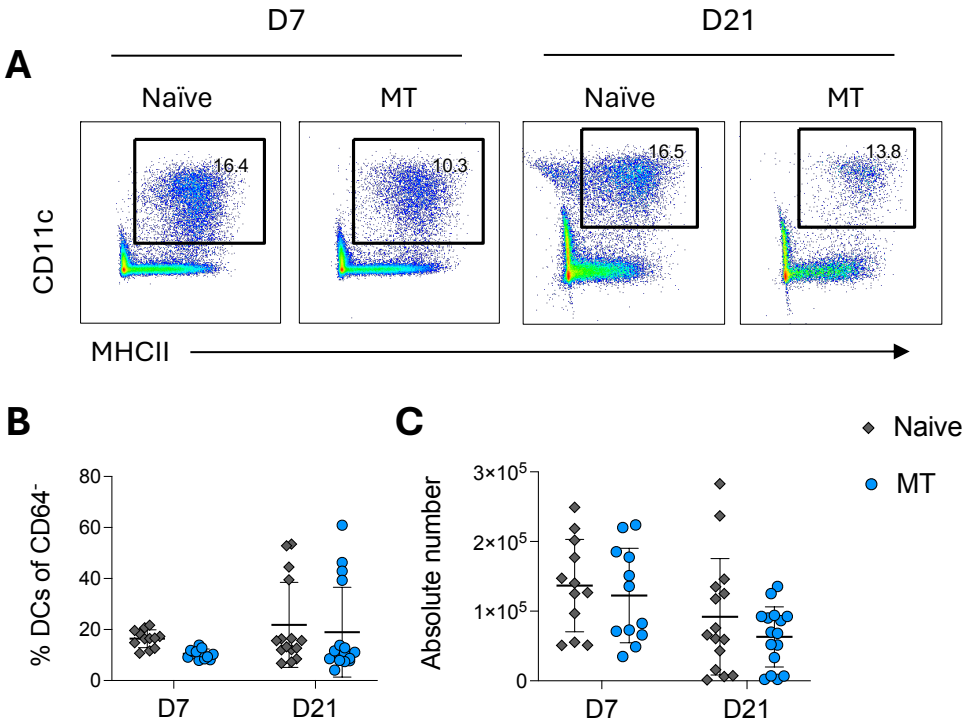


**Figure 4-5: *Hh*⁺ MT does not alter colonic cDC levels**
C57BL/6 littermate cohorts were left untreated (Naïve) or colonized with *Hh*⁺ microbiota (MT) for 7- or 21-days. Representative dot plots of colonic $CD64^{-}CD11c^{+}MHCII^{+}$ cDCs (A), quantification of cDC frequencies (B) and absolute numbers (C) are shown. Data are shown with mean ± SD and pooled from 3 (D7) or 4 (D21) independent experiments with n=4 per experiment. Statistical significance was determined by 2-way ANOVA (significance *p< 0.05, **p<0.01, ***p< 0.001, ****p< .0001).

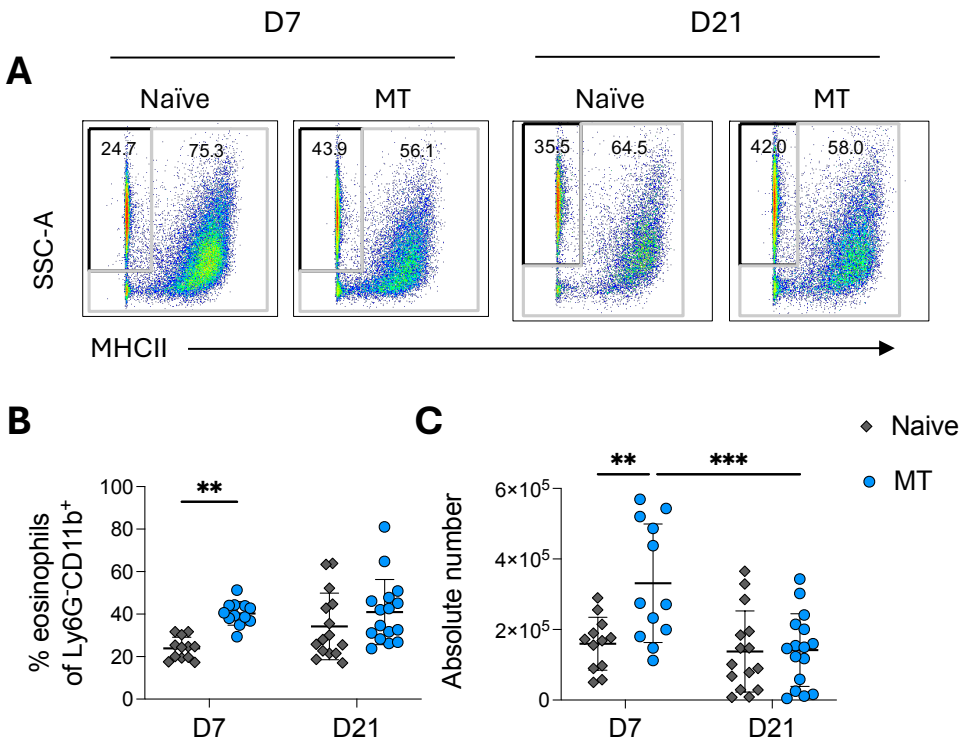


**Figure 4-6: *Hh*⁺ MT drives increased levels of colonic eosinophils at day 7**
C57BL/6 littermate cohorts were left untreated (Naïve) or colonized with *Hh*⁺ microbiota (MT) for 7- or 21-days. Representative dot plots of colonic CD11b⁺SSC$^{hi}$MHCII⁻ eosinophils (A), quantification of eosinophil frequencies (B) and absolute numbers (C) are shown. Data are shown with mean ± SD and pooled from 3 (D7) or 4 (D21) independent experiments with n=4 per experiment. Statistical significance was determined by 2-way ANOVA (significance *p< 0.05, **p<0.01, ***p< 0.001, ****p< .0001).

We then repeated these experiments with direct *Hh* infection to determine whether *Hh* was sufficient to drive the observed responses, or if they were due to the influx of other microbes in *Hh*⁺ MT recipients. Mice were directly infected with *Hh* as previously and cLPL analysed at the indicated timepoints. We found that direct *Hh* infection did not drive significant changes to numbers of CD45⁺ or CD11b⁺ cells in the colon (Figure 4-7A-B). However, numbers of CD64⁺ monocyte-macrophages were significantly increased at day 7 post infection with *Hh* compared to controls, and again this was reduced to control levels by day 21 (Figure 4-7C). Unlike the *Hh*⁺ MT recipients, a proportion of mice directly infected with *Hh* showed increased colonic neutrophils at day 7, but there was no significant difference between the groups at day 21 (Figure 4-8). *Hh*-infected mice also displayed significantly elevated levels of infiltrating monocytes at both day 7 and day 21 (Figure 4-9). Intermediate monocyte-macrophages were substantially increased at day 7 following *Hh* infection but were comparable with controls by day 21 (Figure 4-10A). *Hh* drove only proportional changes to macrophage frequencies and numbers of these cells were not affected by the

infection at either timepoint (Figure 4-10B). As observed in the *Hh*$^+$ MT experiments, cDC levels were also unaffected by direct *Hh* colonization (Figure 4-11). Finally, and in contrast to *Hh*$^+$ MT recipients (Figure 4-6), mice infected with *Hh* directly showed no significant differences in eosinophil levels at either timepoint (Figure 4-12), although there was a trend towards increased eosinophil numbers in some *Hh* infected mice. This suggests that changes to eosinophils in the *Hh*$^+$ MT system may be the result of additional microbes transferred and not caused by *Hh*.

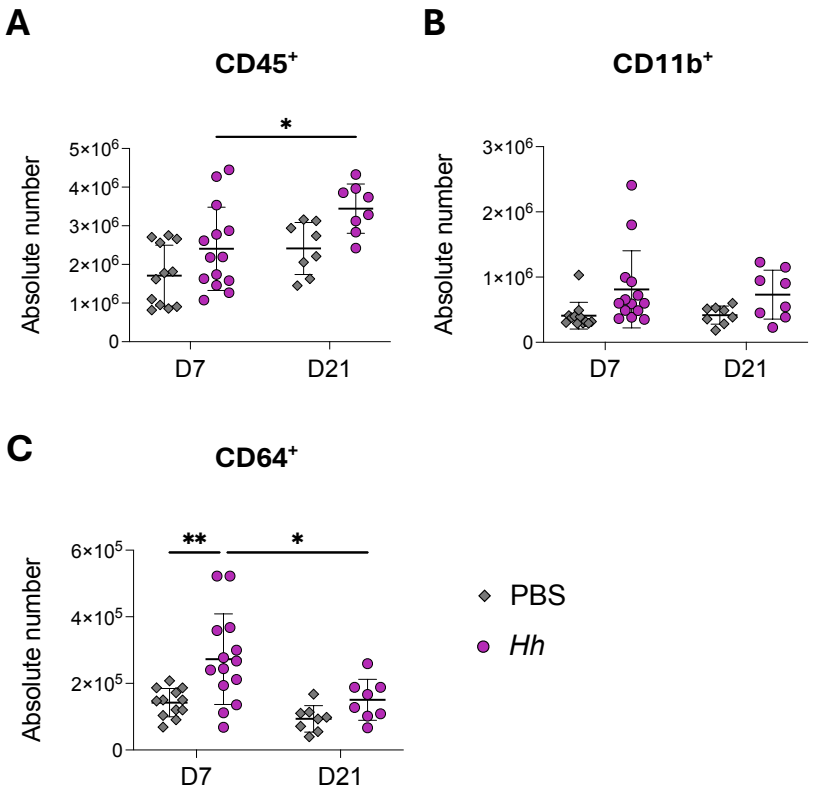


**Figure 4-7: *Hh* colonization drives increased CD64$^+$ monocyte-macrophage levels in the colon at day 7 post-infection**
C57BL/6 littermates were administered 1x10$^8$ CFU *Hh* or given PBS by oral gavage and left for 7- or 21-days post-infection. Colonic LP leukocytes were isolated using enzymatic digestion and the absolute number of CD45$^+$ (A), CD11b$^+$ (B), and CD64$^+$ (C) cells were calculated. Data are shown with mean ± SD and pooled from 3 (D7) or 2 (D21) independent experiments with n=4-6 per experiment. Statistical significance was determined by 2-way ANOVA (significance *p< 0.05, **p<0.01, ***p< 0.001, ****p< .0001).

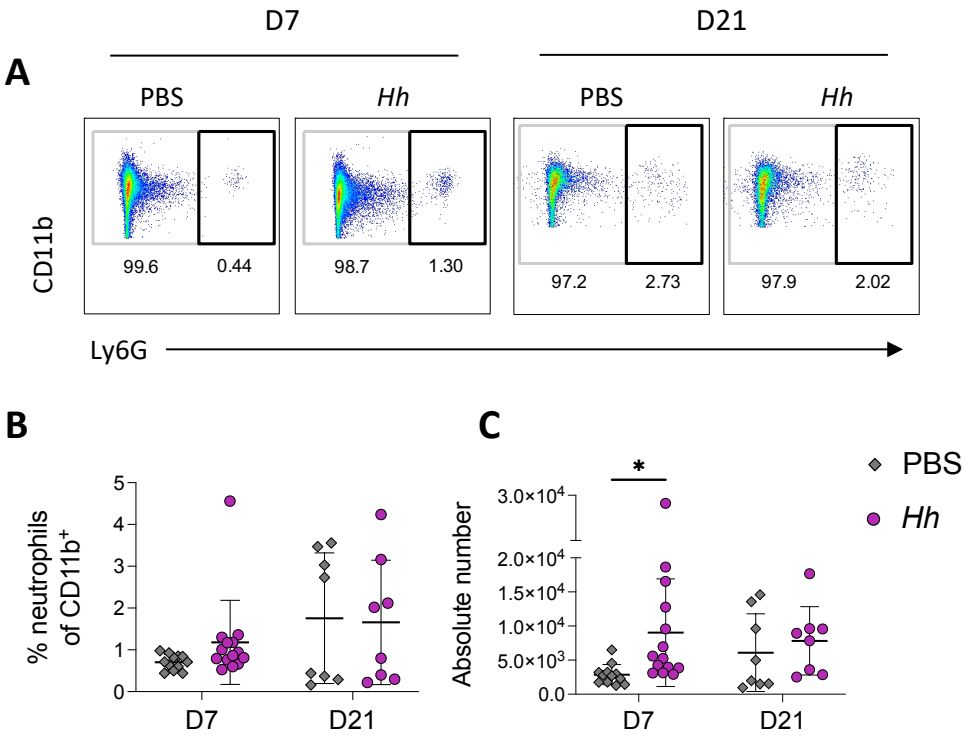


**Figure 4-8: *Hh* colonization induces increased colonic neutrophil accumulation at day 7**
C57BL/6 littermates were administered 1x10$^8$ CFU *Hh* or given PBS by oral gavage and left for 7- or 21-days post-infection. Representative dot plots of colonic CD11b$^+$Ly6G$^+$ neutrophils (A), quantification of neutrophil frequencies (B) and absolute numbers (C) are shown. Data are shown with mean ± SD and pooled from 3 (D7) or 2 (D21) independent experiments with n=4-6 per experiment. Statistical significance was determined by 2-way ANOVA (significance *p< 0.05, **p<0.01, ***p< 0.001, ****p< .0001).

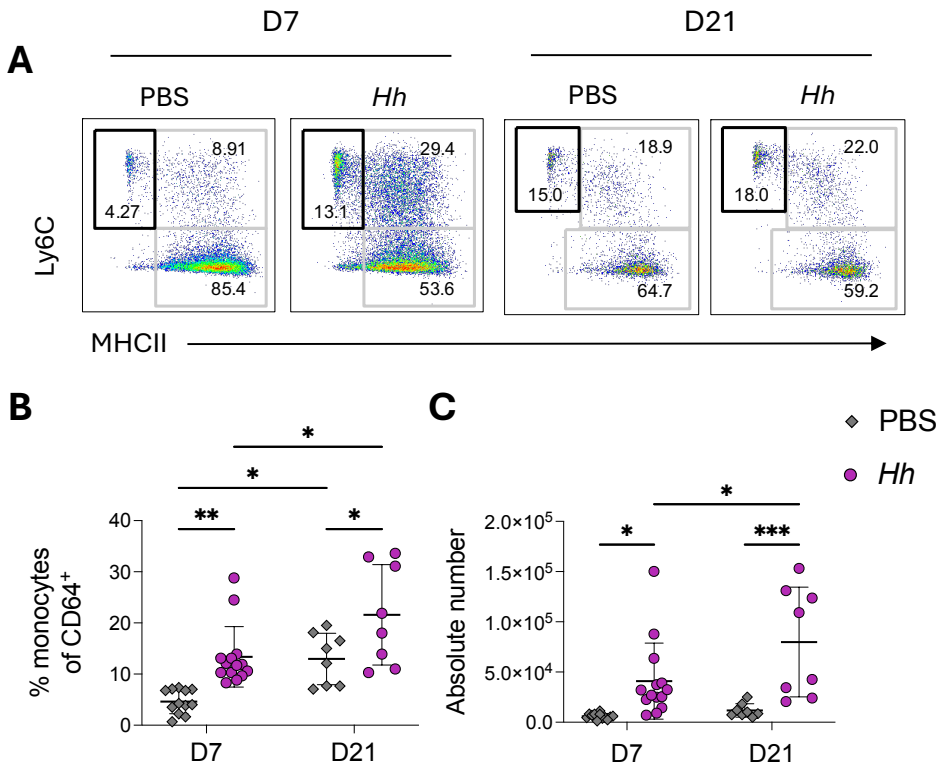


**Figure 4-9: *Hh* colonization induces increased monocyte infiltration to the colon**
C57BL/6 littermates were administered 1x10$^8$ CFU *Hh* or given PBS by oral gavage and left for 7- or 21-days post-infection. Representative dot plots of colonic CD11b$^+$CD64$^+$ monocyte-macrophages (A), quantification of Ly6C$^+$MHCII$^-$ monocyte frequencies (B) and absolute numbers (C) are shown. Data are shown with mean ± SD and pooled from 3 (D7) or 2 (D21) independent experiments with n=4-6 per experiment. Statistical significance was determined by 2-way ANOVA (significance *p< 0.05, **p<0.01, ***p< 0.001, ****p< .0001).

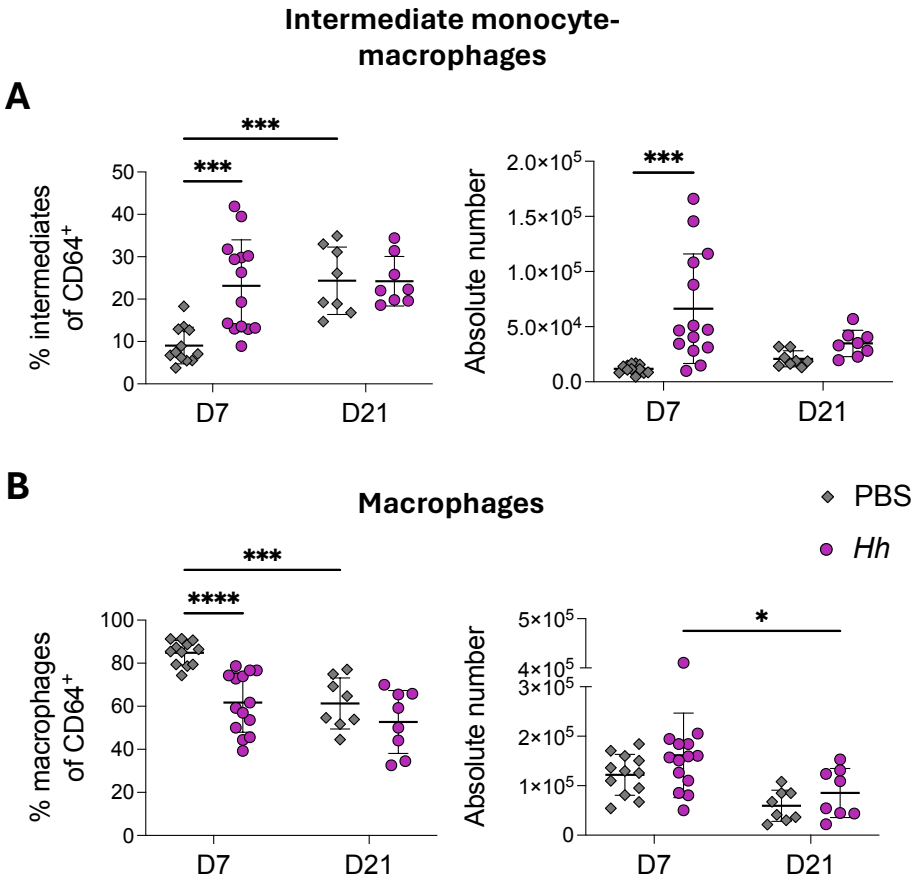


**Figure 4-10: *Hh* colonization drives increased accumulation of colonic intermediate monocyte-macrophages at day 7**
C57BL/6 littermates were administered 1x10$^8$ CFU *Hh* or given PBS by oral gavage and left for 7- or 21-days post-infection. The frequency and absolute number of colonic Ly6C$^+$MHCII$^+$ intermediate monocyte-macrophages (A) and Ly6C$^-$MHCII$^+$ mature macrophages (B) are shown. Data are shown with mean ± SD and pooled from 3 (D7) or 2 (D21) independent experiments with n=4-6 per experiment. Statistical significance was determined by 2-way ANOVA (significance *p< 0.05, **p<0.01, ***p< 0.001, ****p< .0001).

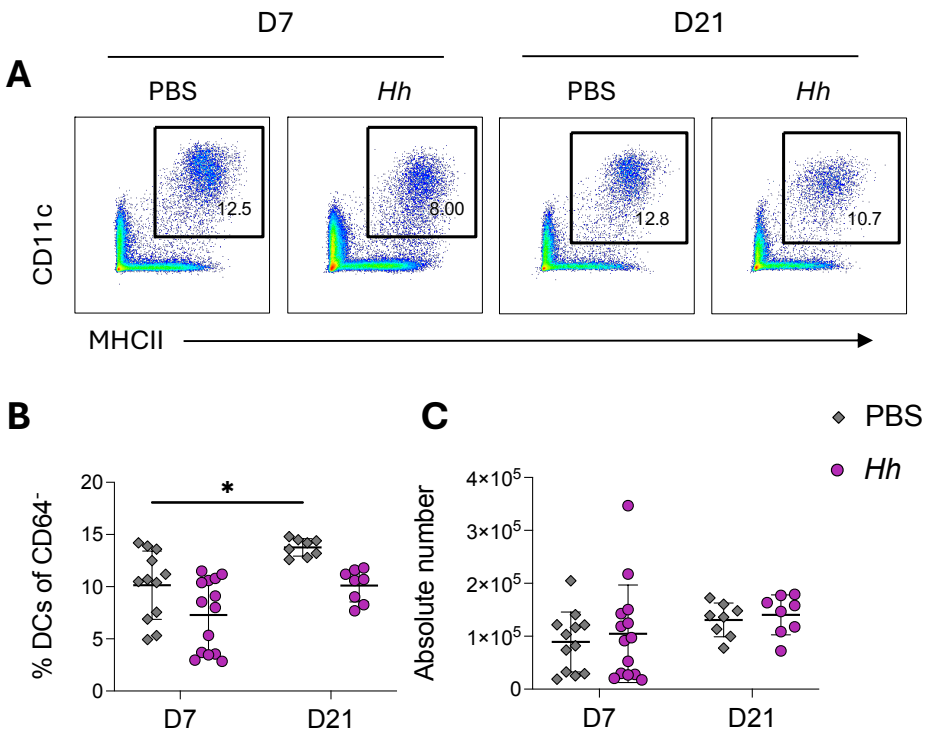


**Figure 4-11: *Hh* colonization does not drive changes to colonic cDC levels**
C57BL/6 littermates were administered 1x10$^8$ CFU *Hh* or given PBS by oral gavage and left for 7- or 21-days post-infection. Representative dot plots of colonic CD64$^-$CD11c$^+$MHCII$^+$ cDCs (A), quantification of cDC frequencies (B) and absolute numbers (C) are shown. Data are shown with mean ± SD and pooled from 3 (D7) or 2 (D21) independent experiments with n=4-6 per experiment. Statistical significance was determined by 2-way ANOVA (significance *p< 0.05, **p<0.01, ***p< 0.001, ****p< .0001).

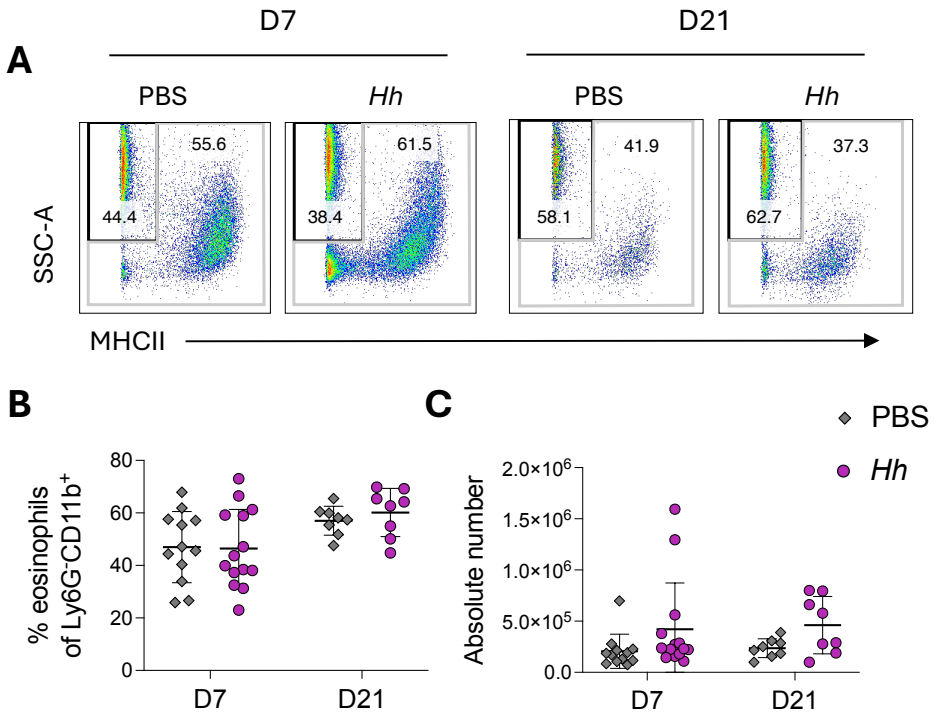


**Figure 4-12: *Hh* colonization does not significantly impact colonic eosinophil accumulation**
C57BL/6 littermates were administered 1x10$^8$ CFU *Hh* or given PBS by oral gavage and left for 7- or 21-days post-infection. Representative dot plots of colonic CD11b$^+$SSC$^{hi}$MHCII$^-$ eosinophils (A), quantification of eosinophil frequencies (B) and absolute numbers (C) are shown. Data are shown with mean ± SD and pooled from 3 (D7) or 2 (D21) independent experiments with n=4-6 per experiment. Statistical significance was determined by 2-way ANOVA (significance *p< 0.05, **p<0.01, ***p< 0.001, ****p< .0001).

Together, these data indicate that colonization with *Hh* drives early recruitment of myeloid cells to the large intestine, suggesting that there is an initial innate immune response stimulated by *Hh*. By day 21, this response appears to have mostly resolved, with only some animals showing a maintained increase in monocyte infiltration at the later timepoint. *Hh*$^+$ MT and direct *Hh* infection had similar effects on the myeloid pool, with the most notable difference being a significant increase in eosinophil levels in *Hh*$^+$ MT recipients at day 7 that was not fully recapitulated in mice infected with *Hh* alone.

### 4.3.2 *Hh* has minimal effects on colonic macrophage and cDC phenotypes at steady state

To further explore the effect of *Hh* on the myeloid compartment at steady state, we assessed colonic macrophages and cDCs following *Hh* colonization. It is well documented that, as these cells mature in the tissue, they exhibit phenotypic differences driven by the local environment (Chang et al., 2014, Schridde et al., 2017, Kang et al., 2020, Cabeza-Cabrerizo et al., 2021). In the direct *Hh* infection system, we assessed colonic macrophages for expression of CD11c, a

marker expressed on inflammatory macrophages (Corbin et al., 2020). At day 7 there were no differences in CD11c expression by colonic macrophages in both groups (Figure 4-13A), but by day 21 CD11c expression was significantly lower in colonic macrophages from *Hh* infected mice (Figure 4-13A). We also measured macrophage PD-L1 expression, another indicator of an inflammatory macrophage phenotype (Yamazaki et al., 2002), and found no significant difference in expression by colonic macrophages in both groups (Figure 4-13B).

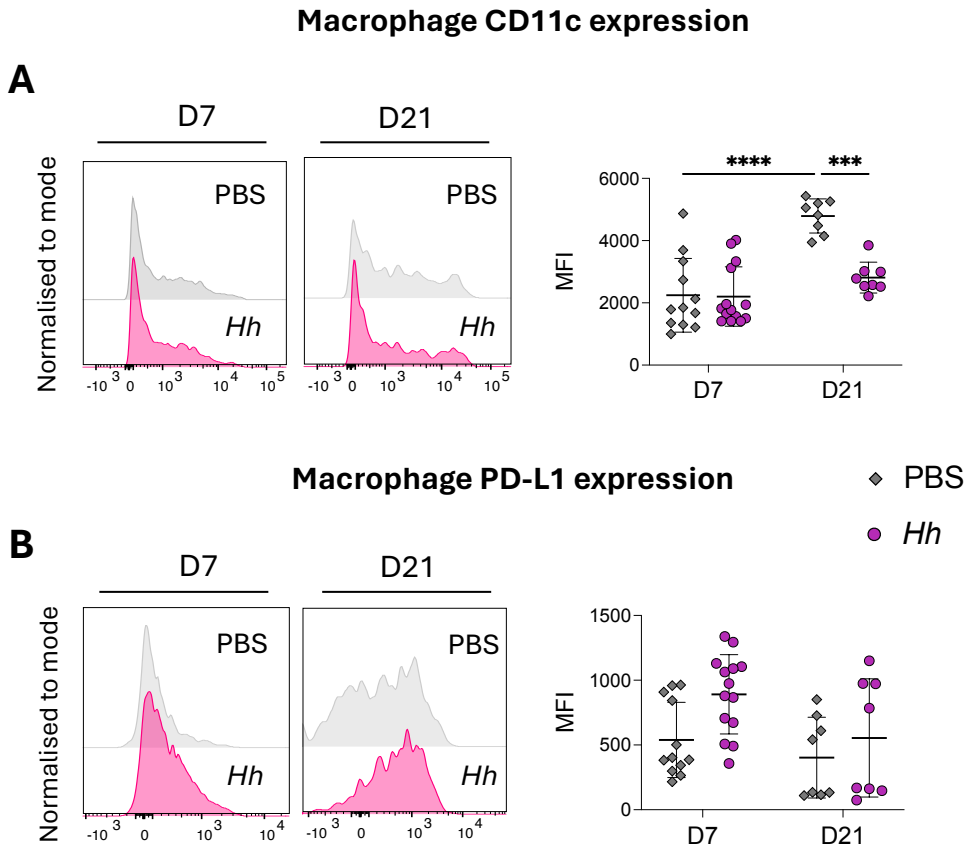


**Figure 4-13: Colonic macrophages show lower CD11c expression on day 21 post-infection with *Hh***
C57BL/6 littermates were administered 1x10$^8$ CFU *Hh* or given PBS by oral gavage and left for 7- or 21-days post-infection. Colonic macrophages were identified as CD11b$^+$CD64$^+$Ly6C$^-$MHCII$^+$ and analysed for expression of CD11c (A) and PD-L1 (B). Representative histograms showing the proportion of CD11c/PD-L1-expressing macrophages (left) and quantification of MFI (right) are shown. Data are shown with mean ± SD and pooled from 3 (D7) or 2 (D21) independent experiments with n=4-6 per experiment. Statistical significance was determined by 2-way ANOVA (significance *p< 0.05, **p<0.01, ***p< 0.001, ****p< .0001).

Expression of the mannose receptor (CD206) is associated with activation of macrophages by IL-4 and IL-13, often referred to as "M2" or "alternatively activated" macrophages (Smith et al., 2016). While intestinal macrophages do not fit comfortably into this paradigm, CD206 expression is often used to denote repair-associated macrophages, and its upregulation is induced by IL-10

signalling (Bain and Mowat, 2014). We saw no differences in CD206$^+$ colonic macrophages following *Hh* infection, although the proportions of CD206$^+$ colonic macrophages were reduced on day 21 in both groups (Figure 4-14). We then measured colonic macrophage CD80 expression and found it to be unaffected by *Hh* infection (Figure 4-15A-B). In contrast, the proportions of CD86$^+$ colonic macrophages were significantly decreased in *Hh* colonized mice at day 21 post-infection (Figure 4-15C-D). Similarly, we saw no differences in CD80 expression on colonic cDCs from both groups (Figure 4-16A-B), but observed a significant reduction in CD86$^+$ colonic cDCs from *Hh*-infected mice at day 21 post-infection (Figure 4-16C-D).

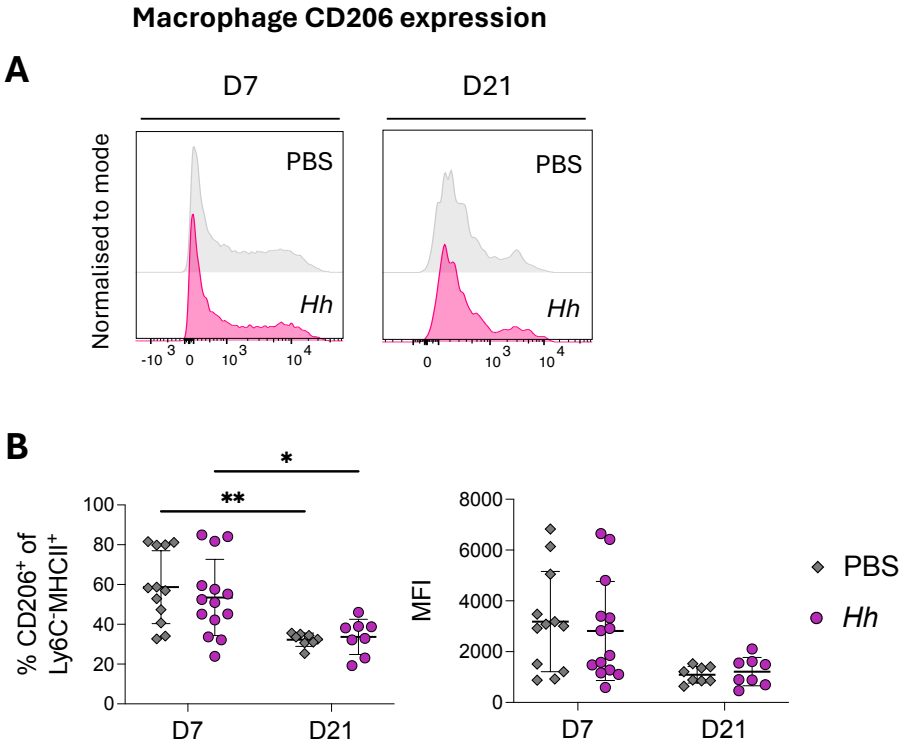


**Figure 4-14: *Hh* colonization does not alter macrophage expression of CD206**
C57BL/6 littermates were administered 1x10$^8$ CFU *Hh* or given PBS by oral gavage and left for 7- or 21-days post-infection. Colonic macrophages were identified as CD11b$^+$CD64$^+$Ly6C$^-$MHCII$^+$ and analysed for expression of CD206. Representative histograms showing the proportion of CD206-expressing macrophages (A) and quantification of frequency and MFI (B) are shown. Data are shown with mean ± SD and pooled from 3 (D7) or 2 (D21) independent experiments with n=4-6 per experiment. Statistical significance was determined by 2-way ANOVA (significance *p< 0.05, **p<0.01, ***p< 0.001, ****p< .0001).

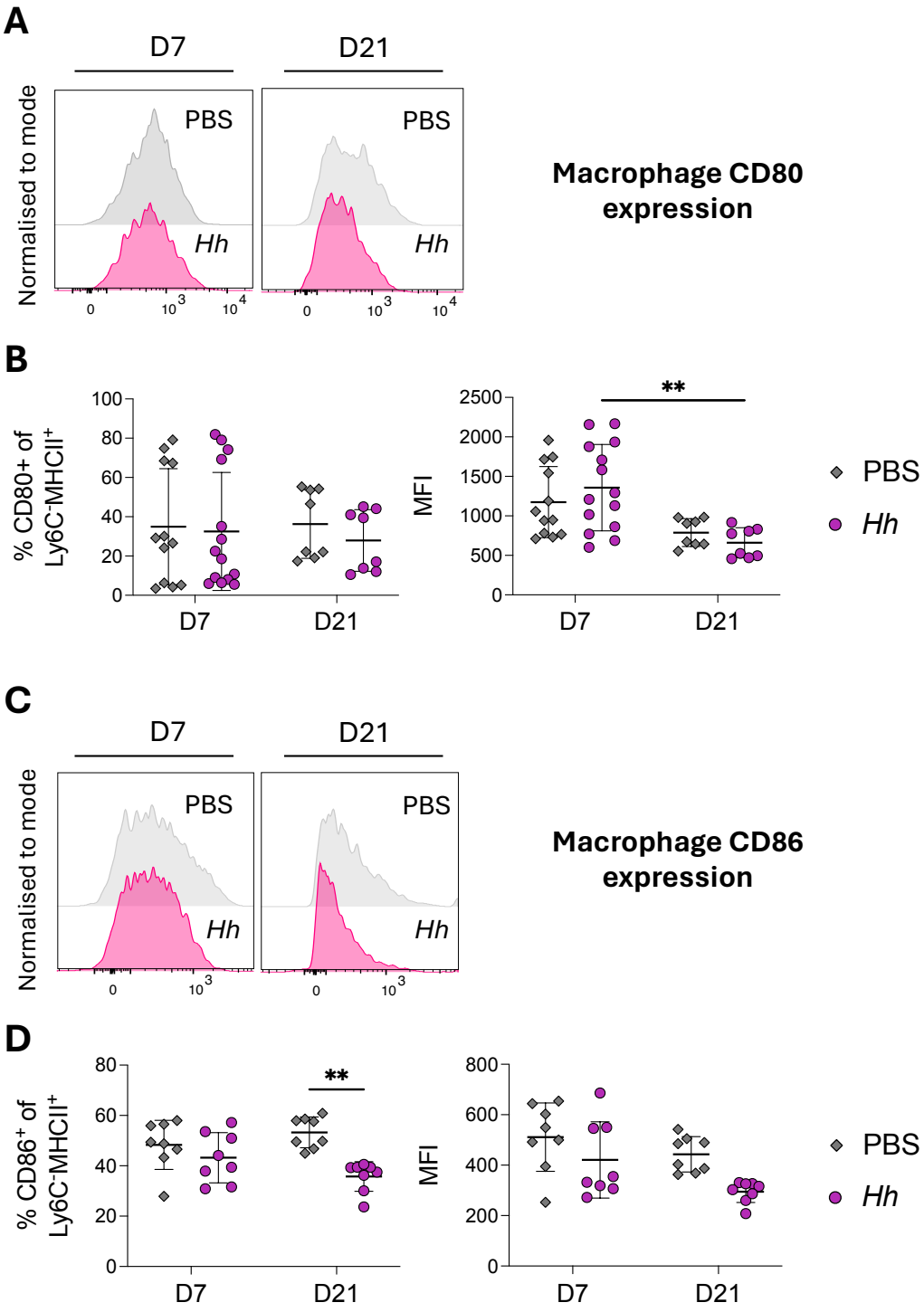


**Figure 4-15: *Hh* colonization reduces CD86⁺ colonic macrophages at day 21 post-infection**
C57BL/6 littermates were administered 1x10$^8$ CFU *Hh* or given PBS by oral gavage and left for 7- or 21-days post-infection. Colonic macrophages were identified as CD11b⁺CD64⁺Ly6C⁻MHCII⁺ and analysed for expression of CD80 (A, B) and CD86 (C, D). Representative histograms showing the proportion of CD80/86-expressing macrophages (A, C) and quantification of frequency and MFI (B, D) are shown. Data are shown with mean ± SD and pooled from 3 (D7) or 2 (D21) independent experiments with n=4-6 per experiment. Statistical significance was determined by 2-way ANOVA (significance *p< 0.05, **p<0.01, ***p< 0.001, ****p< .0001).

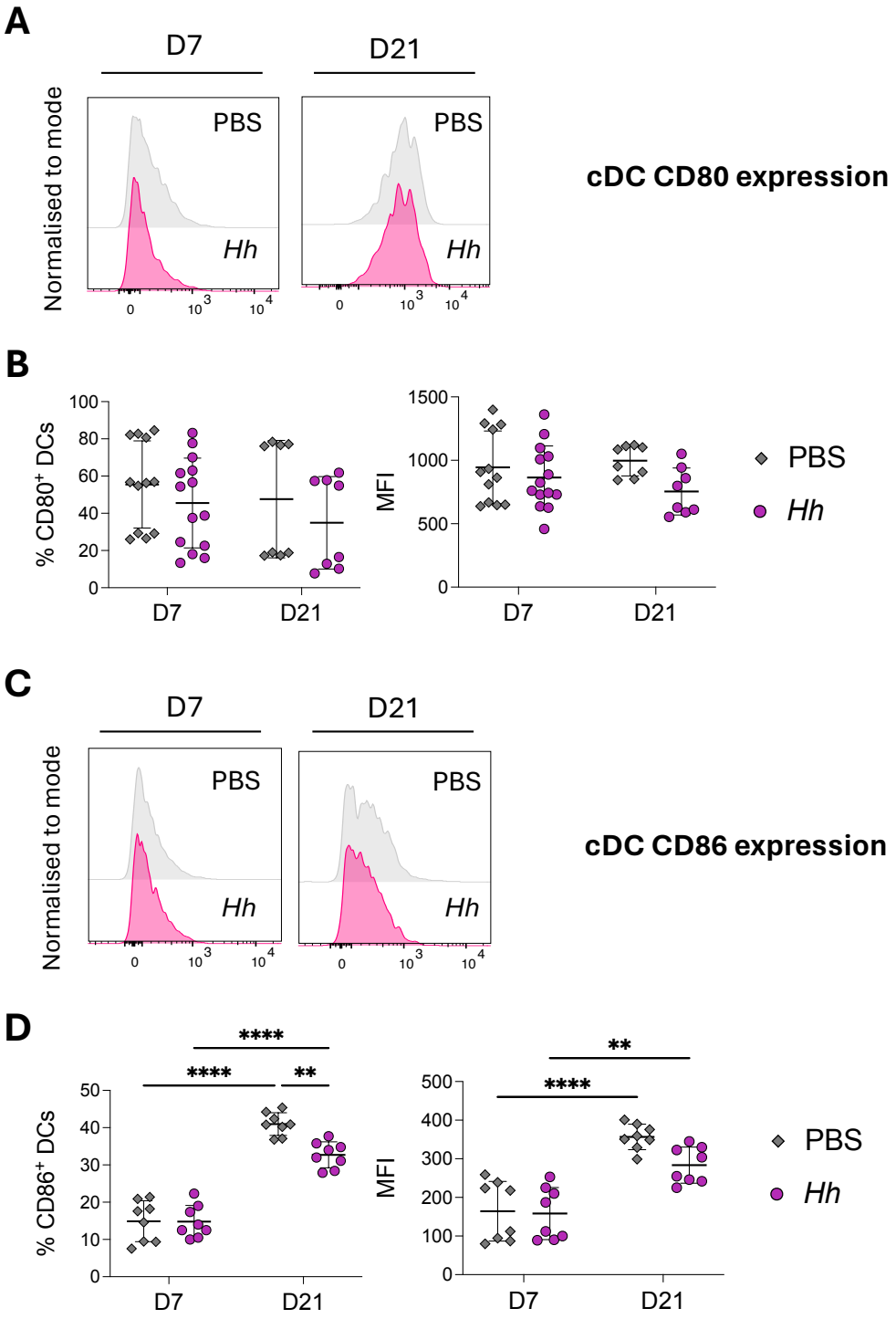


**Figure 4-16: *Hh* colonization reduces CD86⁺ colonic cDC at day 21 post-infection**
C57BL/6 littermates were administered 1x10$^8$ CFU *Hh* or given PBS by oral gavage and left for 7- or 21-days post-infection. Colonic cDCs were identified as CD64$^-$CD11c$^+$MHCII$^+$ and analysed for expression of CD80 (A, B) and CD86 (C, D). Representative histograms showing the proportion of CD80/86-expressing cDCs (A, C) and quantification of frequency and MFI (B, D) are shown. Data are shown with mean ± SD and pooled from 3 (D7) or 2 (D21) independent experiments with n=4-6 per experiment. Statistical significance was determined by 2-way ANOVA (significance *p< 0.05, **p<0.01, ***p< 0.001, ****p< .0001).

Although the majority of gut macrophages are constantly replenished from BM monocytes (Bain et al., 2014), a recently described population of intestinal macrophages, defined as CD4⁺Tim4⁺, appear to be long-lived resident cells in the

gut that are self-maintained in the tissue (Shaw et al., 2018). We assessed whether *Hh* infection altered the abundance of these cells, but we saw no differences in either the frequency or number of these CD4$^+$Tim4$^+$ macrophages at either timepoint (Figure 4-17).

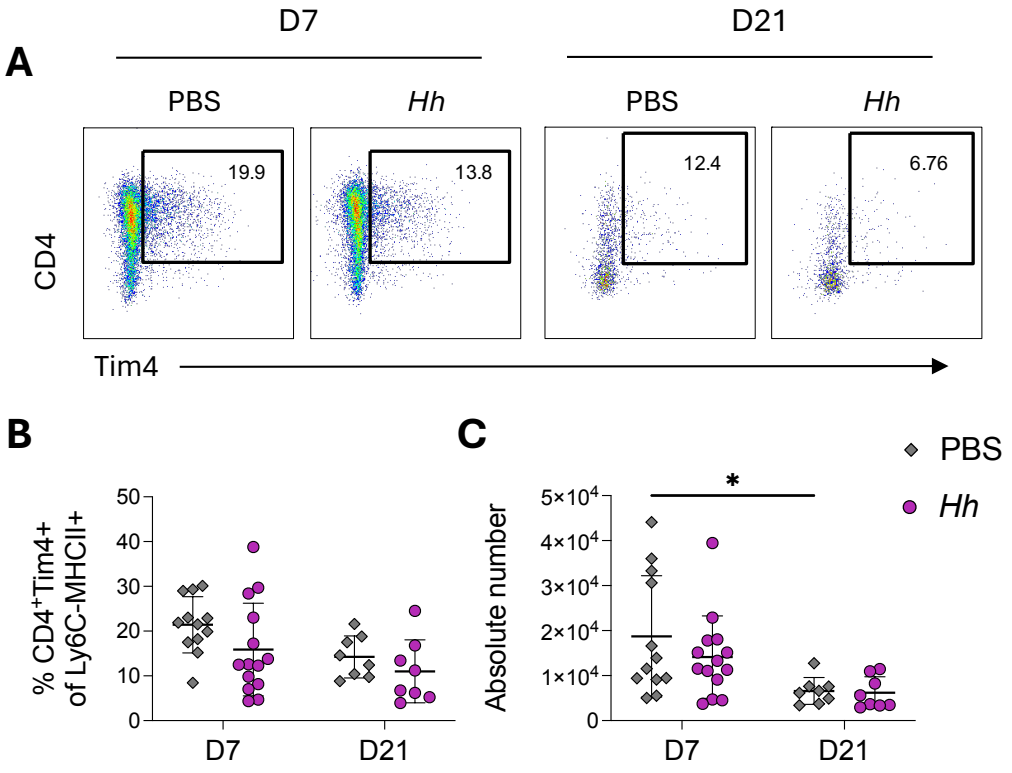


**Figure 4-17: Levels of CD4$^+$Tim4$^+$ macrophages are not changed by *Hh* colonization**
C57BL/6 littermates were administered 1x10$^8$ CFU *Hh* or given PBS by oral gavage and left for 7- or 21-days post-infection. Colonic macrophages were identified as CD11b$^+$CD64$^+$Ly6C$^-$MHCII$^+$ and representative dot plots of CD4$^+$Tim4$^+$ macrophages (A), quantification of frequencies (B) and absolute numbers (C) are shown. Data are shown with mean ± SD and pooled from 3 (D7) or 2 (D21) independent experiments with n=4-6 per experiment. Statistical significance was determined by 2-way ANOVA (significance *p< 0.05, **p<0.01, ***p< 0.001, ****p< .0001).

To conclude, we observed that colonic macrophages and cDCs were generally very similar between uninfected and *Hh*-colonized mice. Following *Hh* colonization, no changes at day 7 post-infection were observed, while at day 21 there were reduced proportions of CD86$^+$ colonic cDCs and macrophages in *Hh*-infected mice. There were also reduced proportions of CD11c$^+$ colonic macrophages in *Hh*-infected mice at the later timepoint only. These data suggest that, when directly infected with *Hh*, macrophages and cDCs show subtle phenotypic differences which take time to become apparent.

### 4.3.3 Colonic transcription of *Tnfα*, *Ifnγ*, and *Il17a* is altered at different timepoints post-infection

Having determined that *Hh* colonization drives an early myeloid response in the colon, we next explored whether there were accompanying changes to cytokine expression. We first assessed inflammatory cytokine transcription in whole distal colon tissue and found that at day 7 post infection, there was a significant upregulation of *Ifnγ* expression in *Hh*-infected mice, although this difference was not significant at day 21 (Figure 4-18). However, at day 21, we observed significant upregulation of *Tnfa* and *Il17a* in the colons of *Hh*-infected mice which was not present at day 7, indicating that there are differences in the response to *Hh* over time. We did not observe differences in expression of *Il1β*, *Il6*, or *Il22* at either timepoint (Figure 4-18). We next measured expression of *Il10* and, despite the slight trend towards increased expression at day 21, there were no significant differences in colonic *Il10* at either timepoint (Figure 4-19). Finally, we measured expression of *Nos2*, which is upregulated following exposure to inflammatory cytokines (Soufli et al., 2016). Again, although there was a trend towards increased expression of *Nos2* in the colon samples from *Hh*-infected mice, these differences did not reach statistical significance (Figure 4-20).

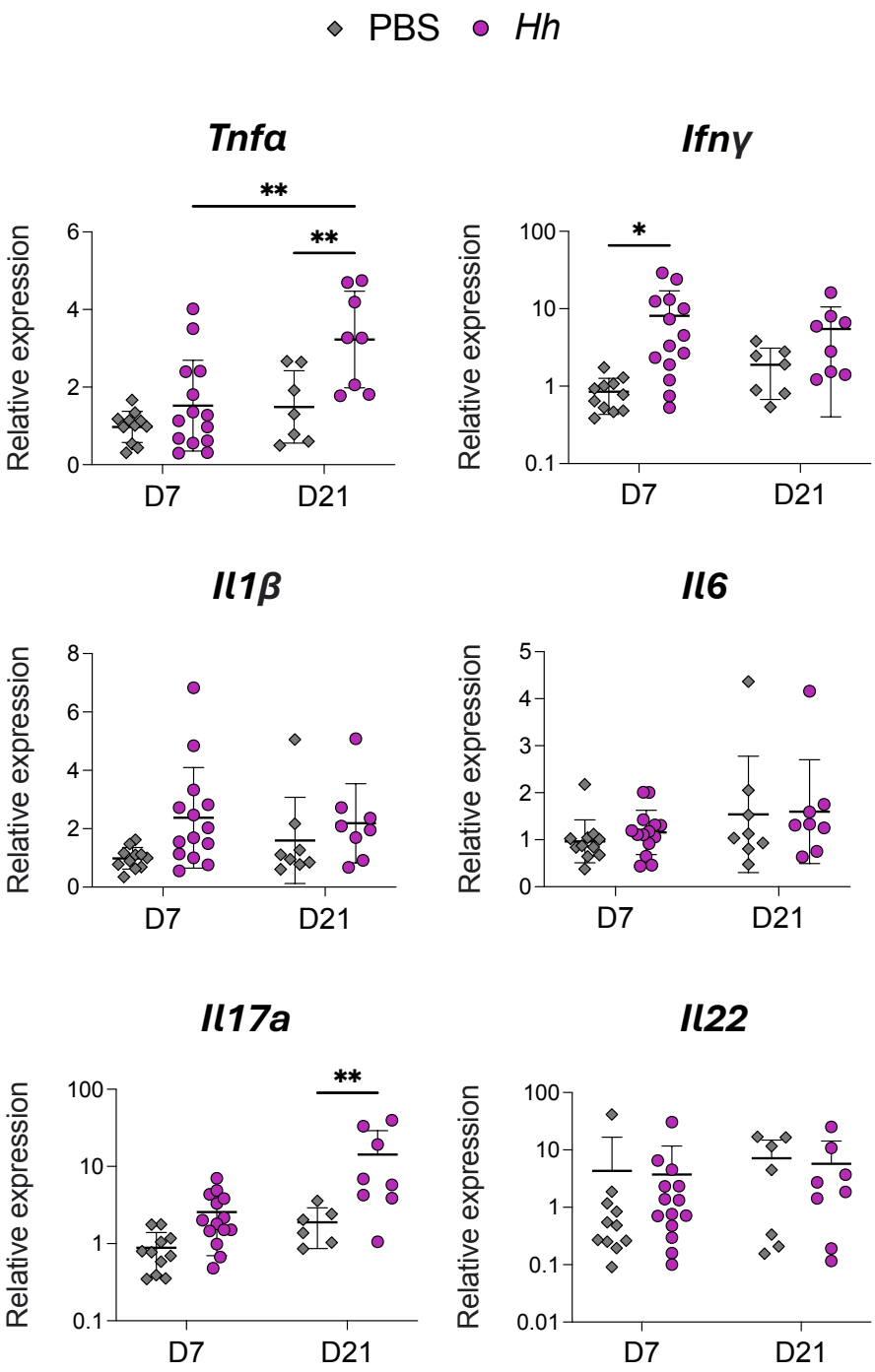


**Figure 4-18: Increased inflammatory cytokine gene expression in the colon after Hh colonization**
C57BL/6 littermates were administered 1x10$^8$ CFU *Hh* or given PBS by oral gavage and left for 7- or 21-days post-infection. A section of distal colon was harvested and expression of indicated genes measured using qPCR. Differences in gene expression were determined using the $2^{-\Delta\Delta C(t)}$ method, with gene expression normalised to the housekeeping gene *Rps29* and data shown as fold change relative to the D7 PBS controls. Data are shown with mean ± SD and pooled from 3 (D7) or 2 (D21) independent experiments with n=4-6 per experiment. Statistical significance was determined by 2-way ANOVA (significance *p< 0.05, **p<0.01, ***p< 0.001, ****p< .0001).

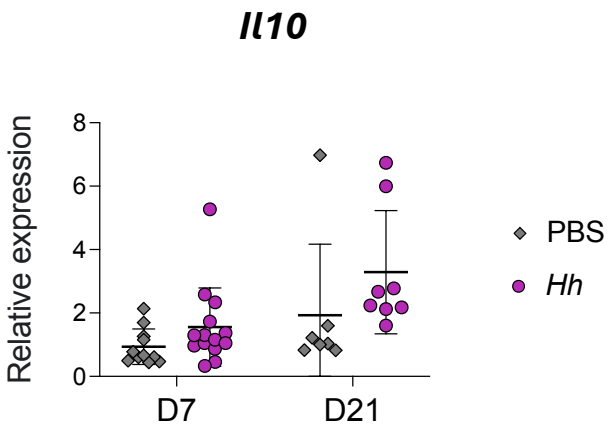


**Figure 4-19: *Hh* colonization does not alter transcription of *Il10* in the colon**
C57BL/6 littermates were administered 1x10$^8$ CFU *Hh* or given PBS by oral gavage and left for 7- or 21-days post-infection. A section of distal colon was harvested and expression of *Il10* measured using qPCR. Differences in gene expression were determined using the $2^{-\Delta\Delta C(t)}$ method, with gene expression normalised to the housekeeping gene *Rps29* and data shown as fold change relative to the D7 PBS controls. Data are shown with mean ± SD and pooled from 3 (D7) or 2 (D21) independent experiments with n=4-6 per experiment. Statistical significance was determined by 2-way ANOVA (significance *p< 0.05, **p<0.01, ***p< 0.001, ****p< .0001).

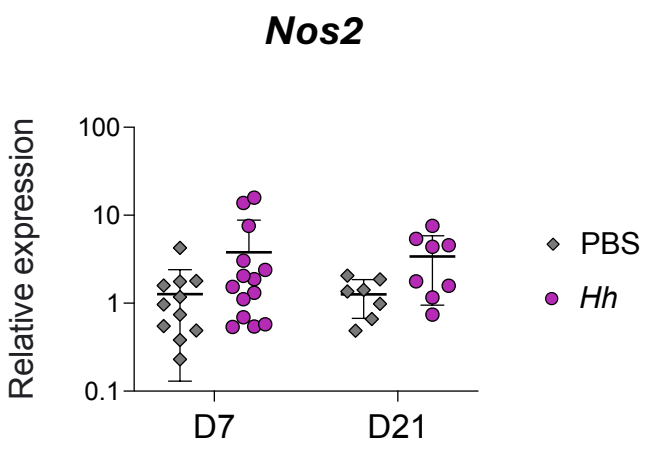


**Figure 4-20: *Hh* colonization does not significantly alter transcription of *Nos2* in the colon**
C57BL/6 littermates were administered 1x10$^8$ CFU *Hh* or given PBS by oral gavage and left for 7- or 21-days post-infection. A section of distal colon was harvested and expression of *Nos2* measured using qPCR. Differences in gene expression were determined using the $2^{-\Delta\Delta C(t)}$ method, with gene expression normalised to the housekeeping gene *Rps29* and data shown as fold change relative to the D7 PBS controls. Data are shown with mean ± SD and pooled from 3 (D7) or 2 (D21) independent experiments with n=4-6 per experiment. Statistical significance was determined by 2-way ANOVA (significance *p< 0.05, **p<0.01, ***p< 0.001, ****p< .0001).

Taken together, it appears that early after infection *Hh* drives transcriptional upregulation of *Ifny*, while at later timepoints there is increased *Tnfa* and *Il17a*. These data demonstrate that the cytokine response to *Hh* varies over time.

### 4.3.4 Small intestinal myeloid cell recruitment is not altered following *Hh* infection

We next aimed to determine whether homeostatic immunity to *Hh* was present only in tissues directly colonized, or if *Hh* induces longer reaching effects on other tissues. *Hh* colonizes the murine cecum and colon (Ward et al., 1994, Chan et al., 2005), so we tested whether there were changes to myeloid infiltration in the non-colonized SI. Mice were directly infected with *Hh* and small intestinal lamina propria (SILP) cells harvested on day 7, as we had observed the greatest myeloid response to *Hh* in the colon at this timepoint (Figure 4-8). However, in the SILP, we observed no significant differences in numbers of CD45$^+$ or CD11b$^+$ cells following *Hh* infection (Figure 4-21A). Likewise, levels of neutrophils and eosinophils were comparable between uninfected and *Hh* colonized mice, both in terms of frequency and number (Figure 4-21B-C). We then examined the monocyte-macrophage pool, which showed the clearest change in the colon following *Hh* infection (Figure 4-9, Figure 4-10). In contrast, in the SILP, we observed no significant differences in either monocyte infiltration or accumulation of intermediate monocyte-macrophages after *Hh* infection (Figure

4-22). Thus, the early myeloid responses to *Hh* infection that we observed in the colon were not recapitulated in the SILP, suggesting that *Hh* primarily elicits responses in directly colonized tissues.

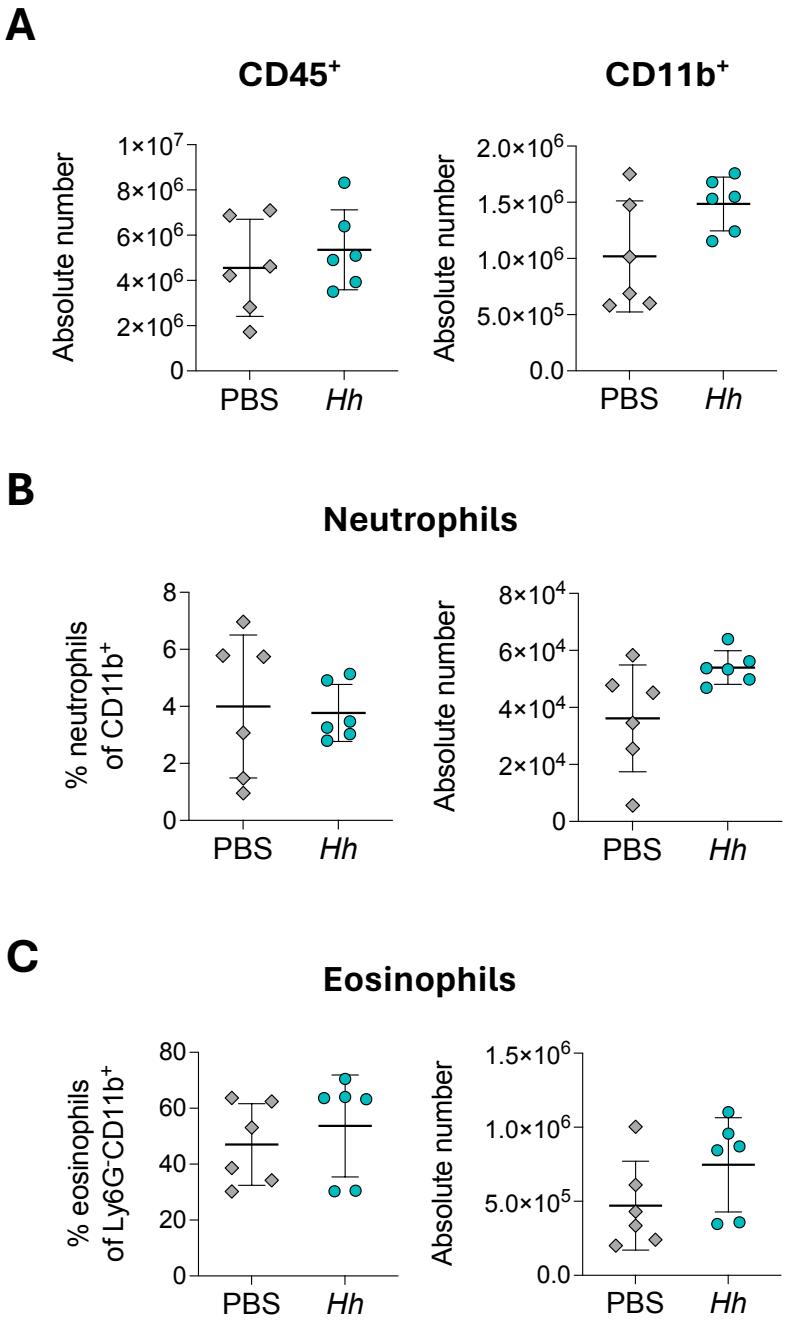


**Figure 4-21: *Hh* colonization does not significantly alter myeloid cell populations in the SILP** C57BL/6 littermates were administered 1x10$^8$ CFU *Hh* or given PBS by oral gavage and left for 7-days post-infection. SILP leukocytes were isolated using enzymatic digestion and the absolute number of CD45$^+$ and CD11b$^+$ leukocytes (A), the frequency and absolute number of CD11b$^+$Ly6G$^+$ neutrophils (B) and CD11b$^+$SSC$^{hi}$MHCII$^-$ eosinophils (C) are shown. Data are shown with mean ± SD and pooled from 2 independent experiments with n=3 per experiment. Data were tested for normality using the Shapiro-Wilk normality test and in cases where data were normally distributed statistical significance was determined by unpaired t test, while otherwise a Mann Whitney test was used (significance *p< 0.05, **p<0.01, ***p< 0.001, ****p< .0001).

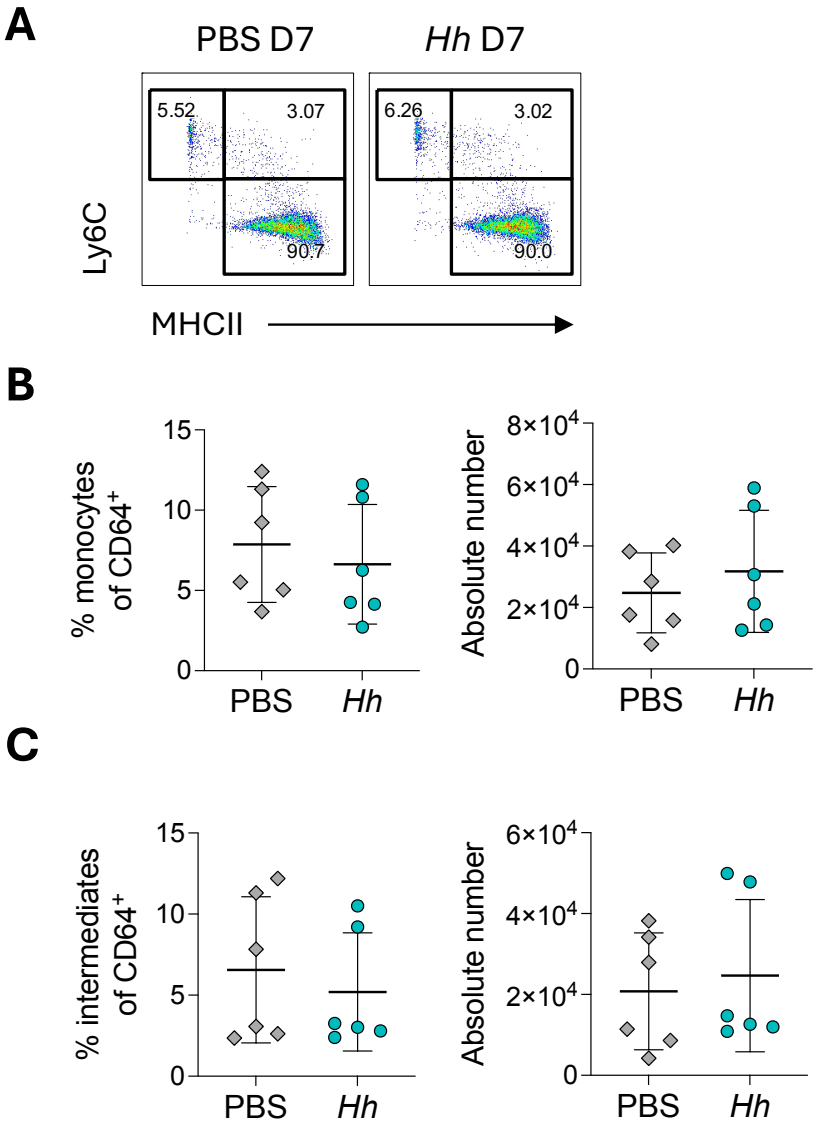


**Figure 4-22: *Hh* colonization does not alter levels of monocytes or intermediate monocyte-macrophages in the SILP**
C57BL/6 littermates were administered 1x10$^8$ CFU *Hh* or given PBS by oral gavage and left for 7-days post-infection. Representative dot plots of SILP CD11b$^+$CD64$^+$ monocyte-macrophages divided by expression of Ly6C and MHCII (A), quantification of Ly6C$^+$MHCII$^-$ monocyte (B) and Ly6C$^+$MHCII$^+$ intermediate monocyte-macrophage (C) frequency and absolute number are shown. Data are shown with mean ± SD and pooled from 2 independent experiments with n=3 per experiment. Data were tested for normality using the Shapiro-Wilk normality test and in cases where data were normally distributed statistical significance was determined by unpaired t test, while otherwise a Mann Whitney test was used (significance *p< 0.05, **p<0.01, ***p< 0.001, ****p< .0001).

### 4.3.5 Quantification of faecal microbial DNA following *Hh* colonization

Finally, to consider how *Hh* affects the local environment in the gut at steady state, we sought to determine whether there were changes to microbiota composition in *Hh*-colonized animals. We first measured whether levels of *Hh* colonization differed over the course of infection. Given that the *Hh*-mediated

protection against DSS-induced disease severity was only present at three weeks and not 1-week post-infection, we postulated that *Hh* colonization levels may increase over time and therefore have a greater effect on host immune function. However, when we quantified levels of faecal *Hh* DNA using qPCR, we observed comparable levels of colonization at day 7, day 14, and day 21 post-infection (Figure 4-23A). When the data were separated based on individual experiments, we saw that there was some variation in the kinetics of colonization, with trends towards levels increasing over time in one experiment, decreasing in another and remaining consistent in a third (Figure 4-23B). However, these trends were not statistically significant. We concluded that, generally, levels of *Hh* do not significantly increase over the course of a three-week infection.

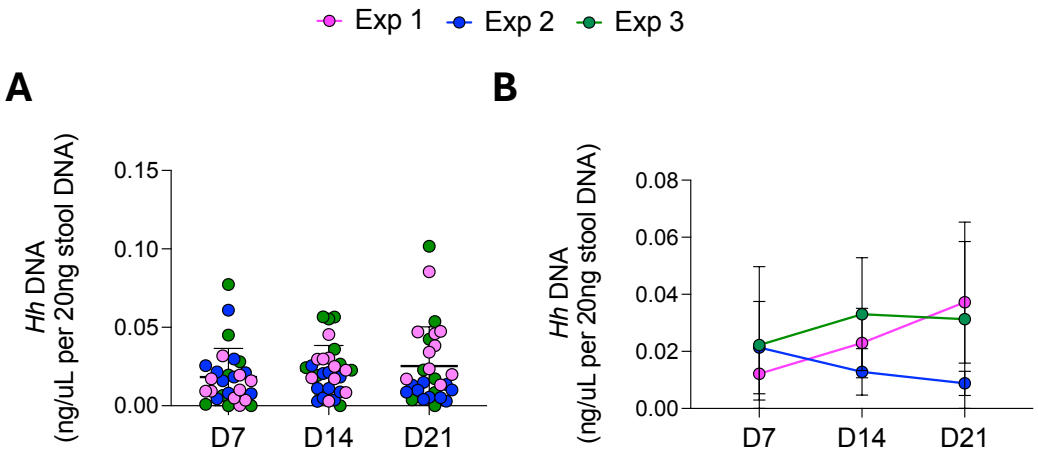


**Figure 4-23: Levels of *Hh* colonization do not change between day 7 and day 21 post-infection**
C57BL/6 littermates were administered 1x10$^8$ CFU *Hh* or given PBS by oral gavage and left for 21-days post-infection. Stool samples were collected on day 7, day 14 and day 21, genomic DNA was extracted and expression of *CdtB* measured using qPCR. Individual data points (A) and mean data separated by experiment (B) are shown. Data are shown with mean ± SD and pooled from 3 independent experiments with n=10 per experiment. Statistical significance was determined by one-way ANOVA with Tukey's multiple comparisons correction (significance *p< 0.05, **p<0.01, ***p< 0.001, ****p< .0001).

To examine whether *Hh* drives broad changes to microbial composition in the gut, we used a qPCR approach to quantify relative expression levels of genes which are specific to different bacterial phyla. We looked first at the Bacteroidetes (now Bacteroidota) and Firmicutes (now Bacillota) phyla, which are known to be depleted in patients with IBD (Frank et al., 2007). We observed no differences in their relative abundance in stool samples between uninfected and *Hh* colonized animals (Figure 4-24A-B). We next measured the relative abundance of Proteobacteria (now Pseudomonadota). Despite *Hh* being a

member of this phylum, we saw no significant differences in Proteobacteria levels in stool samples from *Hh* colonized mice, although there was a trend towards increased levels in some animals (Figure 4-24C). As the phyla level is very broad, we next looked at the relative abundance of more specific bacterial genera and species. We measured levels of Lactobacillus and Bifidobacterium, two genera which are associated with beneficial effects on host physiology and often included in probiotic supplements (van Baarlen et al., 2013, Henrick et al., 2021). We observed no significant differences in their abundance in stool samples in mice with *Hh* colonization (Figure 4-25A-B). We also measured levels of *Escherichia coli*, a species which has the capacity to act as either a commensal or a pathogen depending on the bacterial strain (Stromberg et al., 2018). Again, we observed comparable levels of this species in stool samples from uninfected and *Hh*-colonized animals (Figure 3-25C).

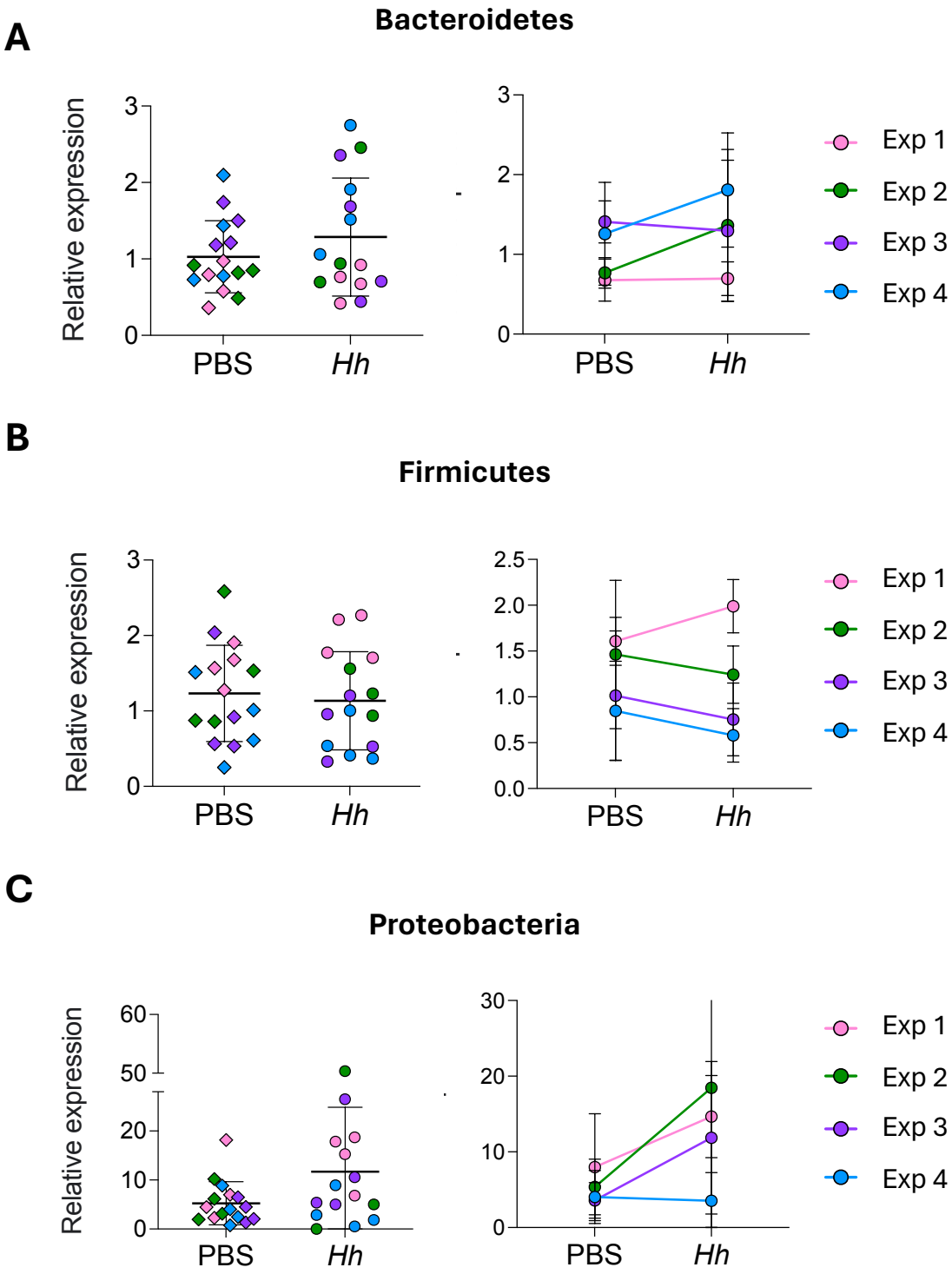


**Figure 4-24: *Hh* colonization does not alter abundance of Bacteroidetes, Firmicutes, or Proteobacteria in the stool**

C57BL/6 littermates were administered 1x10$^8$ CFU *Hh* or given PBS by oral gavage and left for 21-days post-infection. Stool samples were collected, genomic DNA was extracted and expression of genes specific for indicated bacterial phyla analysed by qPCR. Data are shown as fold change relative to the pan-bacteria 16S rRNA gene. Individual data points (left) and mean data separated by experiment (right) are shown. Data are shown with mean ± SD and pooled from 4 independent experiments with n=4 per experiment. Data were tested for normality using the Shapiro-Wilk normality test and in cases where data were normally distributed statistical significance was determined by unpaired t test, while otherwise a Mann Whitney test was used (significance *p< 0.05, **p<0.01, ***p< 0.001, ****p< .0001).

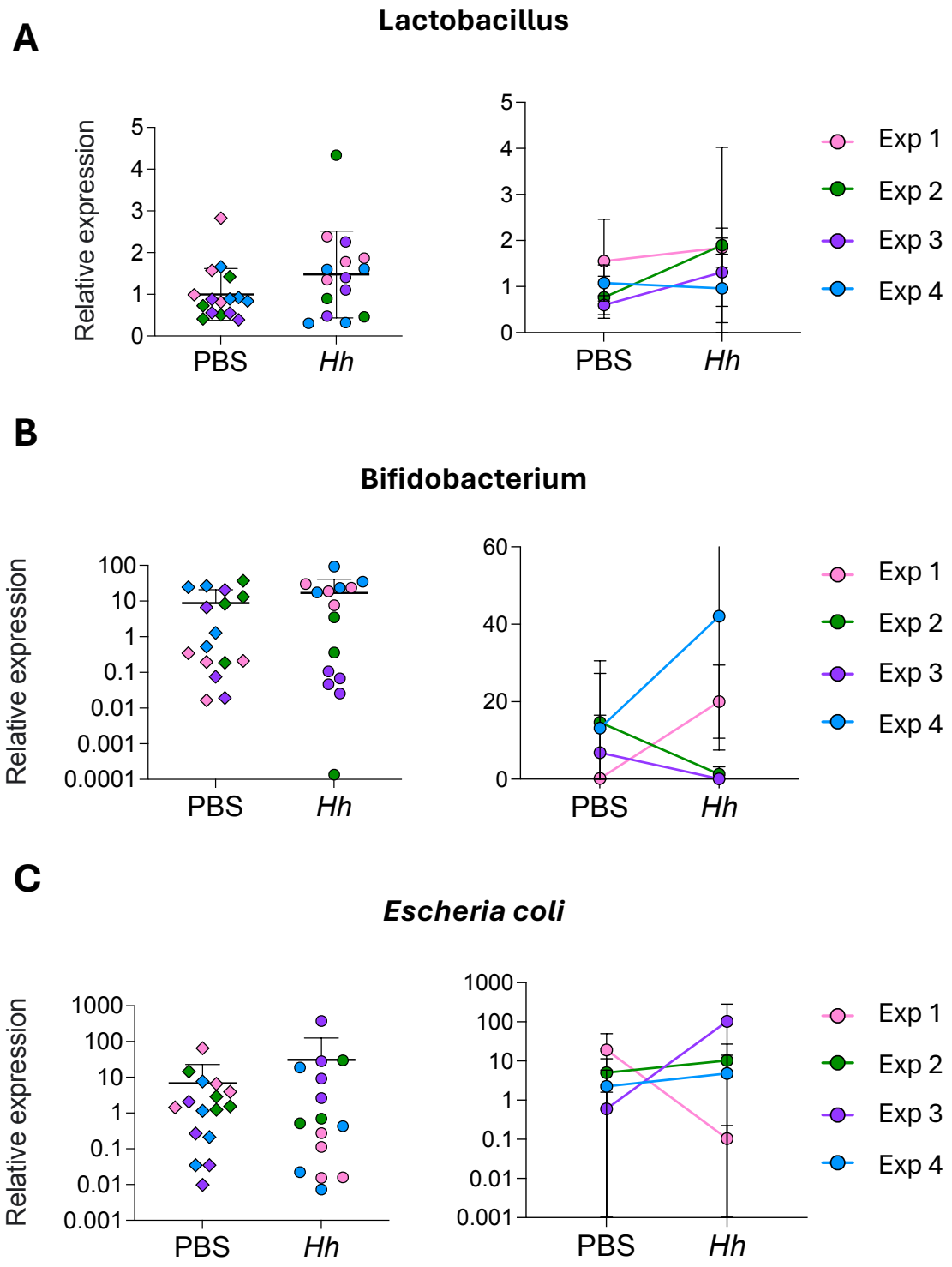


**Figure 4-25: *Hh* colonization does not alter abundance of Lactobacillus, Bifidobacterium, or *Escherichia coli* in the stool**
C57BL/6 littermates were administered 1x$10^8$ CFU *Hh* or given PBS by oral gavage and left for 21-days post-infection. Stool samples were collected, genomic DNA was extracted and expression of genes specific for indicated bacterial genera and species analysed by qPCR. Data are shown as fold change relative to the pan-bacteria 16S rRNA gene. Individual data points (left) and mean data separated by experiment (right) are shown. Data are shown with mean ± SD and pooled from 4 independent experiments with n=4 per experiment. Data were tested for normality using the Shapiro-Wilk normality test and in cases where data were normally distributed statistical significance was determined by unpaired t test, while otherwise a Mann Whitney test was used (significance *p< 0.05, **p<0.01, ***p< 0.001, ****p< .0001).

Lastly, we measured abundance of SFB, a group of bacteria with well-described functional effects on host immunity (Ivanov et al., 2009). We observed a significant increase in the relative abundance of these SFB in mice colonized with *Hh* (Figure 4-26). Together, these data indicate that while *Hh* may not drive distinct changes to microbial composition at the phyla level, there may be subtle differences in the abundance of certain bacterial groups in *Hh*-colonized mice.

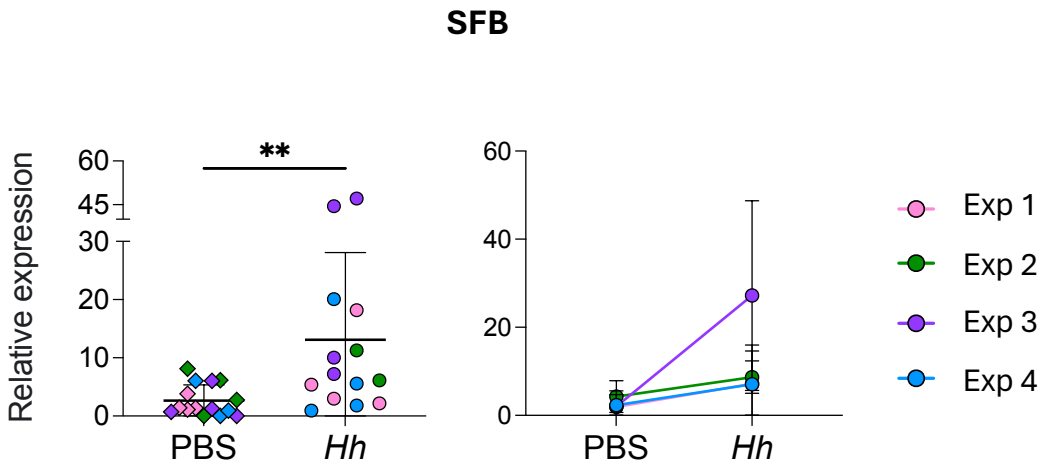


**Figure 4-26: *Hh* colonization increases abundance of SFB in the stool**
C57BL/6 littermates were administered 1x10$^8$ CFU *Hh* or given PBS by oral gavage and left for 21-days post-infection. Stool samples were collected, genomic DNA was extracted and expression of genes specific for SFB analysed by qPCR. Data are shown as fold change relative to the pan-bacteria 16S rRNA gene. Individual data points (left) and mean data separated by experiment (right) are shown. Data are shown with mean ± SD and pooled from 4 independent experiments with n=4 per experiment. Data were tested for normality using the Shapiro-Wilk normality test and in cases where data were normally distributed statistical significance was determined by unpaired t test, while otherwise a Mann Whitney test was used (significance *p< 0.05, **p<0.01, ***p< 0.001, ****p< .0001).

## 4.4 Discussion

Modulation of host immunity by the microbiota underpins immune system development and function. This crosstalk and the mechanisms by which the microbiota influences immune homeostasis have implications for disease outcome and therapeutic approaches, as well as our interpretation of results obtained from animal models (Ansaldo et al., 2021, Rosshart et al., 2019). Pathobiont species such as *Hh* have the capacity to drive a range of host responses depending on the context (Chow and Mazmanian, 2010, Jeffery et al., 2022). Here we aimed to characterise the effect of *Hh* colonization on the intestinal myeloid compartment at steady state, which has not yet been reported. We demonstrate that *Hh* drives increased myeloid recruitment to the site of colonization which is accompanied by transcriptional changes to local

cytokine expression. These changes may alter local immune function and impact how the host responds to secondary challenges.

### 4.4.1 Stimulation of local myeloid responses by *Hh*

We observed increased colonic monocyte infiltration at day 7 after *Hh*$^+$ MT or following direct infection with *Hh*. In mice directly infected, we also observed increases in neutrophil infiltration and abundance of intermediate monocyte-macrophages, while in *Hh*$^+$ MT recipients, eosinophil levels were increased. In contrast, by day 21, the levels of these cells were mostly comparable to uninfected controls, with the exception of colonic monocytes remaining elevated following direct *Hh* infection. Monocyte homing to the intestine is mediated by CCR2 and occurs both at steady state and in the context of inflammation (Bain et al., 2014, Desalegn and Pabst, 2019). From studies in GF mice, it is known that the microbiota stimulates steady state monocyte recruitment to the gut, as adult GF animals show fewer numbers of all colonic monocyte-macrophage subsets (Bain et al., 2014, Kang et al., 2020). Additionally, the microbiota drives myelopoiesis in the BM (Balmer et al., 2014a, Yan et al., 2022, Khosravi et al., 2014), and this can be inhibited by antibiotic treatment (Deshmukh et al., 2014, Josefsdottir et al., 2017). It is unclear whether increased monocyte infiltration as a result of *Hh* colonization is due simply to increased gut-homing, or whether it represents an increase in BM myelopoiesis. The levels of mature macrophages were not altered in infected mice, indicating that the increase in monocyte recruitment does not result in an enlarged intestinal macrophage pool. However, to elucidate the mechanism driving increased colonic monocyte numbers with *Hh* infection, further work should be done to examine the BM pool for monocytes and myeloid precursors.

Additionally, the microbiota stimulates BM granulocytosis (Deshmukh et al., 2014, Tada et al., 1996), so it is also possible that the increased colonic neutrophil and eosinophil numbers shown here are a result of systemic effects of *Hh* or *Hh*$^+$ MT on the BM compartment. However, as these changes were not maintained at day 21 post-infection, it appears that *Hh* does not drive chronic increases to intestinal granulocyte numbers. The elevated granulocyte levels at day 7 may represent a transient response to infection which is eventually controlled. Gut eosinophil numbers in GF mice have been shown to be

comparable to conventionally housed animals (Mishra et al., 1999), suggesting that the microbiota may not stimulate intestinal eosinophil recruitment. However, the GI tract is home to large populations of resident eosinophils which expand following enteric infection, for example with *H. pylori* (Arnold et al., 2018). A role for eosinophils in suppressing Th1 and Th17 responses has been described, and in this context depleting eosinophils can improve clearance of bacterial pathogens such as *H. pylori* and *C. rodentium* by removing suppression of effector T cell responses (Arnold et al., 2018). One suggested mechanism for this is the production of TGFß by eosinophils, which promotes differentiation of RORγt$^{+}$ Tregs in response to bacterial infections, including infection with *Hh* (Fallegger et al., 2022). At steady state, intestinal eosinophils play a role in maintaining symbiosis with the microbiota by promoting IgA class switching and stimulating mucus secretion, and mice with depleted eosinophils show altered microbiota compositions (Chu et al., 2014, Jung et al., 2015). Interestingly, we only observed significantly increased eosinophil numbers in mice which received *Hh*$^{+}$ MT, although there was a trend towards increased numbers in directly *Hh*-infected animals. This indicates that there may be a different element of the transferred microbiota which drives colonic eosinophil expansion independently from *Hh*, although *Hh* may have a subtle effect alone. Regardless, the role of eosinophils in maintaining homeostasis in *Hh*-colonized mice remains to be determined, but it is likely that production of TGFß and Treg induction contribute to suppressing pathologic effector T cell responses in this context.

A proportion of mice directly infected with *Hh* showed increased colonic neutrophils at day 7 post-infection. Neutrophil production in the BM is regulated by the microbiota (Zhang et al., 2015), and while their numbers are reduced following antibiotic treatment, they can be restored by transfer of a normal microbiota (Khosravi et al., 2014, Deshmukh et al., 2014). Neutrophil functions are also regulated by microbiota-derived signals, as those from GF animals show reduced phagocytic killing (Clarke et al., 2010) and have an impaired ability to migrate towards an inflammatory stimulus (Karmarkar and Rock, 2013). Neutrophils play a key role in the host's response to enteric infections, with functions including phagocytosis, production of antimicrobial peptides and ROS, and release of NETs (Perez-Lopez et al., 2016). It appears that infection with *Hh* stimulates a low level of immune activity, including a neutrophil response, which

does not cause pathology. This response is controlled over time, with all animals showing normal neutrophil levels by day 21. It remains to be tested whether neutrophils and other myeloid cells from *Hh* infected mice have altered functionality. The microbiota has been shown to prime neutrophil responses through the release of peptidoglycan into the circulation which enhances BM neutrophil functions, thus priming the host to respond efficiently to bacterial infections (Clarke et al., 2010). Whether *Hh* elicits effects on the BM through a similar mechanism remains to be explored.

Phenotypically, colonic macrophages and cDCs from *Hh*-colonized animals were largely comparable to uninfected controls. The most notable difference was at day 21 post-infection, when macrophages from infected mice showed reduced expression of CD11c and CD86. This difference in CD86 expression was also present on cDCs. CD86 is upregulated on APCs following stimulation with PAMPs, for example bacterial LPS or outer membrane vesicles (Alaniz et al., 2007), so it is interesting that infection with *Hh* appears to have the opposite effect. Similarly, colonic macrophage CD11c expression is associated with inflammation (Corbin et al., 2020). Our data suggest that colonization with *Hh* may have a suppressive effect on macrophage and cDC responses, particularly as CD86 plays a role in T cell costimulation by APCs (Park et al., 2023). It is unclear why *Hh* appears to elicit changes to CD86 but not CD80 expression on macrophages and cDCs. CD80 and CD86 share the same receptor, CD28, expressed on T cells, although it has been suggested that CD86 is the dominant ligand which drives Treg proliferation and survival (Halliday et al., 2020). It will be important to determine whether these subtle phenotypic differences have an effect on macrophage or cDC function. To explore this, the ability of APCs from *Hh*-colonized animals to induce a T cell response could be tested *in vitro* using ovalbumin antigen and the OT-II transgenic system (Helft et al., 2015). Other macrophage phenotypic markers, PD-L1 and CD206, were unchanged with *Hh* colonization, as were the population of $CD4^{+}Tim4^{+}$ macrophages which are reported to self-renew in the gut independently of BM monocytes (Shaw et al., 2018). Together, it appears that *Hh* has a limited effect on macrophage and cDC phenotypes at steady state. Whether the infection has a functional effect on colonic macrophages will be explored in Chapter 5.

While analysing these data, we noted that in addition to changes as a result of *Hh*$^+$ MT or direct *Hh* infection, there were differences in the composition of the myeloid pool in the control animals between day 7 and day 21. Eosinophil frequencies were higher in many control mice at day 21 compared to day 7, though not to a statistically significant level (Figure 4-6, Figure 4-12). Similarly, neutrophil levels were elevated in a proportion of animals at the later timepoint (Figure 4-2, Figure 4-8). In the direct *Hh* infection experiments, this trend was also present in monocyte levels (Figure 4-9), although this was not recapitulated in the *Hh*$^+$ MT experiments (Figure 4-3). It is possible that these differences are due to animal age between the two timepoints. At day 7 post *Hh*$^+$ MT or *Hh* infection, mice were ~8 weeks, while at the later timepoint they were ~10 weeks. Mice reach sexual maturity at ~10 weeks (Dutta and Sengupta, 2016), so it is possible that these differences represent maturing of the intestinal immune compartment as mice age.

### 4.4.2 *Hh*-induced cytokine responses

At both timepoints *Hh* elicited changes to colonic cytokine transcription. At day 7 the most notable change was an upregulation of *Ifnγ*, while at day 21 this was at a similar level to uninfected controls. At day 7, the source of IFNγ is likely to be innate. Neutrophils have been shown to produce IFNγ during *Salmonella typhimurium* infection as early as day 2 after inoculation (Spees Alanna et al., 2014). Intestinal ILCs also produce IFNγ in response to bacterial infection, for example following infection with *Campylobacter jejuni* (Muraoka et al., 2021) or *S. typhimurium* (Kästele et al., 2021). We have not yet assessed ILC phenotypes in the context of *Hh* infection, although they have been shown to play a role in *Hh*-induced colitis where they produce IFNγ and IL-17a (Buonocore et al., 2010, Coccia et al., 2012). At day 21, we observed an increase in transcription of *Tnfa* and *Il17a*. In *Hh*-induced colitis, there is expansion of IL-17A$^+$ and IFNγ$^+$ CD4$^+$ T cells (Morrison et al., 2013), while CD11b$^+$ and CD11c$^+$ myeloid cells are key producers of TNFα (Arnold et al., 2016, Bain et al., 2018). Further work to determine which cells are producing these cytokines at each timepoint remains to be done. However, these data confirm that at steady state *Hh* is not ignored by the host immune system, and in fact stimulates a low-level inflammatory response without causing pathologic inflammation. The cytokine transcription likely correlates with the increased colonic neutrophil and monocyte

recruitment discussed previously, although other cell types such as ILCs and T cells probably contribute too. It is possible that the presence of microbes such as *Hh* which stimulate active responses help to prime the host immune system to better cope with secondary infections through enhancement of cytokine responses. This hypothesis could be explored by testing how *Hh* colonization affects the outcome of a co-infection with an enteric pathogen, for example *C. rodentium* or *S. typhimurium*.

### 4.4.3 Local versus systemic effects of the microbiota and *Hh*

To examine whether *Hh* has effects beyond the primary site of infection, we tested whether *Hh* altered the myeloid compartment in the SILP. We found that *Hh* infection did not stimulate an increase in myeloid recruitment in the SILP at day 7 post-infection, with neutrophil, eosinophil, monocyte and total $CD45^+$ immune cell numbers remaining comparable with uninfected controls. This suggests that *Hh* preferentially drives specific infiltration of myeloid cells to the site of primary infection, although to confirm this the caecal LP should also be analysed for immune cell populations, given that this tissue hosts the highest levels of *Hh* colonization (Kuehl et al., 2005, Chan et al., 2005). Despite this, *Hh* may have other effects on systemic immunity which remain to be characterised. The effect of the microbiota on BM myelopoiesis, as well as the priming of BM neutrophil functions, has been discussed previously. It is also of interest to consider the potential effects of *Hh* on other extraintestinal tissues. The liver receives blood from the intestine via the portal vein, and in situations where gut-derived commensal bacteria enter the bloodstream, they are captured in the liver by Kupffer cells and phagocytosed to prevent systemic spread (Balmer et al., 2014b). Liver resident immune cells may therefore be exposed to commensal-derived signals and metabolites, both from bacteria in the bloodstream and bacterial products. Whether *Hh* has any phenotypic or functional effects in the liver has not yet been reported, although the infection was initially associated with liver pathology in certain immunodeficient mouse strains (Ward et al., 1994, Fox et al., 1994), and has been shown to colonize the bile canaliculi in some contexts (Fox et al., 1996). Exploring potential systemic effects of *Hh* will provide insight into whether this infection modulates disease and infection outcomes in different tissues.

### 4.4.4 Modulation of microbiota composition by *Hh*

Triggers such as infection, antibiotic treatment, or dietary changes, can all result in alterations to microbial composition and overall function of the microbiota (Stecher et al., 2013). These alterations can have negative outcomes for the host, an effect which is termed dysbiosis and is often associated with disease (Levy et al., 2017). Conversely, modulation of the microbiota can promote beneficial effects for the host and much research is now being done on how beneficial probiotic species may modulate immune function (Turroni et al., 2014). Following infection, *Hh* becomes the dominant community member colonizing the caecal mucosa, thus driving a decrease in microbial diversity at this site with potential knock-on effects (Kuehl et al., 2005). As our analyses focussed on the colon, we aimed to determine whether *Hh* drives changes to microbial composition detected in stool. Firstly, our data indicate that *Hh* colonization levels do not consistently change from 7 to 21 days post-infection. In the caecal mucosa, *Hh* levels have been reported to increase between day 2 and day 8, and then again from day 8 to day 14 post-infection (Kuehl et al., 2005), but the colonization kinetics may be different in the colon. However, this suggests that the difference in DSS colitis outcomes at the timepoints described in Chapter 3 is not a result of increased colonic *Hh* levels and therefore increased exposure to the bacteria and its products. Rather, it is likely to be a result of *Hh*-mediated changes to the local environment and immune function which take an extended period of time to develop.

At the phyla level, we observed no significant differences in abundance of Bacteroidetes, Firmicutes or Proteobacteria in the stool following *Hh* colonization. Changes in the abundance of these phyla have been associated with various human diseases, including IBD. For example, Crohn's disease has been associated with increased abundance of Firmicutes, *Enterobacteriaceae* and other Proteobacteria, and decreased Bacteroidetes (Willing et al., 2010, Gevers et al., 2014). It is unclear whether these changes are a correlation with disease or play a causal role in pathogenesis. However, the phyla level is a broad classification, and in the absence of overt inflammation it may be unlikely that we would see changes at this level. More specifically, there were also no differences in relative abundance of the Lactobacillus and Bifidobacterium genera, or *E. coli* species, suggesting that *Hh* may have limited effects on

microbial structure in the colon. While infections with pathogens such as *C. rodentium* have been shown to cause marked changes to microbiota composition (Hoffmann et al., 2009), it may be that colonization with *Hh* at steady state has less of an effect. Host inflammation has been suggested as the key driver of microbiota changes following pathogenic infection, rather than the infection itself (Lupp et al., 2007, Stecher et al., 2007). Additionally, colonization with *Campylobacter jejuni*, a species which is not a natural mouse pathogen and does not cause pathology in mice, has been shown to drive only minimal changes to the microbiota compared to *C. rodentium* infection (Lupp et al., 2007).

We detected an increase in the relative abundance of SFB DNA following *Hh* infection. This was surprising as SFB colonizes the SI (Ivanov et al., 2009), while *Hh* occupies the caecum and colon (Chan et al., 2005). It is unclear whether this difference indicates a direct mechanism by which *Hh* modulates the environment so that SFB colonization increases. It is known that different microbes can mediate the ability of other species to colonize the GI tract. For example, there is evidence that colonization with SFB can protect against enteric infection with *S. typhimurium*, through a mechanism involving intestinal sensory neurons called nociceptors (Lai et al., 2020). The authors describe a neuronal circuit in which nociceptors regulated M cell development in Peyer's patches, thus regulating SFB colonization and in turn inhibiting systemic *S. typhimurium* dissemination (Lai et al., 2020). It is interesting to consider whether *Hh* colonization also drives activation of neuronal pathways, which could employ a similar circuit to that described by Lai *et al*. Firstly, to validate these data, 16S RNA sequencing should be performed to provide a more complete and unbiased analysis of the microbiome. This could include sequencing of SI contents to determine whether *Hh* drives changes to microbial community structure in the niche occupied by SFB. However, it has been shown that profiling of the microbiota in stool is insufficient to capture changes in mucosal-associated communities, which may be where disease-correlating dysbiosis occurs (Gevers et al., 2014). Given that *Hh* colonizes the mucosa rather than the intestinal lumen (Chan et al., 2005), it is particularly important to analyse the microbial community in this niche, as the community in stool is thought to mostly reflect that of the distal colon lumen (Riva et al., 2019). In future, microbial DNA should be isolated from colon tissue rather than stool to allow for examination of this niche. This would also allow

for microbial analysis at specific regions of the colon, as it is known that community structure varies along the length of the colon as well as the whole GI tract (Riva et al., 2019, Lkhagva et al., 2021).

### 4.4.5 Concluding remarks

In this chapter, we have shown that colonization with *Hh* drives increases in myeloid infiltration to the colon. Early after infection, we documented a neutrophil and monocyte response which was accompanied by heightened transcription of *Ifny*. At later timepoints, neutrophil levels resolved while monocytes remained elevated, and transcription of *Tnfa* and *Il17a* were increased. These changes were observed in the colon but not the SILP, suggesting that the increased myeloid recruitment is specific to the site of infection. We also showed that while *Hh* does not have notable effects on faecal microbial composition at the broad phyla level, colonization appears to increase the relative abundance of SFB DNA in stool. This indicates that there may be a feedback mechanism by which *Hh* colonization alters SFB levels, despite these species occupying different niches. These data provide evidence of homeostatic immunity to *Hh*, as well as potential changes to microbiota composition as a result of *Hh* colonization. These changes may alter how the immune system responds in the event of a disease or infectious challenge.

# 5 Colonic macrophage functions are altered following *Helicobacter hepaticus* infection

## 5.1 Introduction

Macrophages play key roles in the maintenance of intestinal homeostasis and are functionally specialised to the tissue environment. Intestinal macrophages are highly phagocytic and bactericidal (Bujko et al., 2017, Kang et al., 2020), yet unlike those in other tissues, are resistant to stimulation with PAMPs and produce limited cytokine responses when stimulated *ex vivo* (Smythies et al., 2005, Ogino et al., 2013). These properties allow macrophages to capture and remove bacteria which enter the intestinal lamina propria (LP), without induction of a pathologic inflammatory response.

Intestinal macrophages exist in a differentiation continuum, where they enter the gut as $Ly6C^{+}MHCII^{-}$ monocytes and, via an intermediate state, differentiate into mature macrophages characterised by expression of MHCII and CD64 (Tamoutounour et al., 2012). As these cells differentiate in the tissue, this process is influenced by the local tissue environment (Lavin et al., 2014). In the intestine, the differentiation of mature macrophages from monocytes requires TGFß signalling (Schridde et al., 2017), and is modulated by the microbiota, as GF animals show altered proportions of differentiated macrophage subsets (Kang et al., 2020). The microbiota also impacts macrophage functions, with evidence that the bacterial metabolite butyrate regulates production of pro-inflammatory mediators, such as IL-6 and nitric oxide (Chang et al., 2014). Butyrate also promotes macrophage antimicrobial functions and thereby improves resistance to infection with enteric pathogens *S. typhimurium* and *C. rodentium* (Schulthess et al., 2019). Similarly, treatment with the microbiota derived metabolites itaconate and succinate have been shown to improve resistance to infection by *E. coli* in BMDMs *in vitro* (O'Callaghan et al., 2021). In contrast, treatment with antibiotics *in vivo* appears to drive a pro-inflammatory macrophage phenotype, characterised by increased production of TNFα (Scott et al., 2018).

Changes in cellular metabolism appear to be associated with the effects of the microbiota on macrophage function. For example, the imprinting of an

antimicrobial phenotype by butyrate is accompanied by a shift in macrophage metabolism away from glycolysis, together with reduced mammalian target of rapamycin (mTOR) activity (Schulthess et al., 2019). Treatment of mice with antibiotics appears to have the opposite effect on intestinal macrophages, driving increased glycolysis and increased mitochondrial function (Scott et al., 2022). Macrophages from different tissues exhibit altered metabolic phenotypes reflecting the local environment of each location, with SILP and cLP macrophages appearing more similar to each other than those from other tissues, including the liver, lung, and spleen (Heieis et al., 2023). Metabolic heterogeneity also exists within the intestinal macrophage pool. As recruited monocytes differentiate into mature macrophages, there are marked differences in their expression of metabolic proteins, including decreased GLUT1, which is consistent with decreased glycolysis (Heieis et al., 2023). Different macrophage phenotypes are also associated with distinct metabolic states. From the literature, classically activated macrophages are associated with glycolysis, while alternatively activated macrophages rely on mitochondrial oxidative phosphorylation (O'Neill et al., 2016). This dichotomy is now known not to be representative of most tissue macrophages, including intestinal macrophages, and it is of interest to determine how the local environment in each tissue affects metabolic function.

The unique environment of the intestine therefore influences macrophage differentiation, function, and metabolic phenotype. The role of the microbiota in these processes is not fully understood, and little is known about the effects of *Hh* on macrophage functions at steady state. One mechanism has been described by which *Hh* drives an anti-inflammatory transcriptional program in macrophages. This occurs through a *Hh*-derived polysaccharide which is recognised directly by TLR2 and induces production of IL-10 (Danne et al., 2017). Whether there are other mechanisms by which *Hh* influences macrophage functions at steady state has not been reported. We have previously identified an increase in colonic monocyte recruitment following *Hh* colonization, as well as subtle differences in macrophage phenotypes, including reduced expression of CD11c and CD86. Here, we aimed to build on these findings by exploring the effect of *Hh* on macrophage functions using the *in vivo* infection models described previously.

## 5.2 Aims

In this chapter I aimed to test whether *Hh* colonization modulates colonic macrophage functions at steady state, which might contribute to the difference in disease outcomes described in Chapter 3. I also aimed to test and optimise various systems to measure macrophage functions *ex vivo*, including using FACS for cell isolation, testing different methods for measuring phagocytosis, and using flow cytometry-based assays for measuring metabolic function.

## 5.3 Results

### 5.3.1 *Hh* impairs colonic macrophage *ex vivo* cytokine production

To test whether *Hh* colonization has functional effects on colonic macrophages, we first aimed to optimise a system to study the functional output of these cells *ex vivo*. Many studies investigating the effects of bacteria or bacterial metabolites on immune cells use *in vitro* systems to test immune functions (Sterzenbach et al., 2007, Danne et al., 2017, Schulthess et al., 2019, O'Callaghan et al., 2021). These systems lack the environmental context of an *in vivo* infection, and it is likely that species such as *Hh* exert quite different effects on host cells *in vitro* as opposed to in their natural niche in the intestine, where they are spatially segregated from immune cells by the epithelial barrier. Furthermore, *Hh* requires low oxygen concentrations for survival (Fox et al., 1994, Ward et al., 1994) which would need to be factored into an *in vitro* setting and would have functional implications for immune cells (Lin and Simon, 2016). We therefore chose to use an *ex vivo* approach to study macrophage functions.

In Chapter 3 we noted that *Hh*-induced protection against DSS disease was present at day 21 but not day 7 post-infection, suggesting that the longer time period is required for protective conditioning of the host by *Hh*. Here, we used a system in which mice either received $Hh^{+}$ MT or were directly infected with *Hh* as previously and colons were harvested on day 21 to allow time for this conditioning *in vivo*. We then used fluorescence-activated cell sorting (FACS) to isolate colonic macrophages, which were placed in culture overnight with different PAMPs. Culture supernatants were harvested, and the concentration of various cytokines measured by cytometric bead array (CBA) (Figure 5-1). When

initially optimising this system using *Hh*$^+$ MT recipients, macrophages were defined by expression of CD45, CD11b and CD64. However, the CD64$^+$ pool in the intestine contains monocytes and intermediate monocyte-macrophages as well as mature macrophages (Bain et al., 2013). This should be considered when interpreting the results from these first experiments.

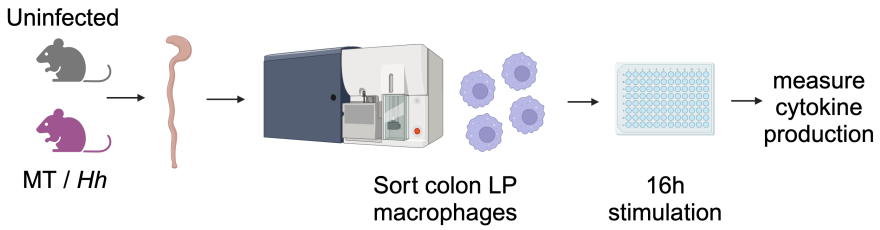


**Figure 5-1: Schematic of colonic macrophage isolation and ex vivo stimulation**
C57BL/6 littermate cohorts were left untreated (Naïve), colonized with *Hh*$^+$ microbiota (MT) or were infected with 1x10$^8$ CFU *Hh* or given PBS by oral gavage before being left for 21-days post-infection. cLPL were isolated using enzymatic digestion and CD11b$^+$CD64$^+$ macrophages purified by FACS. In later experiments macrophages were defined as CD11b$^+$CD64$^+$Ly6C$^-$MHCII$^+$. Macrophages were seeded in 96-well culture plates in presence of PAMPs for 16 hours. The concentration of cytokines in culture supernatants was measured by cytometric bead array (CBA).

Sorted macrophages were either left unstimulated, treated with *E. coli* LPS, or incubated with live *Hh*. We measured production of inflammatory cytokines IL-6 and TNFα, the chemokine monocyte chemoattractant protein-1 (MCP-1, also called CCL2), and IL-10. In every condition, we observed that intestinal macrophages from *Hh*$^+$ MT recipients showed significantly reduced cytokine output compared to those from naïve mice (Figure 5-2). Interestingly, this appeared to be independent of any stimulus, as we observed this difference even in unstimulated macrophages (Figure 5-2). Macrophages from both naïve and *Hh*$^+$ MT recipients produced markedly increased cytokine responses following stimulation with LPS, while the responses to live *Hh* were similar to that of unstimulated cells (Figure 5-2). This may be due to *Hh* death when incubated under standard oxygen conditions, so we did not pursue live *Hh* as a stimulation condition further.

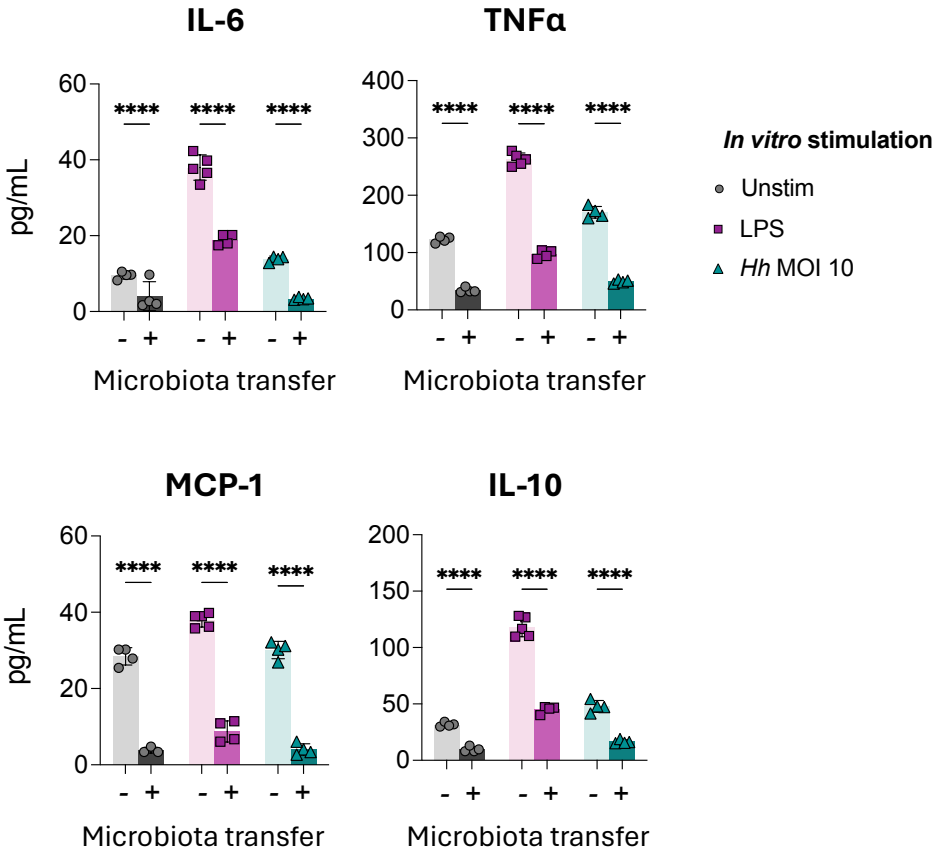


**Figure 5-2: Intestinal macrophages from *Hh*⁺ MT recipient mice show suppressed cytokine production**
C57BL/6 littermate cohorts were left untreated (Naïve) or colonized with *Hh*⁺ microbiota (MT) for 21-days. $CD11b^{+}CD64^{+}$ colonic macrophages were seeded at $3x10^{4}$ cells per well in a 96 well plate and either left unstimulated, treated with 100ng/mL *E. coli* LPS, or incubated with live *Hh* at MOI 10. After 16h, culture supernatants were harvested and the concentration of IL-6, TNFα, MCP-1, and IL-10 measured by CBA. Data points are technical replicates pooled from 4 mice per group (naïve/MT). Data are shown with mean ± SD and are representative of 3 independent experiments. Statistical significance was determined by 2-way ANOVA (significance *p< 0.05, **p<0.01, ***p< 0.001, ****p< .0001).

Bacterial LPS is recognised specifically by TLR4 (Poltorak et al., 1998), so we next assayed responses to additional PAMPs. Pam3csk4 is a synthetic molecule recognised specifically by TLR2 (Aliprantis et al., 1999), while zymosan is a fungal cell wall component recognised by TLR2 and Dectin-1 (Underhill, 2003, Herre et al., 2004). We observed that intestinal macrophages from *Hh*⁺ MT recipients showed reduced cytokine production in response to these PAMPs (Figure 5-3). Pam3csk4 triggered increased production of IL-6 and IL-10, but not TNFα or MCP-1, from intestinal macrophages, while those stimulated with zymosan produced comparable cytokine levels to unstimulated cells (Figure 5-3). In a later experiment, a higher concentration of zymosan was used which did elicit production of all cytokines tested, and *Hh*⁺ MT recipient macrophages still showed significantly reduced cytokine output compared to those from naïve

controls (data not shown). We therefore concluded that colonic macrophages from *Hh*$^+$ MT recipients have an impaired ability to produce cytokines *ex vivo*, and that this difference is present regardless of the stimulus.

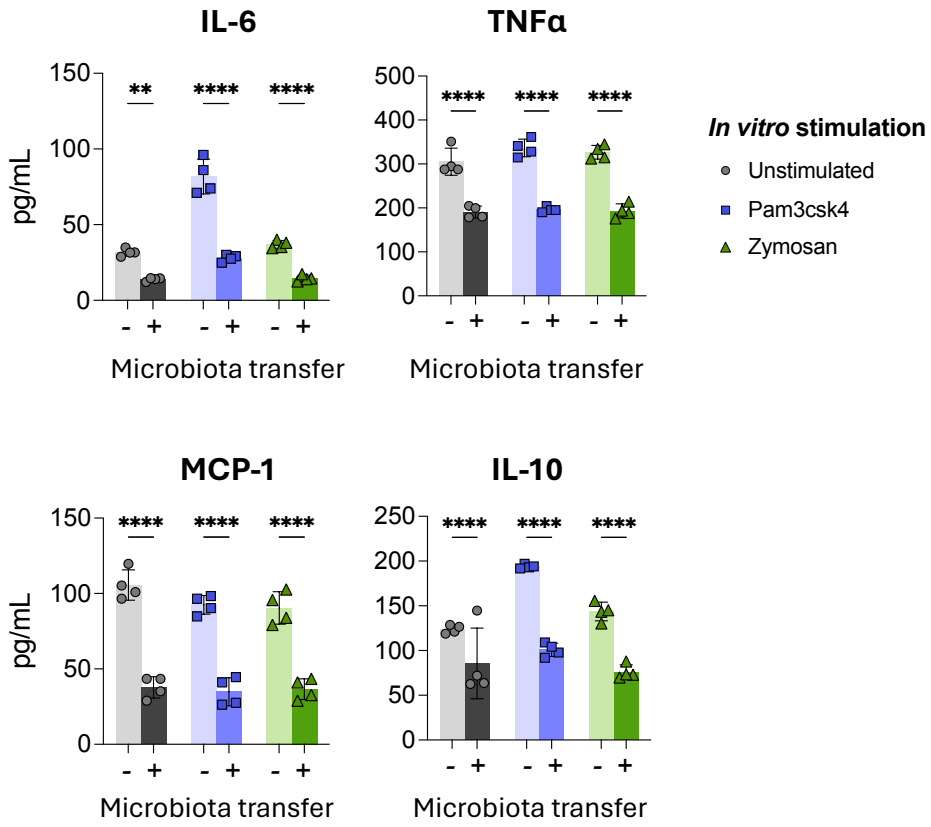


**Figure 5-3: Suppressed cytokine responses of intestinal macrophages from *Hh*$^+$ MT recipients are not stimulus-dependent**
C57BL/6 littermate cohorts were left untreated (Naïve) or colonized with *Hh*$^+$ microbiota (MT) for 21-days. CD11b$^+$CD64$^+$ colonic macrophages were seeded at 3x10$^4$ cells per well in a 96 well plate and either left unstimulated, treated with 100ng/mL Pam3csk4, or 1µg/mL zymosan. After 16h, culture supernatants were harvested and the concentration of IL-6, TNFα, MCP-1, and IL-10 measured by CBA. Data points are technical replicates pooled from 4 mice per group (naïve/MT). Data are shown with mean ± SD and are representative of 2 independent experiments. Statistical significance was determined by 2-way ANOVA (significance *p< 0.05, **p<0.01, ***p< 0.001, ****p< .0001).

We next tested whether *Hh* colonization alone was sufficient to attenuate macrophage cytokine output. Mice were directly infected with *Hh* as previously for 21 days. For these experiments, we FACS-sorted intestinal macrophages defined as CD45$^+$CD11b$^+$CD64$^+$Ly6C$^-$MHCII$^+$, a more stringent definition of mature macrophages that excludes monocytes and intermediate cells (Bain and Mowat, 2014). Sorted intestinal macrophages were left unstimulated or treated with LPS or Pam3csk4 as previously. We observed that mature macrophages showed a reduced response to stimulation compared to mixed monocyte-macrophages (Figure 5-4, cf. Figure 5-2 and Figure 5-3). LPS treatment triggered production of

IL-6, TNFα, and IL-10 from mature intestinal macrophages, but to a lesser extent than the total CD64$^{+}$ population used previously (Figure 5-4, cf. Figure 5-2 and Figure 5-3). This is likely due to the fact that mature intestinal macrophages are refractory to stimulation by PAMPs (Smythies et al., 2005, Ogino et al., 2013), while newly recruited monocytes have a greater capacity for cytokine production (Bain et al., 2013). Pam3csk4 treatment did not increase cytokine production when compared to unstimulated intestinal macrophages (Figure 5-4). Nonetheless, intestinal macrophages isolated from *Hh* colonized mice again showed significantly reduced cytokine production compared to those from naïve mice (Figure 5-4). Again, this was independent of the stimulus, as the trend was present in unstimulated macrophages as well as LPS or Pam3csk4 treated cells (Figure 5-4).

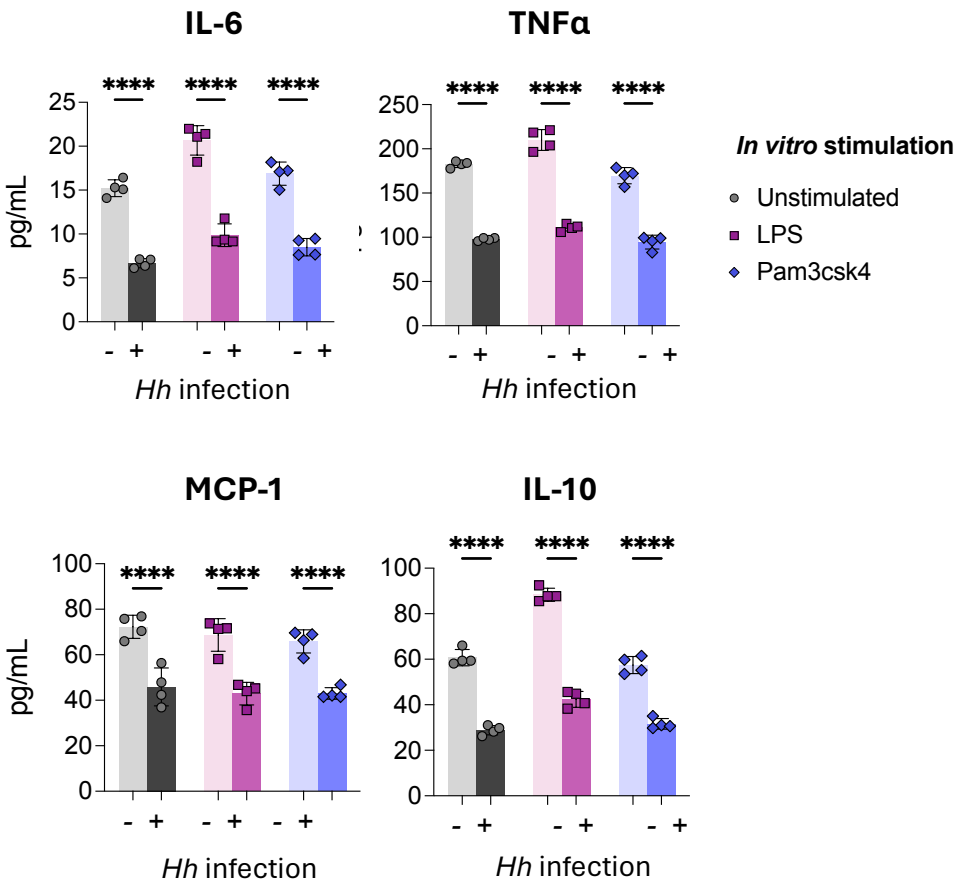


**Figure 5-4: *Hh* colonization is sufficient to attenuate intestinal macrophage cytokine production**
C57BL/6 littermates were administered 1x10$^8$ CFU *Hh* or given PBS by oral gavage and left for 21-days post-infection. CD11b$^+$CD64$^+$Ly6C$^-$MHCII$^+$ colonic macrophages were seeded at 3x10$^4$ cells per well in a 96 well plate and either left unstimulated, treated with 100ng/mL *E. coli* LPS, or 100ng/mL Pam3csk4. After 16h, culture supernatants were harvested and the concentration of IL-6, TNFα, MCP-1, and IL-10 measured by CBA. Data points are technical replicates pooled from 4 mice per group (PBS/*Hh*). Data are shown with mean ± SD and are representative of 2 independent experiments. Statistical significance was determined by 2-way ANOVA (significance *p< 0.05, **p<0.01, ***p< 0.001, ****p< .0001).

It was possible that the reduced cytokine output from intestinal macrophages from *Hh*-infected mice could be caused by increased cell death. We therefore tested the viability of the isolated cells at various stages of the experimental process. First, following isolation by enzymatic digestion, live cLPL were counted manually using trypan blue. No differences in the number of live isolated cells were noted with *Hh*$^+$ MT or *Hh* infection (Figure 5-5A-B). Second, as intestinal macrophages were obtained using FACS, samples were assessed using a fluorescent viability dye, and we saw no differences in viability between macrophages from *Hh*$^+$ MT or *Hh* infection compared to naïve controls (Figure 5-5A-B). Following sorting, the isolated macrophages from each mouse group were counted again using trypan blue. Again, no differences in the yield of live macrophages were present between *Hh*$^+$ MT or *Hh* infection compared to naïve

controls (Figure 5-5A-B). Although, these analyses confirmed comparable viability of cLPL and sorted colonic macrophages across all groups, it remained possible that differences in viability may become apparent after the cells were cultured *ex vivo*. We therefore used the alamarBlue cell viability reagent to measure viability during the culture (Pott et al., 2018). Again, we did not see differences in alamarBlue absorbance between intestinal macrophages isolated from naïve and *Hh*$^{+}$ MT recipients (Figure 5-5C), or those from *Hh*-infected mice (Figure 5-5D). Together, these data indicate that the reduced intestinal macrophage cytokine output is not due to increased cell death. Further work to determine the mechanism causing impaired macrophage cytokine responses in this setting remains to be done.

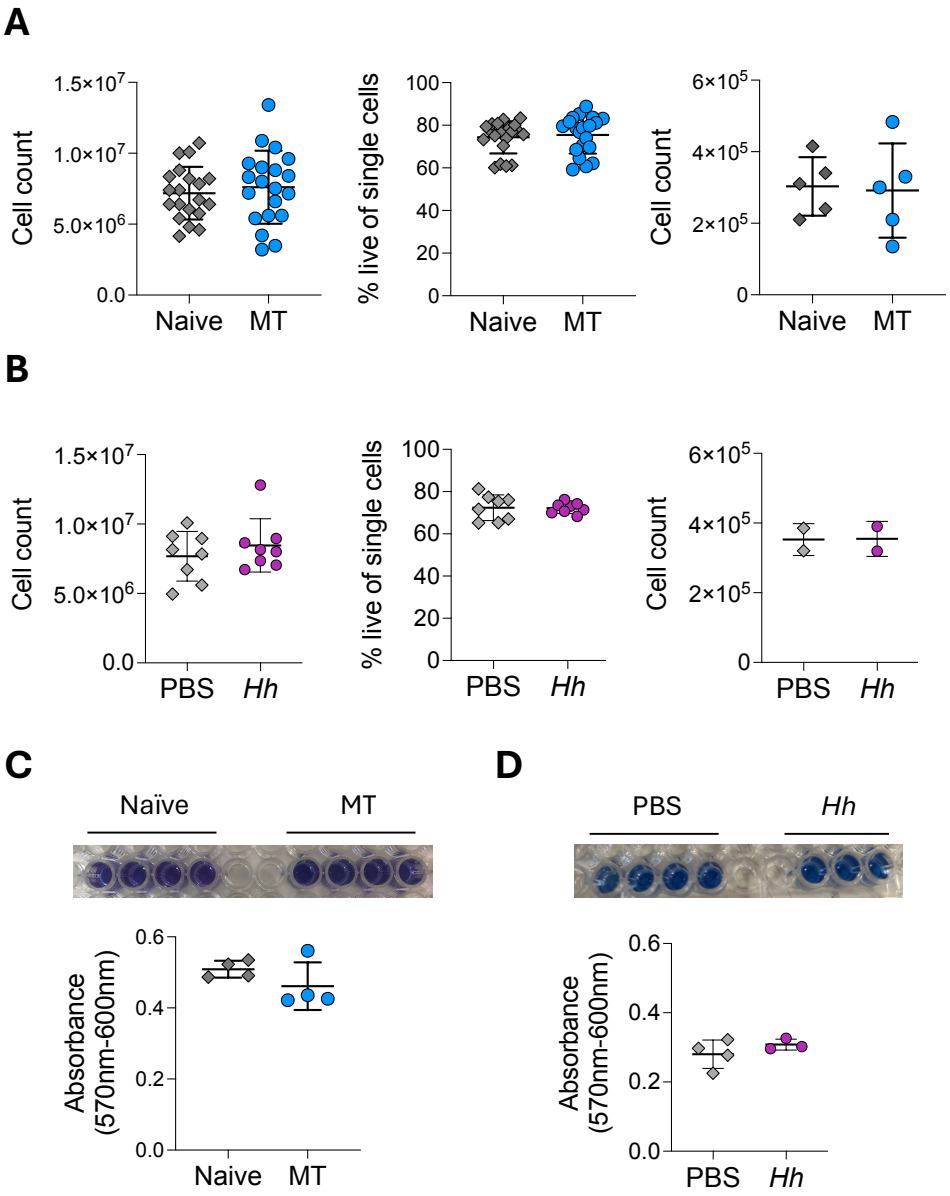


**Figure 5-5: Intestinal macrophages isolated from *Hh*⁺ MT recipients or direct *Hh* colonized mice do not show impaired viability**
C57BL/6 littermates were administered 1x10$^8$ CFU *Hh* or given PBS by oral gavage and left for 21-days post-infection. cLPL were isolated and viable cells counted using trypan blue (A-B, left). Cells were assessed for viability during sorting with viability dye (A-B, centre), and viable purified CD11b$^+$CD64$^+$Ly6C$^-$MHCII$^+$ macrophages were pooled from each experimental group and counted using trypan blue (A-B, right). Macrophage viability during overnight culture was assessed by incubation with AlamarBlue for 16h. AlamarBlue absorbance was read on a plate reader at 570nm with reference wavelength 600nm. Data are shown with mean ± SD and are representative of 5 (A) or 2 (B) independent experiments with n=4 per experiment. Data were tested for normality using the Shapiro-Wilk normality test and in cases where data were normally distributed statistical significance was determined by unpaired t test, while otherwise a Mann Whitney test was used (significance *p< 0.05, **p<0.01, ***p< 0.001, ****p< .0001).

## 5.3.2 The impact of *Hh* colonization on colonic macrophage phagocytosis

We next assessed whether other macrophage functions were altered following *in vivo* infection with *Hh* or *Hh*⁺ MT. Phagocytosis is a key function of intestinal

macrophages and contributes to maintenance of homeostasis through the clearance of bacteria which enter the LP, as well as dead cells and debris (Smythies et al., 2005, Bujko et al., 2017). Various microbiota derived metabolites have been shown to differentially influence macrophage uptake and killing of bacteria *in vitro*. Butyrate appears to increase bacterial killing by macrophages (Schulthess et al., 2019), while itaconate and succinate treatment have differential effects on both bacterial uptake and clearance (O'Callaghan et al., 2021). There are also differing reports of the effect of *in vivo* antibiotics treatment on the phagocytic capability of macrophages. One study reported that antibiotics treatment enhanced the phagocytic function of gut macrophages *ex vivo* (Scott et al., 2022), while another reported the opposite effect on alveolar macrophages (Schuijt et al., 2016). Here, we aimed to determine whether *in vivo* infection with *Hh* or *Hh*$^+$ MT affects the phagocytic function of colonic macrophages.

We attempted two methods to test phagocytic activity *ex vivo*. The first utilised the pHrodo assay, in which cells are incubated with *E. coli* coated BioParticles that become fluorescent at low pH, for example inside an acidic endosome or lysosome, and so can be used as an indicator of phagocytosis (Bujko et al., 2017, Scott et al., 2022). The experimental outline is depicted in Figure 5-6, for which cLPL were obtained from naïve or *Hh* colonized mice, and adherent cells isolated by plating and washing off non-adherent cells. Cells were then incubated with pHrodo BioParticles and washed before being stained with flow cytometry antibodies to allow identification of macrophages and detection of pHrodo fluorescence (Figure 5-6). We initially compared naïve and *Hh*$^+$ MT intestinal macrophages and found that almost all macrophages were positive for pHrodo (Figure 5-7A). However, when we assessed the amount of BioParticles taken up per cell, we observed a significant decrease in pHrodo MFI in intestinal macrophages derived from *Hh*$^+$ MT recipients compared to those from naïve controls (Figure 5-7B), suggesting that *Hh*$^+$ MT limits macrophage phagocytosis. However, as almost 100% of the macrophages in both groups had taken up the BioParticles, we repeated the experiment using intestinal macrophages from either naive or directly *Hh* infected animals and using a lower concentration of pHrodo BioParticles, so as not to saturate the assay. Here, we observed that lower proportions of macrophages took up the BioParticles, and that a lower

frequency of intestinal macrophages from *Hh* colonized mice were positive for pHrodo than those from naïve animals (Figure 5-8A). However, when the MFI of pHrodo was measured, there were no significant differences between intestinal macrophages isolated from *Hh* colonized mice or naïve animals (Figure 5-8B). Thus, although both *Hh*$^{+}$ MT and *Hh* appear to have a limiting effect on intestinal macrophage phagocytic function, further tests are required to confirm this.

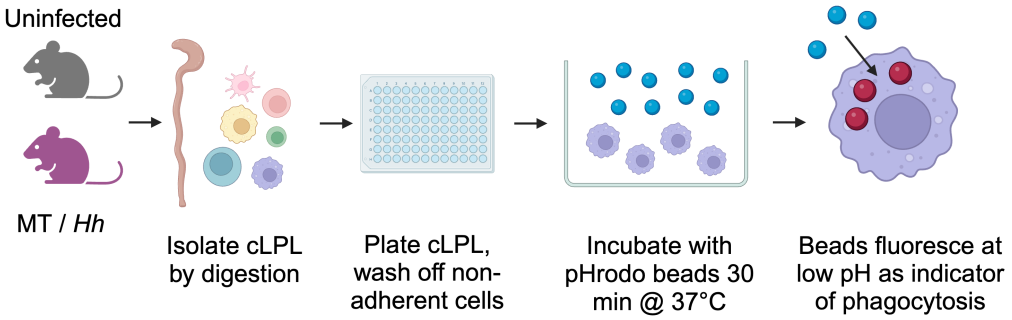


**Figure 5-6: Schematic of pHrodo phagocytosis assay**
C57BL/6 littermate cohorts were left untreated (Naïve), colonized with *Hh*$^{+}$ microbiota (MT) or were infected with 1x10$^{8}$ CFU *Hh* or given PBS by oral gavage before being left for 21-days post-infection. cLPL were isolated using enzymatic digestion and seeded in a 96-well plate before being left for 2h at 37℃. Non-adherent cells were washed off and remaining cells incubated with pHrodo *E. coli* coated BioParticles for 30min at 37℃. Using flow cytometry, macrophages were identified as CD11b$^{+}$CD64$^{+}$Ly6C$^{-}$MHCII$^{+}$ and pHrodo fluorescence quantified in this population.

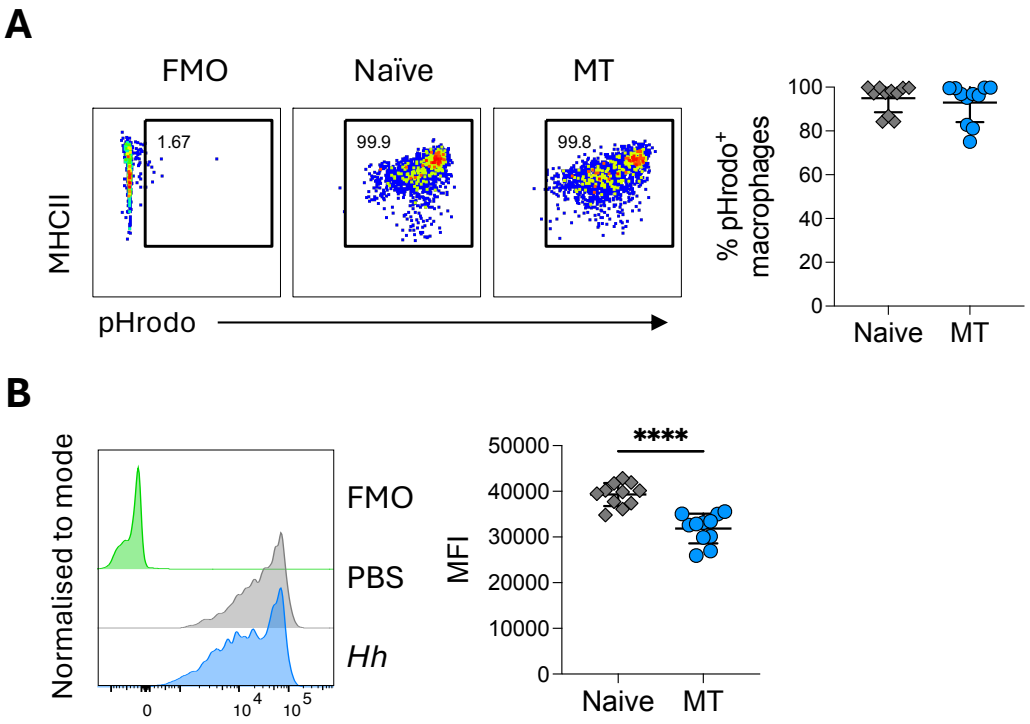


**Figure 5-7: Macrophages from *Hh*⁺ MT recipients exhibit slightly reduced phagocytosis of pHrodo BioParticles**

C57BL/6 littermate cohorts were left untreated (Naïve) or colonized with *Hh*⁺ microbiota (MT) for 21-days. Adherent cells were incubated with 1mg/mL pHrodo BioParticles for 30min at 37℃. Colonic macrophages were identified as $CD11b^{+}CD64^{+}Ly6C^{-}MHCII^{+}$ and dot plots of pHrodo fluorescence within this population are shown (A, left) along with quantification of frequency (A, right). A representative histogram showing the proportion of pHrodo-positive macrophages (B, left) and quantification of pHrodo MFI (B, right) are shown. Data are shown with mean ± SD and pooled from 3 independent experiments with n=3-4 per experiment. Data were tested for normality using the Shapiro-Wilk normality test and in cases where data were normally distributed statistical significance was determined by unpaired t test, while otherwise a Mann Whitney test was used (significance *p< 0.05, **p<0.01, ***p< 0.001, ****p< .0001).

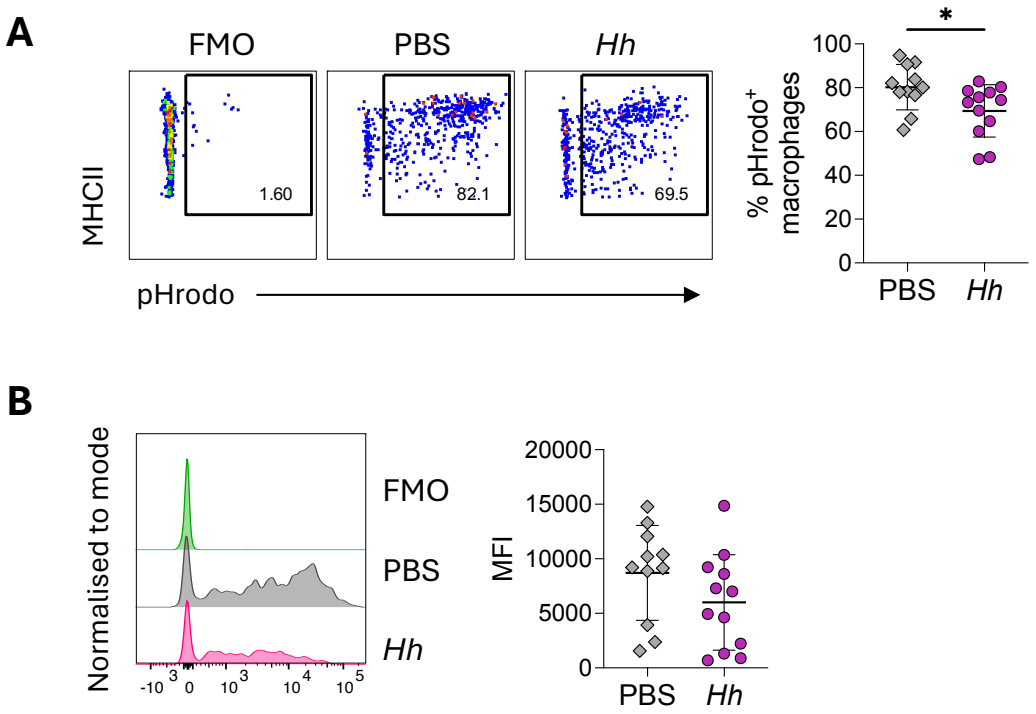


**Figure 5-8: Macrophages from *Hh* colonized mice exhibit slightly reduced phagocytosis of pHrodo BioParticles**
C57BL/6 littermates were administered 1x10$^8$ CFU *Hh* or given PBS by oral gavage and left for 21-days post-infection. Adherent cells were incubated with 0.1mg/mL pHrodo BioParticles for 30min at 37°C. Colonic macrophages were identified as CD11b$^+$CD64$^+$Ly6C$^-$MHCII$^+$ and dot plots of pHrodo fluorescence within this population are shown (A, left) along with quantification of frequency (A, right). A representative histogram showing the proportion of pHrodo-positive macrophages (B, left) and quantification of pHrodo MFI (B, right) are shown. Data are shown with mean ± SD and are pooled from 3 independent experiments with n=3-4 per experiment. Data were tested for normality using the Shapiro-Wilk normality test and in cases where data were normally distributed statistical significance was determined by unpaired t test, while otherwise a Mann Whitney test was used (significance *p< 0.05, **p<0.01, ***p< 0.001, ****p< .0001).

As a second method for testing phagocytosis, we used a gentamicin protection assay, depicted in Figure 5-9, to allow us to assess both uptake and killing ability of macrophages (Schulthess et al., 2019, O'Callaghan et al., 2021). Here, colonic macrophages were isolated from uninfected or *Hh* colonized mice by FACS before being placed in culture overnight. The next day, macrophages were incubated with a commensal strain of *E. coli* for 2 hours. After this incubation, media was removed, and the cells washed with the antibiotic gentamicin to kill extracellular bacteria. Some cells were lysed at this stage to measure bacterial uptake, while others were given fresh media and cultured for various timepoints to assess intracellular bacterial killing over time. Live intracellular bacteria were quantified by lysing cells and plating the lysates on agar plates (Figure 5-9). However, in our first attempt, none of the colonic macrophage lysates yielded bacterial colonies (data not shown). Because isolating colonic macrophages by FACS yields low cell numbers and puts the cells through substantial stress, we

also carried out the assay in parallel using peritoneal macrophages - as they are easy to obtain in larger numbers and do not require any digesting or excessive processing (Pineda-Torra et al., 2015). We were able to successfully obtain bacterial colonies from peritoneal macrophages lysed 2h after incubation with *E. coli*, giving us a readout for bacterial uptake in this population. However, from the later timepoints which were chosen to assess intracellular killing, no bacterial colonies were present, indicating that the macrophages had successfully killed all intracellular bacteria (data not shown). We therefore concluded that the gentamicin protection assay worked well as a phagocytosis readout with the larger cell numbers in the peritoneal macrophage samples but requires further optimisation to work as a readout for bacterial killing. For colonic macrophages, the low cell numbers and experimental processing meant that additional optimisation was required, which we did not have time to carry out.

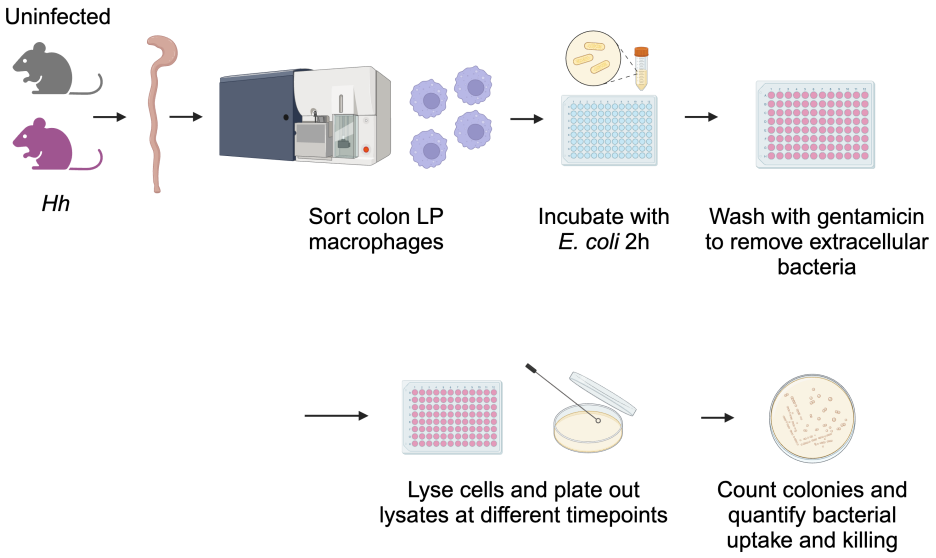


**Figure 5-9: Schematic for gentamicin protection assay**
C57BL/6 littermates were administered 1x10$^8$ CFU *Hh* or given PBS by oral gavage and left for 21-days post-infection. cLPL were isolated using enzymatic digestion and CD11b$^+$CD64$^+$Ly6C$^-$MHCII$^+$ macrophages purified by FACS. Macrophages were seeded in 96-well culture plates overnight before 2h incubation with *E. coli* at MOI 10. Cells were washed with 50µg/mL gentamicin to remove extracellular bacteria before being lysed at various timepoints. Cell lysates were plated on agar plates and incubated overnight at 37℃ before being assessed for bacterial colonies.

### 5.3.3 *Hh*$^+$ MT does not affect colonic macrophage mTOR activation or mitochondrial activity

Finally, we aimed to test whether *Hh* colonization alters the metabolic phenotype of colonic macrophages, which may be linked to the decreased

cytokine production. We used two different broad strokes approaches as readouts for metabolic activity *ex vivo*. First, we made use of 'phospho-flow' to measure mTOR activation. The mTOR complexes mTOR complex 1 (mTORC1) and mTORC2 act as central controllers of cellular metabolism and are involved in regulating various cell processes including transcription and translation, proliferation, and autophagy (Liu et al., 2015b). They also play key roles driving immune functions, particularly during immune cell activation, which involves many metabolically demanding processes such as production of cytokines and other mediators (Weichhart et al., 2015). Downstream of mTORC1 signalling is ribosomal protein S6, which is activated by phosphorylation and is an important driver of protein translation (Weichhart et al., 2015). Similarly, phosphorylation of AKT is downstream of mTORC2, which drives metabolic reprogramming and can also act upstream of mTORC1 (Weichhart et al., 2015). As such, phosphorylated S6 and AKT are indicators of mTOR activation and can be measured by techniques such as flow cytometry or western blot (Tazzari et al., 2002, Schulthess et al., 2019).

Detection of phosphorylated proteins can be difficult due to the transient nature of phosphorylation and the fact that intracellular antibody binding requires cell fixation and permeabilization. Analysis of cells from *ex vivo* tissues brings added complexity, as digestion and processing steps cause cell stress and can alter phosphorylation states. We therefore decided to first test the protocol for phospho-flow on *in vitro*-stimulated cells. We generated murine BMDMs and stimulated them with *E. coli* LPS or live *Hh* before assessing the presence of phosphorylated S6 and AKT (pS6, pAKT). Compared to unstimulated BMDMs, cells stimulated with LPS or *Hh* showed a significant increase in pS6 (Figure 5-10A). Stimulation with *Hh* induced the highest expression of pS6, indicating that incubation with whole bacteria drives greater macrophage metabolic activation than stimulation with LPS alone (Figure 5-10A). In contrast, pAKT was not upregulated to the same extent as pS6, showing only a slight trend towards higher expression in the stimulated BMDMs compared to unstimulated cells, which did not reach statistical significance (Figure 5-10B). This may be because phosphorylation of AKT could be an earlier event following mTOR activation and therefore the phosphorylation lost earlier than on S6. Having determined that pS6 was a good readout for macrophage activation, we went on to quantify its

presence on colonic macrophages from naïve and *Hh*$^{+}$ MT recipient mice. In contrast to the *in vitro* system, colonic macrophages showed much higher expression of both pS6 and pAKT compared to unstimulated BMDMs (Figure 5-10, Figure 5-11). This may reflect a higher level of metabolic activity required for survival in tissue. However, we did not observe differences in expression of pS6 or pAKT between colonic macrophages from naïve or *Hh*$^{+}$ MT recipient animals (Figure 5-11A-B).

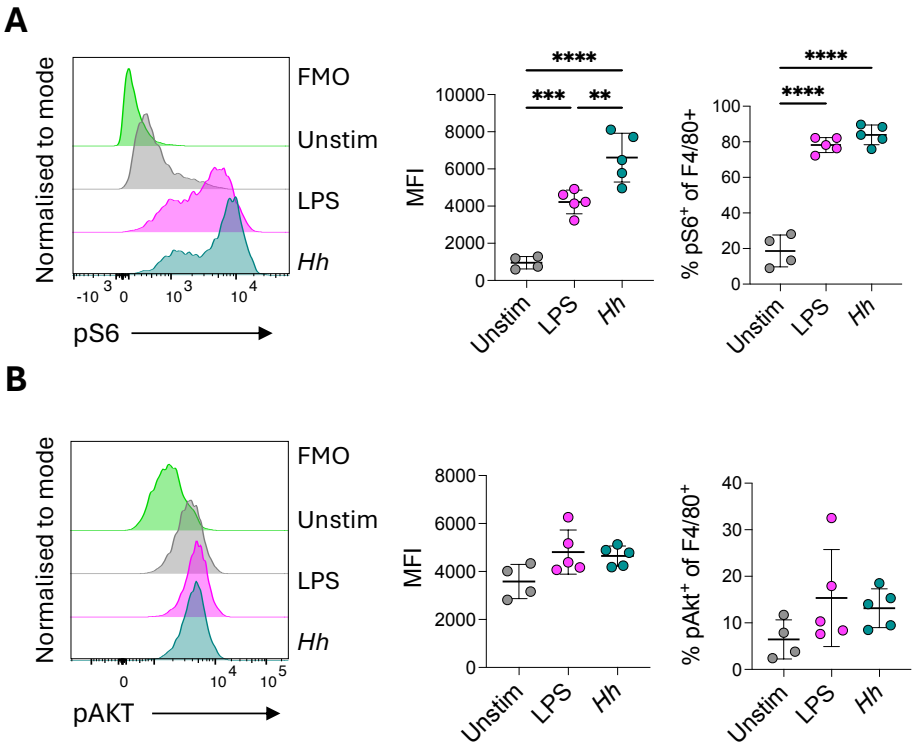


**Figure 5-10: pS6 levels are increased in BMDMs following stimulation with *Hh***
BMDMs were left unstimulated, treated with 100ng/mL *E. coli* LPS, or incubated with live *Hh* at MOI 10 for 16h. BMDMs were identified as F4/80$^{+}$ and the presence of phosphorylated S6 (A) and AKT (B) were assessed by flow cytometry. Representative histograms showing the proportion of pS6/pAKT-expressing BMDMs are shown (left) along with quantification of MFI (centre) and frequency of expression (right). Data are shown with mean ± SD. Data points are technical replicates and are representative of 1 experiment. Data were tested for normality using the Shapiro-Wilk normality test and statistical significance determined by one-way ANOVA with Tukey's multiple comparison correction (significance *p< 0.05, **p<0.01, ***p< 0.001, ****p< .0001).

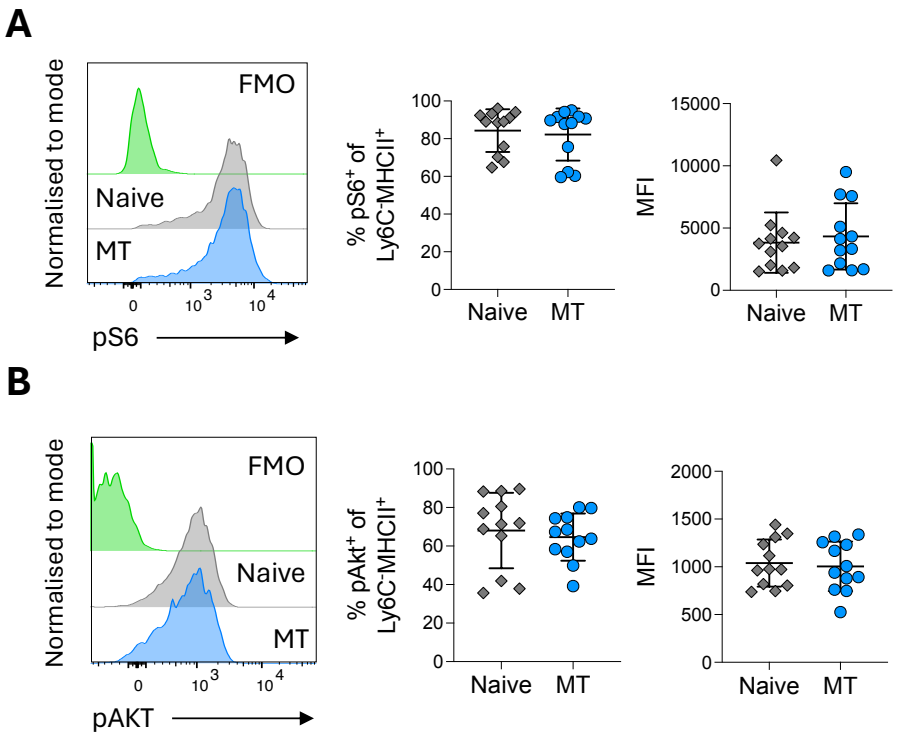


**Figure 5-11: Levels of pS6 and pAKT in colonic macrophages are not altered by *Hh*$^+$ MT**
C57BL/6 littermate cohorts were left untreated (Naïve) or colonized with *Hh*$^+$ microbiota (MT) for 21-days. cLPL were isolated using enzymatic digestion and the presence of pS6 (A) and pAKT (B) were assessed by flow cytometry on CD11b$^+$CD64$^+$Ly6C$^-$MHCII$^+$ macrophages. Representative histograms showing the proportion of pS6/pAKT-expressing macrophages are shown (left) along with quantification of MFI (centre) and frequency of expression (right). Data are shown with mean ± SD and are pooled from 3 independent experiments with n=4 per experiment. Data were tested for normality using the Shapiro-Wilk normality test and in cases where data were normally distributed statistical significance was determined by unpaired t test, while otherwise a Mann Whitney test was used (significance *p< 0.05, **p<0.01, ***p< 0.001, ****p< .0001).

Secondly, we used ‘mitospy’ dyes to measure mitochondrial activity by flow cytometry (Scott et al., 2022, Heieis et al., 2023). Key metabolic pathways take place in the mitochondria, including the TCA cycle and electron transport chain, which support oxidative phosphorylation (O'Neill et al., 2016). Mitospy dyes are fluorescent mitochondrial localisation probes, which enter mitochondria in a manner that is either dependent (red) or independent (green) of mitochondrial membrane potential. Thus, mitospy green identifies all mitochondria independently of membrane potential, and is used to indicate total mitochondrial mass (Pendergrass et al., 2004). Mitochondrial mass is thought to largely correlate with increased activity, with larger mass associated with increased rates of transcription and translation (Miettinen and Björklund, 2017). Mitospy red requires an active membrane potential to label the mitochondria, therefore labelling only active mitochondria as a readout of oxidative phosphorylation (Pendergrass et al., 2004).

Again, we first tested the mitospy dyes on *in vitro*-stimulated BMDMs. For both dyes, 100% of the BMDM population were stained following incubation, indicating that all cells contained active mitochondria (Figure 5-12). We noted subtle differences in MFI for both dyes following BMDM stimulation. Treatment with LPS or *Hh* resulted in a significant decrease in mitospy green in BMDMs, indicative of reduced mitochondrial mass (Figure 5-12A). BMDMs stimulated with *Hh* also showed a modest increase in the MFI of mitospy red (Figure 5-12B), suggesting they may be more metabolically active. Finally, we used the mitospy dyes on colonic macrophages from uninfected and *Hh*$^{+}$ MT recipient mice. However, we found no significant differences in either the proportions or MFI levels of mitospy green or mitospy red staining in colonic macrophages from naïve or *Hh*$^{+}$ MT mice (Figure 5-13). Overall, these data indicate that colonic macrophages from *Hh*$^{+}$ MT recipients appear metabolically similar to those from naïve mice, at least in terms of mTOR and mitochondrial activity.

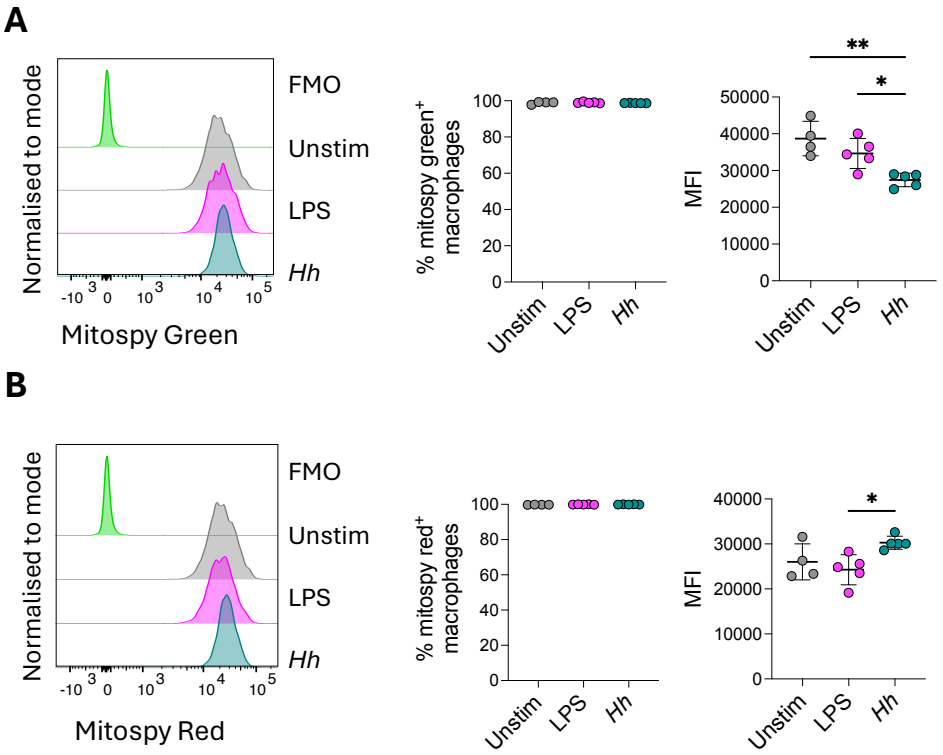


**Figure 5-12: Mitochondrial mass decreases while mitochondrial activity increases in BMDMs following stimulation with *Hh***

BMDMs were left unstimulated, treated with 100ng/mL *E. coli* LPS, or incubated with live *Hh* at MOI 10 for 16h. BMDMs were incubated with Mitospy dyes at 250nM for 30min at 37℃. BMDMs were identified as F4/80$^+$ and the level of Mitospy Green (A) and Mitospy Red (B) assessed by flow cytometry. Representative histograms showing the proportion of Mitospy Red/Green-positive BMDMs are shown (left), along with frequency of expression (centre), and quantification of MFI (right). Data are shown with mean ± SD. Data points are technical replicates and are representative of 1 experiment. Data were tested for normality using the Shapiro-Wilk normality test and statistical significance determined by one-way ANOVA with Tukey's multiple comparison correction (significance *p< 0.05, **p<0.01, ***p< 0.001, ****p< .0001).

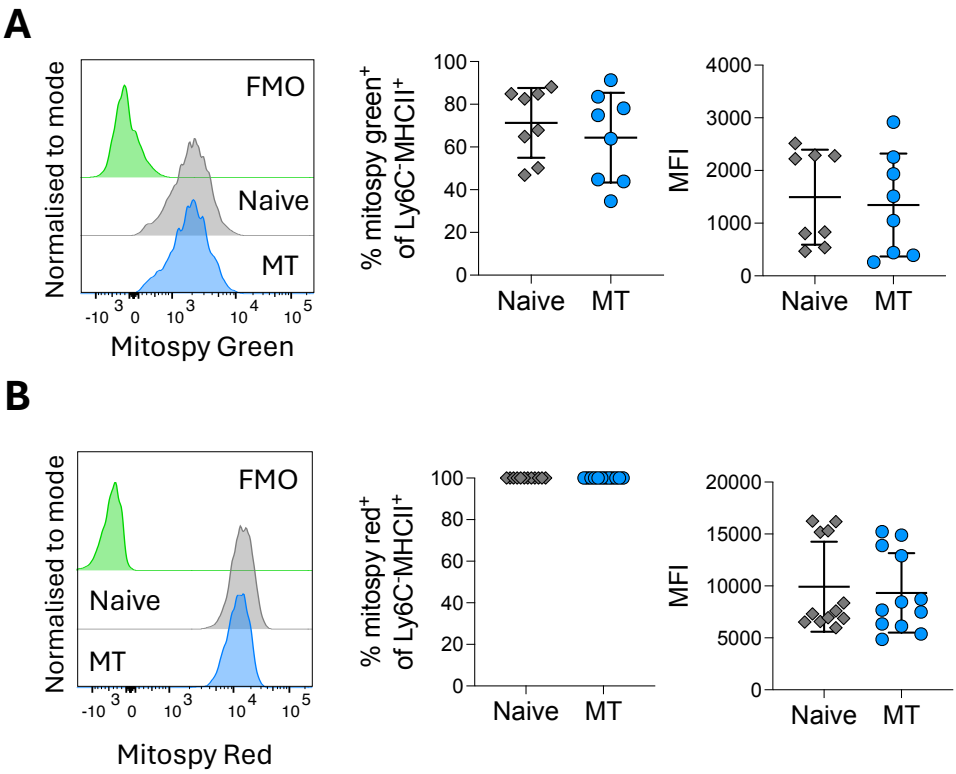


**Figure 5-13: Colonic macrophage mitochondrial mass and activity are not altered by *Hh*$^+$ MT**
C57BL/6 littermate cohorts were left untreated (Naïve) or colonized with *Hh*$^+$ microbiota (MT) for 21-days. cLPL were isolated using enzymatic digestion and incubated with Mitospy dyes at 250nM for 30min at 37℃. Macrophages were identified as CD11b$^+$CD64$^+$Ly6C$^-$MHCII$^+$ and the level of Mitospy Green (A) and Mitospy Red (B) assessed by flow cytometry. Representative histograms showing the proportion of Mitospy Red/Green-positive macrophages are shown (left), along with frequency of expression (centre), and quantification of MFI (right). Data are shown with mean ± SD and are pooled from 3 independent experiments with n=4 per experiment. Data were tested for normality using the Shapiro-Wilk normality test and in cases where data were normally distributed statistical significance was determined by unpaired t test, while otherwise a Mann Whitney test was used (significance *p< 0.05, **p<0.01, ***p< 0.001, ****p< .0001).

## 5.4 Discussion

Intestinal macrophages are specialised to function in the unique environment of the gut, where they are involved in maintaining symbiosis with the microbiota. This crosstalk with the microbiota directly influences macrophage functions. GF animals show changes to intestinal macrophage numbers and subsets (Bain et al., 2014, Kang et al., 2020), while microbiota derived metabolites have been shown to affect macrophage antimicrobial functions and alter metabolic phenotypes (Chang et al., 2014, Schulthess et al., 2019, O'Callaghan et al., 2021). We previously identified a disease-attenuating effect of *Hh* infection in the context of DSS-induced colitis. Here, we aimed to determine whether *Hh* colonization drives changes to macrophage functions at steady state which could contribute to this effect. We demonstrate that macrophages from *Hh* infected

mice have an impaired ability to produce cytokines *ex vivo* and may exhibit reduced phagocytic function.

### 5.4.1 Suppression of macrophage cytokine production by *Hh*

Our results show that colonic macrophages derived from *Hh* colonized animals have an impaired ability to produce cytokines *ex vivo*. This suggests that, either directly or indirectly, *Hh* has a limiting effect on local innate immunity. This ties in with the understanding that intestinal macrophages, unlike those in other tissues, are refractory to stimulation as a result of the large microbial burden in the gut. Compared to monocytes, intestinal macrophages produce fewer cytokines in response to PAMPs (Smythies et al., 2005, Bujko et al., 2017). *Hh* may be one of the species in the microbiota which contribute to this effect, the result of which is continued harmony between the host and its resident microbiota.

It is interesting to consider how this effect on macrophage function may impact the host's response to an inflammatory or infectious challenge. In a setting of pathologic inflammation, such as IBD or murine colitis models, the presence of microbial species which limit the production of proinflammatory cytokines could be beneficial by helping to alleviate inflammation. This is relevant to the data we presented in Chapter 3, as reduced macrophage cytokine output could contribute to the protective effect of *Hh* in DSS colitis. However, colitic inflammation has been shown to be driven by infiltrating monocytes and monocyte-derived macrophages, rather than resident macrophages present in the gut at the time of challenge (Bain et al., 2013, Arnold et al., 2016, Bain et al., 2018). It is unclear whether monocyte cytokine responses are also altered in *Hh* infected mice. In the initial experiments carried out using the *Hh*$^+$ MT system, the total CD64$^+$ monocyte-macrophage pool was isolated for stimulation. In these experiments a greater response to stimulation was observed, likely as a result of the presence of monocytes and their heightened responsiveness compared to macrophages (Smythies et al., 2005, Bujko et al., 2017). Nevertheless, CD64$^+$ cells from *Hh*$^+$ MT recipients still produced substantially less cytokine than those from naïve mice, suggesting that monocytes from *Hh*-infected mice could also show altered function. This hypothesis could be tested by specifically isolating monocytes and repeating the assay.

Additionally, we tested whether the reduction in cytokine production was due to increased cell death in macrophages from *Hh*$^{+}$ MT or *Hh*-infected animals. As we did not observe differences in the number of live cells obtained following cLPL isolation or macrophage sorting, we concluded that macrophages from infected mice did not have an increased propensity for cell death during processing. We used an alamarBlue assay to address the viability of macrophages during culture and also did not detect differences. However, the low cell numbers obtained by FACS were not optimal for the assay, and these results require additional validation (Pott et al., 2018). Other methods of cytokine detection should be used in the future to corroborate the results presented here, for example using flow cytometry to detect intracellular cytokine production.

In Chapter 4, we identified transcriptional upregulation of *Tnfa* and *Il17a* at day 21 following *Hh* colonization. In contrast, here we have shown that macrophages from infected mice produce less TNFα compared to those from naïve mice. This could be due to a difference between transcription and protein production but is more likely to reflect the action of multiple cell types. The transcriptional upregulation was observed in total colon tissue, making it difficult to conclude which cell types may be responsible. With macrophages from infected mice showing reduced cytokine production, the transcriptional upregulation of *Tnfa* could be a T cell response, along with upregulation of *Il17a*. Th1 and Th17 responses have well been documented in *Hh*-induced colitis models, including IL-17A production (Morrison et al., 2013, Xu et al., 2018). The precise source of these cytokines could be identified using flow cytometry to identify various cell types, including T cells, and measuring intracellular cytokine levels. It is also of interest that we observed reduced production of IL-10 by macrophages in addition to reduced pro-inflammatory cytokines. IL-10 has been shown to be critical and non-redundant for maintenance of tolerance towards *Hh*, and its loss results in pathogenic inflammation (Kullberg et al., 2001). As such, homeostatic infection with *Hh* relies on production of IL-10 by Tregs( Maloy et al., 2003), but is presumably supplemented with IL-10 produced by other cell types. A mechanism has been described by which *Hh* promotes IL-10 production by intestinal macrophages at steady state (Danne et al., 2017), which appears in contrast to the data we have presented. However, in the Danne *et al*. study, mice were infected with *Hh* and cytokine levels observed at day 5 post-

infection, as opposed to the day 21 timepoint we have used. It may be the case that extended interactions with *Hh* and its products imprints a phenotype which is not present early after infection. Indeed, at the day 7 timepoint studied in Chapter 4, we observed increased transcription of *Ifnγ* and infiltration of neutrophils and monocytes. It may be that this short-term response is what drives the increased IL-10 production described by Danne *et al.*, and that with time this is resolved.

The mechanism by which *Hh* colonization acts to limit macrophage cytokine production remains unclear. We postulate that *Hh* may have both direct and indirect effects on local myeloid cells, and indirect effects could be mediated by the action of *Hh*-specific T cells which expand upon infection (Xu et al., 2018, Kedmi et al., 2022). Tregs have been shown to be capable of suppressing innate immune pathology *in vivo* (Maloy et al., 2003), and it is likely that their suppressive functions act on local myeloid populations at steady state. *In vitro*, Tregs inhibit the activation and maturation of cDCs upon exposure to TLR ligands, including suppressing cDC cytokine production (Houot et al., 2006). Similarly, monocytes pre-incubated with Tregs show reduced TNFα and IL-6 production when exposed to LPS (Taams et al., 2005). In concordance with the data we presented in Chapter 4, incubation with Tregs also results in reduced expression of costimulatory molecules on monocytes (Taams et al., 2005) and cDCs (Houot et al., 2006), further implicating Tregs as a potential driver of the phenotypic and functional changes we have observed in myeloid cells of *Hh* colonized mice. However, we cannot rule out the possibility that *Hh* may also exert direct effects on myeloid cells which contribute to the functional changes we have described. The mechanism described by Danne *et al.* involves a polysaccharide produced by *Hh* which is recognised by TLR2 (Danne et al., 2017). It is likely that other *Hh* derived products are recognised by macrophages and cDCs in the LP and exert additional functional effects. Several putative virulence factors of *Hh* have been described (Fox et al., 2011) and could be involved in the crosstalk of *Hh* with the host as well as with other microbes. Of interest, the *Hh* flagellin molecule, which is required for motility to allow colonization of its murine host (Sterzenbach et al., 2008), has evolved to evade recognition by TLR5 (Andersen-Nissen et al., 2005), presumably to attenuate inflammatory cytokine responses. Advances in metabolomics and proteomics may allow further

characterisation of *Hh* derived products and identification of additional mechanisms by which the host is influenced by the presence of *Hh*.

### 5.4.2 Optimisation of techniques to measure phagocytosis

Our data suggest that *Hh*$^{+}$ MT and *Hh* may have a limiting effect on macrophage phagocytosis, however further testing is required to validate this. We used two methods to test the phagocytic function of colonic macrophages. Using the pHrodo BioParticles system, we found that the concentration of BioParticles greatly altered the outcome of the assay. At the higher concentration, almost all macrophages successfully phagocytosed the BioParticles, regardless of the experimental group. Despite a difference in the MFI of pHrodo in the MT group, we therefore cannot conclude that MT had a notable effect on phagocytosis, as all macrophages displayed avid phagocytic function. pHrodo is non-fluorescent at neutral pH and therefore should not fluoresce if simply bound to the cell surface. However, studies using this assay often include an additional control group of cells kept at 4℃ during incubation (Scott et al., 2022), as this should largely inhibit phagocytosis, and as such is a more suitable negative control for the assay than a FMO alone. When we repeated this assay using a lower concentration of BioParticles, we were able to discern a subtle difference in the frequency of macrophages which phagocytosed the BioParticles. However, in these samples, no difference in MFI was present, leading us to conclude that further validation of this result is required. Additionally, while the pHrodo system allows for the measurement of phagocytosis independently of live bacteria, which removes the confounding effect of bacterial invasion versus phagocytosis (Lenzo et al., 2016), it is not without limitations. The assay as used here provides an endpoint reading, meaning that it cannot detect differences in the rate of phagocytosis, which may be important. Additionally, further optimisation of the endpoint timing is required. One study tested the use of different BioParticle concentrations and incubation times and reported that the MFI of pHrodo fluorescence reached a plateau at 30-60 mins incubation, depending on the concentration used (Lindner et al., 2020). At the 30-minute timepoint used here, it is therefore possible that this plateau had been reached, meaning that macrophages were saturated and differences in phagocytosis difficult to discern.

We then used the gentamicin protection assay with the aim of validating the result of the pHrodo system. The advantage of this assay is that both bacterial uptake and killing can be investigated. The killing of phagocytosed bacteria is an important mechanism by which phagocytes such as macrophages and neutrophils eliminate pathogens (Flannagan et al., 2009). Microbiota derived signals have been shown to enhance the bactericidal functions of macrophages (Schulthess et al., 2019) and neutrophils (Clarke et al., 2010), with beneficial effects on the outcome of subsequent infections with *S. typhimurium*, *C. rodentium*, and *Staphylococcus aureus*. Alterations to killing ability may therefore have a greater impact on infection outcomes than phagocytosis alone. However, this assay required additional optimisation. We were not able to detect live bacterial colonies at either the uptake or killing timepoints in colonic macrophages. We postulate that this is due to the low cell numbers obtained by FACS. We used a commensal strain of *E. coli* at MOI 10, and with the low cell numbers it may not have been enough to retrieve live bacteria. One solution could be to increase the MOI used, for example to MOI 100, although this may have a detrimental effect on macrophage viability (Schwan et al., 2000). A different bacterial strain could also be used, for example a pathogenic strain of *E. coli* or another pathogen such as *S. typhimurium* or *C. rodentium*, as it may be the case that commensal strains are not phagocytosed with the same efficiency as pathogens. As we could successfully validate the assay using larger numbers of peritoneal macrophages, we concluded that the assay worked in principal but requires further optimisation for colonic macrophages.

### 5.4.3 Metabolic phenotype as a functional readout

We lastly aimed to assess the metabolic phenotype of colonic macrophages, which is closely linked to functional state (Heieis et al., 2023). We identified no differences in mTOR activity or mitochondrial activity in colonic macrophages following *Hh*$^{+}$ MT. However, these approaches were very broad, and do not rule out the possibility that there may be more subtle differences in immunometabolism following *Hh*$^{+}$ MT or direct infection with *Hh*. To test this further, more specialised metabolic assays could be implemented. For example, the Seahorse assay tests metabolic function by measuring extracellular acidification rates (ECAR) and oxygen consumption rates (OCR) as readouts of glycolysis and mitochondrial respiration, respectively (Caines et al., 2022, Scott

et al., 2022). Another common example is the BODIPY assay which is an indicator of fatty acid uptake (Scott et al., 2022, Heieis et al., 2023). Additionally, several groups have described methods for using high dimensional spectral flow cytometry to measure the expression of various proteins associated with different metabolic phenotypes (Ahl et al., 2020, Heieis et al., 2023), which could provide a more complete picture of how *Hh*$^{+}$ MT or *Hh* colonization affect macrophage metabolism.

One caveat of measuring metabolic output of *ex vivo* cells is the fact that cell isolation methods from tissues often involve excessive processing and digestion steps, which can cause cellular stress and alter metabolic states. As such, the majority of work in the immunometabolism field has been carried out *in vitro* (Verberk et al., 2022). We noted that, in contrast to the BMDMs, the frequency of colonic macrophages positive for mitospy green was quite variable and <100%, while all macrophages were positive for mitospy red in both settings. It is not clear whether this reflects a fault in the mitospy green assay or is perhaps due to the additional processing required to isolate macrophages from *ex vivo* tissue. As techniques are becoming more refined and the field of immunometabolism is growing, it is likely that more information about how the microbiota affects immune cell metabolism *in vivo* will become available.

### 5.4.4 Concluding remarks

We have demonstrated that *Hh* colonization results in a suppression of intestinal macrophage cytokine responses. Despite evidence in the literature that *Hh* drives production of IL-10, we have shown that IL-10 production is reduced to the same extent as production of pro-inflammatory cytokines such as TNFα. *Hh* may also drive a reduction in phagocytic function, although these results remain to be validated. While we did not detect differences in colonic macrophage metabolism, we conclude that *Hh* has significant effects on macrophage functions which may contribute to disease and infection outcomes. Whether these effects are mediated by direct interactions with *Hh*, or through an indirect mechanism, for example involving Tregs, remains to be characterised.

# 6 Attenuation of disease severity by *Helicobacter hepaticus* is independent of TLR2

## 6.1 Introduction

We have previously described effects of *Hh* colonization on intestinal homeostasis and macrophage functions at steady state, and on disease outcome in the DSS colitis model. While these findings provide insight into the effects of *Hh* on the host, it remains unclear how these effects are mediated and which cell types, bacterial products, and immune signalling pathways are involved. It is likely that much of the crosstalk between *Hh* and the host involves conserved pathways which are active between a range of bacterial species and the mammalian immune system. Defining the mechanisms which drive this crosstalk will therefore help to further our understanding of host-microbiota interactions, with future implications for translational medicine (Belkaid and Harrison, 2017).

*Hh* is recognised directly by a range of immune cells, through both innate and adaptive receptors. We have predominantly highlighted the effects of *Hh* on the intestinal myeloid compartment, and postulate that these effects may be mediated by direct recognition of *Hh*, or indirectly through the functions of other immune cells. We know that *Hh* drives expansion of Tregs (Xu et al., 2018, Kedmi et al., 2022), and have previously discussed the possibility of Treg-mediated suppression of myeloid driven inflammation. However, it has also been documented that *Hh* can directly modulate macrophage functions (Danne et al., 2017), and a role for innate recognition in *Hh* mediated colitis has been described (Boulard et al., 2010, Asquith et al., 2010). Variants of genes associated with innate microbial recognition have been identified as risk factors for IBD (Jostins et al., 2012), highlighting the importance of these pathways in maintaining symbiosis with the microbiota. Similarly, TLR mediated recognition of commensals is critical for maintenance of intestinal homeostasis and is protective against epithelial injury in models of colitis (Rakoff-Nahoum et al., 2004, Asquith et al., 2010).

MyD88 is an important signalling adaptor molecule which functions downstream of TLR ligation. It has been reported that *Hh*-induced colitis is dependent on expression of MyD88 on myeloid cells (Asquith et al., 2010), indicating that

innate recognition of *Hh* is a key step in the pathogenesis of disease, even when the inflammation is driven by T cells. However, TLR responses to *Hh* do not cause disease in the presence of IL-10 signalling, and there is evidence that these signals actually promote anti-inflammatory responses at steady state. Danne *et al*. report one such mechanism, in which a *Hh* derived polysaccharide is recognised by TLR2 and signals through MyD88 to induce IL-10 production by macrophages (Danne et al., 2017). Despite the documented ability of TLR2 to recognise *Hh* (Mandell et al., 2004, Danne et al., 2017), mice lacking this receptor are equally as susceptible as WT mice to both T cell mediated and innate mediated colitis induced by *Hh* (Boulard et al., 2010). This could indicate a level of redundancy in the TLR system, but may also suggest that TLR2 signals promote homeostatic, rather than inflammatory, responses to *Hh*.

Identification of the innate signalling pathways responding to the microbiota not only provides information about the host's response, but also about the bacterial signals driving these responses. This is important for identifying mechanisms which may be shared between microbial species. For example, many species of flagellated bacteria have evolved to evade recognition by TLR5, including *Hh* and various species found in humans, such as *H. pylori* and *Campylobacter jejuni* (Andersen-Nissen et al., 2005). It has also been reported that *Hh* LPS has an inhibitory effect on subsequent TLR4 and TLR5 responses (Sterzenbach et al., 2007), suggesting that the presence of certain species could influence the host's response to other components of the microbiota. Dissecting how specific microbes interact with the host in different contexts will be critical for understanding how alterations to microbial composition affect disease and therapeutic outcomes (Rosshart et al., 2019).

## 6.2 Aims

The aim of this chapter was to gain an understanding of the mechanisms by which *Hh* affects intestinal homeostasis. I aimed to test the specific hypothesis that TLR2 signals may contribute to the attenuating effect of *Hh* infection on DSS colitis. I first attempted to validate a TLR2 antibody blockade approach *in vivo*, using challenge with a TLR2 agonist. I next assessed whether the disease protective effect of *Hh* on DSS colitis was dependent on recognition of *Hh* by TLR2.

## 6.3 Results

### 6.3.1 Validation of TLR2 blockade using an *in vivo* agonist challenge

To block TLR2 signalling *in vivo*, we employed an anti-TLR2 mAb that was reported previously to achieve this effect (Sung et al., 2019). To validate its efficacy, we utilised the specific TLR2 agonist Pam3csk4 (Aliprantis et al., 1999) and first performed a pilot experiment to determine the optimal dose of Pam3csk4. There are several examples in the literature of *in vivo* Pam3csk4 challenges at different doses. One study challenged mice with 100µg per mouse (Martínez et al., 2018), while others used a dose of 1mg/kg (Mersmann et al., 2010, Murayama et al., 2019), which equates to 20µg for a mouse weighing 20g. As we wanted to avoid a severe sickness response, we chose to test a lower dose of 10µg per mouse, as well as a higher dose of 100µg, given by intraperitoneal (ip) injection. Mice were left for 4 hours following Pam3csk4 treatment before ending the experiment and harvesting serum for cytokine analysis. We observed no sickness responses during this timeframe, and found that serum concentrations of IL-6, TNFα, and MCP-1 increased in a dose-dependent manner following Pam3csk4 treatment (Figure 6-1). Serum IL-10 was also increased following treatment, although showed greater variation in response at the lower dose. Due to the lack of sickness response at either dose, we opted to use the higher dose of 100µg per mouse for subsequent experiments as this elicited the greatest cytokine response and showed the least variation between animals (Figure 6-1).

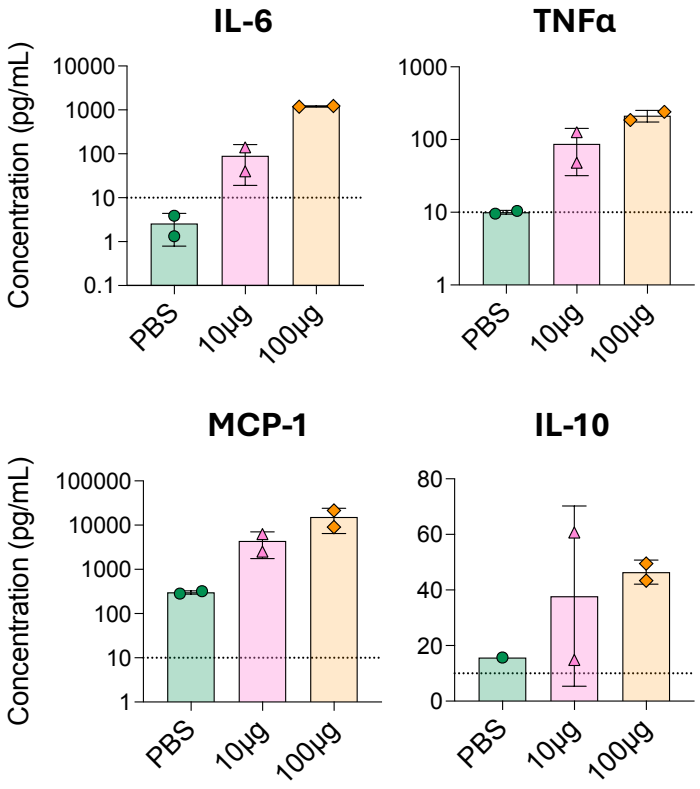


**Figure 6-1: Pam3csk4 drives increases in serum cytokine concentrations in a dose-dependent manner**
C57BL/6 mice were administered 100μg αTLR2 mAb or isotype control mAb and challenged 4d later by ip injection of either 10μg or 100μg Pam3csk4 or PBS. Mice were culled after 4 hours and concentrations of IL-6, TNFα, MCP-1, and IL-10 measured in the serum by CBA. Data are shown with mean ± SD and are representative of one experiment with n=2. The lower detection limits of the assays are indicated by the dotted lines.

To test the efficacy of the αTLR2 mAb for blocking TLR2 signalling *in vivo*, cohorts of mice were first treated with either the αTLR2 mAb or an isotype control mAb, then left for 4 days before being challenged by ip injection of 100μg Pam3csk4 and culled 4h later (Figure 6-2).

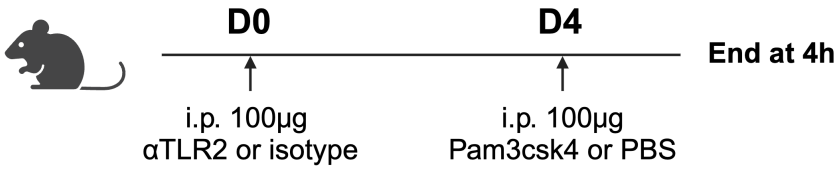


**Figure 6-2: Schematic for in vivo Pam3csk4 challenge with TLR2 blockade**
C57BL/6 mice were administered 100μg αTLR2 mAb or isotype control mAb. On day 4 animals received 100μg Pam3csk4 or PBS by i.p. injection and were culled after 4 hours.

We harvested serum for cytokine measurement and colons for analysis of cLPL populations. In the isotype control mAb treated group, we observed significant increases of IL-6 and MCP-1 in the serum following Pam3csk4 treatment (Figure 6-3). There was also a trend towards increased TNFα and IL-10, although these did not reach statistical significance (Figure 6-3). In contrast, mice which received αTLR2 mAb showed significantly reduced responsiveness to Pam3csk4 treatment, with serum IL-6 and MCP-1 responses almost completed ablated (Figure 6-3). We also saw a similar trend of reduced production of TNFα, although this did not reach statistical significance (Figure 6-3). While the cytokine response to Pam3csk4 was not completely blocked in these mice, it was reduced to a level statistically comparable with untreated controls. These data indicate that the tested dose of αTLR2 mAb successfully inhibits TLR2-mediated recognition of Pam3csk4 *in vivo*.

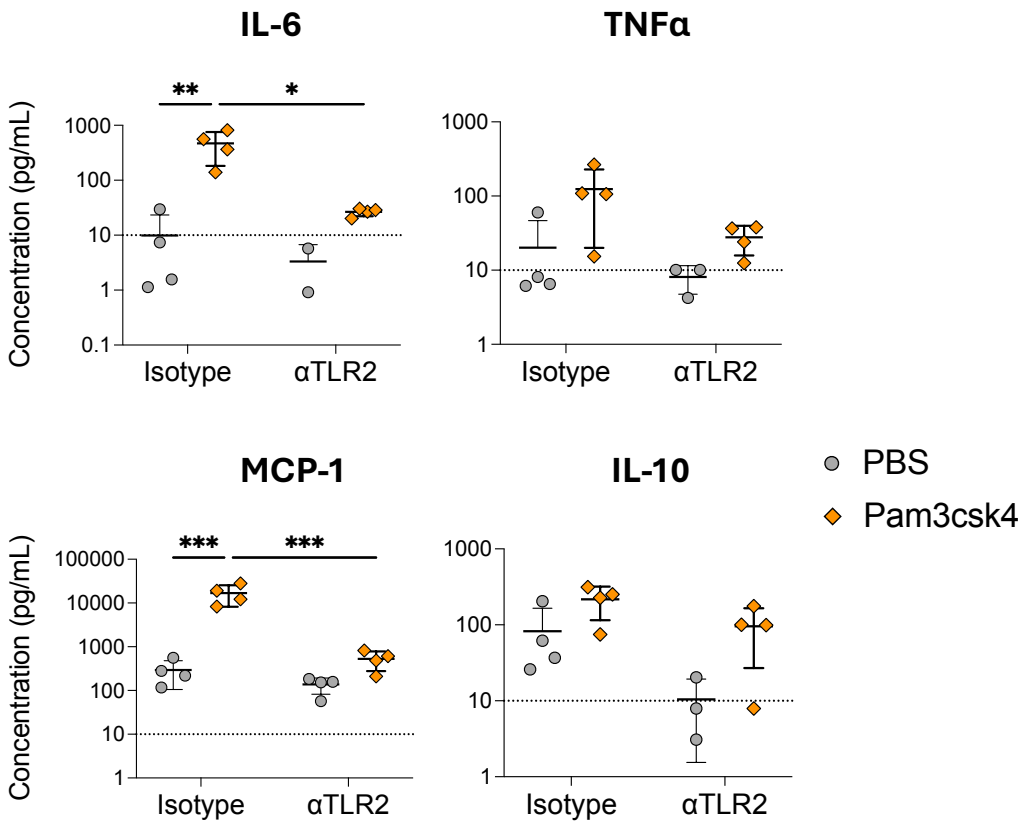


**Figure 6-3: Anti-TLR2 mAb attenuates Pam3csk4 induced inflammatory cytokine production *in vivo***
C57BL/6 mice were administered 100µg αTLR2 mAb or isotype control mAb and challenged 4d later by ip injection of either 100µg Pam3csk4 or PBS. Mice were culled after 4 hours and concentrations of IL-6, TNFα, MCP-1, and IL-10 measured in the serum by CBA. Data are shown with mean ± SD and are representative of one experiment with n=4. Statistical significance was determined by 2-way ANOVA (significance *p< 0.05, **p<0.01, ***p< 0.001, ****p< .0001). The lower detection limits of the assays are indicated by the dotted lines.

In parallel, we also examined the cLPL pool for changes following Pam3csk4 challenge. Levels of most cLPL populations were unchanged following Pam3csk4 treatment (data not shown); however, colonic neutrophil infiltration was significantly increased (Figure 6-4). As with serum cytokine levels, the colonic neutrophil response to Pam3csk4 was highly attenuated in mice which received αTLR2 (Figure 6-4), indicating that TLR2 blockade effectively inhibited the response to Pam3csk4 in the colon. Together, these results show that the dose of αTLR2 mAb used here was successful at blocking TLR2-mediated recognition of Pam3csk4 *in vivo*, confirming that this strategy could be employed to test the role of TLR2 signals in *Hh*-induced protection from DSS colitis.

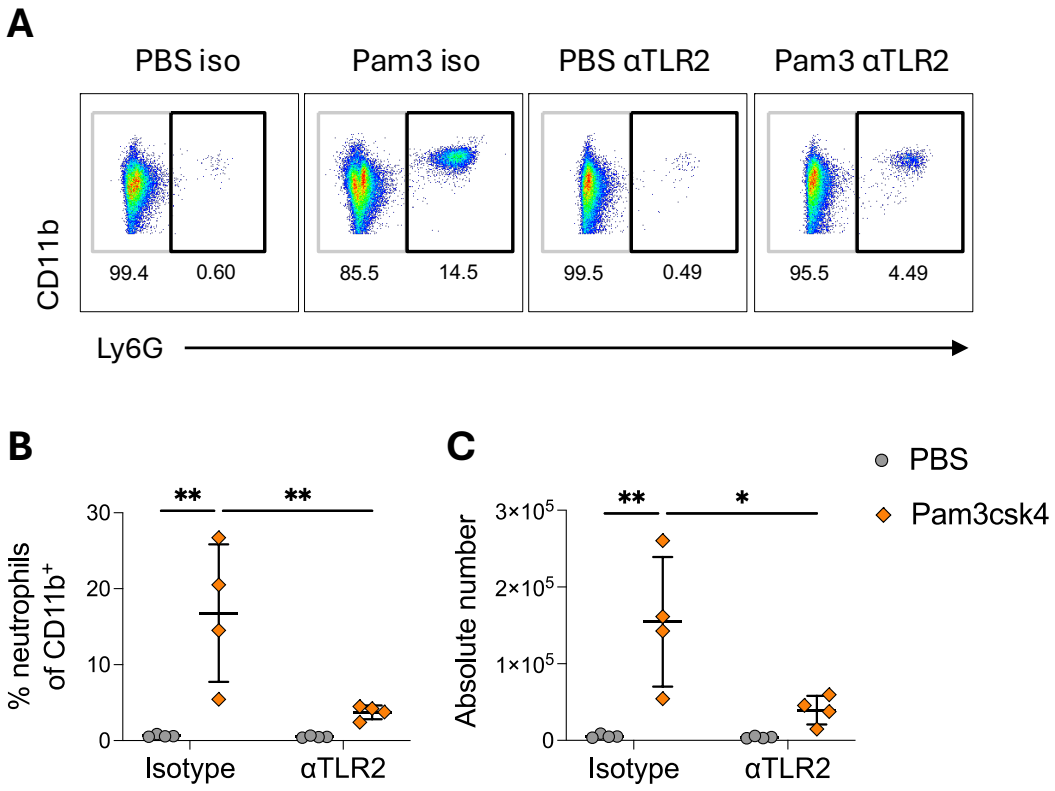


**Figure 6-4: Anti-TLR2 mAb attenuates Pam3csk4 induced neutrophil infiltration into the intestine *in vivo***

C57BL/6 mice were administered 100µg αTLR2 or isotype control then challenged 4d later by ip injection of either 100µg Pam3csk4 or PBS and culled after 4 hours. Representative dot plots of colonic neutrophils (A), quantification of neutrophil frequencies (B) and absolute numbers (C) are shown. Data are shown with mean ± SD and are representative of one experiment with n=4 per experiment. Statistical significance was determined by 2-way ANOVA (significance *p< 0.05, **p<0.01, ***p< 0.001, ****p< .0001).

### 6.3.2 TLR2 is not required for *Hh* mediated protection against disease severity

Due to the evidence that *Hh* is recognised by TLR2 and drives an anti-inflammatory response through this pathway (Mandell et al., 2004, Danne et al., 2017), we opted to test whether TLR2 signals were required for the disease protective effect of *Hh* documented previously. We infected mice with *Hh* and allowed 21 days for conditioning of the immune system before challenging all animals with 2% DSS (Figure 6-5A). For the duration of the experiment, mice received weekly doses of αTLR2 treatment to block recognition of *Hh* by TLR2. This method was preferential to using *Tlr2*$^{-/-}$ mice as it ensured that animals had a normal relationship with their microbiota during development and did not show genotype related differences in microbial composition – either as a result of familial transmission or directly because of the genotype (Ubeda et al., 2012). We then confirmed that TLR2 blockade did not affect levels of *Hh* colonization (Figure 6-5B).

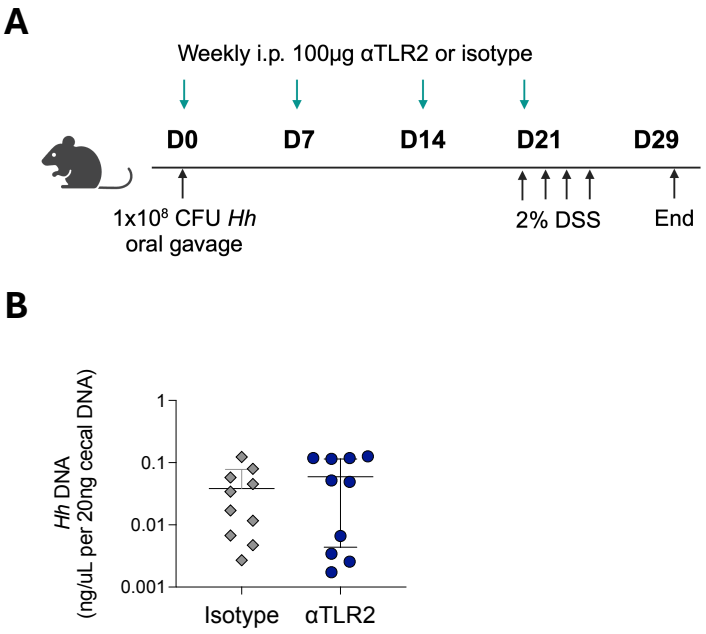


**Figure 6-5: Schematic for TLR2 blockade and effect of treatment on *Hh* colonization**
C57BL/6 mice were administered 1x10$^8$ CFU *Hh* or PBS by oral gavage and left for 21 days to allow bacterial colonization. On day 21 all mice were administered 2% DSS in drinking water for 4 days before being switched back to normal water for a final 4 days. Mice received 100µg αTLR2 mAb or mouse IgG1, κ isotype control mAb once weekly by i.p. injection (A). *Hh* colonization was quantified in caecal content by qPCR of *CdtB* (B). Data are shown with mean ± SD and pooled from 2 independent experiments with n=5 per experiment. Statistical significance was determined by 2-way ANOVA (significance *p< 0.05, **p<0.01, ***p< 0.001, ****p< .0001).

Of the mice which received the isotype control, those infected with *Hh* showed significantly reduced disease activity and DSS-induced weight loss compared to uninfected animals, as previously described (Figure 6-6A-B). TLR2 blockade appeared to slightly attenuate the severity of DSS symptoms, with uninfected mice which received αTLR2 mAb showing a trend towards reduced disease activity and weight loss compared to the isotype treated group (Figure 6-6A-B). This was also the case for the *Hh* colonized animals, with those receiving αTLR2 showing a non-significant trend towards greater disease reduction than those which received the isotype control (Figure 6-6A-B). Nevertheless, TLR2 blockade did not abrogate the protective effect of *Hh* colonization, as *Hh* infected mice which received αTLR2 mAb showed significantly reduced clinical symptoms compared to uninfected αTLR2 mAb treated mice (Figure 6-6A). Of the mice in the isotype group, those colonized with *Hh* showed increased colon length compared to uninfected (Figure 6-6C), which is an indicator of reduced disease severity (Yan et al., 2009). TLR2 blockade also resulted in an increase in colon length and was not different between uninfected and *Hh* colonized mice (Figure 6-6C).

We then assessed the mid and distal colon for DSS-induced intestinal pathology. In the uninfected mice, we observed that treatment with αTLR2 mAb slightly reduced the severity of pathology, although not to a statistically significant level (Figure 6-7). However, infection with *Hh* significantly reduced the levels of histological inflammation, both in the isotype mAb and αTLR2 mAb-treated groups (Figure 6-7). We observed no significant difference in the severity of intestinal pathology between the *Hh*-infected mice in the different mAb treatment groups (Figure 6-7). Together, these data indicate that αTLR2 mAb treatment may have a slight attenuating effect on DSS-induced intestinal pathology, but this effect is not as significant as the attenuating effect of *Hh* infection. Importantly, loss of TLR2 signalling did not inhibit the ability of *Hh* to protect against DSS induced disease severity.

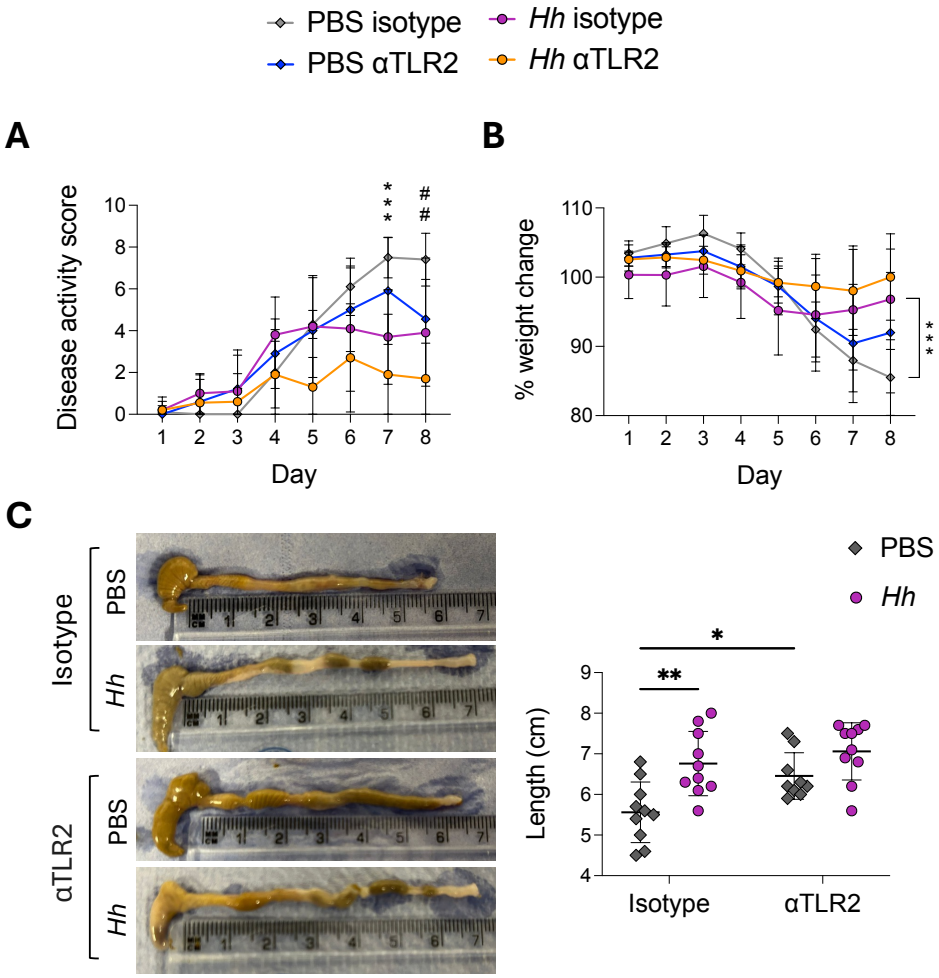


**Figure 6-6: TLR2 blockade does not abrogate *Hh*-mediated attenuation of DSS disease**
C57BL/6 mice were infected with 1x10$^8$ CFU *Hh* or PBS by oral gavage and administered 2% DSS in drinking water. Mice received either αTLR2 mAb or isotype control mAb once weekly for experiment duration. Following DSS administration mice were assessed daily for clinical disease activity (A) and weight change (B). Representative pictures of colon length are shown (C – left) with lengths quantified (C – right). Data are shown as mean ± SD and pooled from 2 independent experiments with n=5 per experiment. Statistical significance was determined by 2-way ANOVA (significance *p< 0.05, **p<0.01, ***p< 0.001, ****p< .0001). In (A) the statistical significance is shown on D7 between the PBS and *Hh* αTLR2 groups (represented by *) and on D8 between the PBS and *Hh* isotype groups (represented by #). In (B) the statistical significance is shown on D8 between the PBS and *Hh* isotype groups.

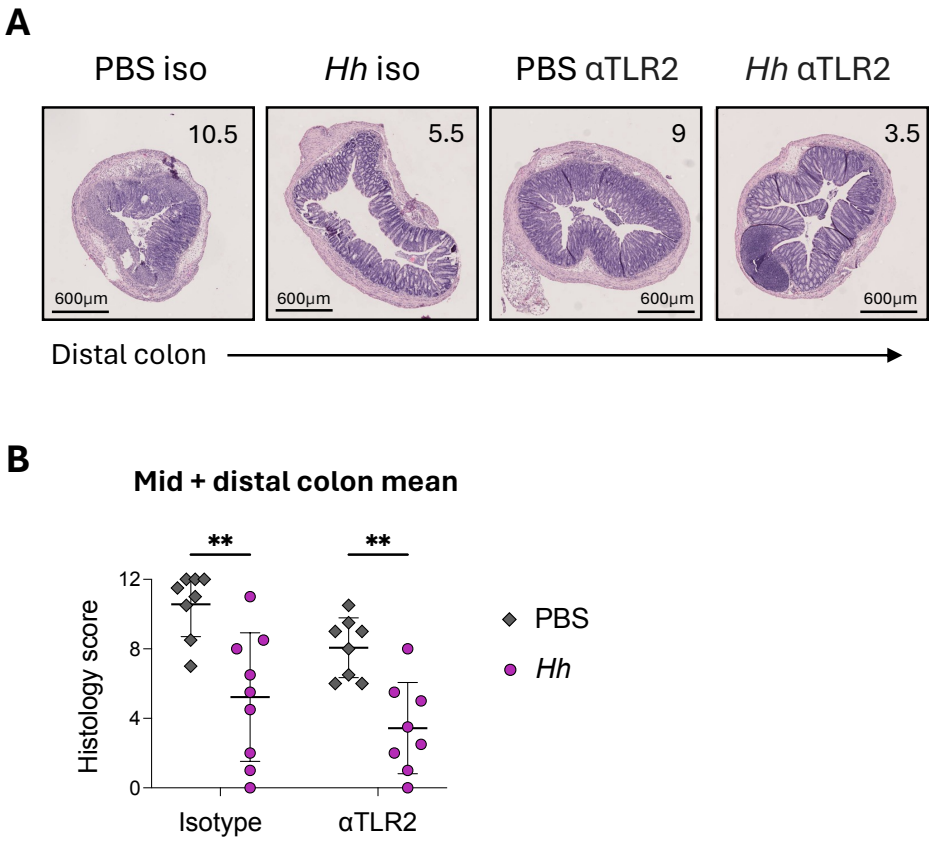


**Figure 6-7: TLR2 blockade does not abrogate *Hh*-mediated attenuation of DSS colitis**
C57BL/6 mice were infected with 1x$10^8$ CFU *Hh* or PBS by oral gavage and administered 2% DSS in drinking water. Mice received either αTLR2 mAb or isotype control mAb once weekly for experiment duration. Representative H&E staining of distal colon sections, with histological scores shown in the top right of each image (A). Sections were scored blind for signs of histological inflammation and the mean scores from the mid and distal colon were quantified (B). Data are shown with mean ± SD and pooled from 2 independent experiments with n=5 per experiment. Statistical significance was determined by 2-way ANOVA (significance *p< 0.05, **p<0.01, ***p< 0.001, ****p< .0001).

In parallel, we assessed the cLP for immune cell populations. Following DSS treatment, *Hh* colonized mice had significantly fewer $CD45^+$ leukocytes and $CD11b^+$ myeloid cells in the cLP compared to uninfected animals, regardless of αTLR2 mAb treatment (Figure 6-8A-C). *Hh* infection also significantly reduced the number of $CD64^+$ monocyte-macrophages in the isotype mAb-treated group (Figure 6-8D). This trend was present in the mice which received αTLR2 mAb treatment, although not to a statistically significant level (Figure 6-8D). We then assessed levels of colonic neutrophils in the different treatment groups. Of the uninfected mice, those receiving αTLR2 mAb showed significantly reduced neutrophil levels compared to those receiving the isotype control mAb (Figure 6-9). However, in both mAb treatment groups, infection with *Hh* resulted in a marked reduction in neutrophil levels compared to the uninfected mice (Figure 6-9). Indeed, the *Hh*-infected, αTLR2 mAb-treated group showed the lowest

levels of neutrophil infiltration, suggesting that αTLR2 mAb did not inhibit the disease attenuating effect of *Hh* but instead provided an additional reductive effect. Furthermore, αTLR2 mAb treatment significantly reduced the levels of monocyte infiltration in uninfected mice (Figure 6-10). *Hh* infection also caused a significant reduction in monocyte levels in the isotype mAb-treated group (Figure 6-10). Of the mice which received αTLR2 mAb, *Hh* infection resulted in a non-significant decrease in monocyte levels, which meant that this group showed the lowest levels of colonic monocyte accumulation, suggesting an additive effect of *Hh* infection and αTLR2 mAb treatment (Figure 6-10).

Numbers of intermediate monocyte-macrophages were reduced in both *Hh* infected groups, regardless of αTLR2 mAb treatment (Figure 6-11A), whereas mature macrophage numbers were comparable between all treatment groups (Figure 6-11B). In Chapter 3 we observed phenotypic differences in the cLP macrophage pool following DSS treatment which were altered with *Hh* colonization. We therefore examined the expression of these markers to determine the contribution of TLR2 signalling to this effect. As previously, expression of the costimulatory molecule CD80 was reduced on cLP macrophages from *Hh* infected mice, and this was unaffected by TLR2 blockade (Figure 6-12A). In contrast, CD86 expression by cLP macrophages was comparable across all groups, with the exception of those isolated from the *Hh* infected and αTLR2 treated group, which showed increased CD86 levels (Figure 6-12B). Finally, PD-L1 expression on cLP macrophages was substantially reduced with *Hh* colonization, and this was again independent of TLR2 blockade (Figure 6-12C).

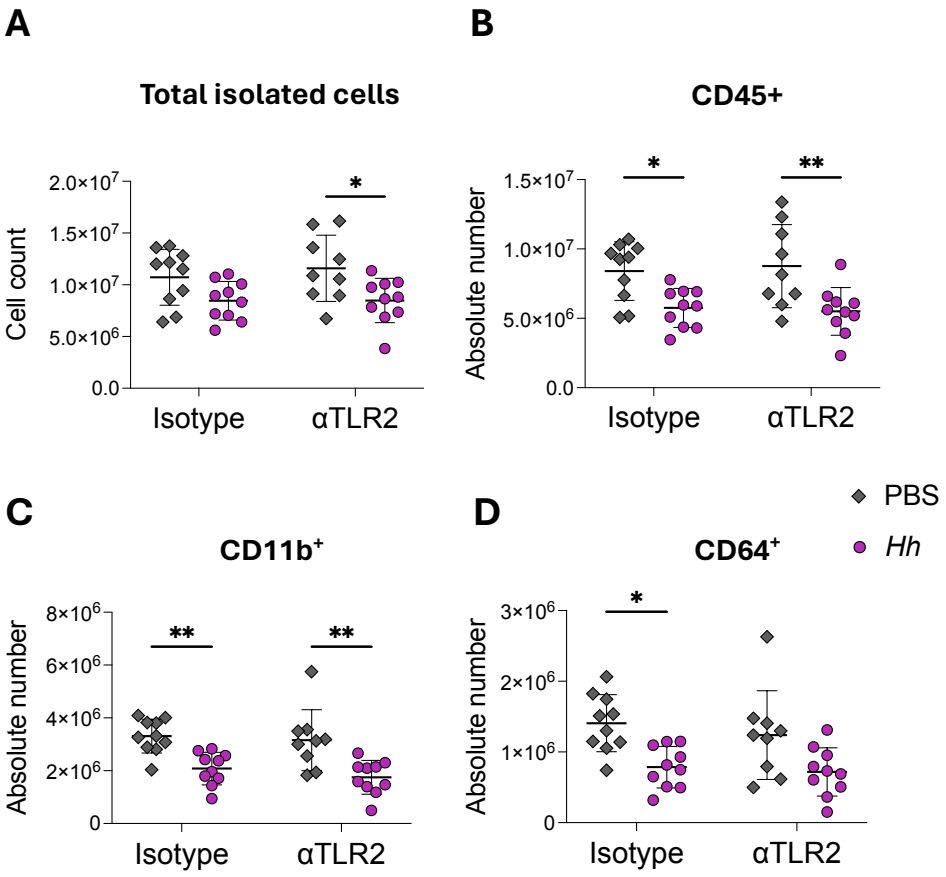


**Figure 6-8: *Hh* attenuates DSS-induced inflammatory leukocyte infiltration regardless of αTLR2 treatment**

C57BL/6 mice were infected with 1x$10^8$ CFU *Hh* or PBS by oral gavage and administered 2% DSS in drinking water. Mice received either αTLR2 mAb or isotype control mAb once weekly for experiment duration. Colonic LP leukocytes were isolated using enzymatic digestion and the total isolated cells counted manually using trypan blue (A). Cells were assessed by flow cytometry and the absolute number of $CD45^+$ (B), $CD11b^+$ (C), and $CD64^+$ (D) cells were calculated. Data are shown with mean ± SD and are pooled from 2 independent experiments with n=5 per experiment. Statistical significance was determined by 2-way ANOVA (significance *p< 0.05, **p<0.01, ***p< 0.001, ****p< .0001).

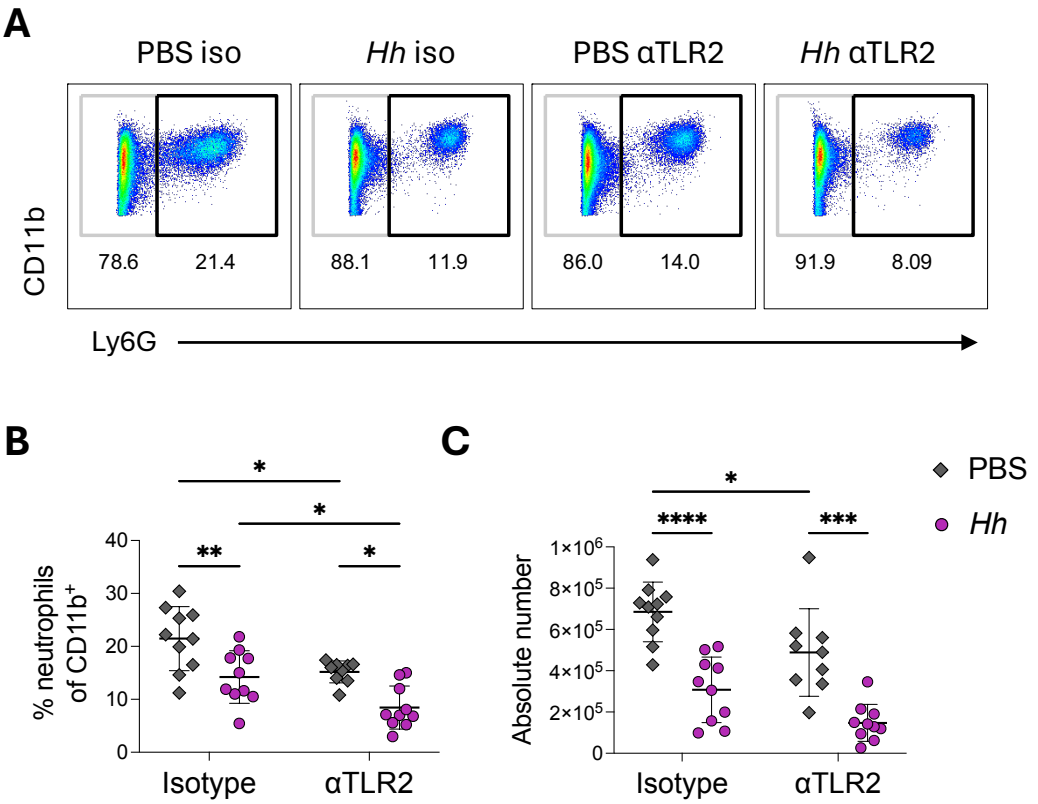


**Figure 6-9: *Hh* attenuates DSS-induced cLP neutrophil infiltration regardless of αTLR2 treatment**

C57BL/6 mice were infected with 1x10$^8$ CFU *Hh* or PBS by oral gavage and administered 2% DSS in drinking water. Mice received either αTLR2 mAb or isotype control mAb once weekly for experiment duration. Representative dot plots of colonic neutrophils (A), quantification of neutrophil frequencies (B) and absolute numbers (C) are shown. Data are shown with mean ± SD and are pooled from 2 independent experiments with n=5 per experiment. Statistical significance was determined by 2-way ANOVA (significance *p< 0.05, **p<0.01, ***p< 0.001, ****p< .0001).

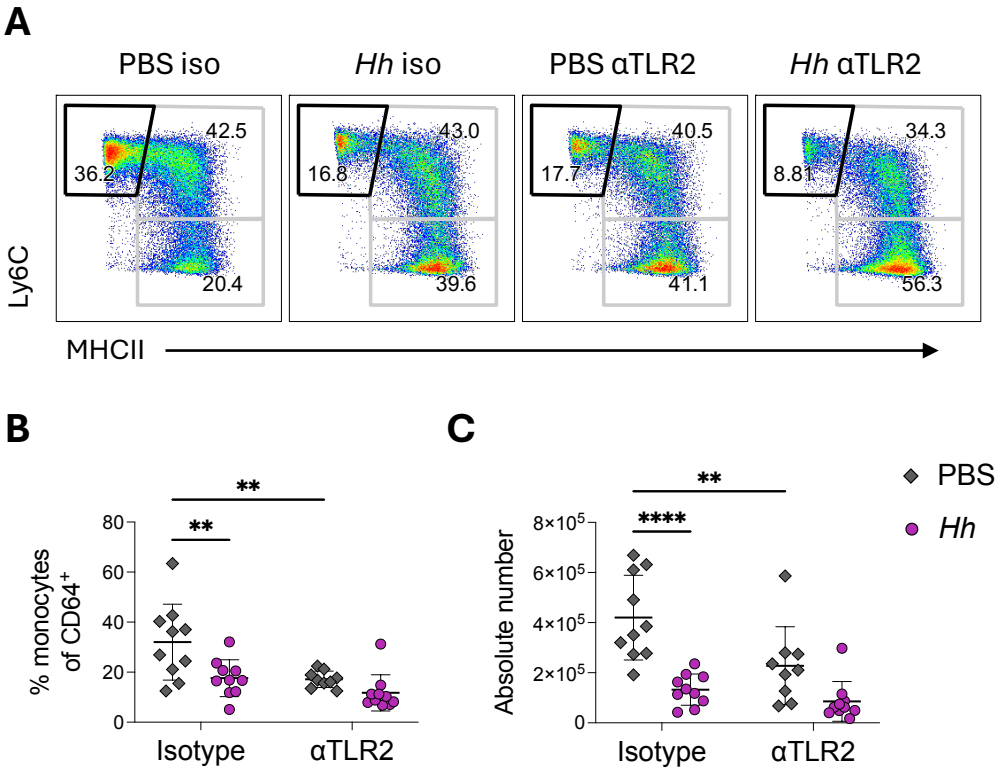


**Figure 6-10: DSS-induced cLP monocyte infiltration is attenuated by both *Hh* and αTLR2 treatment**

C57BL/6 mice were infected with 1x10$^8$ CFU *Hh* or PBS by oral gavage and administered 2% DSS in drinking water. Mice received either αTLR2 mAb or isotype control mAb once weekly for experiment duration. Representative dot plots of colonic monocytes, defined in bold regions (A), quantification of monocyte frequencies (B) and absolute numbers (C) are shown. Data are shown with mean ± SD and are pooled from 2 independent experiments with n=5 per experiment. Statistical significance was determined by 2-way ANOVA (significance *p< 0.05, **p<0.01, ***p< 0.001, ****p< .0001).

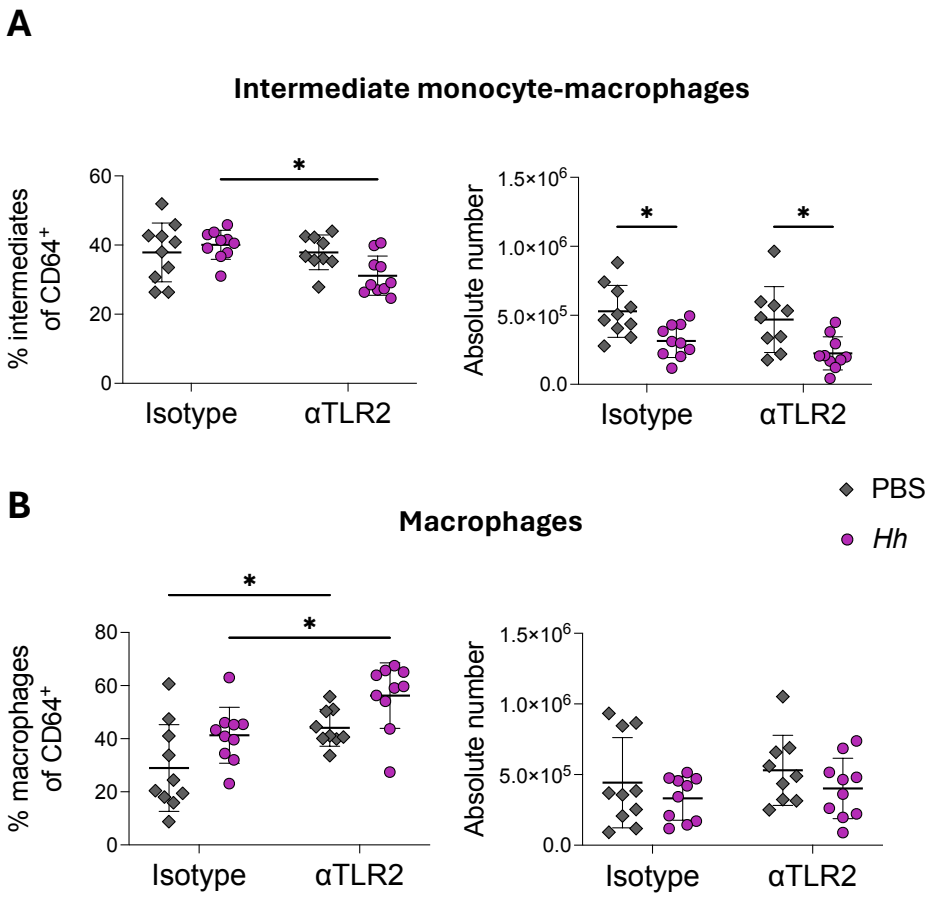


**Figure 6-11: Levels of cLP intermediate monocyte-macrophages are attenuated by *Hh* colonization regardless of αTLR2 treatment**
C57BL/6 mice were infected with 1x$10^8$ CFU *Hh* or PBS by oral gavage and administered 2% DSS in drinking water. Mice received either αTLR2 mAb or isotype control mAb once weekly for experiment duration. The frequency and absolute number of colonic intermediate monocyte-macrophages (A) and mature macrophages (B) are shown. Data are shown with mean ± SD and are pooled from 2 independent experiments with n=5 per experiment. Statistical significance was determined by 2-way ANOVA (significance *p< 0.05, **p<0.01, ***p< 0.001, ****p< .0001).

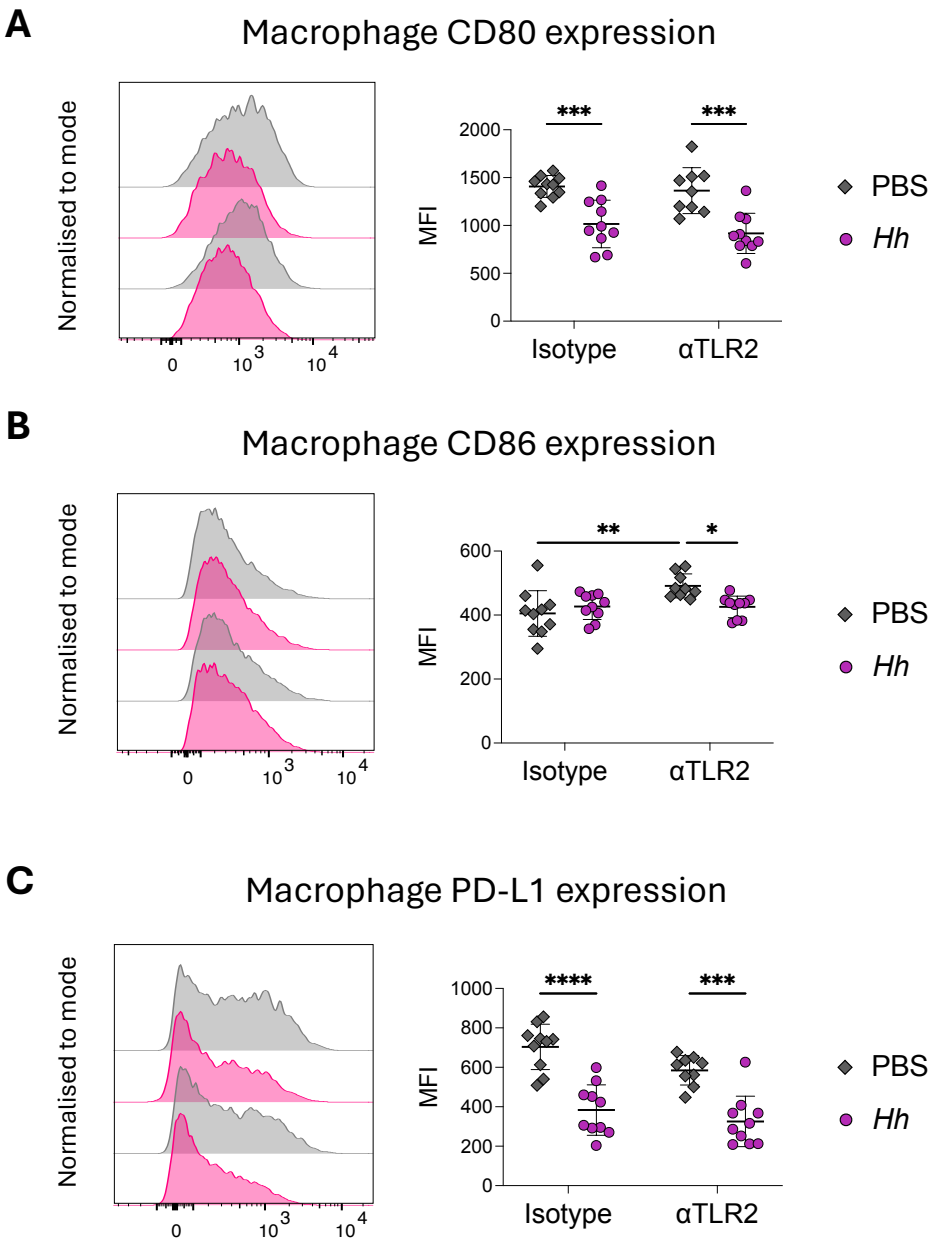


**Figure 6-12: Hh attenuates DSS-induced expression of cLP macrophage inflammatory markers regardless of αTLR2 treatment**
C57BL/6 mice were infected with 1x10$^8$ CFU *Hh* or PBS by oral gavage and administered 2% DSS in drinking water. Mice received either αTLR2 mAb or isotype control mAb once weekly for experiment duration. Colonic macrophages were identified as CD11b$^+$CD64$^+$Ly6C$^-$MHCII$^+$ and analysed for expression of CD80 (A), CD86 (B), and PD-L1 (C). Representative histograms (left) and quantification of MFI (right) are shown. Data are shown with mean ± SD and are pooled from 2 independent experiments with n=5 per experiment. Statistical significance was determined by 2-way ANOVA (significance *p< 0.05, **p<0.01, ***p< 0.001, ****p< .0001).

Lastly, we measured levels of Calprotectin in the stool as an additional readout of DSS-induced inflammation. We had previously observed that *Hh* colonization resulted in significantly reduced faecal Calprotectin levels following DSS treatment and we reproduced this effect again here in the isotype mAb-treated, *Hh*-infected group (Figure 6-13). We also found that TLR2 blockade alone did not

have a significant effect on Calprotectin levels, although there was a trend towards reduced concentrations in mice receiving αTLR2 mAb, and the lowest Calprotectin levels were found in *Hh* colonized, αTLR2-treated mice (Figure 6-13).

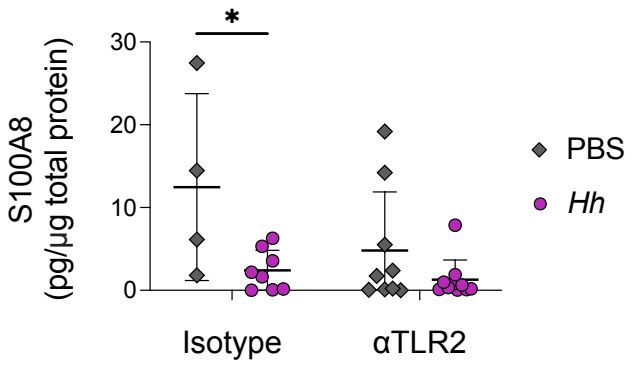


**Figure 6-13: DSS-induced faecal Calprotectin levels are reduced by *Hh* regardless of αTLR2 treatment**
C57BL/6 mice were infected with 1x10$^8$ CFU *Hh* or PBS by oral gavage and administered 2% DSS in drinking water. Mice received either αTLR2 mAb or isotype control mAb once weekly for experiment duration. Stool was collected at experiment endpoint and the concentration of S100A8 measured by ELISA. Concentrations were normalised to total protein content measured by BCA. Data are shown with mean ± SD and are pooled from 2 independent experiments with n=5 per experiment. Statistical significance was determined by 2-way ANOVA (significance *p< 0.05, **p<0.01, ***p< 0.001, ****p< .0001).

Taken together, our data demonstrate that blockade of TLR2 had an attenuating effect on the severity of DSS-induced colitis. However, *Hh* infection appeared to produce a more robust attenuation of DSS disease, and this attenuation was not inhibited by loss of TLR2 signalling.

## 6.4 Discussion

TLR2 is among the host innate receptors which recognise *Hh*, driving downstream signalling responses following bacterial recognition. Genetic deletion of TLR2 does not affect the induction of either innate immune-mediated or T cell-mediated colitis by *Hh* (Boulard et al., 2010), however, there is evidence that recognition of *Hh* through TLR2 instead drives an anti-inflammatory response (Danne et al., 2017). We have previously described a disease attenuating effect of *Hh* colonization in the context of DSS colitis, as well as changes to myeloid responses and macrophage phenotype and function following *Hh* infection at steady state. In this Chapter, we aimed to determine whether these effects involved TLR2-mediated recognition of *Hh*. We validated this approach by

confirming that *in vivo* treatment with an αTLR2 mAb is effective at blocking TLR2-mediated responses to Pam3csk4 *in vivo*. We then demonstrated that blockade of TLR2 signalling does not abrogate the protective effect of *Hh* against DSS induced disease.

### 6.4.1 TLR2-independent attenuation of DSS induced disease

Our results indicate that loss of TLR2 signalling does not impede the ability of *Hh* to attenuate disease in the DSS colitis model. This indicates that the protection we have described is independent of TLR2-mediated recognition of *Hh* and is likely caused by a different mechanism.

While our data suggest that *Hh* mediated disease protection is independent of TLR2 signalling, we do not rule out the possibility that innate recognition of *Hh* drives a protective response which contributes to this effect. Indeed, TLR2 mediated recognition of *Hh* may drive an anti-inflammatory host response in combination with other mechanisms, and when blocked its function may be compensated by other pathways. A level of redundancy exists within innate host defences, for example between the TLR and NLR pathways (Lindsay et al., 2010, Nish and Medzhitov, 2011). There is evidence that *Helicobacter muridarum*, a related murine commensal, activates both TLR2 and NOD1 responses (Chaouche-Drider et al., 2009), while a role for NOD2 has been described in limiting *Hh* colonization levels (Petnicki-Ocwieja et al., 2009), suggesting responses to *Hh* may also occur through this pathway. Given that loss of MyD88, the signalling adaptor downstream of many innate PRRs, removes the ability of *Hh* to induce colitis in susceptible mice (Asquith et al., 2010), it would be interesting to test whether loss of this adaptor abrogates the disease protective effect of *Hh* described here. Use of MyD88 $^{-/-}$ mice could be a useful system to study the contribution of broad innate recognition in the host's response to *Hh*, particularly as it was demonstrated that T cells do not require MyD88 expression for their regulatory or pathogenic functions (Asquith et al., 2010).

Additionally, we postulate that *Hh*-mediated effects on other cell types may have an indirect effect on the inflammatory responses of myeloid cells during DSS colitis. $CD4^+$ T cells are known to respond to *Hh* infection with a variety of responses, including the induction of Tregs and Th1/17 effectors, as well as

developing into Tfh cells in the caecal patch (Kullberg et al., 2002, Xu et al., 2018). We hypothesise that the *Hh*-induced expansion of Tregs may act to limit local myeloid responses both at steady state and in the context of DSS colitis. Tregs are able to suppress innate-driven immune pathology in murine colitis models (Maloy et al., 2003), as well as inhibiting myeloid cytokine production and costimulatory molecule expression *in vitro* (Taams et al., 2005, Houot et al., 2006*)*. Microbial species and products which attenuate DSS disease severity have been associated with an altered balance of intestinal Tregs and Th1/Th17 effector T cells, resulting in increased Treg numbers and decreased pro-inflammatory cytokine production (Hartog et al., 2015, Park et al., 2018, Zhang et al., 2018). This evidence supports the hypothesis that *Hh*-mediated disease attenuation may be driven by Tregs, and thus unaffected by the absence of TLR2 signalling. However, it has been suggested that TLR2 expression on Tregs may be required for their recognition and tolerance towards the commensal species *Bacteroides fragilis* (Round et al., 2011). The authors report that Tregs isolated from *Tlr2*$^{-/-}$ mice had an impaired ability to suppress effector CD4$^{+}$ T cell responses towards *B. fragilis* and suggest that TLR2 signalling may be an important component of Treg functions (Round et al., 2011). Contrastingly, another report using *Tlr2*$^{-/-}$ mice demonstrated that Tregs isolated from these animals showed comparable suppression of intestinal inflammation to those isolated from WT counterparts (Boulard et al., 2010). This suggests that in most contexts, Treg functions are not dependent on TLR2 signalling, although this has not been specifically studied in the context of steady state *Hh* infection and the disease attenuating effect we have observed.

Studying the role of Tregs in the host's relationship with *Hh* at steady state may be challenging, as these cells are required to prevent development of colitis in response to *Hh* colonization (Kullberg et al., 2002). Techniques which ablate Tregs for a very short time, for example immediately prior to DSS treatment onset, may be feasible to test their requirement for protection as *Hh*-induced colitis can take several weeks to develop (Kullberg et al., 2002). One such technique could be to use an anti-CD25 mAb administered *in vivo*, which has been demonstrated to deplete ~70% of Tregs in peripheral blood following a single dose (Setiady et al., 2010). Alternatively, techniques which deplete the entire CD4 T cell compartment could be used to study the role of T cells in this

context, as loss of Th1 and Th17 cells should alleviate *Hh*-induced pathology (Morrison et al., 2015, Morrison et al., 2013). Importantly, *Hh*-induced colitis develops in $RAG^{-/-}$ mice which lack T and B cells, and in this case is driven by innate mechanisms (Maloy et al., 2003). However, pathology takes longer to develop in these mice, with studies using a timepoint 8-12 weeks post infection to assess intestinal inflammation (Maloy et al., 2003). This suggests that depletion of CD4 T cells for a brief time period, such as immediately prior to DSS onset and during treatment, could provide a non-specific system in which the loss of Tregs can be studied without induction of *Hh*-induced colitis.

Finally, although we have demonstrated that loss of TLR2 does not remove the protective effect of *Hh* in the context of DSS colitis, we have not tested whether the blockade alters effects of *Hh* on the myeloid compartment at steady state. In Chapters 4 and 5, we identified differences in macrophage and cDC phenotypes following steady state infection with *Hh*, as well as a marked reduction in the ability of macrophages to produce cytokines *ex vivo*. It is currently unconfirmed whether these changes are caused by the same mechanism driving attenuated disease severity or the result of a different pathway. The requirement for TLR2 signalling in this context could be tested in the future by performing TLR2 blockade of *Hh* colonized mice in the absence of DSS treatment. Similarly, it would be of interest to test whether macrophage phenotypes and functions are altered by *Hh* at steady state in $MyD88^{-/-}$ mice (Asquith et al., 2010). This could clarify whether these effects are a result of direct innate bacterial recognition or due to an indirect mechanism, for example Treg expansion. Regardless, it is likely that *Hh* is recognised and responded to by various host cell types, and multiple mechanisms may work in conjunction to allow chronic colonization of *Hh* without induction of pathology.

### 6.4.2 Reduced disease severity in naïve animals with TLR2 blockade

Even in the absence of *Hh* infection, we observed a reduction in DSS disease severity in mice treated with αTLR2, which was most notable in uninfected animals. This difference varied in significance with different readouts of inflammation. For example, naïve mice which received TLR2 blockade showed significantly increased colon length, as well as reduced neutrophil and monocyte

levels, compared to naïve untreated mice. In contrast, other readouts of inflammation did not show differences, such as expression of macrophage inflammatory markers, or only showed trends towards being different, such as histopathology scores. These results suggest that loss of TLR2 signalling has an alleviating effect on DSS disease, although less prominent than the protective effect of *Hh* colonization.

This finding was surprising as it is in contrast to reports in the literature. It has previously been shown that TLR2$^{-/-}$ mice display increased mortality and disease severity when challenged with DSS (Rakoff-Nahoum et al., 2004, Cario et al., 2007). This phenotype was also observed in TLR4$^{-/-}$ mice (Rakoff-Nahoum et al., 2004, Shi et al., 2019), and to an even greater extent with MyD88$^{-/-}$ (Rakoff-Nahoum et al., 2004). Rakoff-Nahoum *et al*. suggest that TLR-dependent interactions with commensals are protective against disease as they maintain epithelial homeostasis (Rakoff-Nahoum et al., 2004). Similarly, it has been proposed that TLR2 signalling is critical for maintaining tight junctions in the epithelial barrier, which helps to prevent epithelial injury (Cario et al., 2007). However, there are studies whose results are consistent with the findings described here. Heimesaat *et al*. show reduced DSS disease severity in TLR2$^{-/-}$ and TLR4$^{-/-}$ mice compared to wild-type, a phenotype which is even more apparent in double TLR2/TLR4$^{-/-}$ animals (Heimesaat et al., 2007). As DSS colitis is driven by inflammatory responses targeted at the microbiota, it makes sense that inhibiting the ability of innate cells to recognise and respond to microbes reduces the extent of inflammation in this model.

It is also well known that the severity of DSS colitis is largely dependent on the microbiota (Forster et al., 2022), and differences in the outcome of disease severity in knockout mice may be due to differences in microbiota composition. Regardless of whether differences are driven by the genotype itself, or familial transmission (Ubeda et al., 2012), this could explain the contrasting reports seen in the literature. A benefit of using an antibody treatment to block TLR2 signalling is that it removes confounding effects of genotype on microbiota composition between experimental animals. Additionally, blocking signalling for a short-term period prior to colitis onset, rather than a genetic knockout present throughout the animal's life, may help to maintain a normal relationship between the host and its microbiota during development. This ensures that the

homeostatic effects of TLR signalling described by Rakoff-Nahoum *et al*. and Cario *et al*. are present for most of the animal's life and could be why we do not see increased disease severity in αTLR2 recipients.

### 6.4.3 Using Pam3csk4 responsiveness as a measure of TLR2 signalling

To test whether loss of TLR2 function affects the ability of *Hh* to modulate host responses, we blocked TLR2 signalling for the 29-day duration in which animals were infected with *Hh*. Animals received once weekly doses of 100μg αTLR2 over the 4-week experiment. We used a clone of αTLR2 mAb which had been used in a previous *in vivo* study, where they also administered 100μg per dose, but animals received 4 doses over a 6-day period (Sung et al., 2019). As this was the only cited use of the clone, and we administered the antibody less frequently than Sung *et al*., we aimed to provide validation that the blockade was successful in our hands.

We treated mice with αTLR2 mAb before administering Pam3csk4 *in vivo* and measuring their response to the challenge. Pam3csk4 challenge drives a fever and sickness response in mice, accompanied by early innate immune activation and cytokine production (Murayama et al., 2019). We found that the serum cytokine response to Pam3csk4 was significantly reduced in αTLR2 mAb recipient animals, and these mice also displayed reduced colonic neutrophil infiltration compared to mice which received the isotype control. We concluded that the antibody had successfully inhibited the response to Pam3csk4 and was effective at blocking TLR2 signalling in this context. However, it has been shown that TLR2 signalling as a result of the *Hh* polysaccharide drives an altered response compared to canonical TLR2 agonists such as Pam3csk4 (Danne et al., 2017). Danne *et al*. compared genes specifically upregulated in macrophages following stimulation with either *Hh* polysaccharide or Pam3csk4. They found that many of the genes upregulated by Pam3csk4 were activated by NF-κB signalling, while *Hh* polysaccharide drove induction of genes downstream of cyclic AMP response-element binding protein (CREB) (Danne et al., 2017). This indicates that there are differences in the signalling responses induced by each of these stimuli, despite both signalling through TLR2. Interestingly, the response to *Hh* polysaccharide was dependent on MSK1/2 (Danne et al., 2017), two kinases

which are required for phosphorylation of CREB and function as negative regulators of TLR signalling (Ananieva et al., 2008). While we have demonstrated that the TLR2 blockade was effective at inhibiting the response to Pam3csk4, we cannot rule out the possibility that the non-canonical signalling response to *Hh* may not have been blocked to the same extent. However, these data support the conclusion that the αTLR2 mAb treatment functioned as expected.

### 6.4.4 Concluding remarks

We report that the disease attenuating effect of *Hh* colonization is maintained in the absence of TLR2 signalling, indicating that the mechanism driving the protection is independent of TLR2. The blockade of TLR2 was validated by challenging mice with the agonist Pam3csk4, where we observed that αTLR2 mAb treatment inhibited the response to this challenge. These data provide insight as to how *Hh* may be modulating host responses and suggest that the disease attenuating effect is mediated by a different mechanism. This mechanism may be T cell mediated, or dependent on other innate recognition pathways.

# 7 The epithelial barrier in *Helicobacter hepaticus* infection

## 7.1 Introduction

The epithelial barrier in the intestine is comprised of a single layer of IECs, which separate the LP from the intestinal lumen and microbiota. IECs have many important functions, including nutrient and water absorption, hormone secretion, and production of antimicrobial peptides (Haber et al., 2017). They also contribute to immune responses through the production of cytokines and other mediators which influence both innate and adaptive immunity (Haber et al., 2017, Peterson and Artis, 2014). IECs show distinct TLR expression based on their anatomical location from the SI to the distal colon (Price et al., 2018), allowing specialised responses in different niches. Furthermore, IEC expression of MHCII allows antigen presentation to $CD4^+$ T cells, which has been shown to alter the cytokine profile of the Th cell response (Heuberger et al., 2024).

IESCs reside at the crypt base and provide constant renewal of the epithelial barrier. These cells give rise to all lineages of differentiated IEC, which in turn show specialised functions (Haber et al., 2017). The majority of IECs are absorptive enterocytes, with important functions for nutrient absorption. Similarly, enteroendocrine cells secrete a range of hormones involved in digestive functions (Peterson and Artis, 2014). Goblet cells produce mucins as well as other components of the mucus layer which overlays the epithelium and acts as a physical and biochemical barrier against microbes in the lumen (Kim and Ho, 2010). Goblet cell frequencies increase from the small intestine to the distal colon, correlating with bacterial load (Kim and Ho, 2010), and are reduced in GF animals, suggesting a mechanism by which the microbiota stimulates their differentiation (Kandori et al., 1996). Tuft cells are chemosensory cells which are key orchestrators of type 2 immune responses (Drurey et al., 2021). Paneth cells reside around the stem cell niche and produce various growth factors needed for IESC survival, as well as AMPs (Sato et al., 2011). The differentiation of IESCs is tightly regulated in homeostasis and can be perturbed during inflammation or infection. Cytokines have been shown to alter the differentiation process to promote the expansion of different IEC lineages. For example, IL-10 drives stem cell proliferation, resulting in increased stem and

progenitor cells, while IL-13 drives expansion of Tuft cells, the key IEC type involved in type 2 immunity (Biton et al., 2018).

The effect of microbial exposure on the differentiation and function of the epithelial barrier has been highlighted in recent years. Infection with *S. typhimurium* drives an increase in enterocytes and Paneth cells, as well as induction of IEC antimicrobial functions (Haber et al., 2017) and MHCII upregulation (Biton et al., 2018). In contrast, the helminth *H. polygyrus* causes massive changes to IESC proliferation, resulting in an immature phenotype characterised by loss of differentiated cells and specific inhibition of Tuft cell development (Nusse et al., 2018, Drurey et al., 2021). During *C. rodentium* infection, expression of MyD88 on IECs drives AMP production and enhances barrier functions, contributing to bacterial resistance (Friedrich et al., 2017). IEC functions are modulated not only by pathogens, but also the microbiota at steady state. One commensal species, *Peptostreptococcus russellii*, has been described to promote epithelial barrier integrity through its production of indoleacrylic acid, which is a tryptophan metabolite (Wlodarska et al., 2017). Infection with this species was protective against DSS colitis, suggesting a mechanism by which enhanced barrier function protects against DSS induced disease (Wlodarska et al., 2017). Interestingly, the microbiota-derived SCFA butyrate has been shown *in vitro* to act as a potent inhibitor of IESC proliferation (Kaiko et al., 2016). *In vivo*, the stem cell niche is protected against the inhibitory effect of butyrate on proliferation, due to uptake and metabolism of butyrate by differentiated enterocytes at the top of the crypts (Kaiko et al., 2016). However, microbes which reside deep within the crypts, such as *Hh* (Chan et al., 2005), are in closer proximity to the IESC niche and may be more likely to exert functional effects.

Whether *Hh* affects the epithelial barrier *in vivo* has not yet been reported. *Hh* has been described to antagonise TLR responses by IECs *in vitro* (Sterzenbach et al., 2007), as well as reportedly downregulating genes associated with NF-κB signalling (Chow and Mazmanian, 2010). Its specialised location in the epithelial mucus layer and deep within the colonic crypts may mean that, compared to other luminal microbes, *Hh* may have a greater effect on IESC function (Chan et al., 2005). Our previous data revealed a disease attenuating effect of *Hh* colonization in the context of DSS colitis. We hypothesise that this attenuation

may be mediated in part by effects of *Hh* on the epithelial barrier. Interactions with pathobiont species may act to strengthen the barrier, for example through increased mucus secretion, or alter the composition of different IEC lineages present, thus affecting overall function.

## 7.2 Aims

Here I aimed to explore the effects of *Hh* colonization on the epithelial barrier. I aimed to test whether *Hh* alters the composition of the epithelial barrier and whether IEC show altered responses to stimuli following *Hh* infection.

## 7.3 Results

### 7.3.1 Transfer of *Hh*$^+$ microbiota does not alter expression of IEC lineage genes, but alters immune related gene transcription in the colon

Enteric bacterial and helminth infections have been described to drive changes to epithelial differentiation and function (Haber et al., 2017, Biton et al., 2018, Nusse et al., 2018). Here, we first aimed to determine whether colonization with *Hh* drives changes to IEC-associated gene expression at steady state, which could indicate changes to epithelial composition and function. We utilised the microbiota transfer model for these experiments, which allowed us to study the effects of *Hh* colonization in combination with the undefined microbiota of University of Glasgow donor mice (*Hh*$^+$ MT, described in Chapter 3). As previously, mice were left for 21d post *Hh*$^+$ MT to allow conditioning of the environment by the new microbiota.

We first assessed the expression of different IEC lineage marker genes within whole colon tissue by qPCR. IESCs in the intestine can be identified based on *Lgr5* expression (Barker et al., 2007), while Goblet cells are denoted by expression of *Muc2*, encoding the primary mucin they produce(Kim and Ho, 2010). Enteroendocrine cells express *ChgA*, which encodes the glycoprotein Chromogranin A (Engelstoft et al., 2015). The transcription factor Math1, encoded by *Atoh1*, is required for secretory lineage cell development, and is often used to target intestinal Paneth cells (Durand et al., 2012). Although Paneth cells are thought not to be present in the colon, populations of ‘Paneth-

like cells' have been described, and *Atoh1* denotes secretory progenitor cells (Lo et al., 2017, Castillo-Azofeifa et al., 2019). *Dclk1* expression in the gut is specific to Tuft cells (Drurey et al., 2021), while *Villin1* is universally expressed by epithelial cells (Pinto et al., 1999). We observed largely comparable expression of lineage marker genes between naïve and *Hh*$^{+}$ MT recipients, with the exception of a slight upregulation of *Dclk1* in the *Hh*$^{+}$ MT group (Figure 7-1). These data suggest that *Hh* colonization at steady state does not drive obvious changes to epithelial barrier composition.

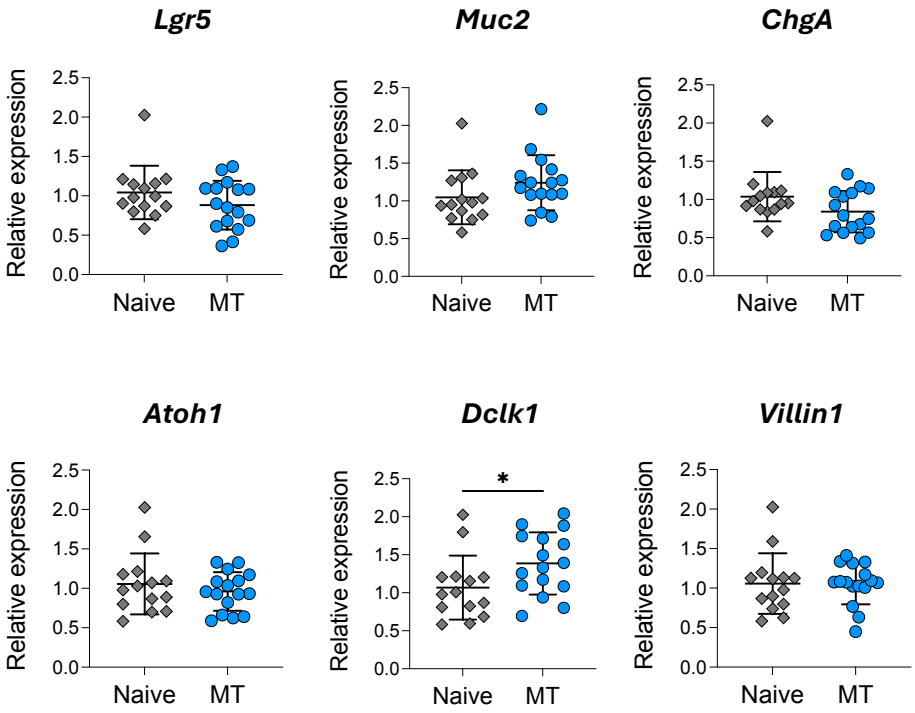


**Figure 7-1: Colonic expression of epithelial lineage genes is unchanged following *Hh*$^{+}$ MT** C57BL/6 littermate cohorts were left untreated (Naïve) or colonized with *Hh*$^{+}$ microbiota (MT) for 21-days. A section of distal colon was harvested and expression of indicated genes measured using qPCR. Differences in gene expression were determined using the $2^{-\Delta\Delta C(t)}$ method, with gene expression normalised to the housekeeping gene *Rps29* and data shown as fold change relative to the naïve group. Data are shown with mean ± SD and are pooled from 4 independent experiments with n=4 per experiment. Data were tested for normality using the Shapiro-Wilk normality test. In cases where data were normally distributed statistical significance was determined by unpaired t test, otherwise a Mann Whitney test was used (significance *p< 0.05, **p<0.01, ***p< 0.001, ****p< .0001).

We next tested whether genes associated with different epithelial responses were altered by *Hh*$^{+}$ MT. Transcription was measured in whole distal colon tissue, so it is important to note that any changes may not be specific to IECs. We first tested a panel of genes associated with antimicrobial responses. Expression of *Retnlb*, encoding RELMß, was significantly increased in *Hh*$^{+}$ MT recipients, while *RegIIIγ* was increased in a proportion of animals (Figure 7-2A).

RELMß plays a key role in maintaining segregation between the host and microbiota (Propheter et al., 2017), while REGIIIγ has bactericidal functions and influences mucus distribution (Loonen et al., 2014). Upregulation of these genes suggests that the influx of new microbes stimulates an active antimicrobial response in *Hh*$^{+}$ MT recipients. However, expression of *Camp*, encoding the AMP Cathelicidin, was unchanged by *Hh*$^{+}$ MT (Figure 7-2A). We then measured expression of various cytokine and chemokine genes. IL-25 is produced by Tuft cells and is a key mediator of type 2 immune responses (Smith et al., 2018), and was significantly upregulated in *Hh*$^{+}$ MT recipients (Figure 7-2B). We also observed an increase in *Ccl20* expression in *Hh*$^{+}$ MT recipients (Figure 7-2B), which has been shown to be upregulated in IECs following TLR stimulation (Price et al., 2018). However, IL-33, an alarmin produced by the epithelium in response to damage (McSorley and Smyth, 2021), was unchanged by *Hh*$^{+}$ MT (Figure 7-2B). Finally, in the *Hh*$^{+}$ MT group colonic tissue, we observed significant increases in *H2Ab1*, encoding MHCII, *Nos2*, encoding iNOS, and *MyD88* (Figure 7-2C). These changes, while not specific to IECs, suggest an increased level of antigen presentation and innate signalling responses in *Hh*$^{+}$ MT recipients. *Nos2* expression is induced following exposure to inflammatory cytokines (Soufli et al., 2016), indicating that increased cytokine production may be a hallmark of *Hh*$^{+}$ MT recipients.

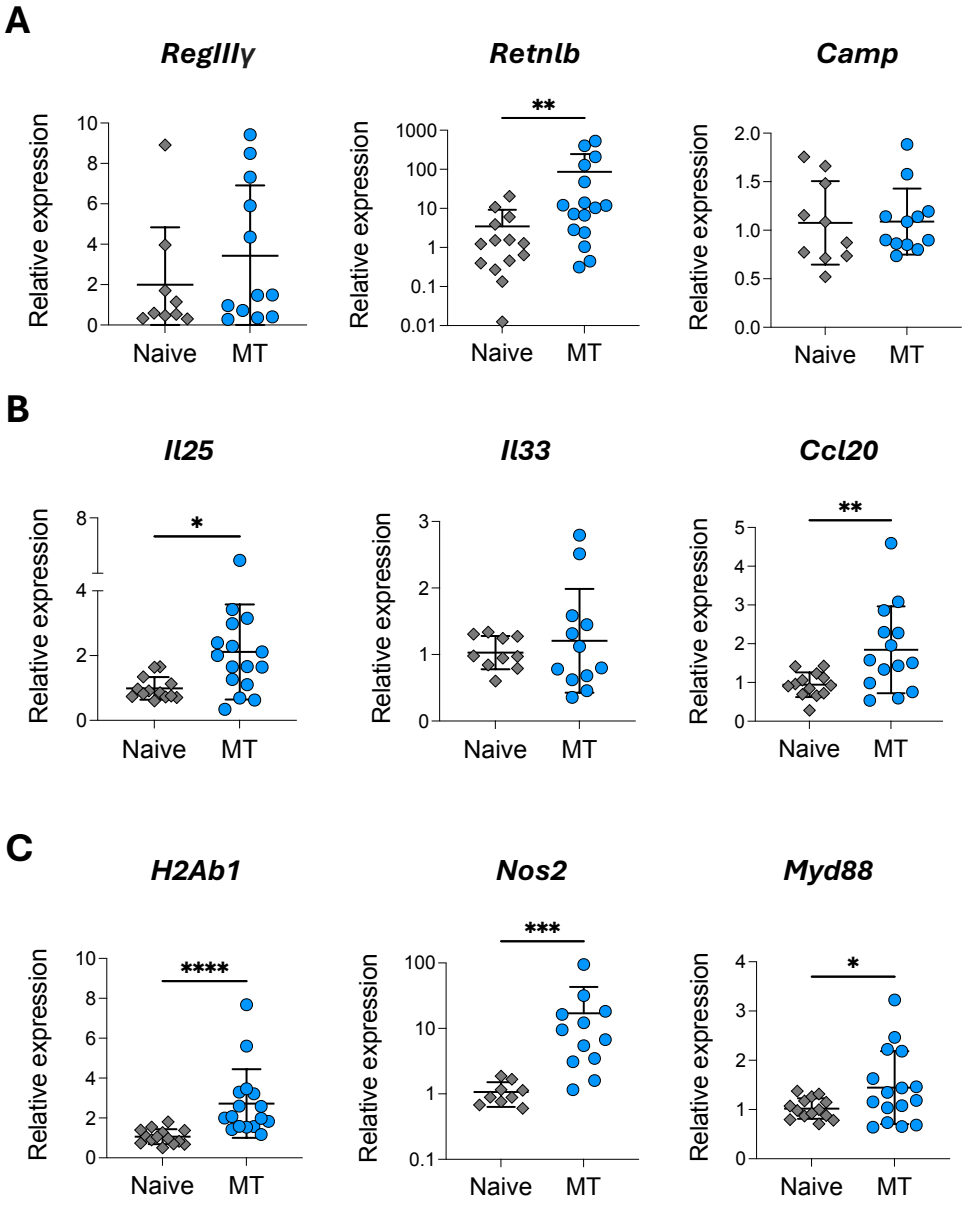


**Figure 7-2: MT drives transcription of epithelial response genes in the colon**
C57BL/6 littermate cohorts were left untreated (Naïve) or colonized with *Hh*$^{+}$ microbiota (MT) for 21-days. A section of distal colon was harvested, and expression of genes associated with antimicrobial responses (A), epithelial cytokines (B), and epithelial immune responses (C) were measured by qPCR. Differences in gene expression were determined using the $2^{-\Delta\Delta C(t)}$ method, with gene expression normalised to the housekeeping gene *Rps29* and data shown as fold change relative to the naïve group. Data are shown with mean ± SD and are pooled from 3-4 independent experiments with n=4 per experiment. Data were tested for normality using the Shapiro-Wilk normality test. In cases where data were normally distributed statistical significance was determined by unpaired t test, otherwise a Mann Whitney test was used (significance *p< 0.05, **p<0.01, ***p< 0.001, ****p< .0001).

Taken together, these data suggest that while *Hh*$^{+}$ MT does not alter the cell type composition of the epithelial barrier at steady state, it may drive changes to functional responses. Although the data described here are obtained from whole colon tissue, and are not specific to IECs, many of these genes are likely to be upregulated in IECs. Later, we will aim to test whether the same changes to gene expression are observed in IECs specifically.

### *7.3.2* Using primary IEC organoids to assess epithelial phenotype and function *ex vivo*

Having observed transcriptional changes in the whole colon following *Hh*$^{+}$ MT, we next aimed to examine the epithelial compartment specifically. We opted to use a primary IEC organoid system, in which epithelial crypts are harvested and provided with growth factors *in vitro* to promote IESC growth (Sato and Clevers, 2013). In this system, IESCs proliferate to form spheroids with an enclosed lumen. After several days, differentiated cells become present, leading to budding of the organoid( Sato and Clevers, 2013). Organoids contain all lineages of differentiated IEC types, resulting in a useful system to study epithelial cells *in vitro* (Lukonin et al., 2020). The organoid culture process is depicted in Figure 7-3A, whereby colonic crypts are isolated and resuspended in basement membrane extract (BME), which allows the IESCs to grow in a 3D structure (Fan et al., 2016) (Figure 7-3A). We followed this method and observed the growth of spheroid structures until around day 4 post seeding in BME (Figure 7-3B). Around day 4-5, we observed budding of organoids, and found that the buds were highly proliferative as evidenced by Ki67 expression (Figure 7-3C). However, as the organoids are 3D, only one focal plane is visible and other areas of the organoid also expressed Ki67, indicating the presence of proliferating IESCs throughout the organoid structure (data not shown).

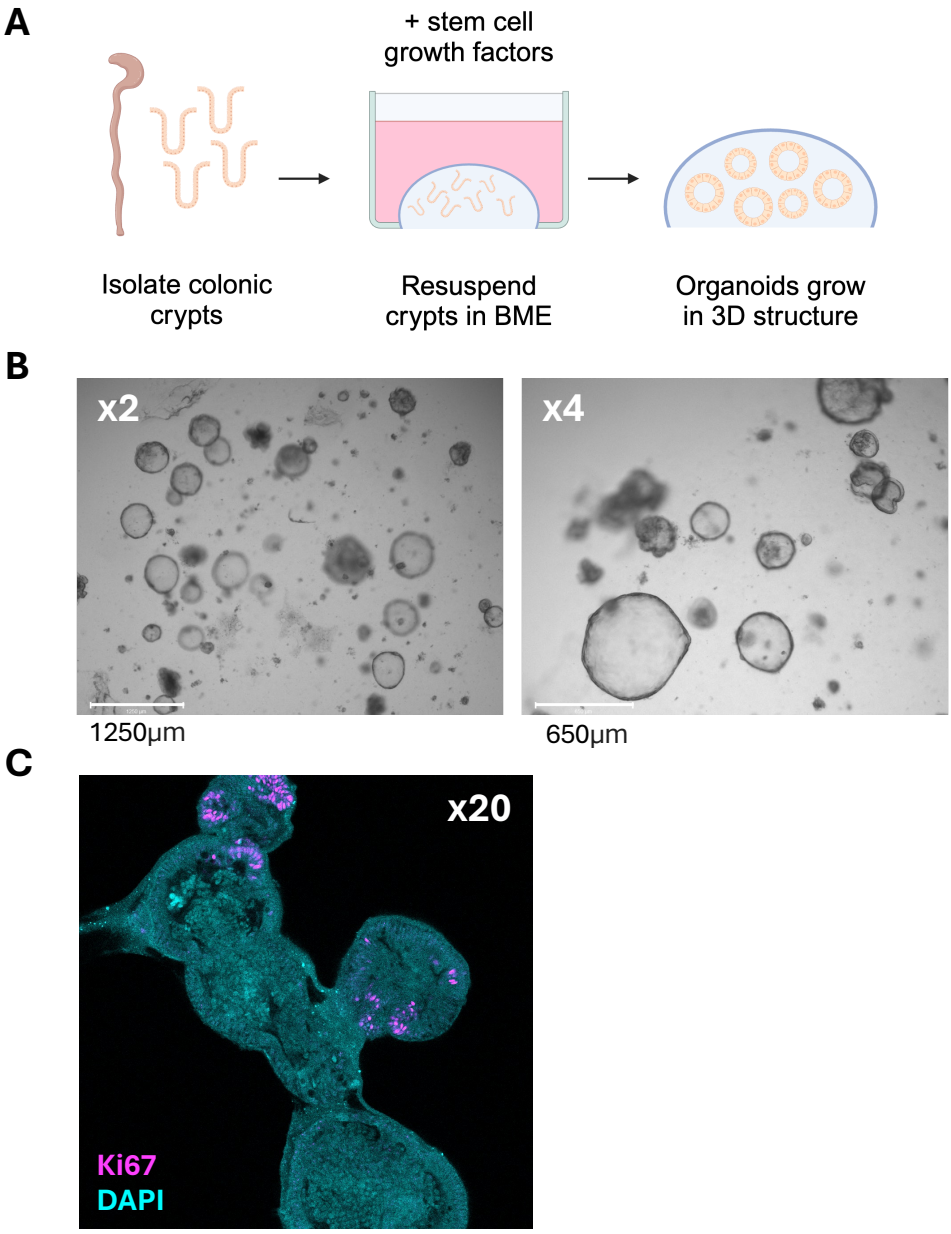


**Figure 7-3: Establishment of primary murine colonic epithelial organoids**
Schematic depicting isolation of epithelial crypts and growth of 3D organoids (A). Brightfield images of spheroids at day 4 post-seeding are shown with magnification of x2 (left) and x4 (right) (B). Day 5 organoids were fixed in paraformaldehyde and stained with an antibody against Ki67, before staining with a fluorescent secondary antibody and DAPI nuclear stain. Image was acquired using a Nikon A1-R confocal microscope at x20 magnification (C).

Initially, we considered using the organoids as a co-culture system to study interactions between *Hh* and the epithelium *in vitro*. However, unlike immune cells, epithelial cells are highly polarised, with expression of various receptors localised to specific sides of the cell (Yu and Gao, 2015). Indeed, it has been shown that TLR ligands elicit different effects when administered to opposite sides of the epithelial cell surface (Stanifer et al., 2020). *In vivo*, the basolateral surface faces towards the intestinal tissue, and may be exposed to immune signals from the LP, while the apical side is exposed to the intestinal lumen, in

closer contact with the microbiota (Co et al., 2021). In traditional organoids, the apical surface faces inwards to the centre of the organoid, while the basolateral side faces outwards and is exposed to the BME and media (Co et al., 2021). This presents a challenge for the use of organoids in co-cultures with microbes, as the surface of the cells which would interact with the microbe *in vivo* is enclosed and inaccessible in an organoid (Puschhof et al., 2021).

Several methods of co-culture have been reported to overcome this challenge (Puschhof et al., 2021). One method involves the microinjection of microbes into the organoid centre, which is technically challenging (Williamson et al., 2018). The most commonly used method is to convert a 3D organoid culture into a 2D monolayer, in which the apical surface faces upwards, allowing microbes to be applied on top (Moon et al., 2014, Roodsant et al., 2020). This method has been employed successfully to study interactions between *H. pylori* and human gastric epithelium (Schlaermann et al., 2016). However, in our hands, we struggled to achieve viability in 2D monolayers and were not able to produce confluent monolayers for co-culture studies (data not shown). Furthermore, the low oxygen concentrations required for *Hh* growth presented an additional challenge for optimisation of a co-culture system (Fox et al., 1994). We therefore opted to use the organoid system to study IEC responses *ex vivo* following *Hh* colonization *in vivo*. There is evidence that epithelial stem cells retain memory of prior injury, resulting in altered responses upon secondary challenge (Naik et al., 2017). In the gut, infection with intestinal helminths has been shown to drive powerful changes to IESC proliferation, and these changes are maintained in organoid cultures derived from infected mice (Nusse et al., 2018, Drurey et al., 2021). We hypothesised that interactions with the microbiota *in vivo* may drive changes to the epithelial stem cell niche which could result in altered responses to stimulation *ex vivo*.

We grew primary IEC organoids derived from naïve and *Hh*$^{+}$ MT recipient mice and tested their responses to various stimuli *in vitro*. First, we challenged organoids with IFNγ, which produces an inflammatory response in IECs and specifically drives upregulation of MHCII and antigen presentation machinery (Heuberger et al., 2024). As expected, we observed significant upregulation of *H2Ab1* and *Nos2* expression in IEC organoids stimulated with IFNγ, but no differences were observed in the response between naïve-derived and *Hh*$^{+}$ MT

recipient-derived organoids (Figure 7-4A). Next, we challenged the IEC organoids with the TLR2 agonist Pam3csk4, which has been shown to drive inflammatory chemokine production by IECs (Price et al., 2018). We found that IEC organoids from both naïve and *Hh*$^{+}$ MT animals produced comparable levels of CXCL1 and CXCL2 in response to Pam3csk4 (Figure 7-4B). Finally, we stimulated the IEC organoids with IL-22, which elicits an antimicrobial response in IECs (Ngo et al., 2018). Transcription of genes encoding the AMPs REGIIIß and REGIIIγ was significantly increased in response to IL-22, however, again no difference was observed between IEC organoids from both naïve and *Hh*$^{+}$ MT animals (Figure 7-4C). Overall, these data indicate that organoids derived from *Hh*$^{+}$ MT recipients show comparable responsiveness to naïve controls. This suggests that *Hh*$^{+}$ MT may not drive changes to epithelial responses *in vivo*, or that any changes may not be maintained for an extended period of time in the absence of *Hh* stimulation.

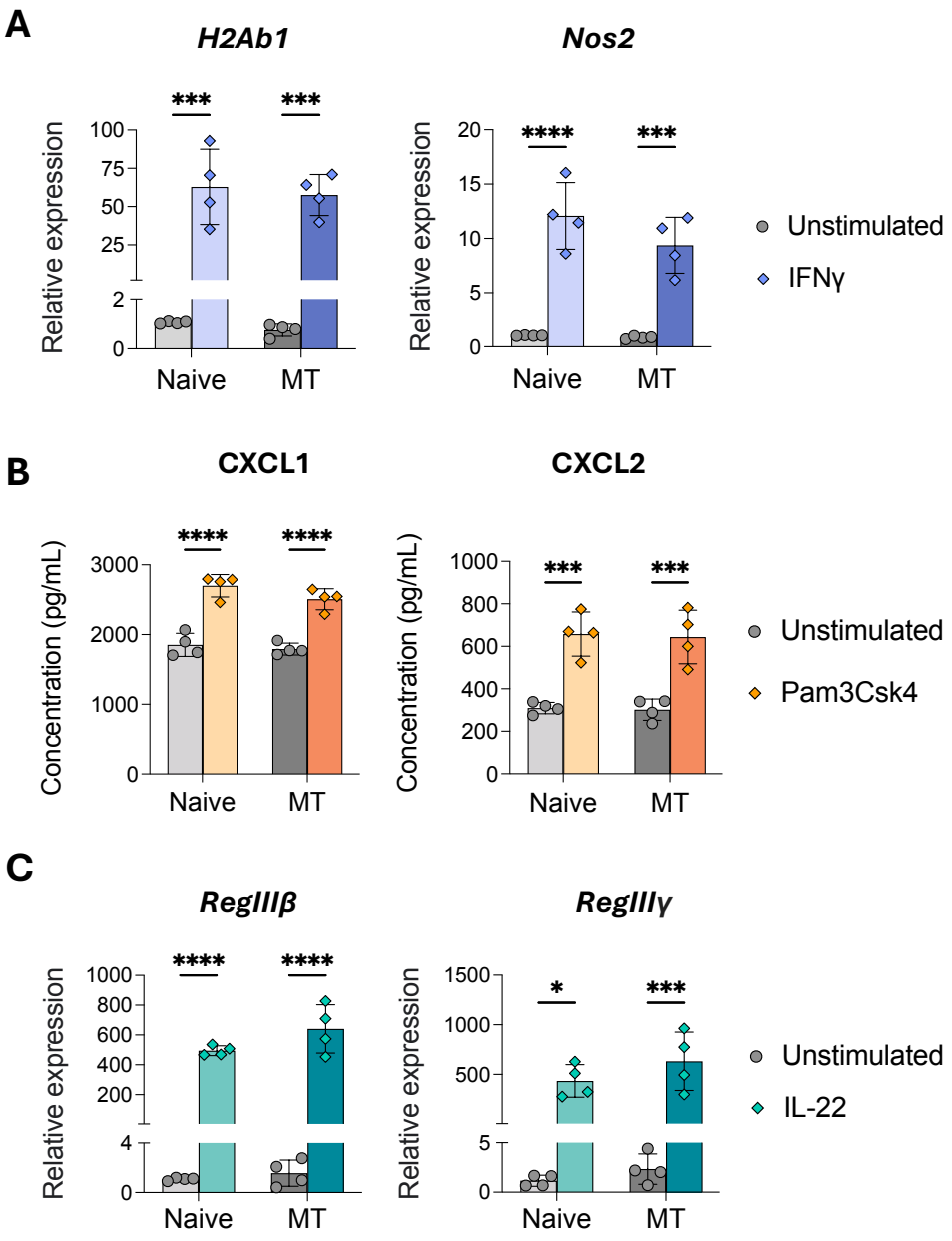


**Figure 7-4: Primary IEC organoids derived from *Hh*⁺ MT recipients show comparable responses to stimulation as those from naïve animals**
C57BL/6 littermate cohorts were left untreated (Naïve) or colonized with *Hh*⁺ microbiota (MT) for 21-days. Colonic crypts were isolated and seeded in BME to allow growth of organoids. After 3 passages, organoids were stimulated with 20ng/mL IFNγ for 6 hours (A), 1µg/mL Pam3csk4 for 16 hours (B), or 20ng/mL IL-22 for 6 hours (C). In (A) and (C) the expression of indicated genes was measured using qPCR. Differences in gene expression were determined using the $2^{-\Delta\Delta C(t)}$ method, with gene expression normalised to the housekeeping gene *Rps29* and data shown as fold change relative to the naïve unstimulated group. In (B) the concentration of indicated chemokines in culture supernatants was measured by ELISA. Data are shown with mean ± SD and are pooled from 2 independent experiments with n=2 per experiment. Data points are average of 3 technical replicates per biological sample. Statistical significance was determined by 2-way ANOVA (significance *p< 0.05, **p<0.01, ***p< 0.001, ****p< .0001).

## 7.3.3 Bulk RNA sequencing of epithelial crypts reveals limited changes following *Hh* colonization

The *ex vivo* organoid stimulation experiments suggested that *Hh*⁺ MT does not drive long-lasting changes to epithelial responses. However, it remained possible

that *Hh*$^{+}$ MT could modulate IEC functions *in vivo*, and that these changes were simply not maintained in the *ex vivo* organoid system. We therefore chose next to examine IEC gene expression using a transcriptomics approach. For these experiments, we infected mice with *Hh* directly for 21 days before colonic crypts were isolated (Fan et al., 2016) to examine the specific effects of *Hh* on IECs. RNA was extracted from IEC crypts and analysed by bulk RNA sequencing, and data analysis was performed by John Cole using Searchlight (Cole et al., 2021) (Figure 7-5).

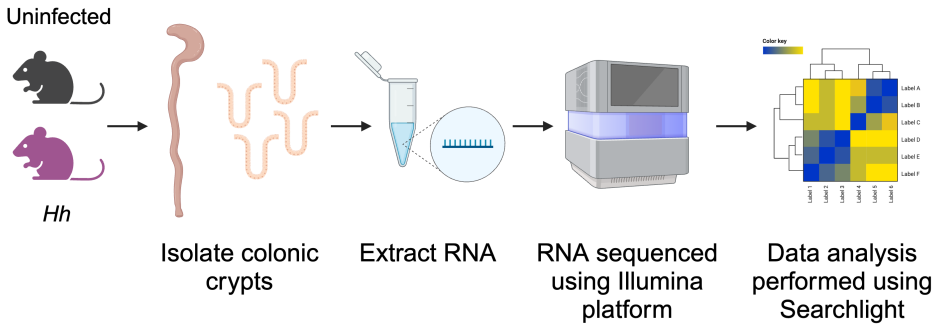


**Figure 7-5: Schematic for bulk RNA sequencing of colonic epithelial crypts**
C57BL/6 littermates were administered 1x10$^{8}$ CFU *Hh* or given PBS by oral gavage and left for 21-days post-infection. Colonic crypts were isolated, and RNA extracted before being sequenced by Novogene using the Illumina platform. Data analysis was performed by John Cole using Searchlight.

First, a principal component analysis (PCA) was performed to provide an indication of sample similarity. PCA uses all gene expression values to determine the main variables (called principal components) which contribute to variation within a dataset. PC1 is the principal component which explains the most variation, followed by PC2. However, we did not observe clear separation of sample groups along either PC1 or PC2 (Figure 7-6). These data suggest that there may be a high level of similarity between the sample groups, indicating that *Hh* colonization may not drive substantial changes to epithelial gene expression.

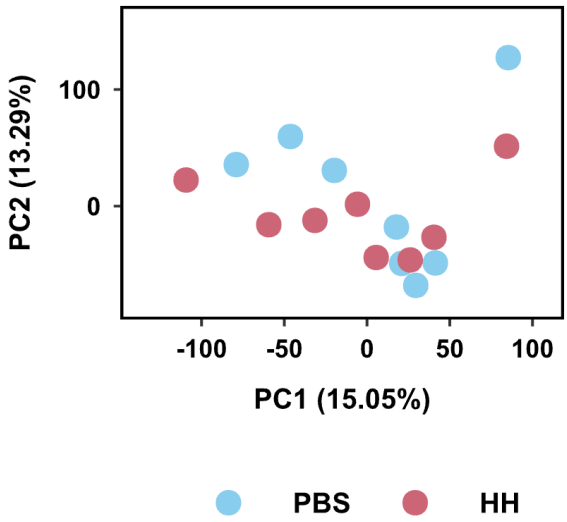


**Figure 7-6: Colonic IEC crypts from uninfected and *Hh* colonized mice do not segregate clearly based on gene expression**
C57BL/6 littermates were administered 1x10$^8$ CFU *Hh* or given PBS by oral gavage and left for 21-days post-infection. Colonic IEC crypts were isolated and RNA was analysed using bulk RNA sequencing with downstream analyses performed using Searchlight. A principal component analysis (PCA) was performed showing variation between samples based on principal components 1 and 2.

Next, the uninfected and *Hh* colonized groups were analysed for differentially expressed genes (DEGs). Initially, the threshold for significance was set as adjusted p-value (p.adj) < 0.05 and absolute log2fold > 1, however, this returned no significant DEGs (data not shown). We next opted to set the threshold for significance to p.adj < 0.1 and absolute log2fold > 0, with the idea that this less stringent threshold would return a higher number of DEGs. Despite this, only 6 genes were identified as significantly different between the uninfected and *Hh* colonized groups (Figure 7-7). A volcano plot was generated to show the relationship between p-value and fold change for each gene, with significantly upregulated genes shown in red, significantly downregulated genes shown in blue, and non-significant genes in grey (Figure 7-7). A heatmap was then generated displaying unsupervised hierarchical clustering of DEG expression. Separation between the two sample groups could be visualised based on expression of the 6 significant DEGs (Figure 7-8). Among the DEGs were *Igha* (encoding the immunoglobulin alpha chain), *Igkc* (encoding immunoglobulin kappa constant region), and *Ighg2b* (encoding immunoglobulin gamma 2B constant region), all of which were upregulated in the *Hh* colonised IEC crypts (Figure 7-8). The presence of immunoglobulin genes likely indicates sample contamination with B cells, although immunoglobulin gene expression has been

described in epithelial cancer cells(Chen et al., 2009). Increased B cell contaminants could reflect an expansion of B cells following *Hh* infection, which stands to reason given that *Hh* induces strong antibody responses (Whary et al., 1998).

The remaining 3 DEGs were *Ceacam2* (encoding carcinoembryonic antigen-related cell adhesion molecule 2) which was upregulated in *Hh* colonised IEC crypts; and *Per2* (encoding period circadian protein homolog 2) and *Cry1* (encoding cryptochrome-1), which were both downregulated in *Hh* colonised IEC crypts (Figure 7-8). Gene set enrichment analysis (GSEA) was performed to gain understanding of potential biological pathways influenced by the DEGs. Among the enriched pathways, several related to circadian rhythm were identified (Figure 7-9). This appears to be due to the presence of *Per2* and *Cry1*, which encode proteins with key roles in regulation of the circadian clock (Smyllie et al., 2022).

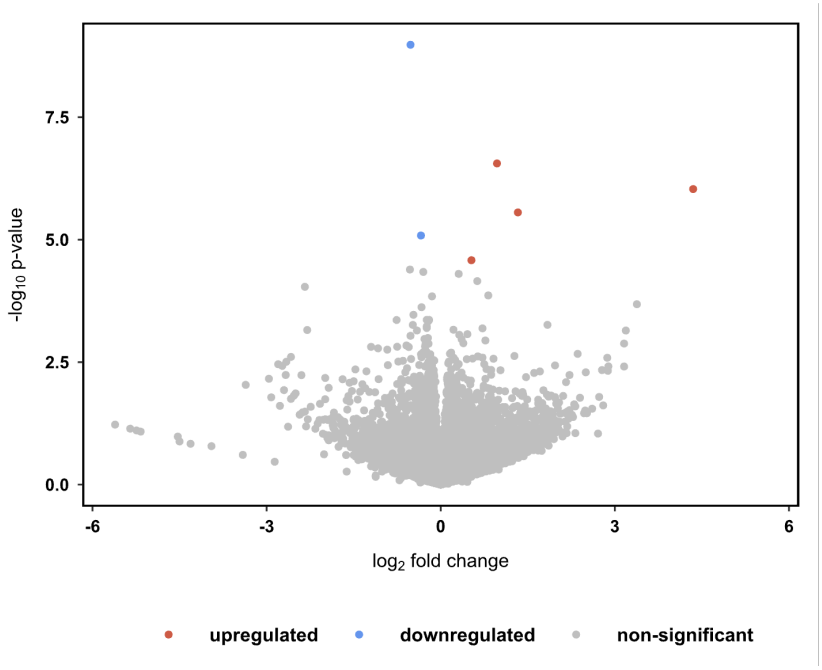


**Figure 7-7: Differential gene expression analysis identifies limited changes in colonic IEC following *Hh* colonization**
C57BL/6 littermates were administered 1x10$^8$ CFU *Hh* or given PBS by oral gavage and left for 21-days post-infection. Colonic IEC crypt RNA was analysed using bulk RNA sequencing with downstream analyses using Searchlight. Differential gene expression was analysed using the DESeq2 package. A volcano plot is shown depicting fold change in $log_2$ and p-value in $-log_{10}$ transformation. Significantly differential genes were defined as p.adj < 0.1, absolute log2fold > 0 and are shown in red if upregulated or blue if downregulated. A positive fold change indicates higher in *Hh* than PBS.

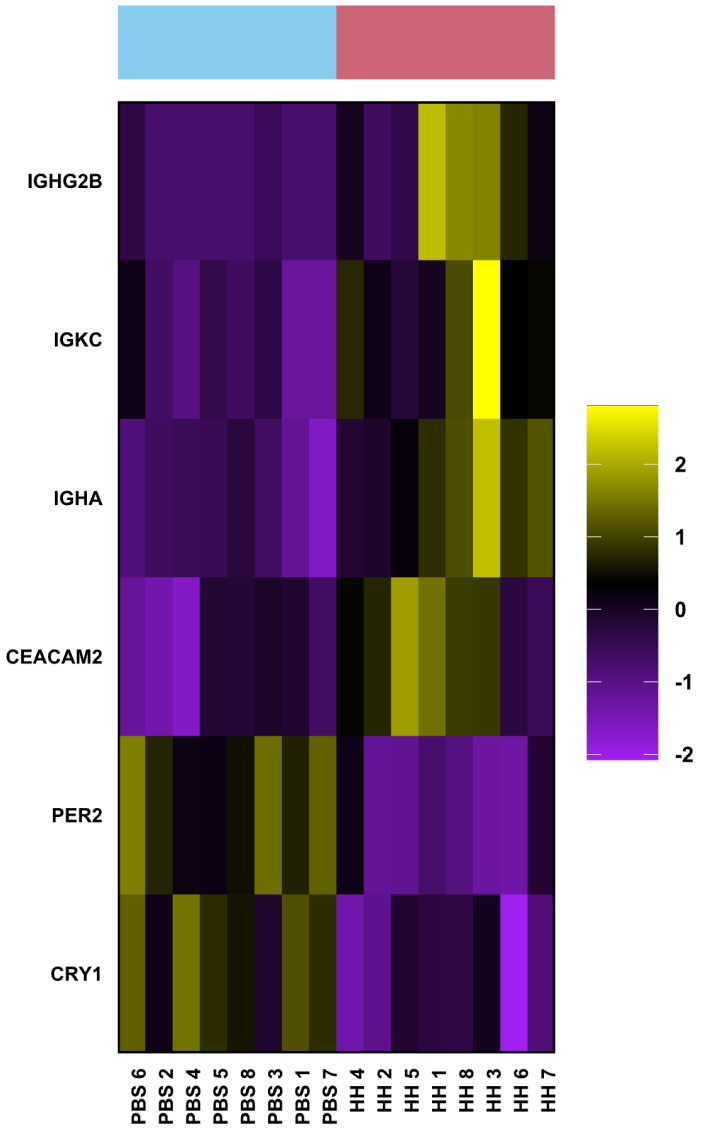


**Figure 7-8: Differentially expressed genes in colonic IEC following *Hh* colonization**
C57BL/6 littermates were administered 1x10$^{8}$ CFU *Hh* or given PBS by oral gavage and left for 21-days post-infection. Colonic IEC crypt RNA was analysed using bulk RNA sequencing with downstream analyses performed using Searchlight. Differential gene expression was analysed using the DESeq2 package. A hierarchically clustered heatmap is shown displaying significantly differentially expressed genes (p.adj < 0.1, absolute log2fold > 0) between the *Hh* and PBS groups. The blue bar above the heatmap (left) indicates the PBS samples while the red bar (right) indicates the *Hh* samples. Expression levels have been row scaled into z-scores.

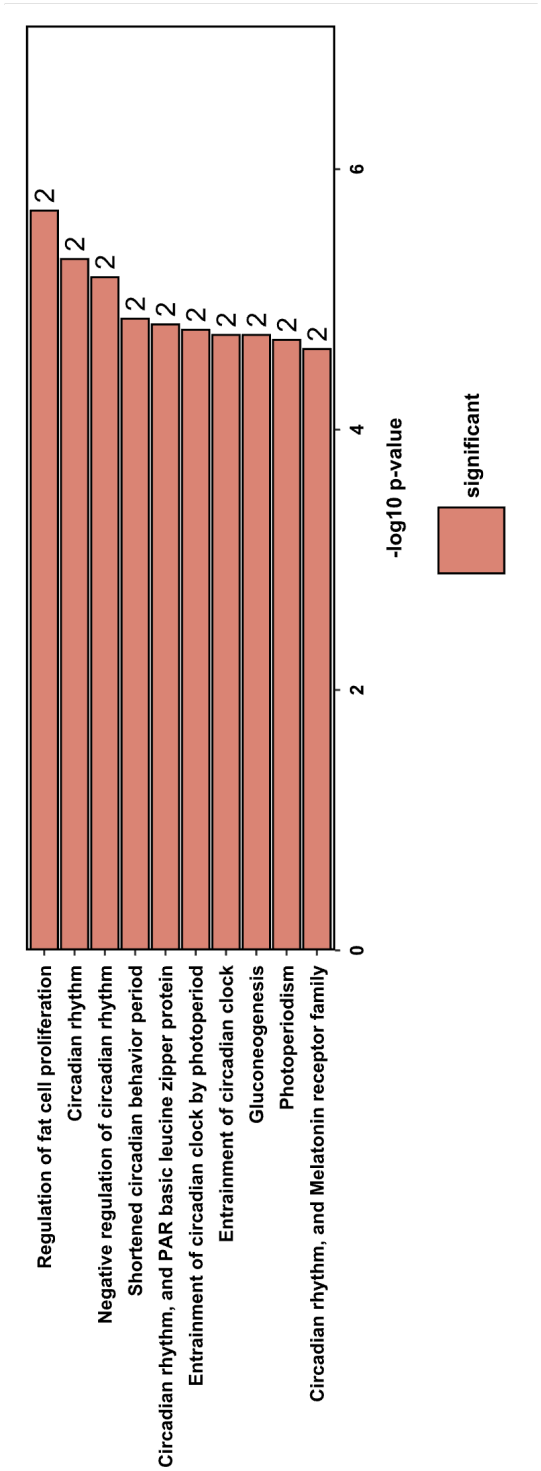


**Figure 7-9: *Hh* colonization drives changes to genes associated with circadian rhythm in colonic IEC**

C57BL/6 littermates were administered 1x10$^8$ CFU *Hh* or given PBS by oral gavage and left for 21-days post-infection. Colonic IEC crypt RNA was analysed using bulk RNA sequencing with downstream analyses performed using Searchlight. Differential gene expression was analysed using the DESeq2 package. A summary bar chart is shown of the 10 most enriched gene sets from the significantly differentially expressed genes (p.adj < 0.1, absolute log2fold > 0) between the *Hh* and PBS groups. The number of significantly differentially expressed genes within each gene set is annotated. Enrichment analysis was performed using Hypergeometric Gene Set Enrichment on the gene database STRING11.5.

Finally, in Figure 7-10, the top 10 upregulated and downregulated DEGs in IEC from *Hh* colonized mice are shown based on p-value (Figure 7-10A) and fold change (Figure 7-10B). Among the most downregulated genes based on fold change were several genes encoding alpha defensins, which are a family of AMPs (*Defa20*, *Defa22*, *Defa30*, *Defa24*, *Defa21*) (Figure 7-10B). However, although these genes were among the most downregulated by fold change, the p.adj values were all >0.999, so it is difficult to conclude whether this represents a meaningful change. Interestingly, based on p-value, among the most downregulated genes in IEC crypts from *Hh* colonised mice was *Klf10,* which encodes Krüppel-like factor 10. This protein acts as a transcriptional regulator of TGFβ and its deficiency has been associated with colitis in mice(Papadakis et al., 2015). Again, it is difficult to postulate whether *Hh* may drive changes to this pathway as the p.adj value was > 0.4.

**A**

**Most upregulated by p value**

| Gene | log2fold | p | p.adj |
|---|---|---|---|
| IGHA | 0.97 | 2.782385e-07 | 0.002795601 |
| IGHG2B | 4.35 | 9.285031e-07 | 0.006219423 |
| IGKC | 1.33 | 2.783079e-06 | 0.013981492 |
| CEACAM2 | 0.53 | 2.629959e-05 | 0.088081713 |
| NR1D2 | 0.31 | 5.000447e-05 | 0.111648866 |
| NR1D1 | 0.63 | 7.023705e-05 | 0.141141357 |
| GM47640 | 0.82 | 1.376626e-04 | 0.222251259 |
| GM4468 | 3.38 | 2.079878e-04 | 0.298536824 |
| LAX1 | 1.84 | 5.488251e-04 | 0.496826762 |
| IL2RB | 0.72 | 6.468665e-04 | 0.496826762 |

**Most downregulated by p value**

| Gene | log2fold | p | p.adj |
|---|---|---|---|
| PER2 | -0.52 | 1.051757e-09 | 2.113506e-05 |
| CRY1 | -0.34 | 8.236112e-06 | 3.310093e-02 |
| BCL6 | -0.53 | 4.078925e-05 | 1.116489e-01 |
| RPL38 | -0.30 | 4.564185e-05 | 1.116489e-01 |
| GAPDH | -2.34 | 9.185169e-05 | 1.677963e-01 |
| LMNB2 | -0.15 | 1.437804e-04 | 2.222513e-01 |
| RORC | -0.33 | 2.395180e-04 | 3.208743e-01 |
| KLF10 | -0.47 | 3.423626e-04 | 4.299861e-01 |
| RPL37 | -0.24 | 4.342332e-04 | 4.603728e-01 |
| SAMD1 | -0.20 | 4.353452e-04 | 4.603728e-01 |

**B**

**Most upregulated by log2fold**

| Gene | log2fold | p | p.adj |
|---|---|---|---|
| IGHG2B | 4.35 | 9.285031e-07 | 0.006219423 |
| GM4468 | 3.38 | 2.079878e-04 | 0.298536824 |
| 5930412G12RIK | 3.19 | 7.169931e-04 | 0.496826762 |
| AC126937.1 | 3.16 | 1.322223e-03 | 0.670724872 |
| NUTM1 | 3.16 | 3.891284e-03 | 0.809856711 |
| ZFP648 | 2.89 | 3.861231e-03 | 0.809856711 |
| 4930405O22RIK | 2.88 | 4.759183e-03 | 0.885516585 |
| GM38509 | 2.87 | 2.582240e-03 | 0.786213921 |
| GM6420 | 2.80 | 2.417761e-02 | 0.999645792 |
| TMPRSS3 | 2.78 | 4.590757e-03 | 0.869813057 |

**Most downregulated by log2fold**

| Gene | log2fold | p | p.adj |
|---|---|---|---|
| DEFA20 | -5.61 | 0.05967251 | 0.9996458 |
| DEFA22 | -5.35 | 0.07221749 | 0.9996458 |
| DEFA30 | -5.24 | 0.07846634 | 0.9996458 |
| AY761184 | -5.17 | 0.08284867 | 0.9996458 |
| DEFA24 | -4.53 | 0.10479728 | 0.9996458 |
| GM7849 | -4.50 | 0.13170158 | 0.9996458 |
| DEFA21 | -4.31 | 0.14676747 | 0.9996458 |
| GM14851 | -3.95 | 0.16425914 | 0.9996458 |
| FAM20A | -3.41 | 0.24755998 | 0.9996458 |
| GM24289 | -3.36 | 0.00920229 | 0.9879621 |

**Figure 7-10: Changes to epithelial gene expression as a result of *Hh* colonization are largely non-significant**
C57BL/6 littermates were administered 1x$10^8$ CFU *Hh* or given PBS by oral gavage and left for 21-days post-infection. Colonic IEC crypt RNA was analysed using bulk RNA sequencing with downstream analyses performed using Searchlight. Differential gene expression was analysed using the DESeq2 package. Tables showing the top 10 upregulated and downregulated genes by p-value (A) and log2fold change (B). Upregulated genes are higher and downregulated genes lower in *Hh* than PBS.

In conclusion, these data suggest that *Hh* colonization drives very minimal changes to colonic epithelial gene expression at steady state. The transcriptional changes identified in Figure 7-2 were not recapitulated in the epithelial bulk RNA sequencing dataset. This may be because they were not the result of epithelial gene expression, or because specific *Hh* infection may not drive the same changes as MT.

## 7.4 Discussion

We have previously described a protective effect of *Hh* colonization in the context of DSS colitis. Here, we demonstrate that, at steady state, *Hh* drives minimal changes to primary colonic IEC gene expression. We also tested IESC-derived organoids for long-term changes to responsiveness to several stimuli but found that organoids from *Hh*-infected mice showed comparable functions to those from naïve animals.

### 7.4.1 Similarity between naïve and *Hh* colonized epithelium at steady state

Our results suggest that *Hh* colonization has minimal effects on colonic epithelial phenotype at steady state. This indicates that epithelial changes may not contribute to the protection against DSS induced disease which we have previously described. We initially analysed whole colon tissue for IEC-related gene expression and found minimal differences in transcription of epithelial lineage genes, aside from a slight increase in expression of *Dclk1*. This suggests that *Hh* colonization has little impact on the differentiation of IEC, with the exception of potentially driving a slight expansion of Tuft cells. Tuft cells are associated with type 2 immune responses (Drurey et al., 2021), which are not generally induced following *Hh* infection (Kullberg et al., 2002, Xu et al., 2018), and it requires further validation to confirm whether increased *Dclk1* expression represents a meaningful increase in Tuft cell numbers. While we observed upregulation of genes associated with antimicrobial and epithelial defence responses in whole colon tissue, such as *Retnlb*, *Ccl20*, and *Nos2*, these changes were not recapitulated in a bulk RNA sequencing dataset specific to IECs. This could suggest that the transcriptional changes we initially observed were the result of other cell types in the colon, rather than IECs. In previous chapters we identified *Hh*-driven changes to colonic myeloid cell recruitment, phenotype and function, so the altered colonic gene transcription observed here could be the result of changes to the myeloid compartment. For example, iNOS (encoded by *Nos2*) is upregulated in intestinal monocytes during acute infection (Grainger et al., 2013). The upregulation we observed in whole colon could therefore be due to increased monocyte numbers following *Hh* colonization, as described in Chapter 4. In future, single-cell RNA sequencing could be performed on total

cells isolated from the colon, thus allowing the identification of specific cell types which are transcriptionally altered (Kolodziejczyk et al., 2015).

Surprisingly, bulk RNA sequencing of colonic IEC crypts revealed very few differences in epithelial gene expression following *Hh* colonization. While this may reflect an absence of *Hh*-induced changes to epithelial phenotype at steady state, there are also notable caveats to the approaches used here. We used a single method to isolate colonic IEC crypts (Fan et al., 2016) and have not yet validated whether the isolated crypts contained representative proportions of all IEC types found *in vivo*. Single-cell RNA sequencing has been used successfully to interrogate the intestinal epithelium and identify individual clusters of IECs within FACS-sorted populations (Haber et al., 2017). This approach could be used here to validate the presence of diverse IECs within the isolated crypt samples and would allow for comparison with published datasets to test that the proportions of isolated cell types are representative. This method would also enable the identification of individual cell clusters showing transcriptional differences, if any, to establish which cells are specifically affected by *Hh* colonization. However, another reason for the observed lack of transcriptional differences could be that not all colonic IEC crypts are equally colonized with *Hh*. Colonization levels are likely to vary throughout the large intestine (Chan et al., 2005), and changes to epithelial gene expression may only be present in cells with close proximity to *Hh*. Other methodologies which allow for spatial analysis in combination with transcriptomics could be a useful approach to address this caveat. ‘Spatial host-microbiome sequencing’ has recently been described (Lötstedt et al., 2023) and allows for sequencing of host transcripts in addition to capturing tissue histology and bacterial 16S sequencing. Techniques such as this could enable the interrogation of IEC gene expression relative to the level of *Hh* colonization, which may reveal *Hh*-induced changes to IEC phenotypes in specific areas of the intestine.

While we did not detect changes to epithelial phenotype at steady state, it does not exclude the possibility that *Hh* may drive altered responses under inflammatory conditions. There may be a level of epigenetic changes which occur following interactions with microbes, which could result in altered responses to stimulation but is not obvious under resting conditions. Epigenetic changes to epithelial stem cells (SCs) have been described in the context of

sterile injury, in which skin SCs retain memory of insult and produce an enhanced wound repair response upon secondary challenge (Naik et al., 2017). Our use of the organoid system attempted to address this, by isolating IESCs from infected mice and analysing their response to various inflammatory stimuli. We observed no differences in the responsiveness of organoids derived from *Hh*-colonized animals to those derived from naïve counterparts, suggesting that *Hh* may not drive long-lasting changes to epithelial barrier function. However, the organoid system requires IESC growth *in vitro* for several passages before use, to ensure the viability and purity of the organoid culture. This results in ~3 weeks of IESC growth *in vitro* prior to stimulation. It is possible that any changes as a result of exposure to *Hh in vivo* may have been lost during this period and could explain the comparable responses between naïve and *Hh* infection derived organoids. An *ex vivo* organoid approach may therefore not be the most suitable system to study *Hh*-induced changes to the epithelium. However, using *in vitro* systems to study the relationship between *Hh* and IECs is technically challenging, due partly to the microaerophilic requirements of the bacteria (Ward et al., 1994), and the enclosed nature of intestinal organoids (Puschhof et al., 2021). While we were unable to optimise a 2D IEC monolayer system, this may remain the most suitable method to study primary IEC-microbe interactions *in vitro* (Moon et al., 2014). To account for the different oxygen requirements of *Hh* and host IECs, an Ussing chamber system could be used to provide specific environments for each component of the co-culture (Clarke, 2009). Alternatively, rather than culturing live *Hh* with IECs, another option could be to isolate *Hh*-secreted metabolites or products which could be administered to IEC organoids or monolayers *in vitro*. This would enable examination of the effects of *Hh* on IEC functions without the technical limitations of using live bacteria. This approach has been used successfully to study a *Hh*-derived polysaccharide isolated from bacterial culture supernatants and its effect on macrophages (Danne et al., 2017), and could be utilised here to study effects on the epithelial compartment.

Finally, how IECs may remain refractory to *Hh* induced changes, while immune cells in the LP show clear differences in phenotype and function, is not yet obvious. From the literature, it is clear that the microbiota plays a key role in shaping epithelial gene expression, as treatment with antibiotics drives notable

changes to colonic IEC transcription (Reikvam et al., 2011). Reikvam *et al*. identified *H2Ab1*, *RegIIIβ*, and *Retnlb* among significantly downregulated genes following antibiotics treatment (Reikvam et al., 2011). This suggests that the microbiota actively stimulates antimicrobial responses in IECs, as well as potentially driving antigen presentation. Many commensal species have been shown to alter epithelial functions, typically strengthening the barrier through stimulation of mucus production or tight junction protein expression (Plovier et al., 2017, Wlodarska et al., 2017, Martín et al., 2019). Despite this evidence, *Hh* appears not to drive obvious changes to colonic IEC functions. However, the primary site of *Hh* colonization is the caecal mucosa (Chan et al., 2005), and it may be the case that the colonic epithelium is less affected due to the lower levels of colonization in this tissue. Indeed, in the caecal mucosa, *Hh* has been shown to be the dominant community member (Kuehl et al., 2005). Our work has focussed on the colon as the location of pathology in the DSS model (Wirtz et al., 2007), but for future study of *Hh* mediated effects on the epithelium it may be useful to focus on the caecum. Nonetheless, we have documented various changes to colonic myeloid phenotypes and functions following *Hh* colonization, and it is interesting that these changes occur while the epithelium remains largely unaffected. The lack of colonic epithelial response to *Hh* likely reflects the need for the epithelium to tolerate repeated exposure to commensal microbes on the luminal side, while maintaining ability to respond to pathogens which invade the tissue. This requirement is partially achieved through the polarisation of IECs, including the asymmetric expression of TLRs and other receptors to distinct sides of the cell (Stanifer et al., 2020). As such, the response to stimulation varies greatly at each cell surface, with the luminal side exposed to the microbiota showing reduced responsiveness (Stanifer et al., 2020). It appears that the intestinal epithelium has evolved to withstand exposure to the microbiota and is tightly regulated to ensure maintenance of homeostasis, which could explain why we have not observed significant changes to the IEC compartment following *Hh* colonization.

### 7.4.2 Concluding remarks

We report that the colonic epithelium shows few transcriptional changes as a result of steady state *Hh* colonization. Similarly, IESCs isolated from infected mice and grown in organoids showed comparable responses to stimulation to

those from naïve animals. These data suggest that the intestinal epithelium is largely refractory to the effects of *Hh in vivo*, despite the documented effects of this microbe on intestinal immune cells. This likely represents a mechanism by which the epithelial barrier tolerates exposure to the microbiota to maintain homeostasis in the gut. Overall, these approaches and results were unable to provide evidence that the disease attenuating effect of *Hh* colonization involves alterations in the IEC barrier, suggesting that effects on other cell types may be responsible.

# 8 Final Discussion

*Hh* is an exemplar pathobiont species which drives inflammatory disease in the absence of immune regulation. However, in normal hosts, the induction of avid regulatory responses allows the host to tolerate chronic *Hh* infection without pathology (Cahill et al., 1997). The effects of *Hh* colonization on immune competent hosts are incompletely understood. Previous literature has described mechanisms whereby *Hh* drives Treg induction (Kullberg et al., 2002, Xu et al., 2018, Kedmi et al., 2022) and an anti-inflammatory macrophage phenotype (Danne et al., 2017), but the consequences of these changes for subsequent immune function were previously unexplored. Here, we aimed to determine whether infection with *Hh* results in an altered response during an inflammatory challenge. We then sought to characterise the effects of *Hh* on the intestinal immune system at steady state, focussing on myeloid populations which have not yet been studied in depth in the context of *Hh* colonization.

## 8.1 *Hh* primes intestinal immune responses, driving changes to homeostasis and disease outcomes

### 8.1.1 Homeostatic immunity

The immune system is constantly responding to microbe-derived signals, leading to the induction of homeostatic immune responses (Belkaid and Harrison, 2017). The outcome of these responses for host physiology and immune function are only beginning to be explored. It is clear that infection with commensal species, such as intestinal *Bacteroides fragilis* or *Staphylococcus epidermis* in the skin, drives tonic immune responses which occur at steady state but can alter the outcome in a disease setting (Mazmanian et al., 2005, Mazmanian et al., 2008, Naik et al., 2015). The induction of a wide range of responses following *Hh* colonization suggests that *Hh* may be another candidate species driving homeostatic immunity, which could alter disease outcomes (Whary et al., 1998, Kullberg et al., 2002, Buonocore et al., 2010, Danne et al., 2017).

In Chapter 4 we reported that, at steady state, *Hh* colonization drives increases to monocyte and neutrophil infiltration to the colon. We also identified *Hh*-induced changes to colonic proinflammatory cytokine transcription, including an

early *Ifny* response which was later followed by elevated levels of *Tnfa* and *Il17a*. Importantly, these responses were not accompanied by pathology, indicating that *Hh* indeed drives homeostatic immune responses in the colon at steady state. These findings are in accordance with reports that the microbiota drives steady state myelopoiesis (Balmer et al., 2014a, Khosravi et al., 2014, Yan et al., 2022), and stimulates monocyte recruitment to the colon in the absence of inflammation (Bain et al., 2014, Kang et al., 2020). Our data suggest that *Hh* may induce similar responses. However, it is currently unclear whether the increased myeloid infiltration we observed is representative of changes to BM myelopoiesis. This is something which should be explored in the future through analysis of BM precursors, monocytes and neutrophils. Microbiota-induced myelopoiesis is dependent on PRRs and their downstream signalling components, including NOD1 (Clarke et al., 2010) and MyD88 (Balmer et al., 2014a). Stimulation of tonic myeloid infiltration by *Hh* is likely to occur through a similar innate recognition pathway and probably represents a shared mechanism common to other bacterial species.

SPF laboratory mice possess a microbiota which differs substantially to that of wild mice, particularly showing a reduction in microbial diversity (Rosshart et al., 2017, Rosshart et al., 2019). Wild mice show differences in steady state immune populations compared to laboratory mice, including increases in effector T cell numbers across various tissues (Beura et al., 2016, Abolins et al., 2017). They also show increased expression of genes associated with immune activity in blood, including chemokines such as *Ccr2* and cytokines such as *Il1B* (Rosshart et al., 2019). These studies further consolidate the idea that a diverse microbiota stimulates increased immune activity at steady state. Our data is in line with this and suggests that *Hh* is a species which contributes to this effect. Despite this, we observed increased myeloid infiltration to the colon but not the SI following *Hh* colonization, indicating that the myeloid response was specific to the site of infection, suggesting that *Hh* mainly affects local innate immune set points. However, whether *Hh* drives wider changes to systemic immune populations, such as in the BM or liver, remains to be explored. *Hh*-specific antibodies are found in the serum following infection (Whary et al., 1998, Kullberg et al., 1998), highlighting that *Hh* can stimulate systemic immune responses. Interestingly, microbiota-specific IgG has been proposed to have a

protective effect against systemic *S. typhimurium* infection (Zeng et al., 2016). Likewise, microbiota-derived metabolites can enter the bloodstream and drive functional changes to immune populations at distal sites, thus increasing protection against bacterial infections (Clarke et al., 2010). Determining whether *Hh* drives similar effects will be important for understanding how colonization might impact the outcome of different disease challenges.

In Chapter 4, we described increases in colonic cytokine transcription following *Hh* colonization. However, in Chapter 5, we stimulated colonic macrophages *ex vivo* and found that macrophages from infected mice showed suppressed cytokine production compared to those from naïve mice. These results present an interesting contrast and suggest that *Hh* has distinct functional effects on different immune cells. A similar phenomenon was described by Abolins *et al.*, who reported that splenocytes from wild mice showed greatly reduced cytokine production when stimulated with PAMPs *ex vivo*, as compared to laboratory mice (Abolins et al., 2017). Similarly, Rosshart *et al.* used a system in which laboratory mouse embryos are implanted into wild mice to produce laboratory strain mice with a wild mouse-like microbiota. They then took genetically identical mice colonized with either a standard SPF microbiota or the 'wild-like' microbiota and challenged them with influenza infection. They found that those with a wild-like microbiota had reduced levels of TNFα, IL-6, and other inflammatory mediators in the lung after infection. Furthermore, those with the wild microbiota had a survival advantage over their standard SPF laboratory counterparts, which they reasoned may be due to the reduction in hyper-active cytokine production (Rosshart et al., 2017). Our data suggests that *Hh* may have a limiting effect on the inflammatory responses of some cell types, such as macrophages, while simultaneously increasing steady state expression of inflammatory cytokines in other cell types. We hypothesise that the source of increased cytokine transcription could instead be lymphoid cells, including ILCs and Th1/Th17 effectors. Studies which blocked IL-10 signalling in the context of *Hh* infection have demonstrated that *Hh* drives IFNγ, IL-1β, TNFα, IL-22, and IL-17A production by these cell types in the absence of immune regulation (Kullberg et al., 2002, Buonocore et al., 2010, Morrison et al., 2013), suggesting that they may also be the source of these cytokines during steady state *Hh* infection. This could be tested using flow cytometry to identify different cell

types and measuring intracellular cytokine production. Nonetheless, it has been proposed that while the microbiota stimulates homeostatic immunity at steady state, it also functions to manage the threshold for immune activation (Ansaldo et al., 2021). This may serve to prevent unnecessary inflammatory responses targeting the microbiota but likely also affects how the immune system responds to other challenges. The balance between microbiota-induced effector responses and regulatory, immune suppressive responses therefore appears to calibrate host immune function and disease outcome, to an extent. Our data, along with the work of others describing *Hh*-specific Treg responses, supports the idea that *Hh* contributes to microbiota-mediated calibration of immune functions at steady state. A summary of *Hh*-induced changes to the colonic immune system at steady state is depicted in Figure 8-1.

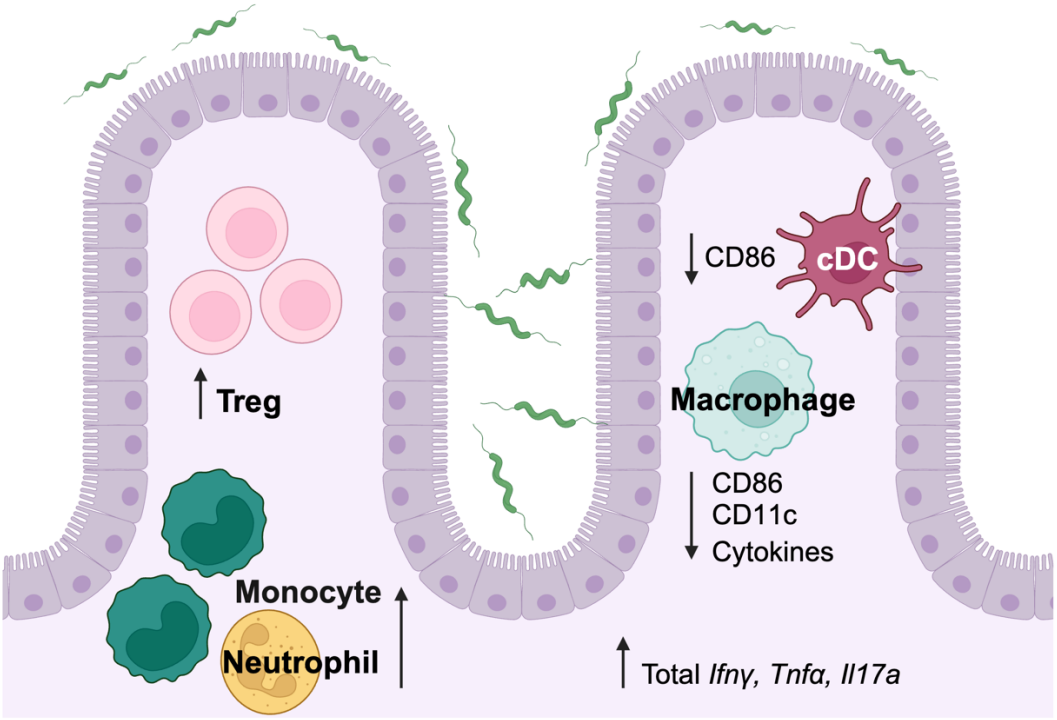


**Figure 8-1: Summary of *Hh*-induced changes to homeostatic intestinal immunity**
*Hh* colonization drives increased Treg expansion, as well as increased infiltration of neutrophils and monocytes to the colon. Macrophages and cDCs show reduced expression of costimulatory CD86, while macrophages also show reduced CD11c expression. Macrophages show suppressed cytokine production *ex vivo*, while the total tissue transcription of *Ifnγ*, *Tnfα*, *Il17a* increases. These changes are not accompanied by pathology. This figure was created using BioRender.com.

## 8.1.2 Effects of *Hh* on disease outcomes

In Chapter 3, we demonstrated that mice colonized with *Hh* show attenuated disease severity when challenged with DSS to induce acute colitis. DSS-induced

weight loss and clinical symptoms were reduced in *Hh* infected animals, along with colonic inflammatory infiltrate. Interestingly, the extent of DSS-induced histopathology showed considerable variation within the *Hh* infected group, but overall, the infected mice had significantly reduced histology scores. It was recently reported that a large cohort of C57BL/6 mice bred and maintained in the same SPF facility showed highly variable disease levels when treated with DSS (Forster et al., 2022). Microbiota sequencing analyses identified specific microbes whose relative abundance correlated with either attenuated or worsened DSS-disease (Forster et al., 2022). They further showed that mono-colonization of GF mice with these individual species could replicate DSS disease outcomes, although importantly none of these animals were colonized with *Hh* (Forster et al., 2022). This corroborates other studies describing how the microbiota can impact outcomes in DSS colitis (Brinkman et al., 2013), including the identification of bacterial species which increase the severity of DSS induced disease (Zhang et al., 2018, Park et al., 2018). *Hh* appears to be another member of the microbiota with the capacity to alter the outcome of DSS colitis, acting as a disease-attenuating factor. However, the variation of DSS disease severity within our cohorts of *Hh*-infected mice suggests that other community members could also be contributing. An important next step will be to perform 16S sequencing to examine the microbial composition of the animals used in our study, with the aim of determining whether other species known to impact DSS severity are present. Furthermore, microbes have the ability to modulate microbiota composition and impact the colonization of other species (Kuehl et al., 2005, Lai et al., 2020). It will be interesting to explore whether *Hh* drives changes to microbial communities which could potentially cause knock-on effects to host immunity and disease outcomes, particularly as there is already evidence that *Hh* can modulate microbial community structure in the caecum (Kuehl et al., 2005).

The extent of pathology induced by DSS is likely impacted by the effects of *Hh* colonization on steady state immune functions. DSS colitis is an immune-mediated disease, driven primarily by innate myeloid cells (Stevceva et al., 2001). Any alterations to neutrophil or monocyte functions would therefore be expected to impact disease outcome. The results presented in Chapter 4 showed that macrophages and cDCs from infected animals expressed lower levels of the

costimulatory molecule CD86, which is involved in T cell activation (Park et al., 2023). Similarly, in Chapter 5, we observed that macrophages from *Hh* colonized mice showed suppressed *ex vivo* cytokine production. These results suggest that *Hh* may have a limiting effect on innate inflammatory responses, although further work is required to test this hypothesis. Functional testing of neutrophils and monocytes from infected mice could reveal whether *Hh* has an intrinsic effect on the functions of these cells. Microbiota-derived signals have been shown to impact the functions of BM neutrophils (Clarke et al., 2010, Balmer et al., 2014a), as well as stimulating BM monocyte development and promoting protection against systemic bacterial infection (Khosravi et al., 2014). It is therefore possible that *Hh*-derived signals modulate the functions of these cells to prevent excessive inflammatory responses, which could impact the inflammation induced by DSS. Another possibility is that *Hh* drives changes to the local environment in the colon, for example by mediating cytokine production, which then has an indirect effect on infiltrating immune cells which are recruited to the tissue following DSS treatment. Potential mechanisms driving the disease attenuation in this model are discussed further in Section 8.1.3.

The homeostatic increase in colonic neutrophil and monocyte infiltration observed in Chapter 4 is somewhat contradictory to the reduced inflammatory infiltrate triggered by DSS in infected animals. We postulate that *Hh* drives a low level of immune activity at steady state, and that the constant interactions between the bacteria and host have functional effects on local immune cells which impact inflammatory responses. This is not dissimilar to the results presented in wild microbiota studies. A diverse, wild-like microbiota promoted reduced inflammatory responses following influenza infection (Rosshart et al., 2017), while simultaneously appearing to drive increased immune activation at steady state (Beura et al., 2016, Abolins et al., 2017, Rosshart et al., 2019). Thus far, we have examined the effect of *Hh* on inflammatory disease in the colon. In the future it will be important to explore whether *Hh* colonization impacts outcomes in other contexts throughout the body, such as pathogenic infections. Our results in Chapter 5 suggest that the phagocytic function of colonic macrophages may be slightly reduced in infected mice, although they still exhibited phagocytic activity. These data require further validation, however, if this is the case, this could be a disadvantage in the context of

bacterial infection. Microbiota-derived metabolites have been described to increase the bactericidal functions of macrophages (Chang et al., 2014, Schulthess et al., 2019), so it would be surprising for *Hh* to have the opposite effect. However, we did not obtain data on the killing functions of macrophages, and this could be independent from the effect we observed on phagocytosis. Similarly, reduced cytokine production by macrophages may be beneficial in the context of inflammatory disease, but unfavourable in a different context where inflammation is required for pathogen clearance. Gaining a more complete understanding of how *Hh* affects different immune functions will be essential for determining how colonization might impact diverse disease situations.

### 8.1.3 Proposed mechanisms of *Hh*-mediated disease attenuation

We postulate that *Hh*-induced attenuation of DSS disease severity is mediated by a combination of direct and indirect bacterial effects on innate immune functions. The induction of *Hh*-specific Tregs has been characterised in detail (Kullberg et al., 2002, Xu et al., 2018, Kedmi et al., 2022), and these cells are indispensable for maintaining tolerance to *Hh*. We propose that the *Hh*-mediated expansion of Tregs may act to limit local myeloid responses, including suppressing cytokine production as described in Chapter 5. This would represent an indirect mechanism by which *Hh* modulates innate immune functions and is in accordance with the understanding that Tregs can suppress innate-driven pathology (Maloy et al., 2003), and limit the responses of monocytes and cDCs to stimulation with PAMPs (Taams et al., 2005, Houot et al., 2006). A recent study exploring the spatial localisation of immune responses in *Hh* infection found that *Hh*-specific Tregs co-localise with $CD206^{+}$ macrophages in the colonic LP at steady state (Gu et al., 2024). These close interactions are likely to impact colonic macrophage functions and may drive the altered cytokine production we reported in Chapter 5. Whether *Hh*-specific Tregs directly interact with infiltrating monocytes and neutrophils in an inflammatory setting has not yet been reported, although Treg-mediated inhibition of neutrophil and monocyte functions has been described (Lewkowicz et al., 2006, Taams et al., 2005). There is also evidence that manipulation of the microbiota, either through colonization with specific species or modulation with treatments, can alter the balance of Th1/Th17 and Treg cells in the intestine (Hartog et al., 2015, Park et al., 2018, Zhang et al., 2018). These changes to intestinal T cell proportions

were associated with attenuated DSS colitis, suggesting that a similar mechanism could drive the disease protection described here. It seems likely that microbes which drive expansion of Tregs to promote tolerance to their own colonization can alter the balance to increase immune regulation, which then limits the extent of inflammation following DSS challenge. However, this is a fine balance, as the intestinal immune system must remain able to respond to pathogens. Microbes which promote immune-regulatory effects may therefore be protective in the context of inflammatory disease but could be detrimental in a setting where inflammatory responses are required for pathogen clearance. It would therefore be interesting to determine how *Hh* alters the outcome of a co-infection with a pathogen.

One remaining question concerns how the inflammatory environment during DSS colitis impacts the phenotype and function of *Hh*-specific Tregs. Commensal antigens preferentially drive Treg expansion at steady state, but it has been proposed that during inflammation this process is circumvented(Hand et al., 2012). Infection with the intestinal parasite *Toxoplasma gondii* was shown to cause bystander activation of commensal-specific T cells, which showed a Th1 phenotype and produced IFNγ (Hand et al., 2012). A similar phenomenon has been reported for *Hh*-specific T cells during pathogenic infection. While *Hh* mostly drives induction of RORγt$^{+}$Foxp3$^{+}$ Tregs at steady state, co-infection with *C. rodentium* results in the expansion of *Hh*-specific RORγt$^{+}$Foxp3$^{-}$ Th17 and Tbet$^{+}$ Th1 effectors (Xu et al., 2018). The authors also tested the fate of *Hh*-specific T cells during DSS colitis and, interestingly, did not observe deviation from the Treg phenotype induced at steady state (Xu et al., 2018). It is worth noting that DSS treatment was commenced on day 2 following *Hh* infection (Xu et al., 2018). This likely explains why the authors did not document the same attenuation of DSS disease severity which we report, as our data in Chapter 3 indicate that this protection is not present immediately after infection. Regardless, this indicates that *Hh*-specific T cells retain their Treg phenotype during colitis, although this requires validation in our own system.

Another potential mechanism driving attenuated disease is the direct modulation of innate immune function by *Hh* and its products. We aimed to explore this idea in Chapter 6, by testing the requirement for TLR2 in *Hh*-mediated disease protection. TLR2 has been described as the primary TLR which responds to *Hh*

(Mandell et al., 2004), but is not required for induction of *Hh*-induced colitis (Boulard et al., 2010). Instead, it has been proposed that TLR2 signalling drives an anti-inflammatory response in macrophages following *Hh* colonization (Danne et al., 2017), which we hypothesised may act to limit local inflammatory responses and drive the attenuation of disease severity documented in Chapter 3. However, upon using an antibody to block TLR2 signalling, we found that this had no impact on the ability of *Hh* to attenuate DSS colitis. This suggests that any anti-inflammatory effects of *Hh* mediated through TLR2 may be largely redundant in this context. This does not rule out the possibility that TLR2 signalling contributes to maintenance of tolerance to *Hh* at steady state. Similarly, other PRRs may be directly influenced by *Hh* and play a role in driving the disease protection described here. The pan-TLR signalling adaptor molecule MyD88 is required for the induction of colitis following *Hh* infection in susceptible hosts (Asquith et al., 2010). It would be interesting to determine whether this molecule is also required for the induction of protective responses to *Hh*. Testing the ability of *Hh* to attenuate DSS colitis in *Myd88*$^{-/-}$ hosts could be a useful system to study this in the future. However, it has been reported that loss of MyD88 worsens the severity of DSS induced disease (Araki et al., 2005), which could make it difficult to interpret the results. Finally, exploring bacterial products which drive different host responses could be another avenue for determining whether *Hh* drives direct functional effects on innate immune cells. Characterisation of additional products, metabolites and virulence factors could provide insight into pathways through which host immunity is impacted by *Hh* and the broader microbiota (Fox et al., 2011). This would also allow for the generation of mutant bacterial strains lacking key factors (Sterzenbach et al., 2008), which could be used to interrogate the role of those factors in conferring protection against DSS disease severity.

A summary of the proposed mechanisms through which *Hh* affects the outcome of DSS colitis is shown in Figure 8-2.

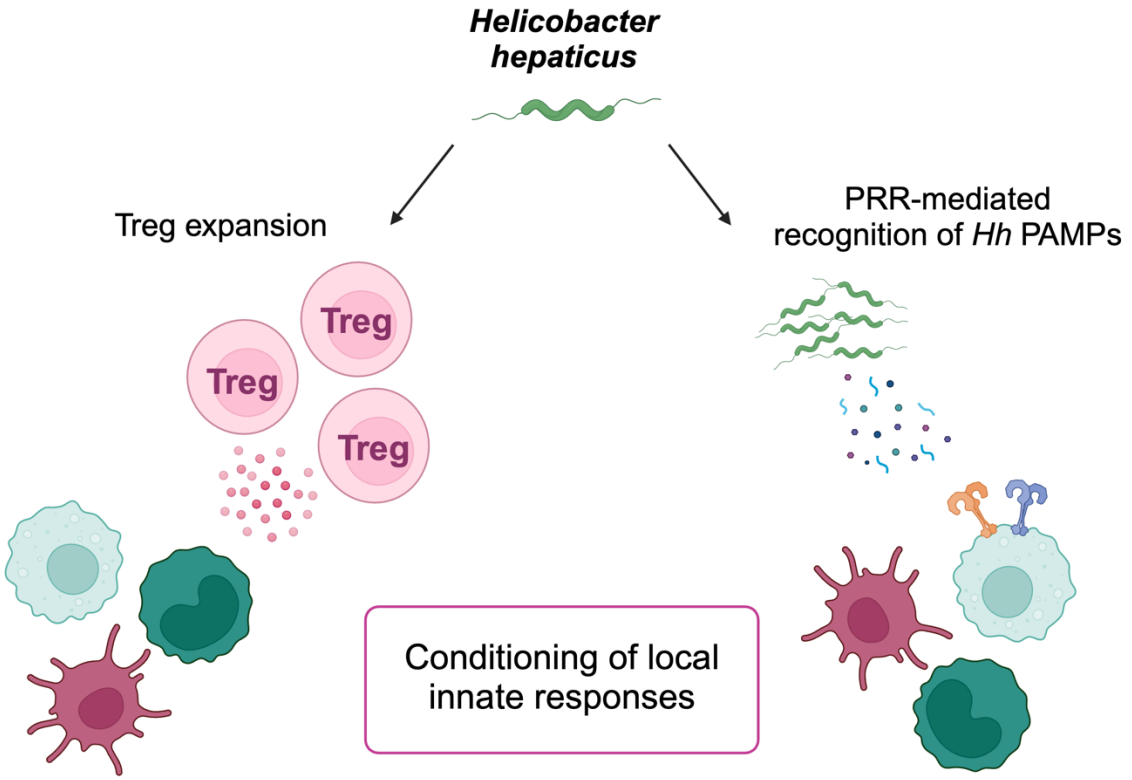


**Figure 8-2: Proposed mechanisms of *Hh*-mediated disease attenuation**
We propose that *Hh*-mediated attenuation of DSS colitis is mediated through a combination of direct and indirect mechanisms. *Hh* induces expansion of *Hh*-specific Tregs which we propose may act on local innate immune cells to indirectly suppress inflammatory responses and allow persistent colonization. *Hh* may also directly modulate innate immune functions through PRR-mediated recognition of *Hh*-derived PAMPs, leading to downregulated inflammatory responses. Both of these mechanisms could result in reduced inflammation and pathology following DSS treatment. This figure was created using BioRender.com.

## 8.2 Pathobionts in human health and disease

Finally, it is important to consider the potential consequences of this work for human health and disease. The human microbiota is far more diverse than that of a laboratory mouse, indicating that there may be a greater level of microbiota-driven immune modulation. As such, reconstitution of laboratory mice with a wild-like microbiota can recapitulate human immune traits and responses (Beura et al., 2016, Rosshart et al., 2019). While *Hh* appears to prime murine immune responses at steady state and reduce the extent of inflammatory disease, similar species may provide this function in humans. Although *Hh* does not colonize the human GI tract, other pathobiont species may occupy similar niches in humans. The most notable example is the related species *Helicobacter pylori*, which colonizes the gastric mucosa and drives disease in some individuals (Malfertheiner et al., 2023). Importantly, *H. pylori* has been described to exert disease-protective effects in certain contexts, such as reportedly reducing the

severity of Barrett's oesophagus (Erőss et al., 2018). Many species found in humans, including *Bacteroides fragilis*, have the capacity to act both as a commensal or an opportunistic pathogen, depending on the context (Patrick, 2022). Another relevant species is *Escherichia coli*. While most *E. coli* strains present in humans behave as commensals, there are some rare types which act as pathogens and are associated with gastroenteritis (Eltai et al., 2020) and IBD (Martinez-Medina and Garcia-Gil, 2014). Despite this, commensal *E. coli* strains have been shown to promote epithelial barrier integrity, thus protecting the host against pathogen invasion and providing disease-protective effects (Alvarez et al., 2019). These context-dependent outcomes of infection resemble the situation with murine *Hh*, although these species interact with the immune system in distinct ways. It is likely that some or all of the mechanisms through which *Hh* modulates host immunity are conserved between other bacterial species, although there is currently no documented microbe in humans which is equivalent to *Hh*. However, gaining understanding of the mechanisms by which *Hh* modulates host immunity will hopefully provide new insight into how the human microbiota may impact disease outcomes.

In conclusion, the microbiota stimulates homeostatic immune responses which lead to an increased level of immune activity at steady state (Ansaldo et al., 2021). Simultaneously, our data and the work of others supports the idea that the microbiota limits the inflammatory responses of local immune cells. A better understanding of these interactions will be crucial for dissecting the role of the microbiota in human disease. This will be particularly important for the development of microbiota-targeted therapeutics and the use of microbiota biomarkers for disease stratification. As laboratory mice are reported to possess an immature immune system (Beura et al., 2016), *Hh* may be an example of a 'keystone' species which stimulates immune maturation through driving increased myeloid infiltration and T cell expansion, modulating cytokine production, and setting the threshold for inflammatory responses (Ansaldo et al., 2021). Similar species are likely to have these effects on the human immune system. Understanding these effects and accounting for them in animal studies may help to provide better models for human disease which more accurately recapitulate human responses (Rosshart et al., 2019).

## 8.3 Concluding remarks

In this thesis, we explored the effects of the pathobiont *Hh* on intestinal immune functions at steady state and in the context of inflammatory disease. We demonstrate that *Hh* colonization protects against disease severity in the DSS colitis model, while also driving homeostatic immune responses in the colon at steady state. Future experiments should focus on elucidating the mechanisms resulting in attenuated disease. This should include deeper phenotypic and functional characterisation of *Hh*-specific T cells, as well as exploring how these cells interact with intestinal myeloid cells. Strategies to deplete T cells prior to DSS administration, for example using an anti-CD4 antibody to deplete all Th cells (Laky and Kruisbeek, 2016) or an anti-CD25 antibody to deplete Tregs (Setiady et al., 2010), could be useful to determine whether these cells are required for the disease-attenuating effect we have observed. It will also be important to perform microbiome sequencing, to determine whether *Hh* drives changes to microbiota composition which may contribute to altered disease outcomes. Finally, the *Hh* colonization and virulence factors which are required to mediate this disease protective effect remain to be explored and may provide parallels with species present in humans. As our understanding of host-microbiota interactions grows, *Hh* infection will continue to provide a valuable tool for studying host-pathobiont interactions *in vivo*. Future studies using this model will hopefully help to define mechanisms of microbiota-mediated immune modulation which are relevant for human health and disease.

# List of References

ABOLINS, S., KING, E. C., LAZAROU, L., WELDON, L., HUGHES, L., DRESCHER, P., RAYNES, J. G., HAFALLA, J. C., VINEY, M. E. & RILEY, E. M. 2017. The comparative immunology of wild and laboratory mice, Mus musculus domesticus. *Nature communications,* 8**,** 14811.

AHL, P. J., HOPKINS, R. A., XIANG, W. W., AU, B., KALIAPERUMAL, N., FAIRHURST, A.-M. & CONNOLLY, J. E. 2020. Met-Flow, a strategy for single-cell metabolic analysis highlights dynamic changes in immune subpopulations. *Communications biology,* 3**,** 305.

AKASHI, K., TRAVER, D., MIYAMOTO, T. & WEISSMAN, I. L. 2000. A clonogenic common myeloid progenitor that gives rise to all myeloid lineages. *Nature,* 404**,** 193-197.

AL NABHANI, Z., DULAUROY, S., MARQUES, R., COUSU, C., AL BOUNNY, S., DéJARDIN, F., SPARWASSER, T., BéRARD, M., CERF-BENSUSSAN, N. & EBERL, G. 2019. A weaning reaction to microbiota is required for resistance to immunopathologies in the adult. *Immunity,* 50**,** 1276-1288. e5.

AL NABHANI, Z., LEPAGE, P., MAUNY, P., MONTCUQUET, N., ROY, M., LE ROUX, K., DUSSAILLANT, M., BERREBI, D., HUGOT, J.-P. & BARREAU, F. 2016. Nod2 deficiency leads to a specific and transmissible mucosa-associated microbial dysbiosis which is independent of the mucosal barrier defect. *Journal of Crohn's and Colitis,* 10**,** 1428-1436.

ALANIZ, R. C., DEATHERAGE, B. L., LARA, J. C. & COOKSON, B. T. 2007. Membrane vesicles are immunogenic facsimiles of Salmonella typhimurium that potently activate dendritic cells, prime B and T cell responses, and stimulate protective immunity in vivo. *The Journal of Immunology,* 179**,** 7692-7701.

ALIPRANTIS, A. O., YANG, R.-B., MARK, M. R., SUGGETT, S., DEVAUX, B., RADOLF, J. D., KLIMPEL, G. R., GODOWSKI, P. & ZYCHLINSKY, A. 1999. Cell Activation and Apoptosis by Bacterial Lipoproteins Through Toll-like Receptor-2. *Science,* 285**,** 736-739.

ALVAREZ, C.-S., GIMéNEZ, R., CAñAS, M.-A., VERA, R., DíAZ-GARRIDO, N., BADIA, J. & BALDOMà, L. 2019. Extracellular vesicles and soluble factors secreted by Escherichia coli Nissle 1917 and ECOR63 protect against enteropathogenic E. coli-induced intestinal epithelial barrier dysfunction. *BMC microbiology,* 19**,** 1-12.

ANANIEVA, O., DARRAGH, J., JOHANSEN, C., CARR, J. M., MCILRATH, J., PARK, J. M., WINGATE, A., MONK, C. E., TOTH, R., SANTOS, S. G., IVERSEN, L. & ARTHUR, J. S. C. 2008. The kinases MSK1 and MSK2 act as negative regulators of Toll-like receptor signaling. *Nature Immunology,* 9**,** 1028-1036.

ANANTHAKRISHNAN, A. N., MCGINLEY, E. L. & BINION, D. G. 2008. Excess hospitalisation burden associated with Clostridium difficile in patients with inflammatory bowel disease. *Gut,* 57**,** 205-210.

ANDERSEN-NISSEN, E., SMITH, K. D., STROBE, K. L., BARRETT, S. L. R., COOKSON, B. T., LOGAN, S. M. & ADEREM, A. 2005. Evasion of Toll-like receptor 5 by flagellated bacteria. *Proceedings of the national academy of sciences,* 102**,** 9247-9252.

ANSALDO, E., FARLEY, T. K. & BELKAID, Y. 2021. Control of immunity by the microbiota. *Annual review of immunology,* 39**,** 449-479.

ARAKI, A., KANAI, T., ISHIKURA, T., MAKITA, S., URAUSHIHARA, K., IIYAMA, R., TOTSUKA, T., TAKEDA, K., AKIRA, S. & WATANABE, M. 2005. MyD88-deficient mice develop severe intestinal inflammation in dextran sodium sulfate colitis. *Journal of gastroenterology,* 40**,** 16-23.

ARANDA, R., SYDORA, B. C., MCALLISTER, P. L., BINDER, S. W., YANG, H. Y., TARGAN, S. R. & KRONENBERG, M. 1997. Analysis of intestinal lymphocytes in mouse colitis mediated by transfer of CD4+, CD45RBhigh T cells to SCID recipients. *Journal of immunology (Baltimore, Md.: 1950),* 158**,** 3464-3473.

ARNOLD, I. C., ARTOLA-BORáN, M., TALLóN DE LARA, P., KYBURZ, A., TAUBE, C., OTTEMANN, K., VAN DEN BROEK, M., YOUSEFI, S., SIMON, H.-U. & MüLLER, A. 2018. Eosinophils suppress Th1 responses and restrict bacterially induced gastrointestinal inflammation. *Journal of experimental medicine,* 215**,** 2055-2072.

ARNOLD, I. C., MATHISEN, S., SCHULTHESS, J., DANNE, C., HEGAZY, A. N. & POWRIE, F. 2016. CD11c(+) monocyte/macrophages promote chronic Helicobacter hepaticus-induced intestinal inflammation through the production of IL-23. *Mucosal Immunol,* 9**,** 352-63.

ASQUITH, M. J., BOULARD, O., POWRIE, F. & MALOY, K. J. 2010. Pathogenic and protective roles of MyD88 in leukocytes and epithelial cells in mouse models of inflammatory bowel disease. *Gastroenterology,* 139**,** 519-29, 529 e1-2.

ATARASHI, K., TANOUE, T., ANDO, M., KAMADA, N., NAGANO, Y., NARUSHIMA, S., SUDA, W., IMAOKA, A., SETOYAMA, H., NAGAMORI, T., ISHIKAWA, E., SHIMA, T., HARA, T., KADO, S., JINNOHARA, T., OHNO, H., KONDO, T., TOYOOKA, K., WATANABE, E., YOKOYAMA, S.-I., TOKORO, S., MORI, H., NOGUCHI, Y., MORITA, H., IVANOV, IVAYLO I., SUGIYAMA, T., NUñEZ, G., CAMP, J. G., HATTORI, M., UMESAKI, Y. & HONDA, K. 2015. Th17 Cell Induction by Adhesion of Microbes to Intestinal Epithelial Cells. *Cell,* 163**,** 367-380.

ATARASHI, K., TANOUE, T., SHIMA, T., IMAOKA, A., KUWAHARA, T., MOMOSE, Y., CHENG, G., YAMASAKI, S., SAITO, T., OHBA, Y., TANIGUCHI, T., TAKEDA, K., HORI, S., IVANOV, I. I., UMESAKI, Y., ITOH, K. & HONDA, K. 2011. Induction of Colonic Regulatory T Cells by Indigenous *Clostridium* Species. *Science,* 331**,** 337-341.

BäCKHED, F., ROSWALL, J., PENG, Y., FENG, Q., JIA, H., KOVATCHEVA-DATCHARY, P., LI, Y., XIA, Y., XIE, H., ZHONG, H., KHAN, MUHAMMAD T., ZHANG, J., LI, J., XIAO, L., AL-AAMA, J., ZHANG, D., LEE, YING S., KOTOWSKA, D., COLDING, C., TREMAROLI, V., YIN, Y., BERGMAN, S., XU, X., MADSEN, L., KRISTIANSEN, K., DAHLGREN, J. & WANG, J. 2015. Dynamics and Stabilization of the Human Gut Microbiome during the First Year of Life. *Cell Host & Microbe,* 17**,** 690-703.

BAIN, C., SCOTT, C., URONEN-HANSSON, H., GUDJONSSON, S., JANSSON, O., GRIP, O., GUILLIAMS, M., MALISSEN, B., AGACE, W. W. & MOWAT, A. M. 2013. Resident and pro-inflammatory macrophages in the colon represent alternative context-dependent fates of the same Ly6C hi monocyte precursors. *Mucosal immunology,* 6**,** 498-510.

BAIN, C. C., BRAVO-BLAS, A., SCOTT, C. L., GOMEZ PERDIGUERO, E., GEISSMANN, F., HENRI, S., MALISSEN, B., OSBORNE, L. C., ARTIS, D. & MOWAT, A. M. 2014. Constant replenishment from circulating monocytes maintains the macrophage pool in the intestine of adult mice. *Nature immunology,* 15**,** 929-937.

BAIN, C. C. & MOWAT, A. M. 2014. The monocyte-macrophage axis in the intestine. *Cellular Immunology,* 291**,** 41-48.

BAIN, C. C., OLIPHANT, C. J., THOMSON, C. A., KULLBERG, M. C. & MOWAT, A. M. 2018. Proinflammatory Role of Monocyte-Derived CX3CR1(int) Macrophages in Helicobacter hepaticus-Induced Colitis. *Infect Immun,* 86.

BALMER, M. L., SCHüRCH, C. M., SAITO, Y., GEUKING, M. B., LI, H., CUENCA, M., KOVTONYUK, L. V., MCCOY, K. D., HAPFELMEIER, S. & OCHSENBEIN, A. F. 2014a. Microbiota-derived compounds drive steady-state granulopoiesis via MyD88/TICAM signaling. *The Journal of Immunology,* 193**,** 5273-5283.

BALMER, M. L., SLACK, E., DE GOTTARDI, A., LAWSON, M. A. E., HAPFELMEIER, S., MIELE, L., GRIECO, A., VAN VLIERBERGHE, H., FAHRNER, R., PATUTO, N., BERNSMEIER, C., RONCHI, F., WYSS, M., STROKA, D., DICKGREBER, N., HEIM, M. H., MCCOY, K. D. & MACPHERSON, A. J. 2014b. The Liver May Act as a Firewall Mediating Mutualism Between the Host and Its Gut Commensal Microbiota. *Science Translational Medicine,* 6**,** 237ra66-237ra66.

BARKER, N., VAN ES, J. H., KUIPERS, J., KUJALA, P., VAN DEN BORN, M., COZIJNSEN, M., HAEGEBARTH, A., KORVING, J., BEGTHEL, H., PETERS, P. J. & CLEVERS, H. 2007. Identification of stem cells in small intestine and colon by marker gene Lgr5. *Nature,* 449**,** 1003-1007.

BASAK, O., VAN DE BORN, M., KORVING, J., BEUMER, J., VAN DER ELST, S., VAN ES, J. H. & CLEVERS, H. 2014. Mapping early fate determination in L gr5+ crypt stem cells using a novel K i67-RFP allele. *The EMBO journal,* 33**,** 2057-2068.

BELKAID, Y. & HARRISON, O. J. 2017. Homeostatic Immunity and the Microbiota. *Immunity,* 46**,** 562-576.

BEN MKADDEM, S., BENHAMOU, M. & MONTEIRO, R. C. 2019. Understanding Fc receptor involvement in inflammatory diseases: from mechanisms to new therapeutic tools. *Frontiers in immunology,* 10**,** 445798.

BENTO, A. F., LEITE, D. F. P., MARCON, R., CLAUDINO, R. F., DUTRA, R. C., COLA, M., MARTINI, A. C. & CALIXTO, J. B. 2012. Evaluation of chemical mediators and cellular response during acute and chronic gut inflammatory response induced by dextran sodium sulfate in mice. *Biochemical pharmacology,* 84**,** 1459-1469.

BERG, D. J., DAVIDSON, N., KüHN, R., MüLLER, W., MENON, S., HOLLAND, G., THOMPSON-SNIPES, L., LEACH, M. W. & RENNICK, D. 1996. Enterocolitis and colon cancer in interleukin-10-deficient mice are associated with aberrant cytokine production and CD4 (+) TH1-like responses. *The Journal of clinical investigation,* 98**,** 1010-1020.

BERGSTROM, K. S. B., MORAMPUDI, V., CHAN, J. M., BHINDER, G., LAU, J., YANG, H., MA, C., HUANG, T., RYZ, N., SHAM, H. P., ZAREPOUR, M., ZAPH, C., ARTIS, D., NAIR, M. & VALLANCE, B. A. 2015. Goblet Cell Derived RELM-β Recruits CD4+ T Cells during Infectious Colitis to Promote Protective Intestinal Epithelial Cell Proliferation. *PLOS Pathogens,* 11**,** e1005108.

BERNIER-LATMANI, J. & PETROVA, T. V. 2017. Intestinal lymphatic vasculature: structure, mechanisms and functions. *Nature reviews Gastroenterology & hepatology,* 14**,** 510-526.

BERSTAD, A., ARSLAN, G. & FOLVIK, G. 2000. Relationship between intestinal permeability and calprotectin concentration in gut lavage fluid. *Scandinavian journal of gastroenterology,* 35**,** 64-69.

BEUMER, J. & CLEVERS, H. 2021. Cell fate specification and differentiation in the adult mammalian intestine. *Nat Rev Mol Cell Biol,* 22**,** 39-53.

BEURA, L. K., HAMILTON, S. E., BI, K., SCHENKEL, J. M., ODUMADE, O. A., CASEY, K. A., THOMPSON, E. A., FRASER, K. A., ROSATO, P. C., FILALI-MOUHIM, A., SEKALY, R. P., JENKINS, M. K., VEZYS, V., HAINING, W. N., JAMESON, S. C. & MASOPUST, D. 2016. Normalizing the environment recapitulates adult human immune traits in laboratory mice. *Nature,* 532**,** 512-516.

BITON, M., HABER, A. L., ROGEL, N., BURGIN, G., BEYAZ, S., SCHNELL, A., ASHENBERG, O., SU, C.-W., SMILLIE, C., SHEKHAR, K., CHEN, Z., WU, C., ORDOVAS-MONTANES, J., ALVAREZ, D., HERBST, R. H., ZHANG, M., TIROSH, I., DIONNE, D., NGUYEN, L. T., XIFARAS, M. E., SHALEK, A. K., VON ANDRIAN, U. H., GRAHAM, D. B., ROZENBLATT-ROSEN, O., SHI, H. N., KUCHROO, V., YILMAZ, O. H., REGEV, A. & XAVIER, R. J. 2018. T Helper Cell Cytokines Modulate Intestinal Stem Cell Renewal and Differentiation. *Cell,* 175**,** 1307-1320.e22.

BODEN, E. K., SHOWS, D. M., CHIOREAN, M. V. & LORD, J. D. 2018. Identification of candidate biomarkers associated with response to vedolizumab in inflammatory bowel disease. *Digestive diseases and sciences,* 63**,** 2419-2429.

BONAKDAR, M., CZUBA, L. C., HAN, G., ZHONG, G., LUONG, H., ISOHERRANEN, N. & VAISHNAVA, S. 2022. Gut commensals expand vitamin A metabolic capacity of the mammalian host. *Cell host & microbe,* 30**,** 1084-1092. e5.

BONFIGLIO, R., GALLI, F., VARANI, M., SCIMECA, M., BORRI, F., FAZI, S., CICCONI, R., MATTEI, M., CAMPAGNA, G., SCHöNBERGER, T., RAYMOND, E., WUNDER, A., SIGNORE, A. & BONANNO, E. 2021. Extensive Histopathological Characterization of Inflamed Bowel in the Dextran Sulfate Sodium Mouse Model with Emphasis on Clinically Relevant Biomarkers and Targets for Drug Development. *International Journal of Molecular Sciences,* 22**,** 2028.

BONNARDEL, J., T'JONCK, W., GAUBLOMME, D., BROWAEYS, R., SCOTT, C. L., MARTENS, L., VANNESTE, B., DE PRIJCK, S., NEDOSPASOV, S. A., KREMER, A., VAN HAMME, E., BORGHGRAEF, P., TOUSSAINT, W., DE BLESER, P., MANNAERTS, I., BESCHIN, A., VAN GRUNSVEN, L. A., LAMBRECHT, B. N., TAGHON, T., LIPPENS, S., ELEWAUT, D., SAEYS, Y. & GUILLIAMS, M. 2019. Stellate Cells, Hepatocytes, and Endothelial Cells Imprint the Kupffer Cell Identity on Monocytes Colonizing the Liver Macrophage Niche. *Immunity,* 51**,** 638-654.e9.

BOULARD, O., ASQUITH, M. J., POWRIE, F. & MALOY, K. J. 2010. TLR2-independent induction and regulation of chronic intestinal inflammation. *Eur J Immunol,* 40**,** 516-24.

BOUSKRA, D., BRéZILLON, C., BéRARD, M., WERTS, C., VARONA, R., BONECA, I. G. & EBERL, G. 2008. Lymphoid tissue genesis induced by commensals through NOD1 regulates intestinal homeostasis. *Nature,* 456**,** 507-510.

BRINKMAN, B. M., BECKER, A., AYISEH, R. B., HILDEBRAND, F., RAES, J., HUYS, G. & VANDENABEELE, P. 2013. Gut microbiota affects sensitivity to acute DSS-induced colitis independently of host genotype. *Inflammatory bowel diseases,* 19**,** 2560-2567.

BUETTNER, M. & LOCHNER, M. 2016. Development and function of secondary and tertiary lymphoid organs in the small intestine and the colon. *Frontiers in immunology,* 7**,** 214811.

BUJKO, A., ATLASY, N., LANDSVERK, O. J. B., RICHTER, L., YAQUB, S., HORNELAND, R., ØYEN, O., AANDAHL, E. M., AABAKKEN, L., STUNNENBERG, H. G., BæKKEVOLD, E. S. & JAHNSEN, F. L. 2017. Transcriptional and functional profiling defines human small intestinal macrophage subsets. *Journal of Experimental Medicine,* 215**,** 441-458.

BUONOCORE, S., AHERN, P. P., UHLIG, H. H., IVANOV, II, LITTMAN, D. R., MALOY, K. J. & POWRIE, F. 2010. Innate lymphoid cells drive interleukin-23-dependent innate intestinal pathology. *Nature,* 464**,** 1371-5.

BYLUND-FELLENIUS, A., LANDSTRöM, E., AXELSSON, L. & MIDTVEDT, T. 1994. Experimental colitis induced by dextran sulphate in normal and germfree mice. *Microbial ecology in health and disease,* 7**,** 207-215.

CABALLERO-FLORES, G., PICKARD, J. M. & NúñEZ, G. 2023. Microbiota-mediated colonization resistance: mechanisms and regulation. *Nature Reviews Microbiology,* 21**,** 347-360.

CABEZA-CABRERIZO, M., CARDOSO, A., MINUTTI, C. M., PEREIRA DA COSTA, M. & REIS E SOUSA, C. 2021. Dendritic cells revisited. *Annual review of immunology,* 39**,** 131-166.

CAHENZLI, J., KöLLER, Y., WYSS, M., GEUKING, M. B. & MCCOY, K. D. 2013. Intestinal microbial diversity during early-life colonization shapes long-term IgE levels. *Cell host & microbe,* 14**,** 559-570.

CAHILL, R. J., FOLTZ, C. J., FOX, J. G., DANGLER, C. A., POWRIE, F. & SCHAUER, D. B. 1997. Inflammatory bowel disease: an immunity-mediated condition triggered by bacterial infection with Helicobacter hepaticus. *Infect Immun,* 65**,** 3126-31.

CAINES, J. K., BARNES, D. A. & BERRY, M. D. 2022. The use of seahorse XF assays to interrogate real-time energy metabolism in cancer cell lines. *Cancer Cell Biology: Methods and Protocols*. Springer.

CAMILLERI, M. 2019. Leaky gut: mechanisms, measurement and clinical implications in humans. *Gut,* 68**,** 1516-1526.

CARIO, E. 2008. Barrier-protective function of intestinal epithelial Toll-like receptor 2. *Mucosal Immunol,* 1 Suppl 1**,** S62-6.

CARIO, E., GERKEN, G. & PODOLSKY, D. 2007. Toll-like receptor 2 controls mucosal inflammation by regulating epithelial barrier function. *Gastroenterology,* 132**,** 1359-1374.

CARUSO, R., ONO, M., BUNKER, M. E., NúñEZ, G. & INOHARA, N. 2019. Dynamic and asymmetric changes of the microbial communities after cohousing in laboratory mice. *Cell Reports,* 27**,** 3401-3412. e3.

CASTILLO-AZOFEIFA, D., FAZIO, E. N., NATTIV, R., GOOD, H. J., WALD, T., PEST, M. A., DE SAUVAGE, F. J., KLEIN, O. D. & ASFAHA, S. 2019. Atoh1+ secretory progenitors possess renewal capacity independent of Lgr5+ cells during colonic regeneration. *The EMBO journal,* 38**,** e99984.

CHAN, V., CROCETTI, G., GREHAN, M., ZHANG, L., DANON, S., LEE, A. & MITCHELL, H. 2005. Visualization of Helicobacter species within the murine cecal mucosa using specific fluorescence in situ hybridization. *Helicobacter,* 10**,** 114-24.

CHANG, P. V., HAO, L., OFFERMANNS, S. & MEDZHITOV, R. 2014. The microbial metabolite butyrate regulates intestinal macrophage function via histone deacetylase inhibition. *Proceedings of the National Academy of Sciences,* 111**,** 2247-2252.

CHAOUCHE-DRIDER, N., KAPARAKIS, M., KARRAR, A., FERNANDEZ, M.-I., CARNEIRO, L. A., VIALA, J., BONECA, I. G., MORAN, A. P., PHILPOTT, D. J. & FERRERO, R. L. 2009. A commensal Helicobacter sp. of the rodent intestinal flora activates TLR2 and NOD1 responses in epithelial cells. *PLoS One,* 4**,** e5396.

CHEN, Z., QIU, X. & GU, J. 2009. Immunoglobulin expression in non-lymphoid lineage and neoplastic cells. *The American journal of pathology,* 174**,** 1139-1148.

CHOW, J. & MAZMANIAN, S. K. 2010. A pathobiont of the microbiota balances host colonization and intestinal inflammation. *Cell host & microbe,* 7**,** 265-276.

CHOW, J., TANG, H. & MAZMANIAN, S. K. 2011. Pathobionts of the gastrointestinal microbiota and inflammatory disease. *Current opinion in immunology,* 23**,** 473-480.

CHU, VAN T., BELLER, A., RAUSCH, S., STRANDMARK, J., ZäNKER, M., ARBACH, O., KRUGLOV, A. & BEREK, C. 2014. Eosinophils Promote Generation and Maintenance of Immunoglobulin-A-Expressing Plasma Cells and Contribute to Gut Immune Homeostasis. *Immunity,* 40**,** 582-593.

CLARKE, L. L. 2009. A guide to Ussing chamber studies of mouse intestine. *Am J Physiol Gastrointest Liver Physiol,* 296**,** G1151-66.

CLARKE, T. B., DAVIS, K. M., LYSENKO, E. S., ZHOU, A. Y., YU, Y. & WEISER, J. N. 2010. Recognition of peptidoglycan from the microbiota by Nod1 enhances systemic innate immunity. *Nat Med,* 16**,** 228-31.

CO, J. Y., MARGALEF-CATALà, M., MONACK, D. M. & AMIEVA, M. R. 2021. Controlling the polarity of human gastrointestinal organoids to investigate epithelial biology and infectious diseases. *Nature protocols,* 16**,** 5171-5192.

COCCIA, M., HARRISON, O. J., SCHIERING, C., ASQUITH, M. J., BECHER, B., POWRIE, F. & MALOY, K. J. 2012. IL-1beta mediates chronic intestinal inflammation by promoting the accumulation of IL-17A secreting innate lymphoid cells and CD4(+) Th17 cells. *J Exp Med,* 209**,** 1595-609.

COLE, J. J., FAYDACI, B. A., MCGUINNESS, D., SHAW, R., MACIEWICZ, R. A., ROBERTSON, N. A. & GOODYEAR, C. S. 2021. Searchlight: automated bulk RNA-seq exploration and visualisation using dynamically generated R scripts. *BMC bioinformatics,* 22**,** 1-21.

COLLINS, N. & BELKAID, Y. 2018. Do the microbiota influence vaccines and protective immunity to pathogens? Engaging our endogenous adjuvants. *Cold Spring Harbor perspectives in biology,* 10**,** a028860.

CORBIN, A. L., GOMEZ-VAZQUEZ, M., BERTHOLD, D. L., ATTAR, M., ARNOLD, I. C., POWRIE, F. M., SANSOM, S. N. & UDALOVA, I. A. 2020. IRF5 guides monocytes

toward an inflammatory CD11c+ macrophage phenotype and promotes intestinal inflammation. *Science immunology,* 5**,** eaax6085.

CUA, D. J., SHERLOCK, J., CHEN, Y., MURPHY, C. A., JOYCE, B., SEYMOUR, B., LUCIAN, L., TO, W., KWAN, S., CHURAKOVA, T., ZURAWSKI, S., WIEKOWSKI, M., LIRA, S. A., GORMAN, D., KASTELEIN, R. A. & SEDGWICK, J. D. 2003. Interleukin-23 rather than interleukin-12 is the critical cytokine for autoimmune inflammation of the brain. *Nature,* 421**,** 744-748.

CUMMINGS, R. J., BARBET, G., BONGERS, G., HARTMANN, B. M., GETTLER, K., MUNIZ, L., FURTADO, G. C., CHO, J., LIRA, S. A. & BLANDER, J. M. 2016. Different tissue phagocytes sample apoptotic cells to direct distinct homeostasis programs. *Nature,* 539**,** 565-569.

CURTSINGER, J. M., LINS, D. C. & MESCHER, M. F. 2003. Signal 3 determines tolerance versus full activation of naive CD8 T cells: dissociating proliferation and development of effector function. *The Journal of experimental medicine,* 197**,** 1141-1151.

D'HAENS, G., PANACCIONE, R., BAERT, F., BOSSUYT, P., COLOMBEL, J.-F., DANESE, S., DUBINSKY, M., FEAGAN, B. G., HISAMATSU, T., LIM, A., LINDSAY, J. O., LOFTUS, E. V., JR., PANéS, J., PEYRIN-BIROULET, L., RAN, Z., RUBIN, D. T., SANDBORN, W. J., SCHREIBER, S., NEIMARK, E., SONG, A., KLIGYS, K., PANG, Y., PIVORUNAS, V., BERG, S., DUAN, W. R., HUANG, B., KALABIC, J., LIAO, X., ROBINSON, A., WALLACE, K. & FERRANTE, M. 2022. Risankizumab as induction therapy for Crohn's disease: results from the phase 3 ADVANCE and MOTIVATE induction trials. *The Lancet,* 399**,** 2015-2030.

DANESE, S., VUITTON, L. & PEYRIN-BIROULET, L. 2015. Biologic agents for IBD: practical insights. *Nature reviews Gastroenterology & hepatology,* 12**,** 537-545.

DANNE, C., RYZHAKOV, G., MARTíNEZ-LóPEZ, M., ILOTT, N. E., FRANCHINI, F., CUSKIN, F., LOWE, E. C., BULLERS, S. J., ARTHUR, J. S. C. & POWRIE, F. 2017. A large polysaccharide produced by Helicobacter hepaticus induces an anti-inflammatory gene signature in macrophages. *Cell host & microbe,* 22**,** 733-745. e5.

DARFEUILLE-MICHAUD, A., NEUT, C., BARNICH, N., LEDERMAN, E., DI MARTINO, P., DESREUMAUX, P., GAMBIEZ, L., JOLY, B., CORTOT, A. & COLOMBEL, J.-F. 1998. Presence of adherent Escherichia coli strains in ileal mucosa of patients with Crohn's disease. *Gastroenterology,* 115**,** 1405-1413.

DAVIS, B. K., PHILIPSON, C., HONTECILLAS, R., EDEN, K., BASSAGANYA-RIERA, J. & ALLEN, I. C. 2014. Emerging significance of NLRs in inflammatory bowel disease. *Inflammatory bowel diseases,* 20**,** 2412-2432.

DE LAFAILLE, M. A. C. & LAFAILLE, J. J. 2009. Natural and adaptive foxp3+ regulatory T cells: more of the same or a division of labor? *Immunity,* 30**,** 626-635.

DEGIRMENCI, B., VALENTA, T., DIMITRIEVA, S., HAUSMANN, G. & BASLER, K. 2018. GLI1-expressing mesenchymal cells form the essential Wnt-secreting niche for colon stem cells. *Nature,* 558**,** 449-453.

DESALEGN, G. & PABST, O. 2019. Inflammation triggers immediate rather than progressive changes in monocyte differentiation in the small intestine. *Nature communications,* 10**,** 3229.

DESHMUKH, H. S., LIU, Y., MENKITI, O. R., MEI, J., DAI, N., O'LEARY, C. E., OLIVER, P. M., KOLLS, J. K., WEISER, J. N. & WORTHEN, G. S. 2014. The microbiota regulates neutrophil homeostasis and host resistance to Escherichia coli K1 sepsis in neonatal mice. *Nature medicine,* 20**,** 524-530.

DIELEMAN, L. A., RIDWAN, B. U., TENNYSON, G. S., BEAGLEY, K. W., BUCY, R. P. & ELSON, C. O. 1994. Dextran sulfate sodium-induced colitis occurs in severe combined immunodeficient mice. *Gastroenterology,* 107**,** 1643-1652.

DOONAN, J., TARAFDAR, A., PINEDA, M. A., LUMB, F. E., CROWE, J., KHAN, A. M., HOSKISSON, P. A., HARNETT, M. M. & HARNETT, W. 2019. The parasitic worm product ES-62 normalises the gut microbiota bone marrow axis in inflammatory arthritis. *Nature communications,* 10**,** 1554.

DRUREY, C., LINDHOLM, H. T., COAKLEY, G., POVEDA, M. C., LöSER, S., DOOLAN, R., GERBE, F., JAY, P., HARRIS, N., OUDHOFF, M. J. & MAIZELS, R. M. 2021. Intestinal epithelial tuft cell induction is negated by a murine helminth and its secreted products. *Journal of Experimental Medicine,* 219**,** e20211140.

DU, Y., ZHANG, H., GUO, Y., SONG, K., ZENG, L., CHEN, Y., XIE, Z. & LI, R. 2021. CD38 deficiency up-regulated IL-1β and MCP-1 through TLR4/ERK/NF-κB pathway in sepsis pulmonary injury. *Microbes and Infection***,** 104845.

DURAND, A., DONAHUE, B., PEIGNON, G., LETOURNEUR, F., CAGNARD, N., SLOMIANNY, C., PERRET, C., SHROYER, N. F. & ROMAGNOLO, B. 2012. Functional intestinal stem cells after Paneth cell ablation induced by the loss of transcription factor Math1 (Atoh1). *Proceedings of the National Academy of Sciences,* 109**,** 8965-8970.

DUTTA, S. & SENGUPTA, P. 2016. Men and mice: relating their ages. *Life sciences,* 152**,** 244-248.

EICHELE, D. D. & KHARBANDA, K. K. 2017. Dextran sodium sulfate colitis murine model: An indispensable tool for advancing our understanding of inflammatory bowel diseases pathogenesis. *World journal of gastroenterology,* 23**,** 6016.

EKEN, A., SINGH, A. K., TREUTING, P. M. & OUKKA, M. 2014. IL-23R+ innate lymphoid cells induce colitis via interleukin-22-dependent mechanism. *Mucosal Immunol,* 7**,** 143-54.

ELTAI, N. O., AL THANI, A. A., AL HADIDI, S. H., AL ANSARI, K. & YASSINE, H. M. 2020. Antibiotic resistance and virulence patterns of pathogenic Escherichia coli strains associated with acute gastroenteritis among children in Qatar. *BMC microbiology,* 20**,** 1-12.

ENGELSTOFT, M. S., LUND, M. L., GRUNDDAL, K. V., EGEROD, K. L., OSBORNE-LAWRENCE, S., POULSEN, S. S., ZIGMAN, J. M. & SCHWARTZ, T. W. 2015. Research resource: a chromogranin A reporter for serotonin and histamine secreting enteroendocrine cells. *Molecular Endocrinology,* 29**,** 1658-1671.

ERICKSON, A. R., CANTAREL, B. L., LAMENDELLA, R., DARZI, Y., MONGODIN, E. F., PAN, C., SHAH, M., HALFVARSON, J., TYSK, C., HENRISSAT, B., RAES, J., VERBERKMOES, N. C., FRASER, C. M., HETTICH, R. L. & JANSSON, J. K. 2012. Integrated metagenomics/metaproteomics reveals human host-microbiota signatures of Crohn's disease. *PLoS One,* 7**,** e49138.

ERőSS, B., FARKAS, N., VINCZE, Á., TINUSZ, B., SZAPáRY, L., GARAMI, A., BALASKó, M., SARLóS, P., CZOPF, L., ALIZADEH, H., RAKONCZAY, Z., JR., HABON, T. & HEGYI, P. 2018. Helicobacter pylori infection reduces the risk of Barrett's esophagus: A meta-analysis and systematic review. *Helicobacter,* 23**,** e12504.

ERRICO, A. 2015. PD-1–PD-L1 axis: efficient checkpoint blockade against cancer. *Nature reviews Clinical oncology,* 12**,** 63-63.

EVANS, D., PYE, G., BRAMLEY, R., CLARK, A., DYSON, T. & HARDCASTLE, J. 1988. Measurement of gastrointestinal pH profiles in normal ambulant human subjects. *Gut,* 29**,** 1035-1041.

FALLEGGER, A., PRIOLA, M., ARTOLA-BORáN, M., NúñEZ, N. G., WILD, S., GURTNER, A., BECHER, B., YOUSEFI, S., SIMON, H.-U., ARNOLD, I. C. & MüLLER, A. 2022. TGF-β production by eosinophils drives the expansion of peripherally induced neuropilin− RORγt+ regulatory T-cells during bacterial and allergen challenge. *Mucosal Immunology,* 15**,** 504-514.

FAN, Y.-Y., DAVIDSON, L. A. & CHAPKIN, R. S. 2016. Murine colonic organoid culture system and downstream assay applications. *Organoids*. Springer.

FANG, F. C. 1997. Perspectives series: host/pathogen interactions. Mechanisms of nitric oxide-related antimicrobial activity. *The Journal of clinical investigation,* 99**,** 2818-2825.

FEAGAN, B. G., SANDBORN, W. J., GASINK, C., JACOBSTEIN, D., LANG, Y., FRIEDMAN, J. R., BLANK, M. A., JOHANNS, J., GAO, L. L., MIAO, Y., ADEDOKUN, O. J., SANDS, B. E., HANAUER, S. B., VERMEIRE, S., TARGAN, S., GHOSH, S., DE VILLIERS, W. J., COLOMBEL, J. F., TULASSAY, Z., SEIDLER, U., SALZBERG, B. A., DESREUMAUX, P., LEE, S. D., LOFTUS, E. V., JR., DIELEMAN, L. A., KATZ, S. & RUTGEERTS, P. 2016. Ustekinumab as Induction and Maintenance Therapy for Crohn's Disease. *N Engl J Med,* 375**,** 1946-1960.

FENG, S., KU, K., HODZIC, E., LORENZANA, E., FREET, K. & BARTHOLD, S. W. 2005. Differential detection of five mouse-infecting helicobacter species by multiplex PCR. *Clinical and Vaccine Immunology,* 12**,** 531-536.

FLANNAGAN, R. S., COSíO, G. & GRINSTEIN, S. 2009. Antimicrobial mechanisms of phagocytes and bacterial evasion strategies. *Nature Reviews Microbiology,* 7**,** 355-366.

FOLTZ, C. J., FOX, J. G., CAHILL, R., MURPHY, J. C., YAN, L., SHAMES, B. & SCHAUER, D. B. 1998. Spontaneous inflammatory bowel disease in multiple mutant mouse lines: association with colonization by Helicobacter hepaticus. *Helicobacter,* 3**,** 69-78.

FORSTER, S. C., CLARE, S., BERESFORD-JONES, B. S., HARCOURT, K., NOTLEY, G., STARES, M. D., KUMAR, N., SODERHOLM, A. T., ADOUM, A., WONG, H., MORóN, B., BRANDT, C., DOUGAN, G., ADAMS, D. J., MALOY, K. J., PEDICORD, V. A. & LAWLEY, T. D. 2022. Identification of gut microbial species linked with disease variability in a widely used mouse model of colitis. *Nature microbiology,* 7**,** 590-599.

FOURNIER, B. & PARKOS, C. 2012. The role of neutrophils during intestinal inflammation. *Mucosal immunology,* 5**,** 354-366.

FOX, J., DEWHIRST, F., TULLY, J., PASTER, B., YAN, L., TAYLOR, N., COLLINS JR, M., GORELICK, P. & WARD, J. 1994. Helicobacter hepaticus sp. nov., a microaerophilic bacterium isolated from livers and intestinal mucosal scrapings from mice. *Journal of clinical microbiology,* 32**,** 1238-1245.

FOX, J., LI, X., YAN, L., CAHILL, R., HURLEY, R., LEWIS, R. & MURPHY, J. 1996. Chronic proliferative hepatitis in A/JCr mice associated with persistent Helicobacter hepaticus infection: a model of helicobacter-induced carcinogenesis. *Infection and immunity,* 64**,** 1548-1558.

FOX, J. G., GE, Z., WHARY, M. T., ERDMAN, S. E. & HORWITZ, B. H. 2011. Helicobacter hepaticus infection in mice: models for understanding lower bowel inflammation and cancer. *Mucosal immunology,* 4**,** 22-30.

FRANK, D. N., ST. AMAND, A. L., FELDMAN, R. A., BOEDEKER, E. C., HARPAZ, N. & PACE, N. R. 2007. Molecular-phylogenetic characterization of microbial community imbalances in human inflammatory bowel diseases. *Proceedings of the national academy of sciences,* 104**,** 13780-13785.

FRANKE, A., BALSCHUN, T., KARLSEN, T. H., SVENTORAITYTE, J., NIKOLAUS, S., MAYR, G., DOMINGUES, F. S., ALBRECHT, M., NOTHNAGEL, M., ELLINGHAUS, D., SINA, C., ONNIE, C. M., WEERSMA, R. K., STOKKERS, P. C., WIJMENGA, C., GAZOULI, M., STRACHAN, D., MCARDLE, W. L., VERMEIRE, S., RUTGEERTS, P., ROSENSTIEL, P., KRAWCZAK, M., VATN, M. H., MATHEW, C. G. & SCHREIBER, S. 2008. Sequence variants in IL10, ARPC2 and multiple other loci contribute to ulcerative colitis susceptibility. *Nat Genet,* 40**,** 1319-23.

FRANKE, A., MCGOVERN, D. P., BARRETT, J. C., WANG, K., RADFORD-SMITH, G. L., AHMAD, T., LEES, C. W., BALSCHUN, T., LEE, J., ROBERTS, R., ANDERSON, C. A., BIS, J. C., BUMPSTEAD, S., ELLINGHAUS, D., FESTEN, E. M., GEORGES, M., GREEN, T., HARITUNIANS, T., JOSTINS, L., LATIANO, A., MATHEW, C. G., MONTGOMERY, G. W., PRESCOTT, N. J., RAYCHAUDHURI, S., ROTTER, J. I., SCHUMM, P., SHARMA, Y., SIMMS, L. A., TAYLOR, K. D., WHITEMAN, D., WIJMENGA, C., BALDASSANO, R. N., BARCLAY, M., BAYLESS, T. M., BRAND, S., BüNING, C., COHEN, A., COLOMBEL, J. F., COTTONE, M., STRONATI, L., DENSON, T., DE VOS, M., D'INCA, R., DUBINSKY, M., EDWARDS, C., FLORIN, T., FRANCHIMONT, D., GEARRY, R., GLAS, J., VAN GOSSUM, A., GUTHERY, S. L., HALFVARSON, J., VERSPAGET, H. W., HUGOT, J. P., KARBAN, A., LAUKENS, D., LAWRANCE, I., LEMANN, M., LEVINE, A., LIBIOULLE, C., LOUIS, E., MOWAT, C., NEWMAN, W., PANéS, J., PHILLIPS, A., PROCTOR, D. D., REGUEIRO, M., RUSSELL, R., RUTGEERTS, P., SANDERSON, J., SANS, M., SEIBOLD, F., STEINHART, A. H., STOKKERS, P. C., TORKVIST, L., KULLAK-UBLICK, G., WILSON, D., WALTERS, T., TARGAN, S. R., BRANT, S. R., RIOUX, J. D., D'AMATO, M., WEERSMA, R. K., KUGATHASAN, S., GRIFFITHS, A. M., MANSFIELD, J. C., VERMEIRE, S., DUERR, R. H., SILVERBERG, M. S., SATSANGI, J., SCHREIBER, S., CHO, J. H., ANNESE, V., HAKONARSON, H., DALY, M. J. & PARKES, M. 2010. Genome-wide meta-analysis increases to 71 the number of confirmed Crohn's disease susceptibility loci. *Nat Genet,* 42**,** 1118-25.

FRIEDRICH, C., MAMARELI, P., THIEMANN, S., KRUSE, F., WANG, Z., HOLZMANN, B., STROWIG, T., SPARWASSER, T. & LOCHNER, M. 2017. MyD88 signaling in dendritic cells and the intestinal epithelium controls immunity against intestinal infection with C. rodentium. *PLoS pathogens,* 13**,** e1006357.

FRIEDRICH, M., POHIN, M. & POWRIE, F. 2019. Cytokine networks in the pathophysiology of inflammatory bowel disease. *Immunity,* 50**,** 992-1006.

FUJINO, S., ANDOH, A., BAMBA, S., OGAWA, A., HATA, K., ARAKI, Y., BAMBA, T. & FUJIYAMA, Y. 2003. Increased expression of interleukin 17 in inflammatory bowel disease. *Gut,* 52**,** 65-70.

FUKATA, M. & ARDITI, M. 2013. The role of pattern recognition receptors in intestinal inflammation. *Mucosal immunology,* 6**,** 451-463.

FUKATA, M., MICHELSEN, K. S., ERI, R., THOMAS, L. S., HU, B., LUKASEK, K., NAST, C. C., LECHAGO, J., XU, R., NAIKI, Y., SOLIMAN, A., ARDITI, M. & ABREU, M. T. 2005. Toll-like receptor-4 is required for intestinal response to epithelial injury and limiting bacterial translocation in a murine model of acute colitis. *Am J Physiol Gastrointest Liver Physiol,* 288**,** G1055-65.

FURUSAWA, Y., OBATA, Y., FUKUDA, S., ENDO, T. A., NAKATO, G., TAKAHASHI, D., NAKANISHI, Y., UETAKE, C., KATO, K., KATO, T., TAKAHASHI, M., FUKUDA, N. N., MURAKAMI, S., MIYAUCHI, E., HINO, S., ATARASHI, K., ONAWA, S., FUJIMURA, Y., LOCKETT, T., CLARKE, J. M., TOPPING, D. L., TOMITA, M., HORI, S., OHARA, O., MORITA, T., KOSEKI, H., KIKUCHI, J., HONDA, K., HASE, K. & OHNO, H. 2013. Commensal microbe-derived butyrate induces the differentiation of colonic regulatory T cells. *Nature,* 504**,** 446-50.

GALLO, R. L. & HOOPER, L. V. 2012. Epithelial antimicrobial defence of the skin and intestine. *Nature Reviews Immunology,* 12**,** 503-516.

GARCIA-VILLATORO, E. L., UFONDU, A., CALLAWAY, E. S., ALLRED, K., SAFE, S. H., CHAPKIN, R. S., JAYARAMAN, A. & ALLRED, C. D. 2024. Aryl Hydrocarbon Receptor Activity in Intestinal Epithelial Cells in the Formation of Colonic Tertiary Lymphoid Tissues. *American Journal of Physiology-Gastrointestinal and Liver Physiology*.

GE, Z., WHITE, D. A., WHARY, M. T. & FOX, J. G. 2001. Fluorogenic PCR-based quantitative detection of a murine pathogen, Helicobacter hepaticus. *Journal of Clinical Microbiology,* 39**,** 2598-2602.

GEISLER, C., LARSEN, J. & PLESNER, T. 1988. Identification of αß and γδ T Cell Receptor-Positive Cells. *Scandinavian journal of immunology,* 28**,** 741-745.

GENSOLLEN, T., IYER, S. S., KASPER, D. L. & BLUMBERG, R. S. 2016. How colonization by microbiota in early life shapes the immune system. *Science,* 352**,** 539-544.

GERASIMIDIS, K., BERTZ, M., HANSKE, L., JUNICK, J., BISKOU, O., AGUILERA, M., GARRICK, V., RUSSELL, R. K., BLAUT, M., MCGROGAN, P. & EDWARDS, C. A. 2014. Decline in presumptively protective gut bacterial species and metabolites are paradoxically associated with disease improvement in pediatric Crohn's disease during enteral nutrition. *Inflamm Bowel Dis,* 20**,** 861-71.

GERBE, F., SIDOT, E., SMYTH, D. J., OHMOTO, M., MATSUMOTO, I., DARDALHON, V., CESSES, P., GARNIER, L., POUZOLLES, M., BRULIN, B., BRUSCHI, M., HARCUS, Y., ZIMMERMANN, V. S., TAYLOR, N., MAIZELS, R. M. & JAY, P. 2016. Intestinal epithelial tuft cells initiate type 2 mucosal immunity to helminth parasites. *Nature,* 529**,** 226-30.

GERMAIN, R. N. 1994. MHC-dependent antigen processing and peptide presentation: providing ligands for T lymphocyte activation. *Cell,* 76**,** 287-299.

GERMAIN, R. N. 2002. T-cell development and the CD4–CD8 lineage decision. *Nature reviews immunology,* 2**,** 309-322.

GEVERS, D., KUGATHASAN, S., DENSON, L. A., VáZQUEZ-BAEZA, Y., VAN TREUREN, W., REN, B., SCHWAGER, E., KNIGHTS, D., SONG, S. J., YASSOUR, M., MORGAN, X. C., KOSTIC, A. D., LUO, C., GONZáLEZ, A., MCDONALD, D., HABERMAN, Y., WALTERS, T., BAKER, S., ROSH, J., STEPHENS, M., HEYMAN, M., MARKOWITZ, J., BALDASSANO, R., GRIFFITHS, A., SYLVESTER, F., MACK, D., KIM, S., CRANDALL, W., HYAMS, J., HUTTENHOWER, C., KNIGHT, R. & XAVIER, R. J. 2014. The treatment-naive microbiome in new-onset Crohn's disease. *Cell Host Microbe,* 15**,** 382-392.

GILBERT, J. A., QUINN, R. A., DEBELIUS, J., XU, Z. Z., MORTON, J., GARG, N., JANSSON, J. K., DORRESTEIN, P. C. & KNIGHT, R. 2016. Microbiome-wide

association studies link dynamic microbial consortia to disease. *Nature,* 535**,** 94-103.

GIRARDIN, S. E., BONECA, I. G., VIALA, J., CHAMAILLARD, M., LABIGNE, A., THOMAS, G., PHILPOTT, D. J. & SANSONETTI, P. J. 2003. Nod2 is a general sensor of peptidoglycan through muramyl dipeptide (MDP) detection. *Journal of Biological Chemistry,* 278**,** 8869-8872.

GOLLWITZER, E. S. & MARSLAND, B. J. 2015. Impact of early-life exposures on immune maturation and susceptibility to disease. *Trends in immunology,* 36**,** 684-696.

GOMES-NETO, J. C., KITTANA, H., MANTZ, S., SEGURA MUNOZ, R. R., SCHMALTZ, R. J., BINDELS, L. B., CLARKE, J., HOSTETTER, J. M., BENSON, A. K., WALTER, J. & RAMER-TAIT, A. E. 2017. A gut pathobiont synergizes with the microbiota to instigate inflammatory disease marked by immunoreactivity against other symbionts but not itself. *Sci Rep,* 7**,** 17707.

GOTO, Y., PANEA, C., NAKATO, G., CEBULA, A., LEE, C., DIEZ, M. G., LAUFER, T. M., IGNATOWICZ, L. & IVANOV, I. I. 2014. Segmented filamentous bacteria antigens presented by intestinal dendritic cells drive mucosal Th17 cell differentiation. *Immunity,* 40**,** 594-607.

GRAINGER, J. R., WOHLFERT, E. A., FUSS, I. J., BOULADOUX, N., ASKENASE, M. H., LEGRAND, F., KOO, L. Y., BRENCHLEY, J. M., FRASER, I. D. & BELKAID, Y. 2013. Inflammatory monocytes regulate pathologic responses to commensals during acute gastrointestinal infection. *Nature medicine,* 19**,** 713-721.

GU, S., CHEN, D., ZHANG, J.-N., LV, X., WANG, K., DUAN, L.-P., NIE, Y. & WU, X.-L. 2013. Bacterial community mapping of the mouse gastrointestinal tract. *PloS one,* 8**,** e74957.

GU, Y., BARTOLOMé-CASADO, R., XU, C., BERTOCCHI, A., JANNEY, A., HEUBERGER, C., PEARSON, C. F., TEICHMANN, S. A., THORNTON, E. E. & POWRIE, F. 2024. Immune microniches shape intestinal Treg function. *Nature***,** 1-9.

GUO, X., OU, J., LIANG, S., ZHOU, X. & HU, X. 2018. Epithelial Hes1 maintains gut homeostasis by preventing microbial dysbiosis. *Mucosal immunology,* 11**,** 716-726.

GURTNER, A., BORRELLI, C., GONZALEZ-PEREZ, I., BACH, K., ACAR, I. E., NúñEZ, N. G., CREPAZ, D., HANDLER, K., VU, V. P., LAFZI, A., STIRM, K., RAJU, D., GSCHWEND, J., BASLER, K., SCHNEIDER, C., SLACK, E., VALENTA, T., BECHER, B., KREBS, P., MOOR, A. E. & ARNOLD, I. C. 2023. Active eosinophils regulate host defence and immune responses in colitis. *Nature,* 615**,** 151-157.

GUTIéRREZ, A., FRANCéS, R., AMORóS, A., ZAPATER, P., GARMENDIA, M., NDONGO, M., CAñO, R., JOVER, R., SUCH, J. & PéREZ-MATEO, M. 2009. Cytokine

association with bacterial DNA in serum of patients with inflammatory bowel disease. *Inflammatory bowel diseases,* 15**,** 508-514.

GUTIéRREZ, A., ZAPATER, P., JUANOLA, O., SEMPERE, L., GARCíA, M., LAVEDA, R., MARTíNEZ, A., SCHARL, M., GONZáLEZ-NAVAJAS, J. M., SUCH, J., WIEST, R., ROGLER, G. & FRANCéS, R. 2016. Gut Bacterial DNA Translocation is an Independent Risk Factor of Flare at Short Term in Patients With Crohn's Disease. *Am J Gastroenterol,* 111**,** 529-40.

HABER, A. L., BITON, M., ROGEL, N., HERBST, R. H., SHEKHAR, K., SMILLIE, C., BURGIN, G., DELOREY, T. M., HOWITT, M. R., KATZ, Y., TIROSH, I., BEYAZ, S., DIONNE, D., ZHANG, M., RAYCHOWDHURY, R., GARRETT, W. S., ROZENBLATT-ROSEN, O., SHI, H. N., YILMAZ, O., XAVIER, R. J. & REGEV, A. 2017. A single-cell survey of the small intestinal epithelium. *Nature,* 551**,** 333-339.

HåKANSSON, Å., TORMO-BADIA, N., BARIDI, A., XU, J., MOLIN, G., HAGSLäTT, M.-L., KARLSSON, C., JEPPSSON, B., CILIO, C. & AHRNé, S. 2015. Immunological alteration and changes of gut microbiota after dextran sulfate sodium (DSS) administration in mice. *Clinical and experimental medicine,* 15**,** 107-120.

HALLIDAY, N., WILLIAMS, C., KENNEDY, A., WATERS, E., PESENACKER, A. M., SOSKIC, B., HINZE, C., HOU, T. Z., ROWSHANRAVAN, B., JANMAN, D., WALKER, L. S. K. & SANSOM, D. M. 2020. CD86 Is a Selective CD28 Ligand Supporting FoxP3+ Regulatory T Cell Homeostasis in the Presence of High Levels of CTLA-4. *Front Immunol,* 11**,** 600000.

HAMADA, T., YOKOTA, K., AYADA, K., HIRAI, K., KAMADA, T., HARUMA, K., CHAYAMA, K. & OGUMA, K. 2009. Detection of Helicobacter hepaticus in human bile samples of patients with biliary disease. *Helicobacter,* 14**,** 545-551.

HAMILTON, S. E., BADOVINAC, V. P., BEURA, L. K., PIERSON, M., JAMESON, S. C., MASOPUST, D. & GRIFFITH, T. S. 2020. New insights into the immune system using dirty mice. *The Journal of Immunology,* 205**,** 3-11.

HAND, T. W., DOS SANTOS, L. M., BOULADOUX, N., MOLLOY, M. J., PAGáN, A. J., PEPPER, M., MAYNARD, C. L., ELSON III, C. O. & BELKAID, Y. 2012. Acute gastrointestinal infection induces long-lived microbiota-specific T cell responses. *Science,* 337**,** 1553-1556.

HARTLEY, G. P., CHOW, L., AMMONS, D. T., WHEAT, W. H. & DOW, S. W. 2018. Programmed cell death ligand 1 (PD-L1) signaling regulates macrophage proliferation and activation. *Cancer immunology research,* 6**,** 1260-1273.

HARTOG, A., BELLE, F. N., BASTIAANS, J., DE GRAAFF, P., GARSSEN, J., HARTHOORN, L. F. & VOS, A. P. 2015. A potential role for regulatory T-cells in the amelioration of DSS induced colitis by dietary non-digestible polysaccharides. *The Journal of Nutritional Biochemistry,* 26**,** 227-233.

HASEGAWA, M., FUJIMOTO, Y., LUCAS, P. C., NAKANO, H., FUKASE, K., NúñEZ, G. & INOHARA, N. 2008. A critical role of RICK/RIP2 polyubiquitination in Nod-induced NF-κB activation. *The EMBO journal,* 27**,** 373-383.

HAUSMANN, M., KIESSLING, S., MESTERMANN, S., WEBB, G., SPöTTL, T., ANDUS, T., SCHöLMERICH, J., HERFARTH, H., RAY, K., FALK, W. & ROGLER, G. 2002. Toll-like receptors 2 and 4 are up-regulated during intestinal inflammation. *Gastroenterology,* 122**,** 1987-2000.

HE, W., WANG, M.-L., JIANG, H.-Q., STEPPAN, C. M., SHIN, M. E., THURNHEER, M. C., CEBRA, J. J., LAZAR, M. A. & WU, G. D. 2003. Bacterial colonization leads to the colonic secretion of RELMβ/FIZZ2, a novel goblet cell-specific protein. *Gastroenterology,* 125**,** 1388-1397.

HEGAZY, A. N., WEST, N. R., STUBBINGTON, M. J. T., WENDT, E., SUIJKER, K. I. M., DATSI, A., THIS, S., DANNE, C., CAMPION, S., DUNCAN, S. H., OWENS, B. M. J., UHLIG, H. H., MCMICHAEL, A., BERGTHALER, A., TEICHMANN, S. A., KESHAV, S. & POWRIE, F. 2017. Circulating and Tissue-Resident CD4(+) T Cells With Reactivity to Intestinal Microbiota Are Abundant in Healthy Individuals and Function Is Altered During Inflammation. *Gastroenterology,* 153**,** 1320-1337.e16.

HEIEIS, G. A., PATENTE, T. A., ALMEIDA, L., VRIELING, F., TAK, T., PERONA-WRIGHT, G., MAIZELS, R. M., STIENSTRA, R. & EVERTS, B. 2023. Metabolic heterogeneity of tissue-resident macrophages in homeostasis and during helminth infection. *Nature Communications,* 14**,** 5627.

HEIMESAAT, M. M., FISCHER, A., SIEGMUND, B., KUPZ, A., NIEBERGALL, J., FUCHS, D., JAHN, H. K., FREUDENBERG, M., LODDENKEMPER, C., BATRA, A., LEHR, H. A., LIESENFELD, O., BLAUT, M., GöBEL, U. B., SCHUMANN, R. R. & BERESWILL, S. 2007. Shift towards pro-inflammatory intestinal bacteria aggravates acute murine colitis via Toll-like receptors 2 and 4. *PLoS One,* 2**,** e662.

HELFT, J., BöTTCHER, J., CHAKRAVARTY, P., ZELENAY, S., HUOTARI, J., SCHRAML, B. U., GOUBAU, D. & E SOUSA, C. R. 2015. GM-CSF mouse bone marrow cultures comprise a heterogeneous population of CD11c+ MHCII+ macrophages and dendritic cells. *Immunity,* 42**,** 1197-1211.

HENRICK, B. M., RODRIGUEZ, L., LAKSHMIKANTH, T., POU, C., HENCKEL, E., ARZOOMAND, A., OLIN, A., WANG, J., MIKES, J., TAN, Z., CHEN, Y., EHRLICH, A. M., BERNHARDSSON, A. K., MUGABO, C. H., AMBROSIANI, Y., GUSTAFSSON, A., CHEW, S., BROWN, H. K., PRAMBS, J., BOHLIN, K., MITCHELL, R. D., UNDERWOOD, M. A., SMILOWITZ, J. T., GERMAN, J. B., FRESE, S. A. & BRODIN, P. 2021. Bifidobacteria-mediated immune system imprinting early in life. *Cell,* 184**,** 3884-3898.e11.

HERBST, T., SICHELSTIEL, A., SCHäR, C., YADAVA, K., BüRKI, K., CAHENZLI, J., MCCOY, K., MARSLAND, B. J. & HARRIS, N. L. 2011. Dysregulation of allergic airway inflammation in the absence of microbial colonization. *American journal of respiratory and critical care medicine,* 184**,** 198-205.

HERNáNDEZ-CHIRLAQUE, C., ARANDA, C. J., OCóN, B., CAPITáN-CAñADAS, F., ORTEGA-GONZáLEZ, M., CARRERO, J. J., SUáREZ, M. D., ZARZUELO, A., SáNCHEZ DE MEDINA, F. & MARTíNEZ-AUGUSTIN, O. 2016. Germ-free and Antibiotic-treated Mice are Highly Susceptible to Epithelial Injury in DSS Colitis. *Journal of Crohn's and Colitis,* 10**,** 1324-1335.

HERRE, J., GORDON, S. & BROWN, G. D. 2004. Dectin-1 and its role in the recognition of β-glucans by macrophages. *Molecular immunology,* 40**,** 869-876.

HEUBERGER, C. E., JANNEY, A., ILOTT, N., BERTOCCHI, A., POTT, S., GU, Y., POHIN, M., FRIEDRICH, M., MANN, E. H., PEARSON, C., POWRIE, F. M., POTT, J., THORNTON, E. & MALOY, K. J. 2024. MHC class II antigen presentation by intestinal epithelial cells fine-tunes bacteria-reactive CD4 T-cell responses. *Mucosal Immunol,* 17**,** 416-430.

HEYLEN, M., RUYSSERS, N. E., GIELIS, E. M., VANHOMWEGEN, E., PELCKMANS, P. A., MOREELS, T. G., DE MAN, J. G. & DE WINTER, B. Y. 2014. Of worms, mice and man: An overview of experimental and clinical helminth-based therapy for inflammatory bowel disease. *Pharmacology & Therapeutics,* 143**,** 153-167.

HILL, M. 1997. Intestinal flora and endogenous vitamin synthesis. *European Journal of Cancer Prevention,* 6**,** S43-S45.

HILLIGAN, K. L. & RONCHESE, F. 2020. Antigen presentation by dendritic cells and their instruction of CD4+ T helper cell responses. *Cellular & molecular immunology,* 17**,** 587-599.

HIROTA, K., DUARTE, J. H., VELDHOEN, M., HORNSBY, E., LI, Y., CUA, D. J., AHLFORS, H., WILHELM, C., TOLAINI, M., MENZEL, U., GAREFALAKI, A., POTOCNIK, A. J. & STOCKINGER, B. 2011. Fate mapping of IL-17-producing T cells in inflammatory responses. *Nat Immunol,* 12**,** 255-63.

HOFFMANN, C., HILL, D. A., MINKAH, N., KIRN, T., TROY, A., ARTIS, D. & BUSHMAN, F. 2009. Community-wide response of the gut microbiota to enteropathogenic Citrobacter rodentium infection revealed by deep sequencing. *Infection and immunity,* 77**,** 4668-4678.

HOOPER, L. V., LITTMAN, D. R. & MACPHERSON, A. J. 2012. Interactions between the microbiota and the immune system. *science,* 336**,** 1268-1273.

HOUOT, R., PERROT, I., GARCIA, E., DURAND, I. & LEBECQUE, S. 2006. Human CD4+ CD25high regulatory T cells modulate myeloid but not plasmacytoid dendritic cells activation. *The Journal of Immunology,* 176**,** 5293-5298.

HOUSTON, S., CEROVIC, V., THOMSON, C., BREWER, J., MOWAT, A. & MILLING, S. 2016. The lymph nodes draining the small intestine and colon are anatomically separate and immunologically distinct. *Mucosal immunology,* 9**,** 468-478.

HUDA-FAUJAN, N., ABDULAMIR, A., FATIMAH, A., ANAS, O. M., SHUHAIMI, M., YAZID, A. & LOONG, Y. 2010. The impact of the level of the intestinal short chain fatty acids in inflammatory bowel disease patients versus healthy subjects. *The open biochemistry journal,* 4**,** 53.

HUE, S., AHERN, P., BUONOCORE, S., KULLBERG, M. C., CUA, D. J., MCKENZIE, B. S., POWRIE, F. & MALOY, K. J. 2006. Interleukin-23 drives innate and T cell-mediated intestinal inflammation. *J Exp Med,* 203**,** 2473-83.

HUEBER, W., SANDS, B. E., LEWITZKY, S., VANDEMEULEBROECKE, M., REINISCH, W., HIGGINS, P. D., WEHKAMP, J., FEAGAN, B. G., YAO, M. D., KARCZEWSKI, M., KARCZEWSKI, J., PEZOUS, N., BEK, S., BRUIN, G., MELLGARD, B., BERGER, C., LONDEI, M., BERTOLINO, A. P., TOUGAS, G. & TRAVIS, S. P. 2012. Secukinumab, a human anti-IL-17A monoclonal antibody, for moderate to severe Crohn's disease: unexpected results of a randomised, double-blind placebo-controlled trial. *Gut,* 61**,** 1693-700.

HUGENHOLTZ, F. & DE VOS, W. M. 2018. Mouse models for human intestinal microbiota research: a critical evaluation. *Cellular and Molecular Life Sciences,* 75**,** 149-160.

IGNACIO, A., SHAH, K., BERNIER-LATMANI, J., KöLLER, Y., COAKLEY, G., MOYAT, M., HAMELIN, R., ARMAND, F., WONG, N. C., RAMAY, H., THOMSON, C. A., BURKHARD, R., WANG, H., DUFOUR, A., GEUKING, M. B., MCDONALD, B., PETROVA, T. V., HARRIS, N. L. & MCCOY, K. D. 2022. Small intestinal resident eosinophils maintain gut homeostasis following microbial colonization. *Immunity,* 55**,** 1250-1267.e12.

IMPELLIZZERI, D., SIRACUSA, R., CORDARO, M., PERITORE, A. F., GUGLIANDOLO, E., MANCUSO, G., MIDIRI, A., DI PAOLA, R. & CUZZOCREA, S. 2018. Therapeutic potential of dinitrobenzene sulfonic acid (DNBS)-induced colitis in mice by targeting IL-1β and IL-18. *Biochemical pharmacology,* 155**,** 150-161.

IVANOV, I. I., ATARASHI, K., MANEL, N., BRODIE, E. L., SHIMA, T., KARAOZ, U., WEI, D., GOLDFARB, K. C., SANTEE, C. A., LYNCH, S. V., TANOUE, T., IMAOKA, A., ITOH, K., TAKEDA, K., UMESAKI, Y., HONDA, K. & LITTMAN, D. R. 2009. Induction of intestinal Th17 cells by segmented filamentous bacteria. *Cell,* 139**,** 485-498.

IWATA, M., HIRAKIYAMA, A., ESHIMA, Y., KAGECHIKA, H., KATO, C. & SONG, S.-Y. 2004. Retinoic acid imprints gut-homing specificity on T cells. *Immunity,* 21**,** 527-538.

IZCUE, A., HUE, S., BUONOCORE, S., ARANCIBIA-CáRCAMO, C. V., AHERN, P. P., IWAKURA, Y., MALOY, K. J. & POWRIE, F. 2008. Interleukin-23 restrains regulatory T cell activity to drive T cell-dependent colitis. *Immunity,* 28**,** 559-570.

JEFFERY, R., ILOTT, N. E. & POWRIE, F. 2022. Genetic and environmental factors shape the host response to Helicobacter hepaticus: insights into IBD pathogenesis. *Current Opinion in Microbiology,* 65**,** 145-155.

JOERIS, T., MüLLER-LUDA, K., AGACE, W. W. & MOWAT, A. M. 2017. Diversity and functions of intestinal mononuclear phagocytes. *Mucosal immunology,* 10**,** 845-864.

JOHANSSON, M. E., GUSTAFSSON, J. K., HOLMéN-LARSSON, J., JABBAR, K. S., XIA, L., XU, H., GHISHAN, F. K., CARVALHO, F. A., GEWIRTZ, A. T., SJöVALL, H. & HANSSON, G. C. 2014. Bacteria penetrate the normally impenetrable inner colon mucus layer in both murine colitis models and patients with ulcerative colitis. *Gut,* 63**,** 281-91.

JOHANSSON, M. E. & HANSSON, G. C. 2016. Immunological aspects of intestinal mucus and mucins. *Nature Reviews Immunology,* 16**,** 639-649.

JOOSSENS, M., HUYS, G., CNOCKAERT, M., DE PRETER, V., VERBEKE, K., RUTGEERTS, P., VANDAMME, P. & VERMEIRE, S. 2011. Dysbiosis of the faecal microbiota in patients with Crohn's disease and their unaffected relatives. *Gut,* 60**,** 631-637.

JøRGENSEN, P. B., FENTON, T. M., MöRBE, U. M., RIIS, L. B., JAKOBSEN, H. L., NIELSEN, O. H. & AGACE, W. W. 2021. Identification, isolation and analysis of human gut-associated lymphoid tissues. *Nature protocols,* 16**,** 2051-2067.

JOSEFSDOTTIR, K. S., BALDRIDGE, M. T., KADMON, C. S. & KING, K. Y. 2017. Antibiotics impair murine hematopoiesis by depleting the intestinal microbiota. *Blood, The Journal of the American Society of Hematology,* 129**,** 729-739.

JOSTINS, L., RIPKE, S., WEERSMA, R. K., DUERR, R. H., MCGOVERN, D. P., HUI, K. Y., LEE, J. C., SCHUMM, L. P., SHARMA, Y., ANDERSON, C. A., ESSERS, J., MITROVIC, M., NING, K., CLEYNEN, I., THEATRE, E., SPAIN, S. L., RAYCHAUDHURI, S., GOYETTE, P., WEI, Z., ABRAHAM, C., ACHKAR, J. P., AHMAD, T., AMININEJAD, L., ANANTHAKRISHNAN, A. N., ANDERSEN, V., ANDREWS, J. M., BAIDOO, L., BALSCHUN, T., BAMPTON, P. A., BITTON, A., BOUCHER, G., BRAND, S., BüNING, C., COHAIN, A., CICHON, S., D'AMATO, M., DE JONG, D., DEVANEY, K. L., DUBINSKY, M., EDWARDS, C., ELLINGHAUS, D., FERGUSON, L. R., FRANCHIMONT, D., FRANSEN, K., GEARRY, R., GEORGES, M., GIEGER, C., GLAS, J., HARITUNIANS, T., HART, A., HAWKEY, C., HEDL, M., HU, X., KARLSEN, T. H., KUPCINSKAS, L., KUGATHASAN, S., LATIANO, A., LAUKENS, D., LAWRANCE, I. C., LEES, C. W., LOUIS, E., MAHY, G., MANSFIELD, J., MORGAN, A. R., MOWAT, C., NEWMAN, W., PALMIERI, O., PONSIOEN, C. Y., POTOCNIK, U., PRESCOTT, N. J., REGUEIRO, M., ROTTER, J. I., RUSSELL, R. K., SANDERSON, J. D., SANS, M., SATSANGI, J., SCHREIBER, S., SIMMS, L. A., SVENTORAITYTE, J., TARGAN, S. R., TAYLOR, K. D., TREMELLING, M., VERSPAGET, H. W., DE VOS, M., WIJMENGA, C., WILSON, D. C., WINKELMANN, J., XAVIER, R. J., ZEISSIG, S., ZHANG, B., ZHANG, C. K., ZHAO, H., SILVERBERG, M. S., ANNESE, V., HAKONARSON, H., BRANT, S. R., RADFORD-SMITH, G., MATHEW, C. G., RIOUX, J. D., SCHADT, E. E., et al. 2012. Host-microbe interactions have

shaped the genetic architecture of inflammatory bowel disease. *Nature,* 491**,** 119-24.

JUKIC, A., BAKIRI, L., WAGNER, E. F., TILG, H. & ADOLPH, T. E. 2021. Calprotectin: from biomarker to biological function. *Gut,* 70**,** 1978-1988.

JUNG, Y. & ROTHENBERG, M. E. 2014. Roles and regulation of gastrointestinal eosinophils in immunity and disease. *The Journal of Immunology,* 193**,** 999-1005.

JUNG, Y., WEN, T., MINGLER, M. K., CALDWELL, J. M., WANG, Y. H., CHAPLIN, D. D., LEE, E. H., JANG, M. H., WOO, S. Y., SEOH, J. Y., MIYASAKA, M. & ROTHENBERG, M. E. 2015. IL-1ß in eosinophil-mediated small intestinal homeostasis and IgA production. *Mucosal Immunology,* 8**,** 930-942.

KAIKO, G. E., RYU, S. H., KOUES, O. I., COLLINS, P. L., SOLNICA-KREZEL, L., PEARCE, E. J., PEARCE, E. L., OLTZ, E. M. & STAPPENBECK, T. S. 2016. The colonic crypt protects stem cells from microbiota-derived metabolites. *Cell,* 165**,** 1708-1720.

KANDORI, H., HIRAYAMA, K., TAKEDA, M. & DOI, K. 1996. Histochemical, lectin-histochemical and morphometrical characteristics of intestinal goblet cells of germfree and conventional mice. *Experimental animals,* 45**,** 155-160.

KANG, B., ALVARADO, L. J., KIM, T., LEHMANN, M. L., CHO, H., HE, J., LI, P., KIM, B.-H., LAROCHELLE, A. & KELSALL, B. L. 2020. Commensal microbiota drive the functional diversification of colon macrophages. *Mucosal Immunology,* 13**,** 216-229.

KAPLAN, G. G. 2015. The global burden of IBD: from 2015 to 2025. *Nature reviews Gastroenterology & hepatology,* 12**,** 720-727.

KARMARKAR, D. & ROCK, K. L. 2013. Microbiota signalling through MyD88 is necessary for a systemic neutrophilic inflammatory response. *Immunology,* 140**,** 483-492.

KäSTELE, V., MAYER, J., LEE, E. S., PAPAZIAN, N., COLE, J. J., CEROVIC, V., BELZ, G., TOMURA, M., EBERL, G., GOODYEAR, C., MACIEWICZ, R. A., WALL, D., CUPEDO, T., WITHERS, D. R. & MILLING, S. 2021. Intestinal-derived ILCs migrating in lymph increase IFNγ production in response to Salmonella Typhimurium infection. *Mucosal Immunology,* 14**,** 717-727.

KEDMI, R., NAJAR, T. A., MESA, K. R., GRAYSON, A., KROEHLING, L., HAO, Y., HAO, S., POKROVSKII, M., XU, M., TALBOT, J., WANG, J., GERMINO, J., LAREAU, C. A., SATPATHY, A. T., ANDERSON, M. S., LAUFER, T. M., AIFANTIS, I., BARTLESON, J. M., ALLEN, P. M., PAIDASSI, H., GARDNER, J. M., STOECKIUS, M. & LITTMAN, D. R. 2022. A RORgammat(+) cell instructs gut microbiota-specific Treg cell differentiation. *Nature*.

KELSALL, B. L. & STROBER, W. 1996. Distinct populations of dendritic cells are present in the subepithelial dome and T cell regions of the murine Peyer's patch. *The Journal of experimental medicine,* 183**,** 237-247.

KHAN, K. J., ULLMAN, T. A., FORD, A. C., ABREU, M. T., ABADIR, A., MARSHALL, J. K., TALLEY, N. J. & MOAYYEDI, P. 2011. Antibiotic therapy in inflammatory bowel disease: a systematic review and meta-analysis. *Official journal of the American College of Gastroenterology| ACG,* 106**,** 661-673.

KHOSRAVI, A., YáñEZ, A., PRICE, JEREMY G., CHOW, A., MERAD, M., GOODRIDGE, HELEN S. & MAZMANIAN, SARKIS K. 2014. Gut Microbiota Promote Hematopoiesis to Control Bacterial Infection. *Cell Host & Microbe,* 15**,** 374-381.

KIESLER, P., FUSS, I. J. & STROBER, W. 2015. Experimental models of inflammatory bowel diseases. *Cellular and molecular gastroenterology and hepatology,* 1**,** 154-170.

KIM, K. S., HONG, S.-W., HAN, D., YI, J., JUNG, J., YANG, B.-G., LEE, J. Y., LEE, M. & SURH, C. D. 2016. Dietary antigens limit mucosal immunity by inducing regulatory T cells in the small intestine. *Science,* 351**,** 858-863.

KIM, Y. S. & HO, S. B. 2010. Intestinal goblet cells and mucins in health and disease: recent insights and progress. *Current gastroenterology reports,* 12**,** 319-330.

KOJOUHAROFF, G., HANS, W., OBERMEIER, F., MäNNEL, D. N., ANDUS, T., SCHöLMERICH, J., GROSS, V. & FALK, W. 1997. Neutralization of tumour necrosis factor (TNF) but not of IL-1 reduces inflammation in chronic dextran sulphate sodium-induced colitis in mice. *Clin Exp Immunol,* 107**,** 353-8.

KOLIARAKI, V., CHALKIDI, N., HENRIQUES, A., TZAFERIS, C., POLYKRATIS, A., WAISMAN, A., MULLER, W., HACKAM, D. J., PASPARAKIS, M. & KOLLIAS, G. 2019. Innate Sensing through Mesenchymal TLR4/MyD88 Signals Promotes Spontaneous Intestinal Tumorigenesis. *Cell Reports,* 26**,** 536-545.e4.

KOLODZIEJCZYK, A. A., KIM, J. K., SVENSSON, V., MARIONI, J. C. & TEICHMANN, S. A. 2015. The technology and biology of single-cell RNA sequencing. *Molecular cell,* 58**,** 610-620.

KONIKOFF, M. R. & DENSON, L. A. 2006. Role of fecal calprotectin as a biomarker of intestinal inflammation in inflammatory bowel disease. *Inflammatory Bowel Diseases,* 12**,** 524-534.

KROEMER, G. & ZITVOGEL, L. 2018. The breakthrough of the microbiota. *Nature Reviews Immunology,* 18**,** 87-88.

KUEHL, C. J., WOOD, H. D., MARSH, T. L., SCHMIDT, T. M. & YOUNG, V. B. 2005. Colonization of the cecal mucosa by Helicobacter hepaticus impacts the diversity of the indigenous microbiota. *Infection and immunity,* 73**,** 6952-6961.

KüHL, A. A., KAKIRMAN, H., JANOTTA, M., DREHER, S., CREMER, P., PAWLOWSKI, N. N., LODDENKEMPER, C., HEIMESAAT, M. M., GROLLICH, K., ZEITZ, M., FARKAS, S. & HOFFMANN, J. C. 2007. Aggravation of different types of experimental colitis by depletion or adhesion blockade of neutrophils. *Gastroenterology,* 133**,** 1882-92.

KüHN, R., LöHLER, J., RENNICK, D., RAJEWSKY, K. & MüLLER, W. 1993. Interleukin-10-deficient mice develop chronic enterocolitis. *Cell,* 75**,** 263-274.

KULLBERG, M. C., ANDERSEN, J. F., GORELICK, P. L., CASPAR, P., SUERBAUM, S., FOX, J. G., CHEEVER, A. W., JANKOVIC, D. & SHER, A. 2003. Induction of colitis by a CD4+ T cell clone specific for a bacterial epitope. *Proceedings of the National Academy of Sciences,* 100**,** 15830-15835.

KULLBERG, M. C., JANKOVIC, D., FENG, C. G., HUE, S., GORELICK, P. L., MCKENZIE, B. S., CUA, D. J., POWRIE, F., CHEEVER, A. W., MALOY, K. J. & SHER, A. 2006. IL-23 plays a key role in Helicobacter hepaticus-induced T cell-dependent colitis. *J Exp Med,* 203**,** 2485-94.

KULLBERG, M. C., JANKOVIC, D., GORELICK, P. L., CASPAR, P., LETTERIO, J. J., CHEEVER, A. W. & SHER, A. 2002. Bacteria-triggered CD4(+) T regulatory cells suppress Helicobacter hepaticus-induced colitis. *J Exp Med,* 196**,** 505-15.

KULLBERG, M. C., ROTHFUCHS, A. G., JANKOVIC, D., CASPAR, P., WYNN, T. A., GORELICK, P. L., CHEEVER, A. W. & SHER, A. 2001. Helicobacter hepaticus-induced colitis in interleukin-10-deficient mice: cytokine requirements for the induction and maintenance of intestinal inflammation. *Infection and immunity,* 69**,** 4232-4241.

KULLBERG, M. C., WARD, J. M., GORELICK, P. L., CASPAR, P., HIENY, S., CHEEVER, A., JANKOVIC, D. & SHER, A. 1998. Helicobacter hepaticus triggers colitis in specific-pathogen-free interleukin-10 (IL-10)-deficient mice through an IL-12-and gamma interferon-dependent mechanism. *Infection and immunity,* 66**,** 5157-5166.

LAI, N. Y., MUSSER, M. A., PINHO-RIBEIRO, F. A., BARAL, P., JACOBSON, A., MA, P., POTTS, D. E., CHEN, Z., PAIK, D., SOUALHI, S., YAN, Y., MISRA, A., GOLDSTEIN, K., LAGOMARSINO, V. N., NORDSTROM, A., SIVANATHAN, K. N., WALLRAPP, A., KUCHROO, V. K., NOWARSKI, R., STARNBACH, M. N., SHI, H., SURANA, N. K., AN, D., WU, C., HUH, J. R., RAO, M. & CHIU, I. M. 2020. Gut-Innervating Nociceptor Neurons Regulate Peyer's Patch Microfold Cells and SFB Levels to Mediate Salmonella Host Defense. *Cell,* 180**,** 33-49.e22.

LAKY, K. & KRUISBEEK, A. M. 2016. In vivo depletion of T lymphocytes. *Current Protocols in Immunology,* 113**,** 4.1. 1-4.1. 9.

LAMAS, B., RICHARD, M. L., LEDUCQ, V., PHAM, H. P., MICHEL, M. L., DA COSTA, G., BRIDONNEAU, C., JEGOU, S., HOFFMANN, T. W., NATIVIDAD, J. M., BROT, L., TALEB, S., COUTURIER-MAILLARD, A., NION-LARMURIER, I., MERABTENE, F., SEKSIK, P., BOURRIER, A., COSNES, J., RYFFEL, B., BEAUGERIE, L., LAUNAY, J.

M., LANGELLA, P., XAVIER, R. J. & SOKOL, H. 2016. CARD9 impacts colitis by altering gut microbiota metabolism of tryptophan into aryl hydrocarbon receptor ligands. *Nat Med,* 22**,** 598-605.

LANGLET, C., TAMOUTOUNOUR, S., HENRI, S., LUCHE, H., ARDOUIN, L., GRéGOIRE, C., MALISSEN, B. & GUILLIAMS, M. 2012. CD64 expression distinguishes monocyte-derived and conventional dendritic cells and reveals their distinct role during intramuscular immunization. *The Journal of Immunology,* 188**,** 1751-1760.

LATHROP, S. K., BLOOM, S. M., RAO, S. M., NUTSCH, K., LIO, C.-W., SANTACRUZ, N., PETERSON, D. A., STAPPENBECK, T. S. & HSIEH, C.-S. 2011. Peripheral education of the immune system by colonic commensal microbiota. *Nature,* 478**,** 250-254.

LAVIN, Y., WINTER, D., BLECHER-GONEN, R., DAVID, E., KEREN-SHAUL, H., MERAD, M., JUNG, S. & AMIT, I. 2014. Tissue-resident macrophage enhancer landscapes are shaped by the local microenvironment. *Cell,* 159**,** 1312-1326.

LENZO, J. C., O'BRIEN-SIMPSON, N. M., CECIL, J., HOLDEN, J. A. & REYNOLDS, E. C. 2016. Determination of active phagocytosis of unopsonized Porphyromonas gingivalis by macrophages and neutrophils using the pH-sensitive fluorescent dye pHrodo. *Infection and immunity,* 84**,** 1753-1760.

LEVY, M., KOLODZIEJCZYK, A. A., THAISS, C. A. & ELINAV, E. 2017. Dysbiosis and the immune system. *Nature Reviews Immunology,* 17**,** 219-232.

LEWIS, J. D., CHEN, E. Z., BALDASSANO, R. N., OTLEY, A. R., GRIFFITHS, A. M., LEE, D., BITTINGER, K., BAILEY, A., FRIEDMAN, E. S., HOFFMANN, C., ALBENBERG, L., SINHA, R., COMPHER, C., GILROY, E., NESSEL, L., GRANT, A., CHEHOUD, C., LI, H., WU, G. D. & BUSHMAN, F. D. 2015. Inflammation, Antibiotics, and Diet as Environmental Stressors of the Gut Microbiome in Pediatric Crohn's Disease. *Cell Host Microbe,* 18**,** 489-500.

LEWKOWICZ, P., LEWKOWICZ, N., SASIAK, A. & TCHóRZEWSKI, H. 2006. Lipopolysaccharide-activated CD4+ CD25+ T regulatory cells inhibit neutrophil function and promote their apoptosis and death. *The Journal of immunology,* 177**,** 7155-7163.

LI, B., ALLI, R., VOGEL, P. & GEIGER, T. L. 2014. IL-10 modulates DSS-induced colitis through a macrophage–ROS–NO axis. *Mucosal immunology,* 7**,** 869-878.

LI, B., GURUNG, P., MALIREDDI, R. S., VOGEL, P., KANNEGANTI, T.-D. & GEIGER, T. L. 2015. IL-10 engages macrophages to shift Th17 cytokine dependency and pathogenicity during T-cell-mediated colitis. *Nature communications,* 6**,** 6131.

LI, M. O., WAN, Y. Y. & FLAVELL, R. A. 2007. T cell-produced transforming growth factor-β1 controls T cell tolerance and regulates Th1-and Th17-cell differentiation. *Immunity,* 26**,** 579-591.

LIN, N. & SIMON, M. C. 2016. Hypoxia-inducible factors: key regulators of myeloid cells during inflammation. *The Journal of clinical investigation,* 126**,** 3661-3671.

LINDNER, B., BURKARD, T. & SCHULER, M. 2020. Phagocytosis assays with different pH-sensitive fluorescent particles and various readouts. *Biotechniques,* 68**,** 245-250.

LINDSAY, R. W., DARRAH, P. A., QUINN, K. M., WILLE-REECE, U., MATTEI, L. M., IWASAKI, A., KASTURI, S. P., PULENDRAN, B., GALL, J. G., SPIES, A. G. & SEDER, R. A. 2010. CD8+ T cell responses following replication-defective adenovirus serotype 5 immunization are dependent on CD11c+ dendritic cells but show redundancy in their requirement of TLR and nucleotide-binding oligomerization domain-like receptor signaling. *J Immunol,* 185**,** 1513-21.

LIU, J. Z., VAN SOMMEREN, S., HUANG, H., NG, S. C., ALBERTS, R., TAKAHASHI, A., RIPKE, S., LEE, J. C., JOSTINS, L., SHAH, T., ABEDIAN, S., CHEON, J. H., CHO, J., DAYANI, N. E., FRANKE, L., FUYUNO, Y., HART, A., JUYAL, R. C., JUYAL, G., KIM, W. H., MORRIS, A. P., POUSTCHI, H., NEWMAN, W. G., MIDHA, V., ORCHARD, T. R., VAHEDI, H., SOOD, A., SUNG, J. Y., MALEKZADEH, R., WESTRA, H. J., YAMAZAKI, K., YANG, S. K., BARRETT, J. C., ALIZADEH, B. Z., PARKES, M., BK, T., DALY, M. J., KUBO, M., ANDERSON, C. A. & WEERSMA, R. K. 2015a. Association analyses identify 38 susceptibility loci for inflammatory bowel disease and highlight shared genetic risk across populations. *Nat Genet,* 47**,** 979-986.

LIU, K., VICTORA, G. D., SCHWICKERT, T. A., GUERMONPREZ, P., MEREDITH, M. M., YAO, K., CHU, F.-F., RANDOLPH, G. J., RUDENSKY, A. Y. & NUSSENZWEIG, M. 2009. In vivo analysis of dendritic cell development and homeostasis. *Science,* 324**,** 392-397.

LIU, Y., ZHANG, D.-T. & LIU, X.-G. 2015b. mTOR signaling in T cell immunity and autoimmunity. *International reviews of immunology,* 34**,** 50-66.

LIYANAGE, N. P., DASSANAYAKE, R. P., KUSZYNSKI, C. A. & DUHAMEL, G. E. 2013. Contribution of Helicobacter hepaticus cytolethal distending toxin subunits to human epithelial cell cycle arrest and apoptotic death in vitro. *Helicobacter,* 18**,** 433-443.

LKHAGVA, E., CHUNG, H.-J., HONG, J., TANG, W. H. W., LEE, S.-I., HONG, S.-T. & LEE, S. 2021. The regional diversity of gut microbiome along the GI tract of male C57BL/6 mice. *BMC microbiology,* 21**,** 1-13.

LO, Y. H., CHUNG, E., LI, Z., WAN, Y. W., MAHE, M. M., CHEN, M. S., NOAH, T. K., BELL, K. N., YALAMANCHILI, H. K., KLISCH, T. J., LIU, Z., PARK, J. S. & SHROYER, N. F. 2017. Transcriptional Regulation by ATOH1 and its Target SPDEF in the Intestine. *Cell Mol Gastroenterol Hepatol,* 3**,** 51-71.

LOONEN, L. M., STOLTE, E., JAKLOFSKY, M. T., MEIJERINK, M., DEKKER, J., VAN BAARLEN, P. & WELLS, J. 2014. REG3γ-deficient mice have altered mucus

distribution and increased mucosal inflammatory responses to the microbiota and enteric pathogens in the ileum. *Mucosal immunology,* 7**,** 939-947.

LOSCHKO, J., SCHREIBER, H. A., RIEKE, G. J., ESTERHáZY, D., MEREDITH, M. M., PEDICORD, V. A., YAO, K. H., CABALLERO, S., PAMER, E. G., MUCIDA, D. & NUSSENZWEIG, M. C. 2016. Absence of MHC class II on cDCs results in microbial-dependent intestinal inflammation. *J Exp Med,* 213**,** 517-34.

LöTSTEDT, B., STRAžAR, M., XAVIER, R., REGEV, A. & VICKOVIC, S. 2023. Spatial host–microbiome sequencing reveals niches in the mouse gut. *Nature Biotechnology***,** 1-10.

LUKONIN, I., SERRA, D., CHALLET MEYLAN, L., VOLKMANN, K., BAATEN, J., ZHAO, R., MEEUSEN, S., COLMAN, K., MAURER, F., STADLER, M. B., JENKINS, J. & LIBERALI, P. 2020. Phenotypic landscape of intestinal organoid regeneration. *Nature,* 586**,** 275-280.

LUPP, C., ROBERTSON, M. L., WICKHAM, M. E., SEKIROV, I., CHAMPION, O. L., GAYNOR, E. C. & FINLAY, B. B. 2007. Host-mediated inflammation disrupts the intestinal microbiota and promotes the overgrowth of Enterobacteriaceae. *Cell host & microbe,* 2**,** 119-129.

MALFERTHEINER, P., CAMARGO, M. C., EL-OMAR, E., LIOU, J.-M., PEEK, R., SCHULZ, C., SMITH, S. I. & SUERBAUM, S. 2023. Helicobacter pylori infection. *Nature reviews Disease primers,* 9**,** 19.

MALOY , K. J., SALAUN , L., CAHILL , R., DOUGAN , G., SAUNDERS , N. J. & POWRIE , F. 2003. CD4+CD25+ TR Cells Suppress Innate Immune Pathology Through Cytokine-dependent Mechanisms. *Journal of Experimental Medicine,* 197**,** 111-119.

MANDELL, L., MORAN, A. P., COCCHIARELLA, A., HOUGHTON, J., TAYLOR, N., FOX, J. G., WANG, T. C. & KURT-JONES, E. A. 2004. Intact Gram-Negative Helicobacter pylori, Helicobacter felis, and Helicobacter hepaticus Bacteria Activate Innate Immunity via Toll-Like Receptor 2 but Not Toll-Like Receptor 4. *Infection and Immunity,* 72**,** 6446-6454.

MARTíN, R., CHAMIGNON, C., MHEDBI-HAJRI, N., CHAIN, F., DERRIEN, M., ESCRIBANO-VáZQUEZ, U., GARAULT, P., COTILLARD, A., PHAM, H. P., CHERVAUX, C., BERMúDEZ-HUMARáN, L. G., SMOKVINA, T. & LANGELLA, P. 2019. The potential probiotic Lactobacillus rhamnosus CNCM I-3690 strain protects the intestinal barrier by stimulating both mucus production and cytoprotective response. *Sci Rep,* 9**,** 5398.

MARTíNEZ, A., BONO, C., MEGíAS, J., YáñEZ, A., GOZALBO, D. & GIL, M. L. 2018. Systemic candidiasis and TLR2 agonist exposure impact the antifungal response of hematopoietic stem and progenitor cells. *Frontiers in Cellular and Infection Microbiology,* 8**,** 309.

MARTINEZ-MEDINA, M. & GARCIA-GIL, L. J. 2014. Escherichia coli in chronic inflammatory bowel diseases: An update on adherent invasive Escherichia coli pathogenicity. *World journal of gastrointestinal pathophysiology,* 5**,** 213.

MARTINON, F., BURNS, K. & TSCHOPP, J. 2002. The inflammasome: a molecular platform triggering activation of inflammatory caspases and processing of proIL-ß. *Molecular cell,* 10**,** 417-426.

MASAHATA, K., UMEMOTO, E., KAYAMA, H., KOTANI, M., NAKAMURA, S., KURAKAWA, T., KIKUTA, J., GOTOH, K., MOTOOKA, D., SATO, S., HIGUCHI, T., BABA, Y., KUROSAKI, T., KINOSHITA, M., SHIMADA, Y., KIMURA, T., OKUMURA, R., TAKEDA, A., TAJIMA, M., YOSHIE, O., FUKUZAWA, M., KIYONO, H., FAGARASAN, S., IIDA, T., ISHII, M. & TAKEDA, K. 2014. Generation of colonic IgA-secreting cells in the caecal patch. *Nat Commun,* 5**,** 3704.

MATZIOURIDOU, C., ROCHA, S. D. C., HAABETH, O. A., RUDI, K., CARLSEN, H. & KIELLAND, A. 2018. iNOS- and NOX1-dependent ROS production maintains bacterial homeostasis in the ileum of mice. *Mucosal Immunology,* 11**,** 774-784.

MAZMANIAN, S. K., LIU, C. H., TZIANABOS, A. O. & KASPER, D. L. 2005. An immunomodulatory molecule of symbiotic bacteria directs maturation of the host immune system. *Cell,* 122**,** 107-118.

MAZMANIAN, S. K., ROUND, J. L. & KASPER, D. L. 2008. A microbial symbiosis factor prevents intestinal inflammatory disease. *Nature,* 453**,** 620-625.

MCCOY, K. D., GEUKING, M. B. & RONCHI, F. 2017. Gut microbiome standardization in control and experimental mice. *Current protocols in immunology,* 117**,** 23.1. 1-23.1. 13.

MCDOLE, J. R., WHEELER, L. W., MCDONALD, K. G., WANG, B., KONJUFCA, V., KNOOP, K. A., NEWBERRY, R. D. & MILLER, M. J. 2012. Goblet cells deliver luminal antigen to CD103+ dendritic cells in the small intestine. *Nature,* 483**,** 345-349.

MCSORLEY, H. J., HEWITSON, J. P. & MAIZELS, R. M. 2013. Immunomodulation by helminth parasites: defining mechanisms and mediators. *International journal for parasitology,* 43**,** 301-310.

MCSORLEY, H. J. & SMYTH, D. J. IL-33: a central cytokine in helminth infections. Seminars in Immunology, 2021. Elsevier, 101532.

MéNARD, A. & SMET, A. 2019. other Helicobacter species. *Helicobacter,* 24**,** e12645.

MERAD, M., SATHE, P., HELFT, J., MILLER, J. & MORTHA, A. 2013. The dendritic cell lineage: ontogeny and function of dendritic cells and their subsets in the steady state and the inflamed setting. *Annual review of immunology,* 31**,** 563-604.

MERSMANN, J., BERKELS, R., ZACHAROWSKI, P., TRAN, N., KOCH, A., IEKUSHI, K., DIMMELER, S., GRANJA, T. F., BOEHM, O., CLAYCOMB, W. C. & ZACHAROWSKI, K. 2010. Preconditioning by toll-like receptor 2 agonist Pam3CSK4 reduces CXCL1-dependent leukocyte recruitment in murine myocardial ischemia/reperfusion injury. *Crit Care Med,* 38**,** 903-9.

METIDJI, A., OMENETTI, S., CROTTA, S., LI, Y., NYE, E., ROSS, E., LI, V., MARADANA, M. R., SCHIERING, C. & STOCKINGER, B. 2018. The environmental sensor AHR protects from inflammatory damage by maintaining intestinal stem cell homeostasis and barrier integrity. *Immunity,* 49**,** 353-362. e5.

MIETTINEN, T. P. & BJöRKLUND, M. 2017. Mitochondrial Function and Cell Size: An Allometric Relationship. *Trends in Cell Biology,* 27**,** 393-402.

MISHRA, A., HOGAN, S. P., LEE, J. J., FOSTER, P. S. & ROTHENBERG, M. E. 1999. Fundamental signals that regulate eosinophil homing to the gastrointestinal tract. *The Journal of clinical investigation,* 103**,** 1719-1727.

MIYAUCHI, E., SHIMOKAWA, C., STEIMLE, A., DESAI, M. S. & OHNO, H. 2023. The impact of the gut microbiome on extra-intestinal autoimmune diseases. *Nature Reviews Immunology,* 23**,** 9-23.

MIYOSHI, H. & STAPPENBECK, T. S. 2013. In vitro expansion and genetic modification of gastrointestinal stem cells in spheroid culture. *Nature protocols,* 8**,** 2471-2482.

MOAYYEDI, P., SURETTE, M. G., KIM, P. T., LIBERTUCCI, J., WOLFE, M., ONISCHI, C., ARMSTRONG, D., MARSHALL, J. K., KASSAM, Z., REINISCH, W. & LEE, C. H. 2015. Fecal Microbiota Transplantation Induces Remission in Patients With Active Ulcerative Colitis in a Randomized Controlled Trial. *Gastroenterology,* 149**,** 102-109.e6.

MOON, C., VANDUSSEN, K. L., MIYOSHI, H. & STAPPENBECK, T. S. 2014. Development of a primary mouse intestinal epithelial cell monolayer culture system to evaluate factors that modulate IgA transcytosis. *Mucosal immunology,* 7**,** 818-828.

MORA, J. R., BONO, M. R., MANJUNATH, N., WENINGER, W., CAVANAGH, L. L., ROSEMBLATT, M. & VON ANDRIAN, U. H. 2003. Selective imprinting of gut-homing T cells by Peyer's patch dendritic cells. *Nature,* 424**,** 88-93.

MORRISON, D. J. & PRESTON, T. 2016. Formation of short chain fatty acids by the gut microbiota and their impact on human metabolism. *Gut microbes,* 7**,** 189-200.

MORRISON, P. J., BALLANTYNE, S. J., MACDONALD, S. J., MOORE, J. W., JENKINS, D., WRIGHT, J. F., FOUSER, L. A. & KULLBERG, M. C. 2015. Differential Requirements for IL-17A and IL-22 in Cecal versus Colonic Inflammation Induced by Helicobacter hepaticus. *Am J Pathol,* 185**,** 3290-303.

MORRISON, P. J., BENDING, D., FOUSER, L. A., WRIGHT, J. F., STOCKINGER, B., COOKE, A. & KULLBERG, M. C. 2013. Th17-cell plasticity in Helicobacter hepaticus-induced intestinal inflammation. *Mucosal Immunol,* 6**,** 1143-56.

MOSCHEN, A. R., TILG, H. & RAINE, T. 2019. IL-12, IL-23 and IL-17 in IBD: immunobiology and therapeutic targeting. *Nature Reviews Gastroenterology & Hepatology,* 16**,** 185-196.

MOWAT, A. M. & AGACE, W. W. 2014. Regional specialization within the intestinal immune system. *Nature Reviews Immunology,* 14**,** 667-685.

MUNYAKA, P. M., RABBI, M. F., KHAFIPOUR, E. & GHIA, J. E. 2016. Acute dextran sulfate sodium (DSS)-induced colitis promotes gut microbial dysbiosis in mice. *Journal of basic microbiology,* 56**,** 986-998.

MURAOKA, W. T., KORCHAGINA, A. A., XIA, Q., SHEIN, S. A., JING, X., LAI, Z., WELDON, K. S., WANG, L.-J., CHEN, Y., KUMMER, L. W., MOHRS, M., VIVIER, E., KOROLEVA, E. P. & TUMANOV, A. V. 2021. Campylobacter infection promotes IFNγ-dependent intestinal pathology via ILC3 to ILC1 conversion. *Mucosal Immunology,* 14**,** 703-716.

MURAYAMA, S., KURGANOV, E. & MIYATA, S. 2019. Activation of microglia and macrophages in the circumventricular organs of the mouse brain during TLR2-induced fever and sickness responses. *Journal of Neuroimmunology,* 334**,** 576973.

NAGALINGAM, N. A., ROBINSON, C. J., BERGIN, I. L., EATON, K. A., HUFFNAGLE, G. B. & YOUNG, V. B. 2013. The effects of intestinal microbial community structure on disease manifestation in IL-10-/-mice infected with Helicobacter hepaticus. *Microbiome,* 1**,** 1-15.

NAIK, S., BOULADOUX, N., LINEHAN, J. L., HAN, S. J., HARRISON, O. J., WILHELM, C., CONLAN, S., HIMMELFARB, S., BYRD, A. L., DEMING, C., QUINONES, M., BRENCHLEY, J. M., KONG, H. H., TUSSIWAND, R., MURPHY, K. M., MERAD, M., SEGRE, J. A. & BELKAID, Y. 2015. Commensal-dendritic-cell interaction specifies a unique protective skin immune signature. *Nature,* 520**,** 104-8.

NAIK, S., LARSEN, S. B., GOMEZ, N. C., ALAVERDYAN, K., SENDOEL, A., YUAN, S., POLAK, L., KULUKIAN, A., CHAI, S. & FUCHS, E. 2017. Inflammatory memory sensitizes skin epithelial stem cells to tissue damage. *Nature,* 550**,** 475-480.

NAKASHIGE, T. G., ZHANG, B., KREBS, C. & NOLAN, E. M. 2015. Human calprotectin is an iron-sequestering host-defense protein. *Nature chemical biology,* 11**,** 765-771.

NATSUGA, K., CIPOLAT, S. & WATT, F. M. 2016. Increased bacterial load and expression of antimicrobial peptides in skin of barrier-deficient mice with reduced cancer susceptibility. *Journal of investigative dermatology,* 136**,** 99-106.

NEURATH, M. F. 2014. Cytokines in inflammatory bowel disease. *Nature Reviews Immunology,* 14**,** 329-342.

NGO, V. L., ABO, H., MAXIM, E., HARUSATO, A., GEEM, D., MEDINA-CONTRERAS, O., MERLIN, D., GEWIRTZ, A. T., NUSRAT, A. & DENNING, T. L. 2018. A cytokine network involving IL-36γ, IL-23, and IL-22 promotes antimicrobial defense and recovery from intestinal barrier damage. *Proceedings of the National Academy of Sciences,* 115**,** E5076-E5085.

NI, J., WU, G. D., ALBENBERG, L. & TOMOV, V. T. 2017. Gut microbiota and IBD: causation or correlation? *Nature reviews Gastroenterology & hepatology,* 14**,** 573-584.

NILSSON, I., LINDGREN, S., ERIKSSON, S. & WADSTRöM, T. 2000. Serum antibodies to Helicobacter hepaticus and Helicobacter pylori in patients with chronic liver disease. *Gut,* 46**,** 410.

NISH, S. & MEDZHITOV, R. 2011. Host defense pathways: role of redundancy and compensation in infectious disease phenotypes. *Immunity,* 34**,** 629-636.

NUNES, N. S., KIM, S., SUNDBY, M., CHANDRAN, P., BURKS, S. R., PAZ, A. H. & FRANK, J. A. 2018. Temporal clinical, proteomic, histological and cellular immune responses of dextran sulfate sodium-induced acute colitis. *World Journal of Gastroenterology,* 24**,** 4341.

NUSSE, Y. M., SAVAGE, A. K., MARANGONI, P., ROSENDAHL-HUBER, A. K., LANDMAN, T. A., DE SAUVAGE, F. J., LOCKSLEY, R. M. & KLEIN, O. D. 2018. Parasitic helminths induce fetal-like reversion in the intestinal stem cell niche. *Nature,* 559**,** 109-113.

O'CALLAGHAN, A. A., DEMPSEY, E., IYER, N., STIEGELER, S., MERCURIO, K. & CORR, S. C. 2021. Intestinal metabolites influence macrophage phagocytosis and clearance of bacterial infection. *Frontiers in cellular and infection microbiology,* 11**,** 622491.

O'NEILL, L. A., KISHTON, R. J. & RATHMELL, J. 2016. A guide to immunometabolism for immunologists. *Nature Reviews Immunology,* 16**,** 553-565.

OGINO, T., NISHIMURA, J., BARMAN, S., KAYAMA, H., UEMATSU, S., OKUZAKI, D., OSAWA, H., HARAGUCHI, N., UEMURA, M., HATA, T., TAKEMASA, I., MIZUSHIMA, T., YAMAMOTO, H., TAKEDA, K., DOKI, Y. & MORI, M. 2013. Increased Th17-inducing activity of CD14+ CD163 low myeloid cells in intestinal lamina propria of patients with Crohn's disease. *Gastroenterology,* 145**,** 1380-91.e1.

PAPADAKIS, K. A., KREMPSKI, J., SVINGEN, P., XIONG, Y., SARMENTO, O. F., LOMBERK, G. A., URRUTIA, R. A. & FAUBION, W. A. 2015. Krüppel-like factor KLF10 deficiency predisposes to colitis through colonic macrophage dysregulation. *American Journal of Physiology-Gastrointestinal and Liver Physiology,* 309**,** G900-G909.

PARK, J.-S., CHOI, J. W., JHUN, J., KWON, J. Y., LEE, B.-I., YANG, C. W., PARK, S.-H. & CHO, M.-L. 2018. Lactobacillus acidophilus improves intestinal inflammation in an acute colitis mouse model by regulation of Th17 and Treg cell balance and fibrosis development. *Journal of medicinal food,* 21**,** 215-224.

PARK, J. S., GAZZANIGA, F. S., KASPER, D. L. & SHARPE, A. H. 2023. Microbiota-dependent regulation of costimulatory and coinhibitory pathways via innate immune sensors and implications for immunotherapy. *Experimental & Molecular Medicine,* 55**,** 1913-1921.

PATRICK, S. 2022. A tale of two habitats: Bacteroides fragilis, a lethal pathogen and resident in the human gastrointestinal microbiome. *Microbiology,* 168**,** 001156.

PEI, C., ZHAO, C., WANG, A. J., FAN, A. X., GRINCHUK, V., SMITH, A., SUN, R., XIE, Y., LU, N., URBAN, J. F., JR., SHEA-DONOHUE, T., ZHAO, A. & YANG, Z. 2016. Critical Role for Interleukin-25 in Host Protective Th2 Memory Response against Heligmosomoides polygyrus bakeri. *Infect Immun,* 84**,** 3328-3337.

PENDERGRASS, W., WOLF, N. & POOT, M. 2004. Efficacy of MitoTracker Green™ and CMXrosamine to measure changes in mitochondrial membrane potentials in living cells and tissues. *Cytometry Part A: the journal of the International Society for Analytical Cytology,* 61**,** 162-169.

PÈNE, J. R. M., CHEVALIER, S., PREISSER, L., VÉNÉREAU, E., GUILLEUX, M.-H. L. N., GHANNAM, S., MOLÈS, J.-P., DANGER, Y., RAVON, E., LESAUX, S., YSSEL, H. & GASCAN, H. 2008. Chronically inflamed human tissues are infiltrated by highly differentiated Th17 lymphocytes. *The Journal of Immunology,* 180**,** 7423-7430.

PEREZ-LOPEZ, A., BEHNSEN, J., NUCCIO, S.-P. & RAFFATELLU, M. 2016. Mucosal immunity to pathogenic intestinal bacteria. *Nature Reviews Immunology,* 16**,** 135-148.

PETERSON, L. W. & ARTIS, D. 2014. Intestinal epithelial cells: regulators of barrier function and immune homeostasis. *Nature reviews immunology,* 14**,** 141-153.

PETNICKI-OCWIEJA, T., HRNCIR, T., LIU, Y.-J., BISWAS, A., HUDCOVIC, T., TLASKALOVA-HOGENOVA, H. & KOBAYASHI, K. S. 2009. Nod2 is required for the regulation of commensal microbiota in the intestine. *Proceedings of the National Academy of Sciences,* 106**,** 15813-15818.

PINEDA-TORRA, I., GAGE, M., DE JUAN, A. & PELLO, O. M. 2015. Isolation, culture, and polarization of murine bone marrow-derived and peritoneal macrophages. *Methods in Mouse Atherosclerosis***,** 101-109.

PINTO, D., ROBINE, S., JAISSER, F., EL MARJOU, F. & LOUVARD, D. 1999. Regulatory sequences of the mouse villin gene that efficiently drive transgenic expression in immature and differentiated epithelial cells of small and large intestines. *Journal of Biological Chemistry,* 274**,** 6476-6482.

PISANI, A., RAUSCH, P., BANG, C., ELLUL, S., TABONE, T., MARANTIDIS CORDINA, C., ZAHRA, G., FRANKE, A. & ELLUL, P. 2022. Dysbiosis in the gut microbiota in patients with inflammatory bowel disease during remission. *Microbiology spectrum,* 10**,** e00616-22.

PLOVIER, H., EVERARD, A., DRUART, C., DEPOMMIER, C., VAN HUL, M., GEURTS, L., CHILLOUX, J., OTTMAN, N., DUPARC, T., LICHTENSTEIN, L., MYRIDAKIS, A., DELZENNE, N. M., KLIEVINK, J., BHATTACHARJEE, A., VAN DER ARK, K. C., AALVINK, S., MARTINEZ, L. O., DUMAS, M. E., MAITER, D., LOUMAYE, A., HERMANS, M. P., THISSEN, J. P., BELZER, C., DE VOS, W. M. & CANI, P. D. 2017. A purified membrane protein from Akkermansia muciniphila or the pasteurized bacterium improves metabolism in obese and diabetic mice. *Nat Med,* 23**,** 107-113.

POLTORAK, A., HE, X., SMIRNOVA, I., LIU, M. Y., VAN HUFFEL, C., DU, X., BIRDWELL, D., ALEJOS, E., SILVA, M., GALANOS, C., FREUDENBERG, M., RICCIARDI-CASTAGNOLI, P., LAYTON, B. & BEUTLER, B. 1998. Defective LPS signaling in C3H/HeJ and C57BL/10ScCr mice: mutations in Tlr4 gene. *Science,* 282**,** 2085-8.

POTT, J., KABAT, A. M. & MALOY, K. J. 2018. Intestinal epithelial cell autophagy is required to protect against TNF-induced apoptosis during chronic colitis in mice. *Cell host & microbe,* 23**,** 191-202. e4.

POWRIE, F., LEACH, M. W., MAUZE, S., CADDIE, L. B. & COFFMAN, R. L. 1993. Phenotypically distinct subsets of CD4+ T cells induce or protect from chronic intestinal inflammation in C. B-17 scid mice. *International immunology,* 5**,** 1461-1471.

POWRIE, F., LEACH, M. W., MAUZE, S., MENON, S., CADDLE, L. B. & COFFMAN, R. L. 1994. Inhibition of Thl responses prevents inflammatory bowel disease in scid mice reconstituted with CD45RBhi CD4+ T cells. *Immunity,* 1**,** 553-562.

PRICE, A. E., SHAMARDANI, K., LUGO, K. A., DEGUINE, J., ROBERTS, A. W., LEE, B. L. & BARTON, G. M. 2018. A Map of Toll-like Receptor Expression in the Intestinal Epithelium Reveals Distinct Spatial, Cell Type-Specific, and Temporal Patterns. *Immunity,* 49**,** 560-575 e6.

PROPHETER, D. C., CHARA, A. L., HARRIS, T. A., RUHN, K. A. & HOOPER, L. V. 2017. Resistin-like molecule ß is a bactericidal protein that promotes spatial segregation of the microbiota and the colonic epithelium. *Proceedings of the National Academy of Sciences,* 114**,** 11027-11033.

PUSCHHOF, J., PLEGUEZUELOS-MANZANO, C., MARTINEZ-SILGADO, A., AKKERMAN, N., SAFTIEN, A., BOOT, C., DE WAAL, A., BEUMER, J., DUTTA, D., HEO, I. & CLEVERS, H. 2021. Intestinal organoid cocultures with microbes. *Nat Protoc,* 16**,** 4633-4649.

RAKOFF-NAHOUM, S., PAGLINO, J., ESLAMI-VARZANEH, F., EDBERG, S. & MEDZHITOV, R. 2004. Recognition of commensal microflora by toll-like receptors is required for intestinal homeostasis. *Cell,* 118**,** 229-41.

RAMALINGAM, R., LARMONIER, C. B., THURSTON, R. D., MIDURA-KIELA, M. T., ZHENG, S. G., GHISHAN, F. K. & KIELA, P. R. 2012. Dendritic cell-specific disruption of TGF-β receptor II leads to altered regulatory T cell phenotype and spontaneous multiorgan autoimmunity. *The Journal of Immunology,* 189**,** 3878-3893.

RATH, H. C., SCHULTZ, M., FREITAG, R., DIELEMAN, L. A., LI, F., LINDE, H.-J. R., SCHÖLMERICH, J. R. & SARTOR, R. B. 2001. Different subsets of enteric bacteria induce and perpetuate experimental colitis in rats and mice. *Infection and immunity,* 69**,** 2277-2285.

RAUCH, I., DEETS, K. A., JI, D. X., VON MOLTKE, J., TENTHOREY, J. L., LEE, A. Y., PHILIP, N. H., AYRES, J. S., BRODSKY, I. E., GRONERT, K. & VANCE, R. E. 2017. NAIP-NLRC4 Inflammasomes Coordinate Intestinal Epithelial Cell Expulsion with Eicosanoid and IL-18 Release via Activation of Caspase-1 and -8. *Immunity,* 46**,** 649-659.

REESE, T. A., BI, K., KAMBAL, A., FILALI-MOUHIM, A., BEURA, L. K., BüRGER, M. C., PULENDRAN, B., SEKALY, R. P., JAMESON, S. C., MASOPUST, D., HAINING, W. N. & VIRGIN, H. W. 2016. Sequential Infection with Common Pathogens Promotes Human-like Immune Gene Expression and Altered Vaccine Response. *Cell Host Microbe,* 19**,** 713-9.

REIKVAM, D. H., EROFEEV, A., SANDVIK, A., GRCIC, V., JAHNSEN, F. L., GAUSTAD, P., MCCOY, K. D., MACPHERSON, A. J., MEZA-ZEPEDA, L. A. & JOHANSEN, F.-E. 2011. Depletion of murine intestinal microbiota: effects on gut mucosa and epithelial gene expression. *PloS one,* 6**,** e17996.

REINHARDT, C., BERGENTALL, M., GREINER, T. U., SCHAFFNER, F., ÖSTERGREN-LUNDéN, G., PETERSEN, L. C., RUF, W. & BäCKHED, F. 2012. Tissue factor and PAR1 promote microbiota-induced intestinal vascular remodelling. *Nature,* 483**,** 627-631.

RIVA, A., KUZYK, O., FORSBERG, E., SIUZDAK, G., PFANN, C., HERBOLD, C., DAIMS, H., LOY, A., WARTH, B. & BERRY, D. 2019. A fiber-deprived diet disturbs the fine-scale spatial architecture of the murine colon microbiome. *Nature communications,* 10**,** 4366.

ROBERTSON, S. J., LEMIRE, P., MAUGHAN, H., GOETHEL, A., TURPIN, W., BEDRANI, L., GUTTMAN, D. S., CROITORU, K., GIRARDIN, S. E. & PHILPOTT, D. J. 2019. Comparison of co-housing and littermate methods for microbiota standardization in mouse models. *Cell reports,* 27**,** 1910-1919. e2.

ROGLER, G., HAUSMANN, M., VOGL, D., ASCHENBRENNER, E., ANDUS, T., FALK, W., ANDREESEN, R., SCHöLMERICH, J. & GROSS, V. 1998. Isolation and

phenotypic characterization of colonic macrophages. *Clin Exp Immunol,* 112**,** 205-15.

ROODSANT, T., NAVIS, M., AKNOUCH, I., RENES, I. B., VAN ELBURG, R. M., PAJKRT, D., WOLTHERS, K. C., SCHULTSZ, C., VAN DER ARK, K. C. H., SRIDHAR, A. & MUNCAN, V. 2020. A Human 2D Primary Organoid-Derived Epithelial Monolayer Model to Study Host-Pathogen Interaction in the Small Intestine. *Frontiers in Cellular and Infection Microbiology,* 10.

ROONEY, C. M., MANKIA, K., MITRA, S., MOURA, I. B., EMERY, P. & WILCOX, M. H. 2021. Perturbations of the gut microbiome in anti-CCP positive individuals at risk of developing rheumatoid arthritis. *Rheumatology,* 60**,** 3380-3387.

RøSETH, A. G., AADLAND, E., JAHNSEN, J. & RAKNERUD, N. 1997. Assessment of disease activity in ulcerative colitis by faecal calprotectin, a novel granulocyte marker protein. *Digestion,* 58**,** 176-180.

ROSSEN, N. G., FUENTES, S., VAN DER SPEK, M. J., TIJSSEN, J. G., HARTMAN, J. H., DUFLOU, A., LöWENBERG, M., VAN DEN BRINK, G. R., MATHUS-VLIEGEN, E. M., DE VOS, W. M., ZOETENDAL, E. G., D'HAENS, G. R. & PONSIOEN, C. Y. 2015. Findings From a Randomized Controlled Trial of Fecal Transplantation for Patients With Ulcerative Colitis. *Gastroenterology,* 149**,** 110-118.e4.

ROSSHART, S. P., HERZ, J., VASSALLO, B. G., HUNTER, A., WALL, M. K., BADGER, J. H., MCCULLOCH, J. A., ANASTASAKIS, D. G., SARSHAD, A. A., LEONARDI, I., COLLINS, N., BLATTER, J. A., HAN, S.-J., TAMOUTOUNOUR, S., POTAPOVA, S., FOSTER ST. CLAIRE, M. B., YUAN, W., SEN, S. K., DREIER, M. S., HILD, B., HAFNER, M., WANG, D., ILIEV, I. D., BELKAID, Y., TRINCHIERI, G. & REHERMANN, B. 2019. Laboratory mice born to wild mice have natural microbiota and model human immune responses. *Science,* 365**,** eaaw4361.

ROSSHART, S. P., VASSALLO, B. G., ANGELETTI, D., HUTCHINSON, D. S., MORGAN, A. P., TAKEDA, K., HICKMAN, H. D., MCCULLOCH, J. A., BADGER, J. H., AJAMI, N. J., TRINCHIERI, G., PARDO-MANUEL DE VILLENA, F., YEWDELL, J. W. & REHERMANN, B. 2017. Wild Mouse Gut Microbiota Promotes Host Fitness and Improves Disease Resistance. *Cell,* 171**,** 1015-1028.e13.

ROUND, J. L., LEE, S. M., LI, J., TRAN, G., JABRI, B., CHATILA, T. A. & MAZMANIAN, S. K. 2011. The Toll-Like Receptor 2 Pathway Establishes Colonization by a Commensal of the Human Microbiota. *Science,* 332**,** 974-977.

ROY, U., GáLVEZ, E. J., ILJAZOVIC, A., LESKER, T. R., BłAżEJEWSKI, A. J., PILS, M. C., HEISE, U., HUBER, S., FLAVELL, R. A. & STROWIG, T. 2017. Distinct microbial communities trigger colitis development upon intestinal barrier damage via innate or adaptive immune cells. *Cell Reports,* 21**,** 994-1008.

RUBINO, S. J., SELVANANTHAM, T., GIRARDIN, S. E. & PHILPOTT, D. J. 2012. Nod-like receptors in the control of intestinal inflammation. *Current opinion in immunology,* 24**,** 398-404.

RUBTSOV, Y. P., RASMUSSEN, J. P., CHI, E. Y., FONTENOT, J., CASTELLI, L., YE, X., TREUTING, P., SIEWE, L., ROERS, A., HENDERSON, W. R., JR., MULLER, W. & RUDENSKY, A. Y. 2008. Regulatory T cell-derived interleukin-10 limits inflammation at environmental interfaces. *Immunity,* 28**,** 546-58.

RUGTVEIT, J., BAKKA, A. & BRANDTZAEG, P. 2003. Differential distribution of B7.1 (CD80) and B7.2 (CD86) costimulatory molecules on mucosal macrophage subsets in human inflammatory bowel disease (IBD). *Clinical and Experimental Immunology,* 110**,** 104-113.

SAKAGUCHI, S., SAKAGUCHI, N., ASANO, M., ITOH, M. & TODA, M. 1995. Immunologic self-tolerance maintained by activated T cells expressing IL-2 receptor alpha-chains (CD25). Breakdown of a single mechanism of self-tolerance causes various autoimmune diseases. *Journal of immunology (Baltimore, Md.: 1950),* 155**,** 1151-1164.

SAKAI, J., CAMMAROTA, E., WRIGHT, J. A., CICUTA, P., GOTTSCHALK, R. A., LI, N., FRASER, I. D. & BRYANT, C. E. 2017. Lipopolysaccharide-induced NF-κB nuclear translocation is primarily dependent on MyD88, but TNFα expression requires TRIF and MyD88. *Scientific reports,* 7**,** 1428.

SANDBORN, W. J., FEAGAN, B. G., RUTGEERTS, P., HANAUER, S., COLOMBEL, J. F., SANDS, B. E., LUKAS, M., FEDORAK, R. N., LEE, S., BRESSLER, B., FOX, I., ROSARIO, M., SANKOH, S., XU, J., STEPHENS, K., MILCH, C. & PARIKH, A. 2013. Vedolizumab as induction and maintenance therapy for Crohn's disease. *N Engl J Med,* 369**,** 711-21.

SANDS, B. E., SANDBORN, W. J., PANACCIONE, R., O'BRIEN, C. D., ZHANG, H., JOHANNS, J., ADEDOKUN, O. J., LI, K., PEYRIN-BIROULET, L., VAN ASSCHE, G., DANESE, S., TARGAN, S., ABREU, M. T., HISAMATSU, T., SZAPARY, P. & MARANO, C. 2019. Ustekinumab as Induction and Maintenance Therapy for Ulcerative Colitis. *N Engl J Med,* 381**,** 1201-1214.

SATO, T. & CLEVERS, H. 2013. Growing self-organizing mini-guts from a single intestinal stem cell: mechanism and applications. *Science,* 340**,** 1190-1194.

SATO, T., VAN ES, J. H., SNIPPERT, H. J., STANGE, D. E., VRIES, R. G., VAN DEN BORN, M., BARKER, N., SHROYER, N. F., VAN DE WETERING, M. & CLEVERS, H. 2011. Paneth cells constitute the niche for Lgr5 stem cells in intestinal crypts. *Nature,* 469**,** 415-418.

SCHäLTER, F., FRECH, M., DüRHOLZ, K., LUCAS, S., SARTER, K., LEBON, L., ESSER-VON BIEREN, J., DUBEY, L. K., VOEHRINGER, D., SCHETT, G., HARRIS, N. L. & ZAISS, M. M. 2022. Acetate, a metabolic product of Heligmosomoides polygyrus, facilitates intestinal epithelial barrier breakdown in a FFAR2-dependent manner. *Int J Parasitol,* 52**,** 591-601.

SCHINDELIN, J., ARGANDA-CARRERAS, I., FRISE, E., KAYNIG, V., LONGAIR, M., PIETZSCH, T., PREIBISCH, S., RUEDEN, C., SAALFELD, S., SCHMID, B., TINEVEZ, J. Y., WHITE, D. J., HARTENSTEIN, V., ELICEIRI, K., TOMANCAK, P. & CARDONA, A.

2012. Fiji: an open-source platform for biological-image analysis. *Nat Methods,* 9**,** 676-82.

SCHLAERMANN, P., TOELLE, B., BERGER, H., SCHMIDT, S. C., GLANEMANN, M., ORDEMANN, J., BARTFELD, S., MOLLENKOPF, H. J. & MEYER, T. F. 2016. A novel human gastric primary cell culture system for modelling Helicobacter pylori infection in vitro. *Gut,* 65**,** 202-213.

SCHMITTGEN, T. D. & LIVAK, K. J. 2008. Analyzing real-time PCR data by the comparative CT method. *Nature protocols,* 3**,** 1101-1108.

SCHRIDDE, A., BAIN, C. C., MAYER, J. U., MONTGOMERY, J., POLLET, E., DENECKE, B., MILLING, S. W. F., JENKINS, S. J., DALOD, M., HENRI, S., MALISSEN, B., PABST, O. & MCL MOWAT, A. 2017. Tissue-specific differentiation of colonic macrophages requires TGFß receptor-mediated signaling. *Mucosal Immunol,* 10**,** 1387-1399.

SCHUIJT, T. J., LANKELMA, J. M., SCICLUNA, B. P., DE SOUSA E MELO, F., ROELOFS, J. J., DE BOER, J. D., HOOGENDIJK, A. J., DE BEER, R., DE VOS, A., BELZER, C., DE VOS, W. M., VAN DER POLL, T. & WIERSINGA, W. J. 2016. The gut microbiota plays a protective role in the host defence against pneumococcal pneumonia. *Gut,* 65**,** 575-83.

SCHULTHESS, J., PANDEY, S., CAPITANI, M., RUE-ALBRECHT, K. C., ARNOLD, I., FRANCHINI, F., CHOMKA, A., ILOTT, N. E., JOHNSTON, D. G. W., PIRES, E., MCCULLAGH, J., SANSOM, S. N., ARANCIBIA-CáRCAMO, C. V., UHLIG, H. H. & POWRIE, F. 2019. The Short Chain Fatty Acid Butyrate Imprints an Antimicrobial Program in Macrophages. *Immunity,* 50**,** 432-445.e7.

SCHULZ, O., JAENSSON, E., PERSSON, E. K., LIU, X., WORBS, T., AGACE, W. W. & PABST, O. 2009. Intestinal CD103+, but not CX3CR1+, antigen sampling cells migrate in lymph and serve classical dendritic cell functions. *Journal of Experimental Medicine,* 206**,** 3101-3114.

SCHWAN, W. R., HUANG, X.-Z., HU, L. & KOPECKO, D. J. 2000. Differential bacterial survival, replication, and apoptosis-inducing ability of Salmonella serovars within human and murine macrophages. *Infection and immunity,* 68**,** 1005-1013.

SCOTT, N. A., ANDRUSAITE, A., ANDERSEN, P., LAWSON, M., ALCON-GINER, C., LECLAIRE, C., CAIM, S., LE GALL, G., SHAW, T., CONNOLLY, J. P. R., ROE, A. J., WESSEL, H., BRAVO-BLAS, A., THOMSON, C. A., KäSTELE, V., WANG, P., PETERSON, D. A., BANCROFT, A., LI, X., GRENCIS, R., MOWAT, A. M., HALL, L. J., TRAVIS, M. A., MILLING, S. W. F. & MANN, E. R. 2018. Antibiotics induce sustained dysregulation of intestinal T cell immunity by perturbing macrophage homeostasis. *Sci Transl Med,* 10.

SCOTT, N. A., LAWSON, M. A., HODGETTS, R. J., LE GALL, G., HALL, L. J. & MANN, E. R. 2022. Macrophage metabolism in the intestine is compartment specific and regulated by the microbiota. *Immunology,* 166**,** 138-152.

SELLON, R. K., TONKONOGY, S., SCHULTZ, M., DIELEMAN, L. A., GRENTHER, W., BALISH, E., RENNICK, D. M. & SARTOR, R. B. 1998. Resident enteric bacteria are necessary for development of spontaneous colitis and immune system activation in interleukin-10-deficient mice. *Infection and immunity,* 66**,** 5224-5231.

SETIADY, Y. Y., COCCIA, J. A. & PARK, P. U. 2010. In vivo depletion of CD4+FOXP3+ Treg cells by the PC61 anti-CD25 monoclonal antibody is mediated by FcγRIII+ phagocytes. *European Journal of Immunology,* 40**,** 780-786.

SHAH, K., IGNACIO, A., MCCOY, K. D. & HARRIS, N. L. 2020. The emerging roles of eosinophils in mucosal homeostasis. *Mucosal immunology,* 13**,** 574-583.

SHAMES, B., FOX, J. G., DEWHIRST, F., YAN, L., SHEN, Z. & TAYLOR, N. S. 1995. Identification of widespread Helicobacter hepaticus infection in feces in commercial mouse colonies by culture and PCR assay. *J Clin Microbiol,* 33**,** 2968-72.

SHARIF, O., BOLSHAKOV, V. N., RAINES, S., NEWHAM, P. & PERKINS, N. D. 2007. Transcriptional profiling of the LPS induced NF-κB response in macrophages. *BMC immunology,* 8**,** 1-17.

SHAW, T. N., HOUSTON, S. A., WEMYSS, K., BRIDGEMAN, H. M., BARBERA, T. A., ZANGERLE-MURRAY, T., STRANGWARD, P., RIDLEY, A. J. L., WANG, P., TAMOUTOUNOUR, S., ALLEN, J. E., KONKEL, J. E. & GRAINGER, J. R. 2018. Tissue-resident macrophages in the intestine are long lived and defined by Tim-4 and CD4 expression. *J Exp Med,* 215**,** 1507-1518.

SHI, Y.-J., HU, S.-J., ZHAO, Q.-Q., LIU, X.-S., LIU, C. & WANG, H. 2019. Toll-like receptor 4 (TLR4) deficiency aggravates dextran sulfate sodium (DSS)-induced intestinal injury by down-regulating IL6, CCL2 and CSF3. *Annals of Translational Medicine,* 7.

SHOUVAL, D. S., BISWAS, A., KANG, Y. H., GRIFFITH, A. E., KONNIKOVA, L., MASCANFRONI, I. D., REDHU, N. S., FREI, S. M., FIELD, M., DOTY, A. L., GOLDSMITH, J. D., BHAN, A. K., LOIZIDES, A., WEISS, B., YERUSHALMI, B., YANAGI, T., LUI, X., QUINTANA, F. J., MUISE, A. M., KLEIN, C., HORWITZ, B. H., GLOVER, S. C., BOUSVAROS, A. & SNAPPER, S. B. 2016. Interleukin 1β Mediates Intestinal Inflammation in Mice and Patients With Interleukin 10 Receptor Deficiency. *Gastroenterology,* 151**,** 1100-1104.

SIMPSON, H. L. & CAMPBELL, B. J. 2015. dietary fibre–microbiota interactions. *Alimentary pharmacology & therapeutics,* 42**,** 158-179.

SMITH, K. A., LöSER, S., VARYANI, F., HARCUS, Y., MCSORLEY, H. J., MCKENZIE, A. N. J. & MAIZELS, R. M. 2018. Concerted IL-25R and IL-4Rα signaling drive innate type 2 effector immunity for optimal helminth expulsion. *eLife,* 7**,** e38269.

SMITH, T. D., TSE, M. J., READ, E. L. & LIU, W. F. 2016. Regulation of macrophage polarization and plasticity by complex activation signals. *Integrative Biology,* 8**,** 946-955.

SMITH-GARVIN, J. E., KORETZKY, G. A. & JORDAN, M. S. 2009. T cell activation. *Annual review of immunology,* 27**,** 591-619.

SMYLLIE, N. J., BAGNALL, J., KOCH, A. A., NIRANJAN, D., POLIDAROVA, L., CHESHAM, J. E., CHIN, J. W., PARTCH, C. L., LOUDON, A. S. & HASTINGS, M. H. 2022. Cryptochrome proteins regulate the circadian intracellular behavior and localization of PER2 in mouse suprachiasmatic nucleus neurons. *Proceedings of the National Academy of Sciences,* 119**,** e2113845119.

SMYTHIES, L. E., SELLERS, M., CLEMENTS, R. H., MOSTELLER-BARNUM, M., MENG, G., BENJAMIN, W. H., ORENSTEIN, J. M. & SMITH, P. D. 2005. Human intestinal macrophages display profound inflammatory anergy despite avid phagocytic and bacteriocidal activity. *The Journal of clinical investigation,* 115**,** 66-75.

SOENDERGAARD, C., SEIDELIN, J. B., STEENHOLDT, C. & NIELSEN, O. H. 2018. Putative biomarkers of vedolizumab resistance and underlying inflammatory pathways involved in IBD. *BMJ open gastroenterology,* 5**,** e000208.

SOLER, D., CHAPMAN, T., YANG, L.-L., WYANT, T., EGAN, R. & FEDYK, E. R. 2009. The binding specificity and selective antagonism of vedolizumab, an anti-α4β7 integrin therapeutic antibody in development for inflammatory bowel diseases. *Journal of Pharmacology and Experimental Therapeutics,* 330**,** 864-875.

SOMMER, F. & BäCKHED, F. 2013. The gut microbiota—masters of host development and physiology. *Nature reviews microbiology,* 11**,** 227-238.

SORINI, C., CARDOSO, R. F., GAGLIANI, N. & VILLABLANCA, E. J. 2018. Commensal bacteria-specific CD4+ T cell responses in health and disease. *Frontiers in immunology,* 9**,** 411784.

SOUFLI, I., TOUMI, R., RAFA, H. & TOUIL-BOUKOFFA, C. 2016. Overview of cytokines and nitric oxide involvement in immuno-pathogenesis of inflammatory bowel diseases. *World journal of gastrointestinal pharmacology and therapeutics,* 7**,** 353.

SPEES ALANNA, M., KINGSBURY DAWN, D., WANGDI, T., XAVIER MARIANA, N., TSOLIS RENéE, M. & BäUMLER ANDREAS, J. 2014. Neutrophils Are a Source of Gamma Interferon during Acute Salmonella enterica Serovar Typhimurium Colitis. *Infection and Immunity,* 82**,** 1692-1697.

SPENCER, D. M., VELDMAN, G. M., BANERJEE, S., WILLIS, J. & LEVINE, A. D. 2002. Distinct inflammatory mechanisms mediate early versus late colitis in mice. *Gastroenterology,* 122**,** 94-105.

STANIFER, M. L., MUKENHIRN, M., MUENCHAU, S., PERVOLARAKI, K., KANAYA, T., ALBRECHT, D., ODENDALL, C., HIELSCHER, T., HAUCKE, V., KAGAN, J. C., BARTFELD, S., OHNO, H. & BOULANT, S. 2020. Asymmetric distribution of TLR3 leads to a polarized immune response in human intestinal epithelial cells. *Nat Microbiol,* 5**,** 181-191.

STECHER, B., MAIER, L. & HARDT, W.-D. 2013. 'Blooming'in the gut: how dysbiosis might contribute to pathogen evolution. *Nature Reviews Microbiology,* 11**,** 277-284.

STECHER, B., ROBBIANI, R., WALKER, A. W., WESTENDORF, A. M., BARTHEL, M., KREMER, M., CHAFFRON, S., MACPHERSON, A. J., BUER, J., PARKHILL, J., DOUGAN, G., VON MERING, C. & HARDT, W. D. 2007. Salmonella enterica serovar typhimurium exploits inflammation to compete with the intestinal microbiota. *PLoS Biol,* 5**,** 2177-89.

STENSTAD, H., SVENSSON, M., CUCAK, H., KOTARSKY, K. & AGACE, W. W. 2007. Differential homing mechanisms regulate regionalized effector CD8αβ+ T cell accumulation within the small intestine. *Proceedings of the National Academy of Sciences,* 104**,** 10122-10127.

STERZENBACH, T., BARTONICKOVA, L., BEHRENS, W., BRENNEKE, B., SCHULZE, J., KOPS, F., CHIN, E. Y., KATZOWITSCH, E., SCHAUER, D. B., FOX, J. G., SUERBAUM, S. & JOSENHANS, C. 2008. Role of the Helicobacter hepaticus flagellar sigma factor FliA in gene regulation and murine colonization. *J Bacteriol,* 190**,** 6398-408.

STERZENBACH, T., LEE, S. K., BRENNEKE, B., GOETZ, F. V., SCHAUER, D. B., FOX, J. G., SUERBAUM, S. & JOSENHANS, C. 2007. Inhibitory Effect of Enterohepatic Helicobacter hepaticus on Innate Immune Responses of Mouse Intestinal Epithelial Cells. *Infection and Immunity,* 75**,** 2717-2728.

STEVCEVA, L., PAVLI, P., HUSBAND, A. J. & DOE, W. F. 2001. The inflammatory infiltrate in the acute stage of the dextran sulphate sodium induced colitis: B cell response differs depending on the percentage of DSS used to induce it. *BMC clinical pathology,* 1**,** 1-11.

STROMBERG, Z. R., VAN GOOR, A., REDWEIK, G. A., WYMORE BRAND, M. J., WANNEMUEHLER, M. J. & MELLATA, M. 2018. Pathogenic and non-pathogenic Escherichia coli colonization and host inflammatory response in a defined microbiota mouse model. *Disease models & mechanisms,* 11**,** dmm035063.

SUN, C.-M., HALL, J. A., BLANK, R. B., BOULADOUX, N., OUKKA, M., MORA, J. R. & BELKAID, Y. 2007. Small intestine lamina propria dendritic cells promote de novo generation of Foxp3 T reg cells via retinoic acid. *The Journal of experimental medicine,* 204**,** 1775-1785.

SUNG, P.-S., HUANG, T.-F. & HSIEH, S.-L. 2019. Extracellular vesicles from CLEC2-activated platelets enhance dengue virus-induced lethality via CLEC5A/TLR2. *Nature communications,* 10**,** 2402.

SURANA, N. K. & KASPER, D. L. 2017. Moving beyond microbiome-wide associations to causal microbe identification. *Nature,* 552**,** 244-247.

SVOLOS, V., HANSEN, R., NICHOLS, B., QUINCE, C., IJAZ, U. Z., PAPADOPOULOU, R. T., EDWARDS, C. A., WATSON, D., ALGHAMDI, A., BREJNROD, A., ANSALONE, C., DUNCAN, H., GERVAIS, L., TAYLER, R., SALMOND, J., BOLOGNINI, D., KLOPFLEISCH, R., GAYA, D. R., MILLING, S., RUSSELL, R. K. & GERASIMIDIS, K. 2019. Treatment of Active Crohn's Disease With an Ordinary Food-based Diet That Replicates Exclusive Enteral Nutrition. *Gastroenterology,* 156**,** 1354-1367.e6.

TAAMS, L. S., VAN AMELSFORT, J. M., TIEMESSEN, M. M., JACOBS, K. M., DE JONG, E. C., AKBAR, A. N., BIJLSMA, J. W. & LAFEBER, F. P. 2005. Modulation of monocyte/macrophage function by human CD4+ CD25+ regulatory T cells. *Human immunology,* 66**,** 222-230.

TADA, T., YAMAMURA, S., KUWANO, Y. & ABO, T. 1996. Level of myelopoiesis in the bone marrow is influenced by intestinal flora. *Cellular immunology,* 173**,** 155-161.

TAFAZOLI, F., MAGNUSSON, K.-E. & ZHENG, L. 2003. Disruption of epithelial barrier integrity by Salmonella enterica serovar typhimurium requires geranylgeranylated proteins. *Infection and immunity,* 71**,** 872-881.

TAKEUCHI, O. & AKIRA, S. 2010. Pattern recognition receptors and inflammation. *Cell,* 140**,** 805-820.

TAMOUTOUNOUR, S., HENRI, S., LELOUARD, H., DE BOVIS, B., DE HAAR, C., VAN DER WOUDE, C. J., WOLTMAN, A. M., REYAL, Y., BONNET, D., SICHIEN, D., BAIN, C. C., MOWAT, A. M., REIS E SOUSA, C., POULIN, L. F., MALISSEN, B. & GUILLIAMS, M. 2012. CD64 distinguishes macrophages from dendritic cells in the gut and reveals the Th1-inducing role of mesenteric lymph node macrophages during colitis. *Eur J Immunol,* 42**,** 3150-66.

TANOUE, T., ATARASHI, K. & HONDA, K. 2016. Development and maintenance of intestinal regulatory T cells. *Nature Reviews Immunology,* 16**,** 295-309.

TAYLOR, N. S., XU, S., NAMBIAR, P., DEWHIRST, F. E. & FOX, J. G. 2007. Enterohepatic Helicobacter species are prevalent in mice from commercial and academic institutions in Asia, Europe, and North America. *Journal of clinical microbiology,* 45**,** 2166-2172.

TAZZARI, P. L., CAPPELLINI, A., BORTUL, R., RICCI, F., BILLI, A. M., TABELLINI, G., CONTE, R. & MARTELLI, A. M. 2002. Flow cytometric detection of total and serine 473 phosphorylated Akt. *Journal of cellular biochemistry,* 86**,** 704-715.

TENG, M. W., BOWMAN, E. P., MCELWEE, J. J., SMYTH, M. J., CASANOVA, J.-L., COOPER, A. M. & CUA, D. J. 2015. IL-12 and IL-23 cytokines: from discovery to targeted therapies for immune-mediated inflammatory diseases. *Nature medicine,* 21**,** 719-729.

THOMPSON, M. R., KAMINSKI, J. J., KURT-JONES, E. A. & FITZGERALD, K. A. 2011. Pattern recognition receptors and the innate immune response to viral infection. *Viruses,* 3**,** 920-940.

TODORIC, J., DI CARO, G., REIBE, S., HENSTRIDGE, D. C., GREEN, C. R., VRBANAC, A., CETECI, F., CONCHE, C., MCNULTY, R., SHALAPOUR, S., TANIGUCHI, K., MEIKLE, P. J., WATROUS, J. D., MORANCHEL, R., NAJHAWAN, M., JAIN, M., LIU, X., KISSELEVA, T., DIAZ-MECO, M. T., MOSCAT, J., KNIGHT, R., GRETEN, F. R., LAU, L. F., METALLO, C. M., FEBBRAIO, M. A. & KARIN, M. 2020. Fructose stimulated de novo lipogenesis is promoted by inflammation. *Nat Metab,* 2**,** 1034-1045.

TREUTING, P. M., ARENDS, M. J. & DINTZIS, S. M. 2018a. Lower gastrointestinal tract. *Comparative anatomy and histology*. Elsevier.

TREUTING, P. M., ARENDS, M. J. & DINTZIS, S. M. 2018b. Upper gastrointestinal tract. *Comparative anatomy and histology*. Elsevier.

TURRONI, F., VENTURA, M., BUTTó, L. F., DURANTI, S., O'TOOLE, P. W., MOTHERWAY, M. O. C. & VAN SINDEREN, D. 2014. Molecular dialogue between the human gut microbiota and the host: a Lactobacillus and Bifidobacterium perspective. *Cellular and molecular life sciences,* 71**,** 183-203.

UBEDA, C., LIPUMA, L., GOBOURNE, A., VIALE, A., LEINER, I., EQUINDA, M., KHANIN, R. & PAMER, E. G. 2012. Familial transmission rather than defective innate immunity shapes the distinct intestinal microbiota of TLR-deficient mice. *Journal of Experimental Medicine,* 209**,** 1445-1456.

UEMATSU, S., JANG, M. H., CHEVRIER, N., GUO, Z., KUMAGAI, Y., YAMAMOTO, M., KATO, H., SOUGAWA, N., MATSUI, H., KUWATA, H., HEMMI, H., COBAN, C., KAWAI, T., ISHII, K. J., TAKEUCHI, O., MIYASAKA, M., TAKEDA, K. & AKIRA, S. 2006. Detection of pathogenic intestinal bacteria by Toll-like receptor 5 on intestinal CD11c+ lamina propria cells. *Nat Immunol,* 7**,** 868-74.

UHLIG, H. H. & POWRIE, F. 2018. Translating immunology into therapeutic concepts for inflammatory bowel disease. *Annual review of immunology,* 36**,** 755-781.

UNDERHILL, D. M. 2003. Macrophage recognition of zymosan particles. *Journal of endotoxin research,* 9**,** 176-180.

VAISHNAVA, S., BEHRENDT, C. L., ISMAIL, A. S., ECKMANN, L. & HOOPER, L. V. 2008. Paneth cells directly sense gut commensals and maintain homeostasis at the intestinal host-microbial interface. *Proceedings of the National Academy of Sciences,* 105**,** 20858-20863.

VAN BAARLEN, P., WELLS, J. M. & KLEEREBEZEM, M. 2013. Regulation of intestinal homeostasis and immunity with probiotic lactobacilli. *Trends in immunology,* 34**,** 208-215.

VAN DER POST, S., JABBAR, K. S., BIRCHENOUGH, G., ARIKE, L., AKHTAR, N., SJOVALL, H., JOHANSSON, M. E. & HANSSON, G. C. 2019. Structural weakening of the colonic mucus barrier is an early event in ulcerative colitis pathogenesis. *Gut,* 68**,** 2142-2151.

VAN DER SLUIS, M., DE KONING, B. A., DE BRUIJN, A. C., VELCICH, A., MEIJERINK, J. P., VAN GOUDOEVER, J. B., BüLLER, H. A., DEKKER, J., VAN SEUNINGEN, I., RENES, I. B. & EINERHAND, A. W. 2006. Muc2-deficient mice spontaneously develop colitis, indicating that MUC2 is critical for colonic protection. *Gastroenterology,* 131**,** 117-29.

VAN DER WAAIJ, L. A., LIMBURG, P. C., MESANDER, G. & VAN DER WAAIJ, D. 1996. In vivo IgA coating of anaerobic bacteria in human faeces. *Gut,* 38**,** 348-354.

VEAUTHIER, B. & HORNECKER, J. R. 2018. Crohn's disease: diagnosis and management. *American family physician,* 98**,** 661-669.

VERBERK, S. G., DE GOEDE, K. E., GORKI, F. S., VAN DIERENDONCK, X. A., ARGüELLO, R. J. & VAN DEN BOSSCHE, J. 2022. An integrated toolbox to profile macrophage immunometabolism. *Cell reports methods,* 2.

VOLYNETS, V., REICHOLD, A., BáRDOS, G., RINGS, A., BLEICH, A. & BISCHOFF, S. C. 2016. Assessment of the intestinal barrier with five different permeability tests in healthy C57BL/6J and BALB/cJ mice. *Digestive diseases and sciences,* 61**,** 737-746.

VON MOLTKE, J., JI, M., LIANG, H.-E. & LOCKSLEY, R. M. 2016. Tuft-cell-derived IL-25 regulates an intestinal ILC2–epithelial response circuit. *Nature,* 529**,** 221-225.

WAHLSTRöM, A., SAYIN, S. I., MARSCHALL, H.-U. & BäCKHED, F. 2016. Intestinal crosstalk between bile acids and microbiota and its impact on host metabolism. *Cell metabolism,* 24**,** 41-50.

WAISMAN, A. & BECHER, B. 2014. T-Helper Cells. Springer.

WALKER, A. W. & LAWLEY, T. D. 2013. Therapeutic modulation of intestinal dysbiosis. *Pharmacological research,* 69**,** 75-86.

WANG, S.-L., WANG, Z.-R. & YANG, C.-Q. 2012. Meta-analysis of broad-spectrum antibiotic therapy in patients with active inflammatory bowel disease. *Experimental and therapeutic medicine,* 4**,** 1051-1056.

WARD, J. M., ANVER, M. R., HAINES, D. C., MELHORN, J. M., GORELICK, P., YAN, L. & FOX, J. G. 1996. Inflammatory large bowel disease in immunodeficient mice naturally infected with Helicobacter hepaticus. *Laboratory animal science,* 46**,** 15-20.

WARD, J. M., FOX, J. G., ANVER, M. R., HAINES, D. C., GEORGE, C. V., COLLINS, M. J., JR., GORELICK, P. L., NAGASHIMA, K., GONDA, M. A., GILDEN, R. V., TULLY, J. G., RUSSELL, R. J., BENVENSITE, R. E., PASTER, B. J., DEWHIRST, F. E., DONOVAN, J. C., ANDERSON, L. M. & RICE, J. M. 1994. Chronic Active Hepatitis and Associated Liver Tumors in Mice Caused by a Presistent Bacterial Infection With a Novel Helicobacter Species. *JNCI: Journal of the National Cancer Institute,* 86**,** 1222-1227.

WEICHHART, T., HENGSTSCHLäGER, M. & LINKE, M. 2015. Regulation of innate immune cell function by mTOR. *Nature Reviews Immunology,* 15**,** 599-614.

WELLS, P. M., ADEBAYO, A. S., BOWYER, R. C. E., FREIDIN, M. B., FINCKH, A., STROWIG, T., LESKER, T. R., ALPIZAR-RODRIGUEZ, D., GILBERT, B., KIRKHAM, B., COPE, A. P., STEVES, C. J. & WILLIAMS, F. M. K. 2020. Associations between gut microbiota and genetic risk for rheumatoid arthritis in the absence of disease: a cross-sectional study. *Lancet Rheumatol,* 2**,** e418-e427.

WEN, H., MIAO, E. A. & TING, J. P.-Y. 2013. Mechanisms of NOD-like receptor-associated inflammasome activation. *Immunity,* 39**,** 432-441.

WHARY, M., MORGAN, T., DANGLER, C., GAUDES, K., TAYLOR, N. & FOX, J. 1998. Chronic active hepatitis induced by Helicobacter hepaticus in the A/JCr mouse is associated with a Th1 cell-mediated immune response. *Infection and immunity,* 66**,** 3142-3148.

WHITE, M. P., MCMANUS, C. M. & MAIZELS, R. M. 2020. Regulatory T-cells in helminth infection: induction, function and therapeutic potential. *Immunology,* 160**,** 248-260.

WILLIAMSON, I. A., ARNOLD, J. W., SAMSA, L. A., GAYNOR, L., DISALVO, M., COCCHIARO, J. L., CARROLL, I., AZCARATE-PERIL, M. A., RAWLS, J. F., ALLBRITTON, N. L. & MAGNESS, S. T. 2018. A High-Throughput Organoid Microinjection Platform to Study Gastrointestinal Microbiota and Luminal Physiology. *Cell Mol Gastroenterol Hepatol,* 6**,** 301-319.

WILLING, B. P., DICKSVED, J., HALFVARSON, J., ANDERSSON, A. F., LUCIO, M., ZHENG, Z., JäRNEROT, G., TYSK, C., JANSSON, J. K. & ENGSTRAND, L. 2010. A pyrosequencing study in twins shows that gastrointestinal microbial profiles vary with inflammatory bowel disease phenotypes. *Gastroenterology,* 139**,** 1844-1854. e1.

WIRTZ, S., NEUFERT, C., WEIGMANN, B. & NEURATH, M. F. 2007. Chemically induced mouse models of intestinal inflammation. *Nature protocols,* 2**,** 541-546.

WLODARSKA, M., LUO, C., KOLDE, R., D'HENNEZEL, E., ANNAND, J. W., HEIM, C. E., KRASTEL, P., SCHMITT, E. K., OMAR, A. S., CREASEY, E. A., GARNER, A. L., MOHAMMADI, S., O'CONNELL, D. J., ABUBUCKER, S., ARTHUR, T. D., FRANZOSA, E. A., HUTTENHOWER, C., MURPHY, L. O., HAISER, H. J., VLAMAKIS, H., PORTER, J. A. & XAVIER, R. J. 2017. Indoleacrylic Acid Produced by Commensal

Peptostreptococcus Species Suppresses Inflammation. *Cell Host Microbe,* 22**,** 25-37.e6.

WONGCHANA, W. & PALAGA, T. 2012. Direct regulation of interleukin-6 expression by Notch signaling in macrophages. *Cellular & molecular immunology,* 9**,** 155-162.

XIONG, H., MITTMAN, S., RODRIGUEZ, R., MOSKALENKO, M., PACHECO-SANCHEZ, P., YANG, Y., NICKLES, D. & CUBAS, R. 2019. Anti-PD-L1 treatment results in functional remodeling of the macrophage compartment. *Cancer research,* 79**,** 1493-1506.

XU, H., AGALIOTI, T., ZHAO, J., STEGLICH, B., WAHIB, R., VESELY, M. C. A., BIELECKI, P., BAILIS, W., JACKSON, R., PEREZ, D., IZBICKI, J., LICONA-LIMóN, P., KAARTINEN, V., GEGINAT, J., ESPLUGUES, E., TOLOSA, E., HUBER, S., FLAVELL, R. A. & GAGLIANI, N. 2020. The induction and function of the anti-inflammatory fate of T(H)17 cells. *Nat Commun,* 11**,** 3334.

XU, M., POKROVSKII, M., DING, Y., YI, R., AU, C., HARRISON, O. J., GALAN, C., BELKAID, Y., BONNEAU, R. & LITTMAN, D. R. 2018. c-MAF-dependent regulatory T cells mediate immunological tolerance to a gut pathobiont. *Nature,* 554**,** 373-377.

YAMAZAKI, T., AKIBA, H., IWAI, H., MATSUDA, H., AOKI, M., TANNO, Y., SHIN, T., TSUCHIYA, H., PARDOLL, D. M., OKUMURA, K., AZUMA, M. & YAGITA, H. 2002. Expression of programmed death 1 ligands by murine T cells and APC. *J Immunol,* 169**,** 5538-45.

YAN, H., WALKER, F. C., ALI, A., HAN, H., TAN, L., VEILLON, L., LORENZI, P. L., BALDRIDGE, M. T. & KING, K. Y. 2022. The bacterial microbiota regulates normal hematopoiesis via metabolite-induced type 1 interferon signaling. *Blood Advances,* 6**,** 1754-1765.

YAN, Y., KOLACHALA, V., DALMASSO, G., NGUYEN, H., LAROUI, H., SITARAMAN, S. V. & MERLIN, D. 2009. Temporal and spatial analysis of clinical and molecular parameters in dextran sodium sulfate induced colitis. *PloS one,* 4**,** e6073.

YANG, I., EIBACH, D., KOPS, F., BRENNEKE, B., WOLTEMATE, S., SCHULZE, J., BLEICH, A., GRUBER, A. D., MUTHUPALANI, S., FOX, J. G., JOSENHANS, C. & SUERBAUM, S. 2013. Intestinal microbiota composition of interleukin-10 deficient C57BL/6J mice and susceptibility to Helicobacter hepaticus-induced colitis. *PLoS One,* 8**,** e70783.

YANG, R., CHEN, Z. & CAI, J. 2023. Fecal microbiota transplantation: Emerging applications in autoimmune diseases. *Journal of Autoimmunity***,** 103038.

YI, P. & LI, L. 2012. The germfree murine animal: an important animal model for research on the relationship between gut microbiota and the host. *Veterinary microbiology,* 157**,** 1-7.

YU, S. & GAO, N. 2015. Compartmentalizing intestinal epithelial cell toll-like receptors for immune surveillance. *Cellular and molecular life sciences,* 72**,** 3343-3353.

ZENG, M. Y., CISALPINO, D., VARADARAJAN, S., HELLMAN, J., WARREN, H. S., CASCALHO, M., INOHARA, N. & NúñEZ, G. 2016. Gut microbiota-induced immunoglobulin G controls systemic infection by symbiotic bacteria and pathogens. *Immunity,* 44**,** 647-658.

ZHANG, D., CHEN, G., MANWANI, D., MORTHA, A., XU, C., FAITH, J. J., BURK, R. D., KUNISAKI, Y., JANG, J. E., SCHEIERMANN, C., MERAD, M. & FRENETTE, P. S. 2015. Neutrophil ageing is regulated by the microbiome. *Nature,* 525**,** 528-32.

ZHANG, H., DAI, Y., LIU, Y., WU, T., LI, J., WANG, X. & WANG, W. 2018. Helicobacter pylori colonization protects against chronic experimental colitis by regulating Th17/Treg balance. *Inflammatory Bowel Diseases,* 24**,** 1481-1492.

ZHENG, L., KELLY, C. J., BATTISTA, K. D., SCHAEFER, R., LANIS, J. M., ALEXEEV, E. E., WANG, R. X., ONYIAH, J. C., KOMINSKY, D. J. & COLGAN, S. P. 2017. Microbial-derived butyrate promotes epithelial barrier function through IL-10 receptor–dependent repression of claudin-2. *The Journal of Immunology,* 199**,** 2976-2984.

ZHU, L., SHI, T., ZHONG, C., WANG, Y., CHANG, M. & LIU, X. 2017. IL-10 and IL-10 receptor mutations in very early onset inflammatory bowel disease. *Gastroenterology research,* 10**,** 65.

ZIGMOND, E., BERNSHTEIN, B., FRIEDLANDER, G., WALKER, C. R., YONA, S., KIM, K. W., BRENNER, O., KRAUTHGAMER, R., VAROL, C., MüLLER, W. & JUNG, S. 2014. Macrophage-restricted interleukin-10 receptor deficiency, but not IL-10 deficiency, causes severe spontaneous colitis. *Immunity,* 40**,** 720-33.